Discrete Breathers in One- and Two-Dimensional Lattices

Imran Ashiq Butt, MSc.

Thesis submitted to the University of Nottingham
for the degree of Doctor of Philosophy

July 2006

Acknowledgements

Contents

List of Figures

List of Tables

Abstract

Discrete breathers are time-periodic and spatially localised exact solutions in translationally invariant nonlinear lattices. They are generic solutions, since only moderate conditions are required for their existence. Closed analytic forms for breather solutions are generally not known. We use asymptotic methods to determine both the properties and the approximate form of discrete breather solutions in various lattices.

We find the conditions for which the one-dimensional FPU chain admits breather solutions, generalising a known result for stationary breathers to include moving breathers. These conditions are verified by numerical simulations. We show that the FPU chain with quartic interaction potential supports long-lived waveforms which are combinations of a breather and a kink. The amplitude of classical monotone kinks is shown to have a nonzero minimum, whereas the amplitude of breathing-kinks can be arbitrarily small.

We consider a two-dimensional FPU lattice with square rotational symmetry. An analysis to third-order in the wave amplitude is inadequate, since this leads to a partial differential equation which does not admit stable soliton solutions for the breather envelope. We overcome this by extending the analysis to higher-order, obtaining a modified partial differential equation which includes known stabilising terms. From this, we determine regions of parameter space where breather solutions are expected. Our analytic results are supported by extensive numerical simulations, which suggest that the two-dimensional square FPU lattice supports long-lived stationary and moving breather modes. We find no restriction upon the direction in which breathers can travel through the lattice. Asymptotic estimates for the breather energy confirm that there is a minimum threshold energy which must be exceeded for breathers to exist in the two-dimensional lattice. We find similar results for a two-dimensional FPU lattice with hexagonal rotational symmetry.

Frequently used abbreviations

ODE	ordinary differential equation
PDE	partial differential equation
DB	discrete breather
ILM	intrinsic localised mode
KG	Klein-Gordon (lattice)
sG	sine-Gordon (equation, lattice)
FPU	Fermi-Pasta-Ulam (lattice)
AL	Ablowitz-Ladik (lattice)
NLS	nonlinear Schrödinger (equation)
KdV	Korteweg-de Vries (equation)
RWA	rotating-wave approximation
PN	Peierls-Nabarro (potential)
ST	Sievers-Takeno (mode)
P	Page (mode)
c.c.	complex conjugate
SETL	square electrical transmission lattice
HETL	hexagonal electrical transmission lattice

Chapter 1

Introduction

Many-particle systems may be modelled as spatially discrete if the processes under consideration involve length scales comparable to the interparticle distances in those systems. Modelling of these systems results in a set of ordinary differential equations, each equation corresponding to a constituent particle. A *lattice* (or *crystal*) is a repeating array of particles, atoms or molecules. More formally, a lattice is a discrete system which possesses discrete translational invariance, or equivalently, spatial periodicity.

1.1 Historical development

1.1.1 Localisation in imperfect lattices

Let us first review some known facts about *harmonic* lattices, that is, lattices for which the coupling forces between particles are linear. There is a large body of literature describing the dynamics of perfect harmonic lattices in terms of extended plane wave states (see for example, Maradudin *et al.* [88]).

In nature, one finds that within crystals, the perfect repeating arrangement may extend over several thousand atoms before translational symmetry is interrupted. Typically, this is manifested by the presence of impurities or defects such as atomic vacancies (missing atoms) or interstitial atoms (extra atoms). Or,

it could be that the lattice is disordered, by which we mean that the interparticle couplings are random.

It is well known that localised vibrational modes can occur in harmonic lattices when imperfections of the type mentioned above are present. For instance, Maradudin writes in [87] that, "when an impurity atom is introduced into a crystal the frequencies of the normal modes of vibration of the atoms in the crystal and the pattern of the atomic displacements in these modes can be profoundly altered. Localized vibration modes can appear …in which the vibration amplitudes of the atoms die off faster than exponentially with increasing distance from the defect." A slightly updated review of the theory on lattices with isolated defects is presented by Lifshitz & Kosevich [83].

A similar localisation phenomenon is also known for disordered lattices. The Hamiltonian for such a lattice with nearest-neighbour interactions (NNI) has the form

$$H = \sum_{n=-\infty}^{+\infty} \tfrac{1}{2}\dot{q}_n^2 + \tfrac{1}{2}k_n(q_{n+1} - q_n)^2, \tag{1.1}$$

where $q_n(t)$ gives the position of the nth particle at time t, and the constants k_n, $n \in \mathbb{Z}$ denote the different coupling strengths between adjacent particles. The equation of motion for the nth particle in the lattice is thus

$$\ddot{q}_n = k_n(q_{n+1} - q_n) - k_{n-1}(q_n - q_{n-1}). \tag{1.2}$$

Localised modes also occur in disordered lattices when there is a sufficiently high level of disorder present. Intuitively, certain types of waves become trapped, and the disorder hinders or completely prevents the spreading of any initial wavepacket. This disorder-induced mechanism for localisation in imperfect lattices is known as *Anderson localisation*, and the resulting waveforms are *Anderson modes* [5].

Thus while the possibility of localised modes in imperfect lattices is well known, in perfect harmonic lattices, typically one expects only spatially extended plane wave solutions. As noted by Campbell *et al.* [30], until relatively recently, this notion was thought to extend to any periodic structure free from

extrinsic imperfections. It was therefore surprising when Sievers & Takeno [117] proposed that localised modes could exist quite commonly in perfect but *anharmonic* lattices, that is, lattices with anharmonic (nonlinear) interparticle interactions. Since the occurrence of this new type of localisation depended upon properties of the lattice itself, and not upon extrinsic defects, they referred to the corresponding modes as *intrinsic localised modes* (ILMs). These excitations have since acquired a host of other names, including *discrete breathers* (DBs), *nonlinear localised excitations* (NLEs), *localised oscillations* (LOs), *self-localised anharmonic modes* (SLAMs), and no doubt several others too. Throughout this thesis, we use the most popular of these, namely "discrete breathers", or simply "breathers." We explain the origin of this particular name in Section 1.1.3.

1.1.2 Existence of discrete breathers: an intuitive argument

Discrete breathers are spatially localised time-periodic excitations in translationally invariant (perfect) anharmonic lattices. Pictorially, a typical breather excitation may appear as a discrete nonlinear version of the well-known linear wavepacket. That is, they take the form of a carrier wave with a bell-shaped envelope.

In this thesis, we consider the ability of lattices to support discrete breather solutions. A qualitative discussion of discrete breathers dates back to Ovchinnikov [94], while Kosevich & Kovalev [80] seem to have been the first to attempt to find a solution for breathers in a Klein-Gordon type lattice. However, it was Sievers & Takeno [117] who first conjectured that long-lived discrete breather modes should occur commonly in nonlinear lattices. A much simplified version of their intuitive argument for breather existence and stability against decay is given by Campbell *et al.* [30]. The following is based on the version that appears there, and also in Campbell [29].

We consider the continuum Klein-Gordon partial differential equation $q_{tt} - q_{xx} + V'(q) = 0$ where $V' = q - q^3$, and its discrete analogue, the Klein-Gordon

lattice (which we shall discuss further in Section 1.2.1), namely

$$q_{tt} = q_{xx} - q + q^3, \quad \text{and} \tag{1.3}$$

$$\ddot{q}_n = \frac{1}{(\Delta x)^2}(q_{n+1} - 2q_n + q_{n-1}) - q_n + q_n^3. \tag{1.4}$$

In (1.4), the term $1/(\Delta x)^2$ in the difference operator is included for reasons that will become clear shortly. It may be thought of as a discreteness parameter, with large Δx corresponding to a lattice that is highly discrete, while $\Delta x \to 0$ corresponds to the continuum limit.

We look for small amplitude solutions of equations (1.4). This corresponds to linearising about the zero solution $q_n = 0$ and solving the resulting equation, which is

$$\ddot{q}_n = \frac{1}{(\Delta x)^2}(q_{n+1} - 2q_n + q_{n-1}) - q_n. \tag{1.5}$$

Explicitly, we seek plane wave solutions of the form $q_n(t) = A \exp(\mathrm{i}kn + \mathrm{i}\omega t)$. Inserting this into the linearised equation (1.5) gives a relationship between the temporal frequency ω and the wavenumber k. This is known as the *dispersion relation*, which for (1.5) turns out to be

$$\omega^2 = \frac{4}{(\Delta x)^2}\sin^2\left(\frac{k}{2}\right) + 1. \tag{1.6}$$

From (1.6), we see that different wavenumbers k correspond to different frequencies ω, but for any wavenumber k, the frequency w is bounded above and below with $1 < w^2 < 1 + (2/\Delta x)^2$. In other words, linear waves have a frequency which must lie within this spectrum (known as the *phonon band*). Clearly, the upper bound arises because of the discreteness of the lattice, and in addition, the width of the phonon band depends upon the discreteness of the lattice (of which Δx is a measure).

Compare this with the dispersion relation of the continuum equation (1.3), which is obtained by seeking small amplitude solutions of the form $q(x, t) = A \exp(\mathrm{i}kx + \mathrm{i}\omega t)$ to $q_{tt} = q_{xx} - q$, giving

$$\omega^2 = \frac{1}{(\Delta x)^2}k^2 + 1. \tag{1.7}$$

From (1.7), we see that for the continuum equation (1.3), there is no upper bound on the frequency of linear waves (or phonons).

A common feature of nonlinear vibrations is that (unlike the say, the harmonic oscillator), the frequency is dependent upon the amplitude of oscillation. In fact, the manner in which the frequency is related to the amplitude is sometimes referred to as the *nonlinear dispersion relation* for the system. We find this for the discrete nonlinear equation (1.4). For now, we use a method similar to that described by Remoissenet [103] (see Chapter 4.4 therein), though later (see Section 2.2) we use a more systematic method. We seek small amplitude solutions to (1.4) of the form $q_n(t) = A \exp(\mathrm{i}kn + \mathrm{i}\omega t) + \mathrm{c.c.}$, where c.c. denotes the complex conjugate. We substitute this into (1.4), and apply the rotating-wave approximation (RWA). This means that we retain only those terms which are of frequency w (and for instance, discard terms which oscillate with frequency 3ω). The RWA is discussed more fully in Section 1.7.1. Proceeding thus, we obtain the nonlinear dispersion relation for (1.4).

$$\omega^2 = \frac{4}{(\Delta x)^2} \sin^2\left(\frac{k}{2}\right) + 1 + 3A^2. \tag{1.8}$$

From (1.8), we see that the frequency of oscillation increases with increasing amplitude.

Putting these two facts together, we begin to see how discrete breather excitations are possible in nonlinear discrete lattices. In order to be long-lived, the frequency of the breather w_b must lie outside of the spectrum of linear waves, otherwise the breather is destroyed through resonance with linear phonon modes. In addition, due to the nonlinearity of the lattice, higher harmonics of the excitation are also generated. For stability, we must similarly avoid resonances between the breather's harmonics and linear phonons. Using the nonlinear dispersion relation (1.8), by choosing the amplitude A suitably, we can ensure that the frequency of the breather w_b lies outside (in this case, above) the phonon band. Also, the discreteness of the system implies that the frequency of linear waves is bounded above (see (1.6)). Since the fundamental frequency of the

breather w_b lies above the phonon band, clearly all of its harmonics will also lie above the phonon band, and therefore potentially destructive resonances between the breather's harmonics and phonons are also avoided.

In this intuitive argument, we see how nonlinearity and discreteness are two essential requirements for breather occurrence. Nonlinearity allows for the shifting of the breather fundamental frequency outside the phonon band, while (in general) the discreteness gives rise to gaps and cut-offs in the phonon spectrum so that all the breather's harmonics lie outside this band. Hence, the breather is stable against decay through phonon emission.

As one would expect, there are additional subtleties. For example, one might find that the frequency of small oscillations *decreases* with amplitude. In this case, one sets the breather fundamental frequency below the phonon band. If Δx is large, then from (1.6) the phonon band is very narrow, and so this ensures that the breather's harmonics still lie above here, avoiding resonances once more. Nevertheless, the argument outlined above embodies the essence of the phenomenon.

1.1.3 Breathers in continuous systems

We have seen in the previous section that discrete breathers exist in lattices provided rather moderate conditions are met. As a consequence, they occur widely in a large range of models, which we shall discuss further in Section 1.2.1. The term "breather" was first applied to refer to a soliton solution of the continuum sine-Gordon PDE,

$$u_{tt} = u_{xx} - \sin u, \tag{1.9}$$

which admits a time-periodic solution that is localised in space. This breather solution (so-called because it resembles a "breathing" pulse) has the explicit form (Ablowitz *et al.* [3])

$$u(x,t) = 4\arctan\left[\frac{\gamma \sin\left(\frac{t}{\sqrt{1+\gamma^2}}\right)}{\cosh\left(\frac{\gamma(x-x_0)}{\sqrt{1+\gamma^2}}\right)}\right]. \tag{1.10}$$

It is easily seen that $u(x, t)$ is periodic in time with frequency $w_b = 1/\sqrt{1 + \gamma^2}$, and exponentially localised in space around the point x_0. The fundamental frequency of the breather satisfies $w_b < 1$. Linearising (1.9) (replacing $\sin u$ by u for small values of u), we find that the dispersion relation for the sine-Gordon equation (1.9) is $\omega(k) = \sqrt{1 + k^2}$. Plane wave solutions of (1.9) therefore have a frequency that is always greater than unity, and hence the fundamental frequency of the breather ω_b lies outside (below) the linear spectrum. However, whatever the size of γ, sufficiently high harmonics of the fundamental frequency lie within the linear spectrum (which is not bounded above). One might expect, therefore, that odd harmonics of ω_b would couple with linear waves and decay. However, as explained by Campbell *et al.* [30], these couplings all vanish, and in fact the sine-Gordon breather soliton remains stable.

Indeed, the sine-Gordon equation is exceptional in this respect. It is one of the few PDEs known to support continuum breathers. Many other nonlinear wave equations have been shown not to support breather solutions, see Kichenassamy [74] for instance. Notably, the nonexistence of breather solutions of the ϕ^4 equation, $\phi_{tt} = \phi_{xx} - \phi + \phi^3$, was eventually established by Segur and Kruskal [115].

In closing, we mention the trivial point that discrete breathers in lattices are named thus because of their similarity to continuum breather soliton solutions of PDEs. They are both time-periodic excitations that are localised in space.

1.2 Rigorous results for discrete breathers

In Section 1.1.2, we mentioned the pioneering work of Ovchinnikov [94], Kosevich & Kovalev [80], and Sievers & Takeno [117]. These early advances generated intense interest in discrete breathers, resulting in a vast body of work offering analytic approximations for discrete breather solutions (using a variety of methods), heuristic arguments regarding existence, numerical analysis establishing results on stability, and a range of other topics. Of these, we will not go

into any specific paper in fine detail, but in Section 1.7, we give a broad discussion of some of the methods (and recent improvements thereupon) employed to investigate discrete breathers in various lattice models. Firstly, we review some of the early rigorous work on the abstract properties of discrete breathers. A more exhaustive account is given by Flach & Willis (and Olbrich) [51, 52, 55].

1.2.1   Existence of discrete breathers

It was not until 1994 that a rigorous proof for the existence of discrete breathers was established by Mackay & Aubry [84]. They prove the existence of discrete breathers in Hamiltonian lattices with anharmonic on-site potential and weak coupling, that is, of the Klein-Gordon (KG) type. The Hamiltonian for the Klein-Gordon lattice has the form

$$H = \sum_{n=-\infty}^{+\infty} \tfrac{1}{2}\dot{q}_n^2 + \tfrac{1}{2}\alpha(q_{n+1} - q_n)^2 + V(q_n), \qquad (1.11)$$

where α denotes the interparticle coupling strength, and V is a nonlinear on-site potential. The equation of motion for the nth particle of the Klein-Gordon lattice is

$$\ddot{q}_n = \alpha(q_{n+1} - 2q_n + q_{n-1}) - V'(q_n), \qquad (1.12)$$

where unlike (1.4), we have not specified the exact form of the potential $V(q_n)$.

Their existence proof is based on the principle of the anti-continuum limit, first introduced by Aubry & Abramovici [7] in the study of variational problems. Specifically, one considers the limit in which there is zero coupling in the lattice. Since the parameter α denotes the strength of coupling in the lattice, this limit, called the *anti-continuum limit*, corresponds to $\alpha = 0$. Thus the lattice is reduced to an array of uncoupled oscillators, each governed by

$$\ddot{q}_n = -V'(q_n). \qquad (1.13)$$

At this limit, it is a straightforward matter to find time-periodic spatially localised solutions. For instance, one may take the trivial breather for which only one oscillator is excited, while all others remain at rest.

It is then shown that this trivial breather at $\alpha = 0$ can be continued to small nonzero values of the coupling parameter α to obtain a breather solution of (1.12). This is done in two stages. Firstly it is shown that the trivial breather at the anti-continuum limit has a unique continuation which is a periodic solution of the Klein-Gordon equation (1.12) for small α. This continuation has the same period as the trivial breather. The proof of this requires that relatively weak conditions are satisfied, namely, that $V \in C^2$ (that is, twice continuously differentiable), and that a nonresonance and anharmonicity condition are also satisfied. These may be thought of as formalisations of the intuitive concepts introduced in Section 1.1.2. It is then shown that this continuation decays exponentially in space, and so is the required breather solution of (1.12).

These breather solutions correspond to trivial breather solutions at the anti-continuum limit for which only one particle oscillates. They are thus named "1-site breathers." The existence of "multi-site breathers" (breathers which correspond to anti-continuum solutions for which more than one oscillator is excited) is also established. The proof proceeds in much the same way as before, though several additional technical conditions must also be met.

In fact, one of the remarkable aspects of Mackay & Aubry's work [84] is that immensely useful results can be deduced for much more general networks of oscillators, assuming only minimal additional constraints. For example, Mackay and Aubry outline what further criteria need to be satisfied in order to infer breather existence in networks of nonidentical oscillators at each site, or for which the potential is different at each site. Or, the oscillators could have more than one degree of freedom. The proof can also be extended to establish breather existence in finite networks, or networks with longer-range interactions. Of direct interest to us, breather existence is also established in lattices of any dimension, thus confirming an earlier conjecture of Flach *et al.* [54]. We will have much more to say on higher-dimensional breathers in Chapter 3.

1.2.2 Stability of discrete breathers

Mackay and Aubry [84] establish rigorously that discrete breathers exist in a broad range of networks. An important issue is whether these excitations are stable. A useful general discussion of notions of stability for nonlinear systems can be found in Chapter 2.5 of Scott, [114]. Though Mackay and Aubry do not give a proof, they argue that discrete breathers are linearly stable for α small. Furthermore, they conjecture that breathers are exponentially stable (also referred to as *Nekhoroshev-stable*) by which it is meant that an orbit which starts within a distance of ε of a breather orbit in phase space must stay within $\mathcal{O}(\varepsilon)$ of the breather until at least time $t = C \exp(-K/\varepsilon^{\beta})$, for some C, K and $\beta > 0$.

This was confirmed by Bambusi [11], who proved the exponential stability of breathers. In doing so, Bambusi also gave a different and (slightly simpler) proof of existence of breathers, and additionally provided new details on the their shape (namely, a sharper result on the form of their exponential decay).

1.2.3 Discrete breathers and Anderson modes

It is worth asking whether there is any connection between the two types of localised oscillations that we have discussed so far, namely discrete breathers and Anderson modes. It was thought previously by some that no such link existed. For instance, Scott (Chapter 5.3, [114]) comments that Anderson localisation is completely different from anharmonic localisation. He arrives at this conclusion upon consideration of numerical work carried out by Feddersen [44] on the localisation of vibrational energy in globular proteins. Feddersen's numerics show that Anderson modes delocalise rapidly as anharmonicity is introduced. This is in contrast to anharmonic localised modes, which become strongly localised as anharmonicity is increased.

Scott's assessment is challenged by Archilla *et al.* [6], who consider a model which interpolates between a weakly anharmonic lattice and a disordered harmonic lattice. Using this model, they show numerically that discrete breather

solutions can be continued virtually continuously to Anderson modes.

1.3 Mobility of discrete breathers

Thus far, our discussion has focused on stationary breathers, that is, breathers in which oscillators vibrate but whose envelope as a whole does not move. A natural question to ask is whether breathers can be mobile, that is, whether the envelope can travel laterally through the lattice as the oscillators vibrate. Before we proceed to answer this, it is worth questioning whether such a notion is even meaningful for discrete breathers. After all, if the centre of a breather moves, then the wavepacket as a whole is translated several sites along the lattice, and so the motion is certainly not time-periodic, contravening one of the defining characteristics of a breather.

This problem can be overcome by formulating the notion of a travelling breather more precisely (see Mackay & Sepulchre [85]). Travelling breathers can be thought of as spatially localised solutions with two dynamical degrees of freedom. One of these dictates the spatial location of the breather centre, and the other is a vibrational degree of freedom which evolves periodically in time. A functional form for describing these structures could be written as $q_n(t) = q(t, n - ct, n)$, where the latter is time-periodic with respect to the first variable (that is, $q(t+T, \cdot, \cdot) = q(t, \cdot, \cdot)$), and spatially localised with respect to the second variable (for example, $|q(\cdot, n, \cdot)|$ could be exponentially localised in the space variable n). Other formulations are also possible, see Aubry & Cretegny [8], and Flach & Kladko [50]. Hence the notion of a moving breather can be well-defined mathematically, though of course, this does not tell us anything about the possibility of existence of such an entity.

1.3.1 Early work on moving discrete breathers

One might suspect that exact moving breather solutions do exist, for at least two reasons. Firstly, it is known that, for instance, the continuum breather solu-

tions (1.10) of the sine-Gordon PDE can be mobile. This follows from the invariance of (1.9) under the Lorentz transformation (see Chapter 6.6 of Remoissenet [103] for more details). One might expect this property to carry across to discrete breathers as well. Indeed, a large number of the early papers on the subject report the observation of moving breathers in one-dimensional Fermi-Pasta-Ulam (FPU) lattices, obtained through numerical simulations (Takeno & Hori [64, 65, 125] are a few such examples). The equation of motion for the nth particle of the FPU lattice is

$$\ddot{q}_n = V'(q_{n+1} - q_n) - V'(q_n - q_{n-1}), \tag{1.14}$$

where the interaction potential $V(\phi) = \frac{1}{2}\phi^2 + \frac{1}{2}\alpha\phi^2 + \frac{1}{2}\beta\phi^4$. When the constant $\alpha = 0$ ($\beta = 0$), then the lattice governed by (1.14) is known as the β-FPU (α-FPU) lattice. We derive the equations of motion for the FPU lattice and discuss its properties more fully in Section 2.1.

Considering other early numerical works on breather mobility, a somewhat complicated (and sometimes confusing) picture emerges. For example, Sandusky *et al.* [110] provide further insights into the possibility of moving breathers. They suggest an explanation for breather mobility, relating known unstable breather modes to observed moving breather-like excitations in a β-FPU lattice. They consider the stability of *odd-parity* and *even-parity* breathers. The odd-parity mode, (often referred to as the ST mode) is of the type proposed by Sievers and Takeno [117], and has a displacement pattern $A(\ldots, 0, -\frac{1}{2}, 1, -\frac{1}{2}, 0, \ldots)$. In other words, it is centred on a lattice site. The even parity mode (P mode) proposed by Page [96] has a displacement pattern $A(\ldots, 0, -1, 1, 0, \ldots)$, and is centred between lattice sites. It is shown that the odd-parity breather is unstable against small perturbations of the amplitude and phase, whereas the even-parity breather is stable. However, the instability does not destroy the odd-parity breather, rather, it causes it to move.

Claude *et al.* [33] consider the stability properties of localised modes in both a Fermi-Pasta-Ulam lattice with cubic and quartic nonlinearity, and also a Klein-Gordon lattice with a cubic on-site potential. They show that the FPU lattice

supports moving localised modes, even of large amplitude (or equivalently, strongly localised). However, they report that the Klein-Gordon lattice cannot support localised modes whose amplitude is greater than a certain threshold value. If the amplitude exceeds this value, the localised mode radiates energy and eventually becomes pinned to a lattice site. Bang & Peyrard [12] also report the existence of a critical amplitude for the Klein-Gordon lattice, above which moving breathers cannot exist.

These properties do not necessarily carry across to two-dimensional lattices. Mobility properties for two-dimensional Klein-Gordon lattices are much the same as for one-dimensional models (Tamga *et al.* [128]). Namely, provided that the amplitude of breathers is small (or equivalently, they are weakly localised), they can be mobile in two-dimensions. However, unlike the one-dimensional FPU lattice, Burlakov *et al.* [22] report that the two-dimensional FPU lattice does not support moving breathers of large amplitude.

Hence the overall picture obtained from these early works on breather mobility is somewhat complicated. Both one- and two-dimensional Klein-Gordon lattices support moving breathers provided the amplitude is small. One-dimensional FPU lattices support large-amplitude moving breathers, while two-dimensional FPU lattices do not. Overall, these observations seem to suggest that at the very least, small-amplitude breathers *can* move within lattices. Although these objects resemble breather modes, they have not been proven to be exact breather solutions of the lattice equations. To the best of our knowledge, we are not aware of any rigorous existence proofs for exact moving breather solutions in nonintegrable lattices (exact moving breather solutions do exist in the Ablowitz-Ladik lattice [2], which is integrable).

1.3.2 Travelling kinks and the Peierls-Nabarro barrier

It has been speculated for some time that a concept similar to that of a Peierls-Nabarro (PN) barrier for moving lattice kinks might also be useful for discrete breathers. Unlike a pulse, a kink represents a monotonic change of

amplitude by a certain height as n crosses from $-\infty$ to $+\infty$ in the lattice (see Chapter 6, Remoissenet [103]). As kinks move through a lattice, they experience a potential barrier between one lattice site and the next. More precisely, a PN potential characterises the dependence of the energy E of a kink on its position in a lattice. Since the lattice is a periodic structure, the PN potential is a periodic function of the same period as the lattice. Minima of the PN potential correspond to stable positions, while maxima correspond to unstable positions. The PN barrier height ΔE is equal to the difference between the maximum and minimum energies.

For instance, the sine-Gordon lattice is known to support two stationary kink solutions, one of which is centred at a lattice site, and another which is centred between lattice sites. The first of these has higher energy, and is unstable to collapse into the lower energy solution. In order to propagate along the chain, the kink must be activated with energy exceeding ΔE. In other words, a stable kink may be "depinned" and set in motion if activated with this quantity of energy. Further details may be found in Chapter 5.2 of Scott [114].

At this point, we recall the work of Sandusky *et al.* [110], who connected the ability of certain breathers to be mobile to their instability (see Section 1.3.1). It is tempting to conclude that the unstable ST and stable P breather modes behave in a similar manner to the two unstable and stable static kink solutions of the sine-Gordon lattice. Specifically, one might conjecture that moving discrete breathers also experience an effective PN potential, where the depinning or barrier energy is equal to the difference between the energies of the ST and P modes. In fact, some authors have reported such a phenomenon, even going as far as calculating the depinning energy (see for example, Claude *et al.* [33], and Kivshar & Campbell [76]).

However, further work on the matter conducted since seems to suggest that no simple concept of Peierls-Nabarro potentials can be found for discrete breathers. More details can be found in the paper by Flach & Willis [53]. Similar conclusions on the difficulty of PN potential concepts for breathers are made

by Bang & Peyrard [12]. A more recent discussion is given by Flach & Willis in Section 9 of [52].

1.4   Discrete breathers and bifurcations of plane waves

We now address another active area of research regarding discrete breathers. Namely, we consider whether discrete breather solutions are connected to plane wave solutions of the linearised equations of motion. More generally, the concept of *modulational* or *Benjamin-Feir instability* has been used to establish a connection between solutions of nonlinear systems and (unstable) plane wave solutions of the corresponding linearised system. For instance, Remoissenet [103] shows that the nonlinear Schrödinger (NLS) equation admits a plane wave solution that is unstable against small perturbations of the amplitude and phase. The plane wave breaks into a train of pulses as time evolves. It is possible to show that these pulses are related to bright soliton solutions of the nonlinear equation. We will come across the nonlinear Schrödinger equation often throughout this thesis. A more complete account of modulational instability in nonlinear systems can be found in Chapter 4.6 of Remoissenet [103].

A similar idea can also be applied to localised modes in lattices. In fact, for many systems, it is observed that in the limit of small amplitude, breathers typically widen and increasingly resemble solutions of the linearised equations. In the following, we adopt the approach of Flach [49].

A simple argument indicates that, in looking for a relationship between discrete breathers and plane wave solutions, we expect the connection to occur for band edge plane waves (that is, those with frequencies at an edge of the phonon spectrum; for example, in (1.6), these correspond to $k = 0$ and $k = \pi$). In the limit of small amplitude, discrete breather solutions of the nonlinear equations must approach the solutions of the linear equations. However, for breathers to exist, resonances with the linear spectrum must be avoided (see Section 1.1.2). In other words, the breather frequency w_b (and its integer multiples) cannot co-

incide with any phonon frequency, say ω_q. The only way in which both these requirements can be satisfied is if the breather frequency ω_b tends to an edge ω_e of the phonon spectrum as the amplitude tends to zero.

In the light of these comments, one might suspect that discrete breathers appear through a bifurcation of band edge plane waves. There is certainly evidence which suggests this might be true (see Flach [49], and Sandusky & Page [109]). Furthermore, this has actually been proved for certain one-dimensional Fermi-Pasta-Ulam lattices by James [69]. However, this conjecture has not been proven in general. Lastly, we mention that assuming this conjecture to be true, Flach [49] calculates the critical energy E_c at which this bifurcation occurs. This calculation has important consequences for higher-dimensional systems, as we shall see in Chapter 3.

1.5 Applications: energy localisation and transfer

Discrete breathers are spatially localised excitations. It is widely thought that discrete breathers could act as coherent agents of energy storage and transport in many physical settings, on account of their ability to localise vibrational energy. Many physical phenomena involve the localisation and transport of energy in space. A wealth of examples can be found in a range of physical settings, including the study of DNA denaturation [36, 37, 97], hydrocarbon structures [78], photonic crystal waveguides [92], photosynthesis [66], and the storage and transport of energy in proteins [13].

For example, Hu *et al.* [66] study a photosynthetic unit consisting of an arrangement of chlorophyll molecules. The antenna-like component of this unit captures light photons (sometimes known as "light-harvesting"). Energy self-focusing then takes place and light is transferred in the form of an exciton in a complex process involving pigment proteins. The energy is released upon reaching a photosynthetic unit.

To take another example, experimental results suggest that the continuum

model of the DNA molecule is inadequate (see Zhou & Zhang [142] for a recent review). Peyrard and Bishop [97] propose a discrete model of DNA in which nucleotides of the double helix are represented by point masses. The coupling along each strand is assumed to be harmonic, and the stretched bonds connecting the two strands are assumed to be nonlinear. Dauxois *et al.* [36, 37] consider the phenomenon of DNA transcription in a slightly more complicated model than the one in [97]. The dynamics of DNA transcription is known to involve *local* denaturation of the DNA double helix. This local denaturation then exposes the coding bases to chemical reagents, and it is thought that this may be a preliminary step towards understanding DNA transcription. Local denaturation may be a precursor to *global* denaturation, namely the process through which the two complementary strands of the molecule are separated completely. Dauxois *et al.* show that a mechanism involving an energy localisation may initiate DNA denaturation, and so once more we see the importance of energy localisation.

Tsironis [130] proposes several ways in which discrete breathers could be of specific relevance to biomolecules. In another recent work, Kopidakis *et al.* [79] outline a general mechanism for highly targeted energy transfer which uses discrete breathers as the transfer agents. A specific amount of energy is injected as a discrete breather at a donor system, and then transferred as a discrete breather to a weakly coupled acceptor system. Such a mechanism could be relevant for energy transfer in bioenergetics.

1.6 Experimental observation of discrete breathers

Recently, there have been numerous experimental observations of discrete breathers in physical systems. We do not describe the technical details of the experiments here, though we do mention some of the more prominent sightings. Swanson [121] report the observation discrete of breathers in crystals of the highly discrete and strongly nonlinear halide bridged mixed valence tran-

sition metal complex $\{[Pt(en)_2][Pt(en)_2Cl_2](ClO_4)_4\}$ (hereupon denoted PtCl for brevity), where "en" denotes ethylenediamine. By measuring resonance Raman spectra, localised vibrational states are identified by the redshifts they impose upon the resonances.

Discrete breathers have also been detected in coupled optical waveguides (Eisenberg *et al.* [43]), antiferromagnetic materials (Schwarz *et al.* [113]), Josephson junction arrays (Binder & Ustinov [18]) and molecular crystals (Edler & Hamm [41]). Campbell *et al.* [30] give a highly readable account of several of these experiments, describing some of the difficulties encountered in designing suitable detection methods, as well as how these have been circumvented.

Very recently, Sato & Sievers [111] have reported the sighting of a breather in a quasi-one-dimensional antiferromagnetic solid. The advanced detection capability of their method permits the properties of the individual breathers to be analysed. Campbell [29] gives a simplified account of their experiment and also some of its implications.

1.7   Analytic methods

In Sections 1.1–1.5, we have documented various abstract properties of discrete breathers in lattices, such as their existence or nonexistence, their spatial decay, their mobility and their connection to band edge plane waves *etc.* Thus far, we have said very little about the explicit form of breather solutions. This is no accident, rather, it is because closed analytic forms for breather solutions are unknown or difficult to obtain. Consequently little is known about them. There are some notable exceptions, for example, the (integrable) Ablowitz-Ladik lattice [2]. Ovchinnikov & Flach [95] also present Hamiltonian lattices (if perhaps slightly artificial models) for which two- and three-dimensional discrete breather solutions can be found explicitly.

However, there is a vast body of literature concerned with finding approximations to exact breather solutions. Nowadays, there are a number of sophisti-

cated methods at our disposal for determining approximate solutions. In comparison, some of the methods used in the earlier works may appear a little unrefined at times. Nevertheless, these papers document important progress made in the study of discrete breathers, and their impact upon much of the later rigorous work is plainly evident. In this section, we will not recount the individual results of all of these papers, since this would prove unnecessarily lengthy. However, we will describe some of the most commonly employed methods in determining approximations to breather solutions.

1.7.1   The rotating-wave approximation

The rotating-wave approximation (RWA) (see Chapter 5.1 of Scott [114]) is used frequently in papers that appeared in the late eighties and early nineties, for instance, see [122, 123, 126, 127, 132]. Since breather solutions are time-periodic, they can be expressed as a Fourier series,

$$q_n(t) = \sum_{k=-\infty}^{k=+\infty} A_{nk} \mathrm{e}^{\mathrm{i}\omega t}, \tag{1.15}$$

where A_{nk} are coefficients to be determined, and $\omega = 2\pi/T$, T being the period of the motion. The ansatz (1.15) is substituted into the lattice equations, and one equates coefficients of terms with the same frequency $k\omega$, $k = 0, \pm 1, \pm 2, \ldots$ in the resulting equation. In the simplest approximation, only terms which are resonant with the fundamental frequency $\mathrm{e}^{\mathrm{i}\omega t}$ are retained, and terms with $|k| \geq 2$ (namely, $\mathrm{e}^{2\mathrm{i}\omega t}, \mathrm{e}^{3\mathrm{i}\omega t}, \mathrm{e}^{4\mathrm{i}\omega t}, \ldots$) are neglected. The equations which are retained give a set of nonlinear difference equations for the coefficients A_{nk}.

For many lattices, the resulting system of difference equations is still difficult to solve, and so often further approximations are required to reduce the equations to a simplified set. This can then be dealt with using Green's lattice function method (see Bickham *et al.* [17]), or a numerical scheme (see Takeno [123]).

The RWA has been applied with considerable success to discrete breathers, and yields better results when extended to include second harmonic terms (see

Franchini *et al.* [59]). However, in reducing the set of difference equations to a more manageable set, approximations of the form $\phi_{n+1}^2 + \phi_{n-1}^2 + \phi_{n+1}\phi_{n-1} \approx 3\phi_n^2$ and $(\phi_{n+1} + \phi_{n-1})\phi_n \approx 2\phi_n^2$ are often employed. This makes it hard to quantify the accuracy of the procedure, unlike other asymptotic methods (see Section 1.7.3), which retain information on the size of error terms, and can also be corrected by the calculation of higher-order terms. In fact, several authors point to the limitations of some of the early results derived by applying the RWA, citing its reliance on too many such approximations (see Bickham *et al.* [17]).

1.7.2   Continuum approximations

Another approach to solving equations for a lattice is through the method of *continuum approximation* (see Chapter 2.4 of Remoissenet [103]). In this approach (illustrated using a simple example below), the equations defined on a discrete lattice are replaced by some partial differential equation. The advantages of this are obvious, after all, PDEs are more easily amenable to analysis. Of course, such a procedure is only useful (and moreover, permissable) if the replacement PDE accurately captures the dynamics of the original lattice equations. As one would expect, some information *is* lost in replacing a fully discrete system with an approximate continuous one. Nevertheless, there are increasingly sophisticated ways of performing this which reflect phenomena associated with the discrete lattice with increasing accuracy.

We illustrate some of these methods using the FPU lattice (discussed in Section 1.3.1, see equation (1.14)) as an example. As we shall see in Section 2.2.1 (see equation (2.5)), the equation governing the difference in displacement between adjacent particles $\phi_n = q_{n+1} - q_n$ in the FPU lattice is

$$\ddot{\phi}_n(t) = V'(\phi_{n+1}) - 2V'(\phi_n) + V'(\phi_{n-1}), \tag{1.16}$$

where for example, $V'(\phi) = \phi + \alpha\phi^2 + \beta\phi^3$. In the simplest continuum approximation, also known as the standard continuum approximation, one assumes that the discrete index n can be replaced by a continuous variable x. In other

words,

$$\phi_n(t) \to \phi(x, t). \tag{1.17}$$

This approximation is a reasonable one for excitations consisting of a slowly varying envelope modulating a carrier wave. Terms of the form $\phi_{n\pm1}$ in (1.16) are replaced by derivatives by applying Taylor's theorem and expanding,

$$\phi_{n\pm1}(t) = \phi(x \pm 1, t) = \phi \pm \frac{\partial \phi}{\partial x} \pm \frac{1}{2}\frac{\partial^2 \phi}{\partial x^2} \pm \frac{1}{6}\frac{\partial^3 \phi}{\partial x^3} \pm \frac{1}{24}\frac{\partial^4 \phi}{\partial x^4} \pm \ldots. \tag{1.18}$$

Substituting for $\phi_{n\pm1}$ in (1.16) using the expansion (1.18), and retaining terms to the desired degree of accuracy, we arrive at some PDE (for example, a generalised Boussinesq equation, for which solutions can then be found, see Wattis [134]). However, as pointed out by Remoissenet (Chapter 3.3, [103]), in some cases, the standard continuum approximation is not sufficiently accurate. In addition, Roseneau [104, 105] highlights more serious problems with this approximation (for instance, ill-posedness of the resulting PDE).

Collins & Rice [34, 35] introduce an improved quasi-continuum approximation, of which a simplified account is given later by Roseneau [104, 105]. We follow the account given by Wattis [134]. Let us assume that a travelling wave solution of (1.16) exists and has the form $\phi_n(t) = \phi(n - ct) \equiv \phi(z)$. Then (1.16) becomes the differential delay-advance equation

$$c^2 \phi''(z) = V'(\phi(z+1)) - 2V'(\phi(z)) + V'(\phi(z-1)), \tag{1.19}$$

which we rewrite as an operator equation. We use $\mathbf{D}$ to denote differentiation with respect to z, that is, $\mathbf{D} \equiv \partial_z$. Using the fact that

$$\phi(z \pm 1) = \phi(z) \pm \mathbf{D}\phi \pm \tfrac{1}{2}\mathbf{D}^2\phi \pm \tfrac{1}{6}\mathbf{D}^3\phi \pm \ldots = e^{\pm\mathbf{D}}\phi, \tag{1.20}$$

we find that equation (1.19) can be rewritten

$$c^2\mathbf{D}^2\phi = \left[4\sinh^2(\tfrac{1}{2}\mathbf{D})\right] V'(\phi(z)). \tag{1.21}$$

Integrating this equation twice with respect to z, and taking the constants of integration to be zero (since for localised solutions, we expect $|\phi(z)| \to 0$ as $|z| \to \infty$), we have

$$c^2\phi = \Lambda(\mathbf{D})V'(\phi), \quad \text{where} \quad \Lambda(\mathbf{D}) = \frac{4\sinh^2(\tfrac{1}{2}\mathbf{D})}{\mathbf{D}^2}. \tag{1.22}$$

Approximations to the equation (1.22) can be made by treating $\mathbf{D}$ as a small parameter and expanding the operator $\Lambda(\mathbf{D})$ (this can be justified rigorously, see Wattis [134]). For instance, by taking $\Lambda(\mathbf{D}) \sim \mathbf{I} + \frac{1}{12}\mathbf{D}^2$ (where $\mathbf{I}$ is the identity operator), we recover the standard continuum approximation.

Padé approximants

Padé approximation is a technique whereby a function is approximated by the ratio of two polynomials (see Baker & Graves-Morris [10]). An (M, N) Padé approximant is the ratio of a polynomial of degree M and a polynomial of degree N. Roseneau [104, 105] suggested that this technique can be applied to the operator $\Lambda(\mathbf{D})$, replacing it by a ratio of two polynomials in the operator $\mathbf{D}$. For instance, the $(0, 2)$ Padé approximant is $\Lambda(\mathbf{D}) \sim [\mathbf{I} - \frac{1}{12}\mathbf{D}^2]^{-1}$.

Larger values of M and N result in better approximations to the operator $\Lambda(\mathbf{D})$. However, the resulting continuum approximations become increasingly complicated and thus harder to solve. Wattis [136] shows how this method can be applied to obtain highly accurate approximations to discrete breather solutions in a generalised Klein-Gordon lattice. We will come across Padé approximations again when we consider kink solutions in the FPU chain (see Section 2.4).

Kevrekidis *et al.* [72] assess some of the successes and failures of the method of Padé continuum approximations. For instance, properties such as the dispersion relation for the system, the wave profile and velocity are retained by the continuum models. However, features such as Peierls-Nabarro barriers are not captured.

1.7.3   The semi-discrete multiple-scale method

Another highly productive method for finding approximations to breather solutions is given by Remoissenet [102]. Here, we refer to it as the *semi-discrete multiple-scale* method, and it is valid in the limit of small amplitude when there

is slow variation in time and space. As we explain shortly, in this method, one introduces a small parameter ε, which represents the amplitude of the breather solutions that we seek. We elaborate upon this, since no small parameter ε occurs in the lattice equations that we have presented so far (see for example, the Klein-Gordon lattice, (1.12), or the FPU lattice, (1.14)).

Following Infeld & Rowlands [68], we comment that in general, when presented with a system of nonlinear physical equations, one can set about finding all manner of complex and exotic solutions. By introducing a small parameter, we confine our attention to a restricted class of solutions, for example, those of small amplitude. We assume an expansion for the solution in the amplitude ε. The solution can be found to a higher degree of accuracy by determining more coefficients of ε^n in the expansion. An in-depth survey of small-amplitude formalism applied to nonlinear equations can be found in Chapters 5 and 8 of Infeld and Rowlands [68], and also in Krylov & Bogoliubov [81].

Returning to the semi-discrete multiple-scale method, similarly, there are many types of discrete breather solutions that we could seek (Flach & Willis [52] describe some of the more exotic strains), but we will restrict our attention to breathers of small amplitude. Hence, we shall assume a perturbation expansion for the solution in the amplitude, which we denote ε. In addition, we will assume that the breather envelope varies very slowly in space compared to the rapid carrier wave. Consequently, we apply the method of multiple scales (see Bush [23], Chapter 4), and introduce a hierarchy of new slow variables defined by $X = \varepsilon n$, $\tau = \varepsilon t$ and $T = \varepsilon^2 t$. We consider the displacement $q_n(t)$ to be a function of the independent variables n, t, X, τ and T, so that $q_n(t) = q(n, t, X, \tau, T)$. We thus assume a small amplitude expansion for $q_n(t)$ of the form

$$
\begin{aligned}
q_n(t) = {}& \varepsilon e^{i\psi} F + \varepsilon^2 (G_0 + e^{i\psi} G_1 + e^{2i\psi} G_2) \\
& + \varepsilon^3 (H_0 + e^{i\psi} H_1 + e^{2i\psi} H_2 + e^{3i\psi} H_3) + \cdots + \text{c.c.},
\end{aligned}
\tag{1.23}
$$

where $\psi = pn + \omega t$, the variables F, G_i, H_i, …, are all functions of X, τ and T, and c.c. denotes the complex conjugate. Notice that in the ansatz (1.23), the

oscillations of the carrier wave are treated exactly. This ansatz is then substituted into the lattice equations, and we then equate coefficients of each power of ε at each frequency (that is, at each power of $e^{i\psi}$). This results in a system of equations for the unknown quantities F, G_i, H_i, ..., where F gives the form of the breather envelope at leading order, and G_i, H_i, ..., are higher order correction terms. Unlike other approaches such as the RWA (see Section 1.7.1), this asymptotic approach gives more precise information on the size of the error in the approximate solution. The error can be reduced by determining more of the unknown terms in the expansion (1.23).

We use this method extensively throughout this thesis. As with all approximate methods for breathers, it is vital to know whether approximations generated by it are close to exact breather solutions of the lattice (the notion of "closeness" can be made precise). This is an active area of research, and we note that rigorous results have been established recently. We discuss these in Section 2.5.

1.8 Overview of thesis

In this chapter, we have discussed the existence and properties of discrete breathers. We have also summarised some of the most important work to have been carried out in the field to date. There are still many open questions regarding discrete breathers and their properties. For example, as we have described, breather mobility is just one of many active areas of research within the subject.

As well as abstract properties, we have reviewed several methods used commonly to obtain approximations to breather solutions. These have been employed extensively to yield a great deal of useful information about breathers and their properties in a broad range of lattice models. In addition, they provide direct and tangible information on breather profiles. Often, analytic work has inspired or guided rigorous work, as well as confirming results obtained therein.

In this thesis, we use asymptotic methods (the semi-discrete multiple-scale method) to determine breather existence and properties in lattices of the Fermi-Pasta-Ulam type. We consider both one- and two-dimensional lattices, with several different geometries in the latter case.

We begin by considering a one-dimensional FPU chain in Chapter 2. Using the semi-discrete multiple-scale method, we determine the conditions for which the FPU chain supports moving breather solutions, thereby generalising known conditions for the existence of stationary breathers. We also give leading-order analytic approximations to these solutions. Numerical simulation of the lattice verifies the breather properties determined by the asymptotic analysis. By considering small wavenumbers, we show that the quartic FPU lattice (with no cubic term in the potential energy function) supports waveforms that are combinations of a breather and a kink. We show that the amplitude of these "breathing-kinks" can be arbitrarily small, as opposed to traditional monotone travelling-wave kinks, which have a nonzero minimum amplitude in such systems. Numerical simulations confirm the long-lived nature of the combined modes.

In Chapter 3, we investigate discrete breathers in a two-dimensional square FPU lattice. A third-order multiple scales analysis in the semi-discrete limit is shown to be inadequate, since at this order, the lattice equations reduce to the (2+1)-dimensional cubic nonlinear Schrödinger equation, which does not support stable soliton solutions for the breather envelope. We therefore extend the analysis to higher order and find a generalised $(2 + 1)$-dimensional NLS equation which incorporates higher order dispersive and nonlinear terms as perturbations. We find an ellipticity criterion for the wavenumbers of the carrier wave. Numerical simulations suggest that both stationary and moving breathers are supported by the system. Calculations of the energy show the expected threshold behaviour whereby the energy of breathers does *not* go to zero with the amplitude. In other words, the energy of any breather solution must exceed an excitation threshold. We find that the energy threshold is maximised by stationary breathers, and becomes arbitrarily small as the boundary of the

domain of ellipticity is approached.

In Chapter 4, we consider a two-dimensional FPU lattice with hexagonal symmetry. We aim to determine whether the different rotational symmetry properties of this lattice model affect the properties of discrete breathers found therein. The results obtained are similar to those obtained for the square FPU lattice, though we find that the square and hexagonal lattices exhibit quite different properties in regard to the generation of higher harmonics. The hexagonal lattice equations are reduced to a cubic nonlinear Schrödinger equation at third order. As before, we carry out a higher order analysis, and find a slightly simpler generalised NLS which includes known stabilising terms. We present numerical results which suggest that long-lived stationary and moving breathers are supported by the lattice. We also find asymptotic estimates for the breather energy, and determine a minimum threshold energy below which breathers cannot be found. This energy threshold is again maximised for stationary breathers, and becomes vanishingly small near the boundary of the elliptic domain.

We conclude in Chapter 5 with a brief discussion of the work carried out in this thesis. We also propose several problems and related lattice models which could prove interesting for further study.

Chapter 2

A one-dimensional
Fermi-Pasta-Ulam chain

In this chapter, we consider discrete breathers in a Fermi-Pasta-Ulam (FPU) chain. We have already come across this model in Sections 1.3.1 and 1.7.2. Firstly, we explain the origin of this much studied model, and derive the governing equations. Before discussing discrete breathers in this system, we mention that the FPU lattice has a rich history in itself, which we now review briefly.

2.1   Introduction

The numerical experiments carried out by Fermi, Pasta and Ulam [45] in 1940 are well documented. They were studying the transfer of heat energy in a solid modelled by a one-dimensional chain composed of particles of equal mass connected by identical nonlinear springs. Figure 2.1 (a) shows the arrangement in its equilibrium state, and Figure 2.1 (b) depicts a non-equilibrium state. Selecting any fixed particle to be the zeroth particle in the array, all of the particles can then be labelled with an integer $n \in \mathbb{Z}$. We will suppose that the central particle in Figure 2.1 (a) is the nth particle, and that the adjoining spring on the right-hand side is the nth spring.

The equation of motion governing the nth particle is obtained by a straight-
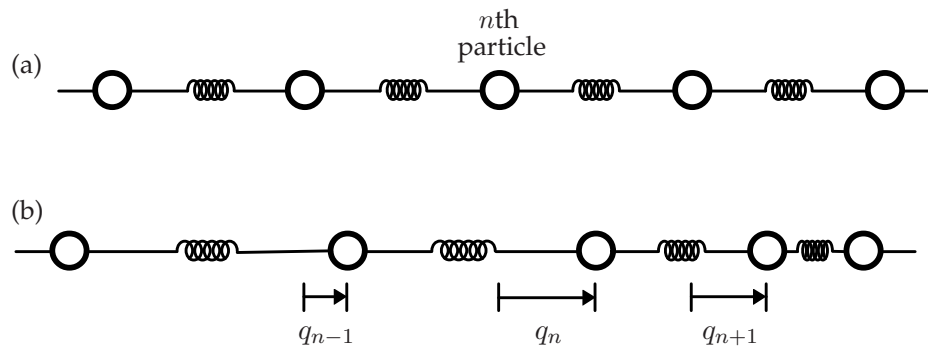
Figure 2.1: A one-dimensional spring-mass system.

forward application of Newton's second law. Letting q_n denote the displacement of the nth particle from its equilibrium position (see Figure 2.1 (b)), the extension in the nth spring is $q_{n+1} - q_n$. Similarly, the extension in the $(n-1)$th spring (to the left of the nth particle) is $q_n - q_{n-1}$. Letting $V(\phi)$ denote the elastic potential energy of each spring as a function of its extension ϕ, the force exerted by each spring is $-V'(\phi)$. Applying Newton's second law to the nth particle, and assuming the particles to be of unit mass, we have

$$\ddot{q}_n(t) = V'(q_{n+1} - q_n) - V'(q_n - q_{n-1}). \tag{2.1}$$

Equation (2.1) is the FPU equation. It can also be derived directly from the Hamiltonian H (which is equal to the total mechanical energy of the system) given by

$$H = \sum_{n=-\infty}^{+\infty} \tfrac{1}{2}p_n^2 + V(q_{n+1} - q_n), \tag{2.2}$$

where the first term in the summand gives the kinetic energy of the nth particle, and the second term is the elastic potential energy of the nth (right-hand) spring. Formally, p_n and q_n are canonically conjugate momenta and displacement variables of the system (see for instance, Chapter 12, Kibble & Berkshire [73]), satisfying

$$\frac{\mathrm{d}q_n}{\mathrm{d}t} = p_n \quad \text{and} \quad \frac{\mathrm{d}p_n}{\mathrm{d}t} = V'(q_{n+1} - q_n) - V'(q_n - q_{n-1}). \tag{2.3}$$

2.1.1 Some historical remarks

We return to the work of Fermi, Pasta and Ulam [45] into heat conduction modelled by the above spring-mass system. They had expected that upon exciting a normal mode, the nonlinear interactions would cause the energy to flow evenly into all the normal modes resulting in energy equipartition (or thermalisation). Computer simulations carried out by them failed to verify this hypothesis. The system did not approach energy equipartition, instead, the energy returned almost periodically to the originally excited mode and a few others nearby. This unexpected phenomenon is known as FPU *recurrence*, and attracted much interest at the time.

One of the most important advances was made by Zabusky and Kruskal [139]. They approximated the FPU spring-mass system by the Korteweg-de Vries (KdV) equation. Results of their numerical investigation allowed them establish a link between FPU recurrence and the nondestructive collisions of soliton solutions of the KdV equation. They proposed the following explanation for the FPU recurrence phenomenon. The initial condition $u(x, 0)$ generates a family of solitons with different velocities moving in the (x, t)-plane. Since the lattice is of finite length, the solitons cannot move indefinitely far apart (reflection at the ends of the lattice prevents this). Thus the solitons collide, but preserve their shapes and velocities. At some later time T_R, the solitons reassemble and approximately recreate the initial condition $u(x, 0)$. The first time at which this occurs is the recurrence time. Whilst this shows a connection between recurrence and solitons in the integrable KdV equation, it is known that the FPU system is not integrable. Even though the FPU chain supports nonlinear waves, they do not interact elastically. Hence, the explanation of recurrence in the FPU chain is not so simple.

The work of Tuck and Menzel [131] provides further insight into the phenomenon of FPU recurrence. By simulating FPU chains over many FPU recurrence times, they found a recurrence with a longer period, the so-called *superperiod*. It was found that more energy is returned to the originally excited mode

after a superperiod recurrence than after a single FPU recurrence. In a later paper, Sholl [116] derives analytic expressions for the FPU recurrence superperiod. A comprehensive historical overview of the FPU problem and suggested resolutions are given by Ford [58].

2.1.2 Discrete breathers in Fermi-Pasta-Ulam lattices

We are interested in whether discrete breathers are supported by FPU lattices. Unfortunately, the anti-continuum method, which has proved so useful in establishing existence in a broad range of other lattice models (see Section 1.2.1), is not applicable to FPU lattices. This is because, as can be seen from the governing equation (2.1), FPU lattices do not posses an uncoupled limit in which trivial breathers exist. Nevertheless, much of the early analytical and numerical work on discrete breathers applied to FPU lattices, indicating that FPU lattices do support breathers. We do not give an exhaustive list of such work but we mention, for example, the work of Bickham *et al.* [17] and Takeno *et al.* [64, 65, 117, 122–127].

For some time, the only rigorous result concerning existence in a certain class of FPU lattices was established by Flach [48], who proves the existence of breathers in FPU lattices with interaction potentials of the form $V(\phi) = \phi^{2m}$ in (2.2), where $m \geq 2$. Aubry *et al.* [9] present a variational method for establishing the existence of breathers whose frequency lies above the phonon band. Their method applies to lattices for which the interaction potential is convex. Discrete breathers are obtained as extrema (in fact, maxima) of a certain variational form. Since this variational method does not rely on the concept of an anti-continuum limit, it can be applied to FPU lattices. Aubry *et al.* apply the method to prove existence of discrete breathers in a class of FPU lattices, namely, those for which the potential V in (2.2) is a convex polynomial of degree 4.

More recently, James [69] gives a more general result, which establishes the existence (nonexistence) of small-amplitude discrete breathers with frequencies slightly above the phonon band in FPU lattices when the potential V satis-

fies (violates) a local hardening condition. Specifically, the existence of such breathers is obtained for $B > 0$, where $B = V^{(4)}(0)/2 - (V^{(3)}(0))^2$, and their nonexistence is proved for $B < 0$. Once more, V is the interaction potential in (2.2), and is chosen to satisfy $V'(0) = 0$ and $V''(0) = 1$. James's proof is based on a centre manifold technique.

Later in this chapter (see Section 2.2.4), we will show how this inequality arises. Specifically, we construct a family of approximate breather solutions parametrised by the carrier's wavenumber, which exist in parameter regions given by the inequality $B > 0$. We show that as B is increased through zero, stationary breathers are the first to exist, satisfying James's inequality exactly.

The results of James [69] are accompanied by numerical work presented later by Sánchez-Rey *et al.* [108]. In this, the range of validity of James's centre manifold technique is tested. Small amplitude breathers are computed numerically and are found to be in very good agreement with approximate leading-order analytical expressions derived by James. The interaction potential V is chosen to be a polynomial of degree 4 (of the same form that we shall consider in Section 2.2.1). The range of validity of James's proof is verified, since breathers are in fact found for $B > 0$.

2.1.3 Overview

In this chapter, we use asymptotic methods (the semi-discrete multiple-scale method) to find leading-order expressions for both stationary and moving discrete breathers in a one-dimensional Fermi-Pasta-Ulam (FPU) lattice with anharmonic potential.

In Section 2.2, the lattice equations are reduced to a nonlinear Schrödinger (NLS) equation at leading order. This equation admits two different types of soliton solution (bright or dark) for the breather envelope, depending on the coefficients of the cubic and quartic terms in the potential energy function. Our asymptotic analysis yields inequalities which illustrate how the sizes of these coefficients determine the type of solution. This leads to conditions for which

the FPU lattice supports bright breathers. Stationary breathers satisfy James's inequality $B > 0$, and for moving breathers, we find a generalised version of James's inequality.

Soliton solutions of the NLS equation are used to construct leading-order analytic forms for bright and dark breathers in the FPU chain. We present results of numerical simulations of the FPU lattice in Section 2.3. We find good agreement with the results obtained through the asymptotic analysis.

In Section 2.4, we show by considering small wavenumbers, that there also exist waveforms which are combinations of a breather and a kink. The order of magnitude of the wavenumber determines which of the two components dominates for such a waveform, and hence whether a breather or kink or a combined *breathing-kink* is exhibited ultimately. We present numerical simulations which show that these combined modes move as travelling waves over intermediate timescales. We show that traditional, monotone, kinks in the quartic FPU lattice have a nonzero minimum amplitude, and that the combined modes allow travelling waves with a kink amplitude below this minimum. Some closing comments are made in Section 2.5.

2.2 Asymptotic analysis

2.2.1 Preliminaries

In this section, we use asymptotic methods to find an approximate form for breather solutions of the one-dimensional FPU chain. Firstly, we introduce a transformation variable ϕ_n, defined as the difference between the displacements of the $(n+1)$th and nth particles, namely

$$\phi_n = q_{n+1} - q_n. \tag{2.4}$$

The FPU equation (2.1) can then be rewritten in terms of the variable ϕ_n. Equation (2.1) becomes $\ddot{q}_n = V'(\phi_n) - V'(\phi_{n-1})$, and so $\ddot{q}_{n+1} = V'(\phi_{n+1}) - V'(\phi_n)$.

Subtracting the former equation from the latter ($\ddot{\phi}_n = \ddot{q}_{n+1} - \ddot{q}_n$) gives

$$\ddot{\phi}_n = V'(\phi_{n+1}) - 2V'(\phi_n) + V'(\phi_{n-1}). \tag{2.5}$$

This is the same as equation (1.16), which we introduced in Section 1.7.2 for our discussion of continuum approximations.

Since we shall be using asymptotic methods to determine the form of small amplitude solutions, we shall only be concerned with the first few terms in the expansion of $V(\phi)$. Thus we may approximate the potential function $V(\phi)$ by a quartic polynomial

$$V(\phi) = \tfrac{1}{2}\phi^2 + \tfrac{1}{3}a\phi^3 + \tfrac{1}{4}b\phi^4, \tag{2.6}$$

where a and b are real constants. The equations of motion (2.5) therefore become

$$\ddot{\phi}_n = (\phi_{n+1} - 2\phi_n + \phi_{n-1}) + a(\phi_{n+1}^2 - 2\phi_n^2 + \phi_{n-1}^2) + b(\phi_{n+1}^3 - 2\phi_n^3 + \phi_{n-1}^3). \tag{2.7}$$

Since we seek localised solutions, we expect the energy to vanish as $n \to \pm\infty$, hence we impose the boundary conditions $q_n \to 0$ as $n \to -\infty$ and $q_n \to q_\infty$ as $n \to +\infty$ for some $q_\infty \in \mathbb{R}$. Recalling the definition of ϕ_n in terms of q_n in (2.4), we find

$$q_n = \sum_{k=-\infty}^{n-1} \phi_k, \tag{2.8}$$

hence we express the latter boundary condition as

$$q_n \to q_\infty = \sum_{n=-\infty}^{\infty} \phi_n \quad \text{as} \quad n \to \infty. \tag{2.9}$$

We shall in general consider both $q_\infty = 0$ and $q_\infty \neq 0$ so that the variable q_n describes a modulated pulse ($q_\infty = 0$) or a modulated kink ($q_\infty \neq 0$) of some description.

2.2.2 Hamiltonian formulations for Fermi-Pasta-Ulam equations

We have seen that by introducing the transformation of variables (2.4), we have derived two formulations of the FPU equation. The first of these (2.1) is expressed in terms of the displacement q_n, and is derived from the Hamiltonian

H given in (2.2). The second (2.5) is expressed in terms of the difference between neighbouring displacements, namely ϕ_n. We note that this formulation can also be derived directly from a Hamiltonian form $\widetilde{H}$ distinct from (2.2). Applying Hamilton's equations to $\widetilde{H}$ defined by

$$\widetilde{H} = \sum_n \tfrac{1}{2}(\psi_{n+1} - \psi_n)^2 + V(\phi_n), \tag{2.10}$$

gives

$$\frac{\mathrm{d}\phi_n}{\mathrm{d}t} = -(\psi_{n+1} - 2\psi_n + \psi_{n-1}) \quad \text{and} \quad \frac{\mathrm{d}\psi_n}{\mathrm{d}t} = -V'(\phi_n), \tag{2.11}$$

from which (2.5) can be recovered. In this form, we note that the nearest-neighbour coupling and nonlinearity have been separated; the coupling now appears in a harmonic term and the nonlinearity involves only one site.

We now show that $\widetilde{H}$ (2.10) and H (2.2) are numerically equal even though they arise from different Hamiltonian formulations. We introduce forward and backward difference operators $\delta^\pm$ defined by $\delta^+ A_n = A_{n+1} - A_n$ and $\delta^- A_n = A_n - A_{n-1}$, where A_n is a quantity referenced by the index n. Then δ^2, defined by $\delta^2 A_n = A_{n+1} - 2A_n + A_{n-1}$, satisfies $\delta^2 = \delta^+ \delta^- = \delta^- \delta^+$. Hamilton's equations applied to (2.10) imply $\dot{\phi}_n = -\delta^2 \psi_n$ (see (2.11)). Since $\phi_n := \delta^+ q_n$ we have $\delta^+ \dot{q}_n = \delta^+ \delta^-(-\psi_n)$, so $\dot{q}_n = p_n = C - \delta^- \psi_n$ for some quantity C, independent of n. Now consider $2(\widetilde{H} - H) = \sum_n (\psi_{n+1} - \psi_n)^2 - \sum_n p_n^2$; then $2(\widetilde{H} - H) = -\sum_n C$ (assuming that both H and $\widetilde{H}$ are finite, and that $\lim_{n\to\pm\infty} \psi_n = 0$). Hence, we deduce $C = 0$, and so $H = \widetilde{H}$, as required.

We shall see the significance of the alternative Hamiltonian formulation $\widetilde{H}$ for Fermi-Pasta-Ulam systems, particularly in reference to non-mechanical models such as those studied in Chapters 3 and 4.

2.2.3 Asymptotic analysis

As we have already discussed in Section 1.7, a closed analytic form for general breather solutions of the FPU lattice (2.7) is not known. We restrict our attention to a class of breather solutions, namely those of small amplitude, and whose envelope varies very slowly compared to the carrier oscillations.

In this case, we apply the semi-discrete multiple-scale method described in Section 1.7.3 to determine approximations to breather solutions. We discuss the validity of this procedure in Section 2.5.

Hence, in addition to the variables n and t, we introduce new slow variables X, τ and T defined by

$$X = \varepsilon n, \quad \tau = \varepsilon t \quad \text{and} \quad T = \varepsilon^2 t. \tag{2.12}$$

We consider the displacement $\phi_n(t)$ to be a function of the independent variables n, t, X, τ and T so that $\phi_n(t) = \phi(n, t, X, \tau, T)$. Applying the chain rule for partial differentiation, the derivative operator $\mathrm{d}/\mathrm{d}t$ is replaced by

$$\frac{\mathrm{d}}{\mathrm{d}t} \equiv \frac{\partial}{\partial t} + \varepsilon \frac{\partial}{\partial \tau} + \varepsilon^2 \frac{\partial}{\partial T}. \tag{2.13}$$

We assume a small-amplitude asymptotic expansion for modulated solutions of (2.7) of the form

$$\begin{aligned}
\phi_n(t) = {}&\varepsilon\, \mathrm{e}^{\mathrm{i}\omega t + \mathrm{i}pn} F(X, \tau, T) + \varepsilon^2 G_0(X, \tau, T) \\
&+ \varepsilon^2 \mathrm{e}^{\mathrm{i}\omega t + \mathrm{i}pn} G_1(X, \tau, T) + \varepsilon^2 \mathrm{e}^{2\mathrm{i}\omega t + 2\mathrm{i}pn} G_2(X, \tau, T) \\
&+ \varepsilon^3 H_0(X, \tau, T) + \varepsilon^3 \mathrm{e}^{\mathrm{i}\omega t + \mathrm{i}pn} H_1(X, \tau, T) \\
&+ \varepsilon^3 \mathrm{e}^{2\mathrm{i}\omega t + 2\mathrm{i}pn} H_2(X, \tau, T) + \varepsilon^3 \mathrm{e}^{3\mathrm{i}\omega t + 3\mathrm{i}pn} H_3(X, \tau, T) + \cdots + \text{c.c.,} \quad (2.14)
\end{aligned}$$

where c.c. denotes the complex conjugate, and ω and p are the frequency and wavenumber of the linear carrier wave respectively. Taylor's theorem enables us to replace terms such as $\phi_{n+1}(t)$ by

$$\begin{aligned}
\phi_{n+1}(t) &= \varepsilon\, \mathrm{e}^{\mathrm{i}\omega t + \mathrm{i}pn + \mathrm{i}p} F(X + \varepsilon, \tau, T) + \cdots + \text{c.c.} \\
&= \varepsilon\, \mathrm{e}^{\mathrm{i}\omega t + \mathrm{i}pn + \mathrm{i}p} \left(F + \varepsilon F_X + \tfrac{1}{2}\varepsilon^2 F_{XX} + \cdots \right) + \cdots + \text{c.c.} \quad (2.15)
\end{aligned}$$

A similar expansion may also be found for terms such as $\phi_{n-1}(t)$.

We then substitute the ansatz (2.14) into the equations of motion (2.7) and equate coefficients of each harmonic in t at each order of ε. This yields the following equations

$\mathcal{O}(\varepsilon\, \mathrm{e}^{\mathrm{i}\omega t + \mathrm{i}pn})$:

$$-\omega^2 F = \mathrm{e}^{\mathrm{i}p} F + \mathrm{e}^{-\mathrm{i}p} F - 2F, \tag{2.16}$$

$\mathcal{O}(\varepsilon^2 e^{i\omega t + ipn})$:

$$\omega F_\tau = \sin(p) F_X, \tag{2.17}$$

$\mathcal{O}(\varepsilon^2 e^{2i\omega t + 2ipn})$:

$$\omega^2 G_2 = \sin^2(p)(G_2 + aF^2), \tag{2.18}$$

$\mathcal{O}(\varepsilon^3 e^{i\omega t + ipn})$:

$$
\begin{aligned}
2i\omega F_T + F_{\tau\tau} + 2i\omega G_{1\tau} &= \cos(p) F_{XX} + 2i\sin(p) G_{1X} \\
&\quad -8a\sin^2\left(\frac{p}{2}\right)[FG_0 + F\overline{G}_0 + \overline{F}G_2] \\
&\quad -12b\sin^2\left(\frac{p}{2}\right)|F|^2 F,
\end{aligned} \tag{2.19}
$$

$\mathcal{O}(\varepsilon^4 e^0)$:

$$G_{0\tau\tau} = G_{0XX} + a\left(|F|^2\right)_{XX}. \tag{2.20}$$

The equation from $\mathcal{O}(\varepsilon^2 e^0)$ is the trivial equation $0 = 0$, and so may be discarded.

We proceed to solve the above set of equations. Equation (2.16) yields the dispersion relation, which relates the temporal frequency of the carrier wave ω to the wavenumber p,

$$\omega^2 = 4\sin^2\left(\frac{p}{2}\right). \tag{2.21}$$

Taking the positive root of (2.21), we conclude that

$$\omega = 2\sin\left(\frac{p}{2}\right). \tag{2.22}$$

A plot of the dispersion relation (2.22) is shown in Figure 2.2(a). From this we see that the temporal frequency ω is maximised at the point $p = \pi$, where $\omega = 2$.

Considering (2.17), this becomes (after substituting for ω from (2.22))

$$F_\tau = \cos\left(\frac{p}{2}\right) F_X. \tag{2.23}$$

Equation (2.23) shows that the temporal derivative F_τ and spatial derivative F_X are multiples of one another. From this we infer that F is a travelling wave of the form

$$F(X, \tau, T) \equiv F(Z, T), \tag{2.24}$$
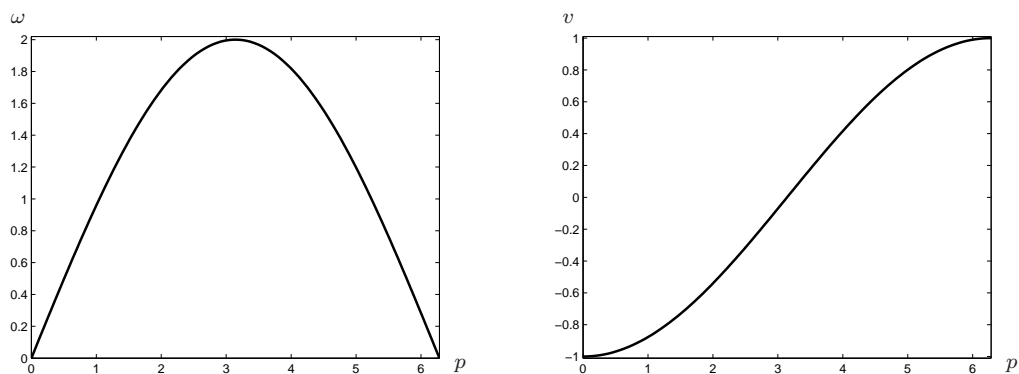
(a) The dispersion relation, ω against p.   (b) The velocity v against p.

Figure 2.2: The dispersion relation ω and velocity v against wavenumber p.

where Z is the travelling wave coordinate given by $Z = X - v\tau$, with velocity $v = -\cos{(p/2)}$. A plot of the velocity against the wavenumber p is shown in Figure 2.2(b). We see from this that for $p = \pi$ we have a stationary wave, and for other values of p a wave which moves with speed below unity.

Equation (2.18) is a straightforward algebraic equation, and hence it is solved easily to give G_2 in terms of F^2. Rearranging, we find after substituting for ω and simplifying that

$$G_2 = a \cot^2\left(\frac{p}{2}\right) F^2. \tag{2.25}$$

Note that for stationary waves (which occur when $p = \pi$), there is no generation of a second harmonic. Note also that when $a \neq 0$ the expression for G_2 becomes singular as $p \to 0$. In particular, from (2.25), we see that if $p = \mathcal{O}(\varepsilon^{1/2})$ or smaller, then the F term in (2.14) is not dominant, but of similar size to the G_2 term.

Turning our attention to (2.19), we anticipate that this should reduce to a nonlinear Schrödinger (NLS) equation in the variable F, as is the case for other lattice models (see Remoissenet [102], or Bang & Peyrard [12]). However, at present, it is clear that (2.19) also includes terms involving G_1 and G_0. These must be found in terms of F before reduction to the NLS equation can occur.

The quantities G_1 and G_0 are higher-order correction terms to the leading order quantity F. If we assume that G_1 and G_0 represent perturbations travelling

at the same velocity as F, we have that

$$G_1(X, \tau, T) = G_1(Z, T) \quad \text{and} \quad G_0(X, \tau, T) = G_0(Z, T), \qquad (2.26)$$

where as before, $Z = X - v\tau$ and $v = -\cos(p/2)$. It follows from the left-hand equality in (2.26) that the terms involving G_1 on either side of (2.19) disappear. Also, using the right-hand equality in (2.26), we find that $G_{0\tau\tau} = v^2 G_{0ZZ}$, and so equation (2.20) becomes

$$(v^2 - 1)G_{0ZZ} = a(|F|^2)_{ZZ}. \qquad (2.27)$$

Integrating this equation twice with respect to Z gives

$$G_0 = \frac{a}{v^2 - 1}|F|^2 = -a\operatorname{cosec}^2\left(\frac{p}{2}\right)|F|^2. \qquad (2.28)$$

Note that in (2.28), we have taken the constants of integration to be zero. This follows from the comments regarding boundary conditions made immediately after (2.7). Also, again, we see that the expression for G_0 (2.28) becomes singular as $p \to 0$.

We now return to (2.19). Substituting for G_2 and G_0 using (2.25) and (2.28) respectively, we arrive at the NLS equation for F as anticipated

$$iF_T + PF_{ZZ} + Q|F|^2 F = 0. \qquad (2.29)$$

In (2.29), the coefficients P and Q of F_{ZZ} and $|F|^2 F$ respectively are given by

$$P = \tfrac{1}{4}\sin\left(\frac{p}{2}\right) \quad \text{and} \quad Q = \frac{2a^2\cos^2\left(\frac{p}{2}\right) - 4a^2 + 3b\sin^2\left(\frac{p}{2}\right)}{\sin\left(\frac{p}{2}\right)}. \qquad (2.30)$$

In other words, the multiple-scale ansatz (2.14) reduces the FPU equations (2.7) defined upon a discrete chain to a continuum partial differential equation (the NLS equation, (2.29)) for the breather envelope F. The next task is to determine soliton solutions of (2.29) which give an analytic formula for the envelope F.

2.2.4 Bright soliton solutions

A vast body of literature on the nonlinear Schrödinger equation is available. It is a generic equation which arises in a wide range of different physical contexts. In general, it describes the propagation of the envelope over a carrier

wave, and is obtained when one takes into account the lowest-order effects of dispersion and nonlinearity upon a wavepacket. It is integrable, and is known to admit soliton solutions. We will not derive the solutions here. However, a concise review of the theoretical properties of the NLS equation can be found in Chapter 4 of Remoissenet [103], or Chapter 3 of Scott [114]. We will quote relevant results from therein when necessary.

It is known that the nonlinear Schrödinger equation (2.29) admits bright soliton solutions (also known as envelope solitons) if the coefficients P and Q are of the same sign, and dark solitons (also known as hole solitons) if P and Q are of opposite sign (see also Dodd et $al.$ [40]). Clearly P is positive for all p in the interval $[0, 2\pi]$ (except at $p = 0$ and $p = 2\pi$). Hence for bright soliton solutions, the above condition reduces to $Q > 0$, which upon rearranging becomes

$$\left(\frac{3b}{2a^2} - 1 \right) \sin^2 \left(\frac{p}{2} \right) > 1. \tag{2.31}$$

A great deal of information can be derived from this inequality, as we now show. In particular, inequality (2.31) is critical for determining the existence and nonexistence of stationary discrete breathers and long-lived moving breather modes in the one-dimensional FPU chain.

In analysing this inequality, it is instructive to consider the (a, b)-parameter-space. For a fixed wavenumber p, we see that in order for the inequality to be satisfied, b must be greater than some simple quadratic function of a, namely

$$b > \frac{2}{3} \left[\text{cosec}^2 \left(\frac{p}{2} \right) + 1 \right] a^2. \tag{2.32}$$

This inequality is illustrated in Figure 2.3, which shows the inequality (2.32) for four distinct wavenumbers $p = j\pi/4$ with $j = 1, 2, 3, 4$. For any given value of a, the lowest possible value of b satisfying (2.32) occurs when $p = \pi$ (that is, when $\text{cosec}^2(p/2)$ is minimised and has value 1). For this wavenumber, for which breathers are stationary, we have $b > \frac{4}{3}a^2$. We mention that this is exactly the inequality proven by James [69] for the existence of stationary breathers that we discussed in Section 2.1.2. From (2.6), we find that $V^{(3)}(0) = 2a$ and

$V^{(4)}(0) = 6b$. Hence James's condition for breather existence in the FPU chain gives $B = 3b - 4a^2 > 0$, which is the same inequality that we arrive at above.

This inequality tells us that no bright breathers at all can exist below the curve which corresponds to $p = \pi$ (see Figure 2.3), and so this is effectively a necessary condition for breather existence in the 1D FPU chain.
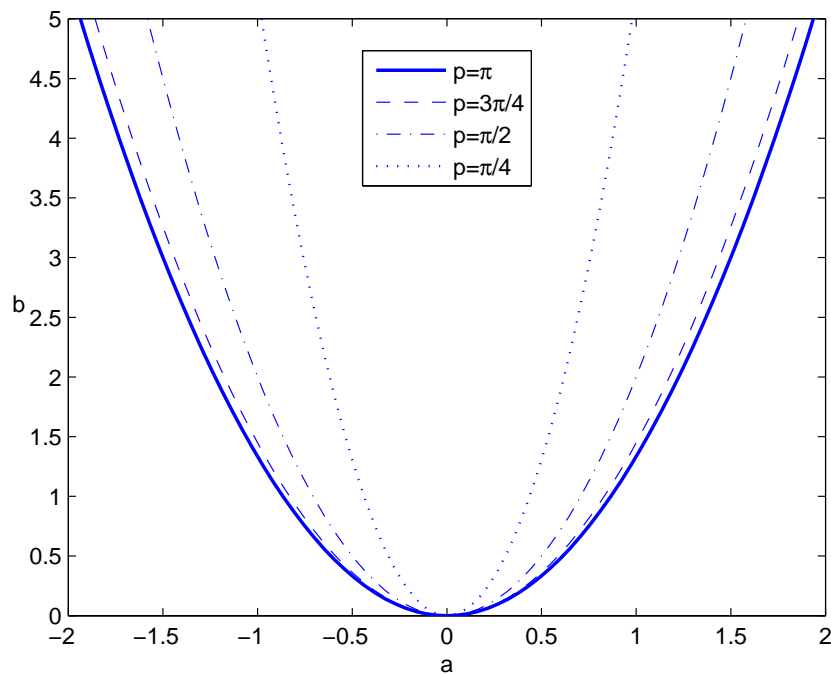
Figure 2.3: Illustration of the inequality (2.32).

Returning to the remaining curves in Figure 2.3 for a moment, we comment that anywhere above the solid curve, stationary breathers with $p = \pi$ exist. Similarly, above the dashed curve $(--)$, breathers with $p \geq 3\pi/4$ exist. These are slowly moving, since $|v| < \cos(3\pi/8) \approx 0.38$ units per second. Above the dash-dotted curve $(-\cdot)$, breathers with $p \geq \pi/2$ exist; these move with speed $|v| < 1/\sqrt{2} \approx 0.707$ units per second. Above the dotted curve $(\cdots)$, breathers with $p \geq \pi/4$ exist. These travel with speed $|v| < \cos(\pi/8) \approx 0.92$ units per second. If we choose to consider arbitrarily small wavenumbers, then it is clear from (2.32) that breathers exist only in a neighbourhood of the b-axis, that is,

when $b \gg a$.

So, given (a, b) satisfying the condition for the existence of a *moving* breather with wavenumber p, namely (2.32), then we also expect to find breathers with larger p values, and in particular $p = \pi$ and hence a *stationary* breather mode to exist. A rearrangement of (2.31) shows there is a threshold wavenumber, $p_{\min}$, above which the inequality (2.31) is satisfied. Explicitly, for bright soliton solutions, the wavenumber p must satisfy $p_{\min} < p < \pi$ where

$$p_{\min} = 2 \sin^{-1} \sqrt{\frac{2a^2}{3b - 2a^2}}. \tag{2.33}$$

In Section 2.3, we investigate the properties of breathers which correspond to wavenumber p, where $p \to p_{\min}^+$. For now, we note that if we consider the special case of a lattice with symmetric quartic potential ($a = 0$), then from (2.30), we see that the condition $Q > 0$ reduces to $b > 0$. In other words, provided $b > 0$, the NLS equation (2.29) yields bright soliton solutions for all $p \in (0, 2\pi)$, and we find no threshold for the wavenumber p (that is, $p_{\min} = 0$). Formally, breathers with $p = 0$ exist only in the case $a = 0$, $b > 0$. This limit is considered in more detail in Section 2.4.

2.2.5 Analytic forms for breather solutions in the FPU chain

In this section, we firstly use formulae for bright soliton solutions to determine an expression for the breather in the difference variable ϕ_n. We then show how this can be used to find a leading-order expression for the breather in the original displacement variable q_n.

In the region above the curve corresponding to a particular wavenumber p in Figure 2.3, we expect to find bright soliton solutions to (2.30) of the form

$$F = A \operatorname{sech}\left(A \sqrt{\frac{Q}{2P}} Z\right) \exp\left(i\frac{Q}{2} A^2 T\right), \tag{2.34}$$

where A is a free parameter which parametrises the soliton amplitude (see Chapter 4.5 of Remoissenet [103]). We note that both the soliton width and

frequency depend upon the amplitude A, with larger amplitude solitons being narrower and having a higher temporal frequency.

The expression (2.34) for the envelope F is then substituted into the breather ansatz (2.14), giving the breather solution of (2.7) in terms of our original variables,

$$
\begin{aligned}
\phi_n(t) \;=\; & 2\varepsilon A \operatorname{sech}\left[\varepsilon A \sqrt{\frac{Q}{2P}}\left(n+\cos\left(\frac{p}{2}\right)t\right)\right]\cos\left(\Omega t + pn\right) \\
& + 2a\varepsilon^2 A^2 \operatorname{cosec}^2\left(\frac{p}{2}\right)\operatorname{sech}^2\left[\varepsilon A \sqrt{\frac{Q}{2P}}\left(n+\cos\left(\frac{p}{2}\right)t\right)\right] \\
& \times\left(\cos^2\left(\frac{p}{2}\right)\cos\left(2\Omega t + 2pn\right)-1\right)+\mathcal{O}(\varepsilon^3),
\end{aligned}
\tag{2.35}
$$

where P and Q are defined in (2.30) above, also

$$
\Omega = 2\sin\left(p/2\right) + Q\varepsilon^2 A^2/2,
\tag{2.36}
$$

and the combination εA is a single free parameter. Note that in (2.35), we have given the form of the breather to second-order, since we have also determined the second-order terms G_0 and G_2 in (2.28) and (2.25) respectively. Equation (2.36) gives the relationship between the frequency and amplitude for the non-linear system. This has been obtained through a more systematic method than that used in Section 1.1.2.

We use the leading-order solution for $\phi_n(t)$ in (2.35) to obtain an expression at leading-order for q_n, the original displacement variable. We assume that q_n is of the form

$$
\begin{aligned}
q_n(t) = {} & 2\varepsilon A[\lambda\cos(\Omega t + pn) + \mu\sin(\Omega t + pn)] \\
& \times \operatorname{sech}\left[\varepsilon A\sqrt{\frac{Q}{2P}}\left(n - vt\right)\right]+\mathcal{O}(\varepsilon^2),
\end{aligned}
\tag{2.37}
$$

where $v = -\cos(p/2)$ is the envelope velocity given in (2.24), and λ and μ are constants to be determined in terms of p, which is taken to be $\mathcal{O}(1)$.

We substitute (2.37) into the defining equation for ϕ_n (2.4) giving a second

expression for $\phi_n(t)$ at leading order. Specifically, we find that

$$q_{n+1}(t) - q_n(t) = 2\varepsilon A\mathrm{sech}\left[\varepsilon A\sqrt{\frac{Q}{2P}}(n - vt)\right]\left\{\cos(\Omega t + pn)[\lambda\cos p + \mu\sin p - \lambda]\right.$$

$$\left. + \sin(\Omega t + pn)[-\lambda\sin p + \mu\cos p - \mu]\right\} + \mathcal{O}(\varepsilon^2).$$

$$(2.38)$$

Equating coefficients of corresponding terms in the two leading-order expressions for ϕ_n (2.35) and (2.38) yields the following simultaneous equations for λ and μ:

$$\lambda\cos p + \mu\sin p - \lambda = 1, \qquad (2.39)$$

$$-\lambda\sin p + \mu\cos p - \mu = 0. \qquad (2.40)$$

The second equation (2.40) is used to find that $\lambda/\mu = -\tan(p/2)$, and substituting this into (2.39) gives $\lambda = -1/2$ and $\mu = (1/2)\cot(p/2)$. Hence overall we obtain an expression for the bright breather to leading-order

$$q_n(t) = -\varepsilon A\left[\cos(\Omega t + pn) - \cot\left(\frac{p}{2}\right)\sin(\Omega t + pn)\right]$$

$$\times\mathrm{sech}\left[\varepsilon A\sqrt{\frac{Q}{2P}}(n - vt)\right] + \mathcal{O}(\varepsilon^2), \qquad (2.41)$$

which is valid when $\varepsilon \ll 1$ and $p = \mathcal{O}(1)$. Note that equations (2.39) and (2.40) are ill-posed in the limit $p \to 0$.

Lastly in this section, we make a few remarks comparing the phase (or crest) velocity v_{crest} and the group (or envelope) velocity v_{envelope} of the carrier wave of the breather solution (2.41). Clearly, $v_{\mathrm{envelope}} = -\cos(p/2)$ is always less than unity. The crest velocity is given by $-\Omega/p$ and so from (2.36) this is also less than unity. For general p the two will differ, since $\sin\theta > \theta\cos\theta$. In the limit of small p, the envelope and crest velocities $-\cos(p/2)$ and $-\Omega/p$ respectively are close, but $v_{\mathrm{crest}} = -\Omega/p$ is always larger in magnitude when the $\mathcal{O}(\varepsilon^2)$ correction term is included. Thus there is no value of p for which $v_{\mathrm{crest}} = v_{\mathrm{envelope}}$.

Also, it is possible to use the existence criterion (2.31) (in particular, its rearrangement (2.33)) to find an upper bound for the envelope velocity v_{envelope}.

Since the wavenumber p is restricted to the range $p_{\min} \leq p \leq \pi$, the breather velocity $v_{\text{envelope}} = -\cos(p/2)$ is restricted to the range

$$|v_{\text{envelope}}| < \sqrt{\frac{3b - 4a^2}{3b - 2a^2}}. \tag{2.42}$$

Thus for nonzero values of a, breather modes have a velocity which is bounded away from the speed of sound in the lattice. The phrase "speed of sound" refers to maximum speed at which linear waves of the form $A \exp(\mathrm{i}pn + \mathrm{i}\omega t)$ can travel through a lattice. The speed of such waves is given by $c = \omega/p$. For an FPU lattice of the form (2.7), the speed $c = 2\sin(p/2)/p$, which has a maximum value $c = 1$ at $p = 0$. Waveforms which travel at greater (lower) speeds than this are referred to as *supersonic* (*subsonic*).

2.2.6 Asymptotic estimate for breather energy

In this section we use our solution for q_n (2.41) to find a leading-order estimate for the total energy of the system, H, defined by (2.2). We see from the potential function V in (2.6) that to leading-order, H is given by

$$H \sim \sum_{n=-\infty}^{\infty} \tfrac{1}{2}\dot{q}_n^2 + \tfrac{1}{2}(q_{n+1} - q_n)^2 = \sum_{n=-\infty}^{\infty} \tfrac{1}{2}\dot{q}_n^2 + \tfrac{1}{2}\phi_n^2. \tag{2.43}$$

An expression for ϕ_n has already been obtained in (2.35). Differentiating q_n (2.41) with respect to time gives

$$\dot{q}_n(t) \sim 2\varepsilon A \sin\left(\frac{p}{2}\right)\left[\sin(\Omega t + pn) + \cot\left(\frac{p}{2}\right)\cos(\Omega t + pn)\right] \operatorname{sech}\left[\varepsilon A\sqrt{\frac{Q}{2P}}(n - vt)\right]. \tag{2.44}$$

Substituting (2.35) and (2.44) into the expression for the energy H (2.43) gives a complicated sum. We replace this sum by an integral since the variable $X = \varepsilon n$ varies slowly with n. Therefore, we have

$$H(t) = I_1 + I_2 + I_3, \tag{2.45}$$

where the integrals I_1, I_2 and I_3 are given by

$$I_1 = \int_{-\infty}^{\infty} 2\varepsilon^2 A^2 \left[1 + \cos^2\left(\frac{p}{2}\right)\right] \cos^2(\Omega t + pn)\operatorname{sech}^2\left[\varepsilon A\sqrt{\frac{Q}{2P}}(n - vt)\right] \, dn,$$

(2.46)

$$I_2 = \int_{-\infty}^{\infty} 2\varepsilon^2 A^2 \sin^2\left(\frac{p}{2}\right) \sin^2(\Omega t + pn)\operatorname{sech}^2\left[\varepsilon A\sqrt{\frac{Q}{2P}}(n - vt)\right] \, dn, \quad (2.47)$$

$$I_3 = \int_{-\infty}^{\infty} \varepsilon^2 A^2 \sin(p) \sin(2\Omega t + 2pn)\operatorname{sech}^2\left[\varepsilon A\sqrt{\frac{Q}{2P}}(n - vt)\right] \, dn. \quad (2.48)$$

Since the energy in the FPU chain (2.43) is conserved, we have that $H(t) = H(0)$, and therefore we may set $t = 0$ in each of the integrands in I_1, I_2 and I_3. Clearly $I_3 = 0$, since the integrand in (2.48) is an odd function. The remaining integrals can be evaluated using the following result (formula 3.982.1 of Gradshteyn & Ryzhik [63]),

$$\int_{-\infty}^{\infty} \cos(\alpha x) \operatorname{sech}^2(\beta x) \, dx = \frac{\alpha\pi}{\beta^2} \operatorname{cosech}\left(\frac{\alpha\pi}{2\beta}\right). \quad (2.49)$$

Using (2.49) to evaluate (2.46) and (2.47), we therefore find a leading-order expression for the energy H

$$H \sim \frac{4\varepsilon A \sin\left(\frac{p}{2}\right)}{\sqrt{(6b - 4a^2)\sin^2\left(\frac{p}{2}\right) - 4a^2}} + \frac{p\pi \sin^2(p)\operatorname{cosech}\left(\frac{p\pi}{\varepsilon A}\sqrt{\frac{2P}{Q}}\right)}{(6b - 4a^2)\sin^2\left(\frac{p}{2}\right) - 4a^2}. \quad (2.50)$$

If we take all parameters to be $\mathcal{O}(1)$ except for $\varepsilon \ll 1$, then the second term on the right-hand side of (2.50) is exponentially small in ε. Hence overall, the energy H is an $\mathcal{O}(\varepsilon)$ quantity. In calculating the estimate for the energy H (2.50), we have used the expression for q_n given in (2.41). Since (2.41) is valid when $p = \mathcal{O}(1)$, it follows that the estimate for H (2.50) is also valid for this parameter regime.

2.2.7 Dark solitons

In the region below the curves in Figure 2.3 corresponding to wavenumbers p where (2.32) fails, we expect to find dark soliton solutions of the NLS equation.

These solutions have the form $F(Z,T) = D(Z,T)e^{i\mu(Z,T)}$, where (see Chapter 4.5 of Remoissenet [103])

$$D(Z,T) = B\left[1 - m^2 \operatorname{sech}^2\left(mB\sqrt{\frac{-Q}{2P}}Z\right)\right]^{\frac{1}{2}},$$ (2.51)

$$\mu(Z,T) = \sqrt{\frac{-Q}{2P}}\left[\sqrt{1-m^2}BZ + \tan^{-1}\left\{\frac{m}{\sqrt{1-m^2}}\tanh\left(mB\sqrt{\frac{-Q}{2P}}Z\right)\right\}\right] - \frac{B^2Q}{2}(3-m^2)T.$$ (2.52)

In (2.52), B is a free parameter (distinct from the quantity introduced in Section 2.1.2) and m $(0 \leq m \leq 1)$ is a parameter that controls the depth of the modulation of amplitude [103]. In this case, the overall solution of (2.7) in terms of the original variables to first order is $\phi_n(t) = 2\varepsilon D_n(t)\cos(\psi_n(t)) + \mathcal{O}(\varepsilon^2)$, where, using B and m as before,

$$D_n(t) = B\left[1 - m^2 \operatorname{sech}^2\left\{mB\varepsilon\sqrt{\frac{-Q}{2P}}\left(n + \cos\left(\frac{p}{2}\right)t\right)\right\}\right]^{\frac{1}{2}},$$ (2.53)

$$\begin{aligned}\psi_n(t) &= B\sqrt{\frac{-Q(1-m^2)}{2P}}\left[n + \cos\left(\frac{p}{2}\right)t\right] - \frac{B^2Q}{2}\varepsilon^2(3-m^2)t + 2\sin\left(\frac{p}{2}\right)t + pn \\ &\quad + \sqrt{\frac{-Q}{2P}}\tan^{-1}\left[\frac{m}{\sqrt{1-m^2}}\tanh\left\{mB\sqrt{\frac{-Q}{2P}}\left(n + \cos\left(\frac{p}{2}\right)t\right)\right\}\right].\end{aligned}$$ (2.54)

These solutions have been observed previously, for example, by Flytzanis *et al.* [57].

2.2.8 The Toda lattice

We illustrate the results of our above analysis by referring to the Toda lattice, [129]. This lattice corresponds to $V(\phi) = \alpha[e^{-\beta\phi} + \beta\phi - 1]/\beta$ in (2.5). Hence $V'(\phi) = \alpha(1 - e^{-\beta\phi})$, giving the Toda lattice equation

$$\ddot{\phi}_n = -\alpha\left(e^{-\beta\phi_{n+1}} - 2e^{-\beta\phi_n} + e^{-\beta\phi_{n-1}}\right).$$ (2.55)

The Toda lattice is an integrable system, and is known to support travelling wave solutions and elastically interacting N-soliton solutions (see Chapter 5 of Scott, [114]).

Performing a Taylor expansion of $V(\phi)$ about $\phi = 0$, we find that $V'(\phi) \sim \alpha\beta[\phi - \beta\phi^2/2 + \beta^2\phi^3/6]$. Comparing this (2.6), we see that for the Toda lattice $a = -\alpha\beta^2/2$ and $b = \alpha\beta^3/6$. It follows that $3b = 2a^2$, and therefore the inequality (2.32) fails to hold for any p. We conclude that bright breathers can never exist in the Toda lattice. This nonexistence result is entirely consistent with the literature on Toda lattice (see [129]).

2.3   Numerical results

In this section we solve the equations for the FPU lattice (2.1) numerically. This infinite system of nonlinear coupled second-order ordinary differential equations can be converted to a first-order system in the variables q_n and p_n, where $p_n = \dot{q}_n$ is the generalised momentum of the nth particle (see equations (2.2) and (2.3)). Hence, the system (2.1) is equivalent to

$$
\begin{aligned}
\dot{q}_n &= p_n, \\
\dot{p}_n &= V'(q_{n+1} - q_n) - V'(q_n - q_{n-1}).
\end{aligned}
\tag{2.56}
$$

We carry out the numerical simulation of the system using a fourth-order Runge-Kutta scheme (see for example, Chapter 8 of Boyce & DiPrima [21]) coded in Fortran90 (see Chapman [31]). Our program solves the equations of motion for N particles where N is any natural number greater than or at least equal to three, but typically around 100.

2.3.1   Initial data and boundary conditions

The first task is to generate initial data for q_n and p_n to input into the numerical routines. This is done using the formula for $\phi_n(t)$ given in (2.35). From the definition of ϕ_n, it may be verified that

$$
q_n(t) = q_1(t) + \sum_{i=1}^{n-1} \phi_i(t) = \sum_{i=1}^{n-1} \phi_i(t),
\tag{2.57}
$$

where for a breather initially located centrally in the lattice, we take $q_1 = 0$ following the comments on our choice of boundary conditions in (2.9). A similar equation holds for p_n. Setting $t = 0$ in (2.57), we evaluate the analytical solution for $\phi_n(0)$ given by (2.35) on the lattice, and then take the cumulative sum to determine initial data for q_n at each lattice site. It also follows from our chosen boundary conditions in (2.9) that the constant $q_\infty = q_N(0)$.

One is entitled to ask why we have used an indirect route (by summing ϕ_i) in (2.57) to determine initial data for q_n, when an analytic expression for q_n (2.41) is already known. This is because, as we have already pointed out after equations (2.41) and (2.50), the expansion for q_n (2.41) is not valid for small p (specifically when $p \sim \varepsilon$). Hence it cannot be assumed that (2.41) gives the form of the breather correctly in this domain. Therefore, we choose to use the sum given by (2.57) instead, since the leading-order expression for $\phi_n(t)$ obtained from (2.35) is valid for arbitrarily small p.

Returning to the system (2.56), we see that the equations are defined for each of the particles $n = 2 \ldots N - 1$. However, the 1st and Nth particles are missing left- and right- neighbours respectively. We remedy this by imposing periodic boundary conditions. That is, the linear chain is effectively formed into a closed ring where the 1st and Nth particles are placed next to one another. To this end, we introduce fictitious particles at either end of the lattice, satisfying

$$q_{N+1}(t) = q_1(t) + q_\infty, \quad \text{and} \quad q_0(t) = q_N(t) - q_\infty,$$
$$p_{N+1}(t) = p_1(t), \quad \text{and} \quad p_0(t) = p_N(t). \tag{2.58}$$

This has the consequence that breathers moving to the right- (left-) hand edge of the chain eventually reemerge from the left- (right-) hand edge.

2.3.2 Results

In this section, we present the results of breather simulations for a range of different parameter values. In particular, we aim to verify the analytical results

of Section 2.2. Amongst other properties, we will observe whether long-lived breather modes exist in the parameter regions where expected, that is, when a, b and p satisfy the inequality (2.31). We will also check if the analysis of Section 2.2 correctly predicts the shape and velocity of stationary and moving waveforms in the chain.

In addition to this, we use the conservation of mechanical energy H (2.2) of the system to check the validity of the numerical routines. The total energy H of the lattice is computed easily since it is a simple combination of the variables q_n and p_n returned by the numerical scheme. We compute this at regular intervals to check that it is conserved. Also, we shall compare the numerically computed total energy with the asymptotic estimate given by (2.50).

Firstly, we present a simulation of a stationary breather with $p = \pi$. We choose the remaining parameter values to be $a = 0.1$, $b = 2.0$, $N = 101$, $A = 1.0$ and $\varepsilon = 0.1$ which satisfy the existence criterion (2.31). The temporal frequency of the carrier wave is $\Omega = 2.2098$, and hence it follows that the period of oscillation is $T = 2\pi/\Omega = 3.0955$. The breather is initially located at the centre of the chain (as is the case for all of our simulations), and is shown in Figure 2.4 (a). The profile of the breather is also shown at later time $t = 32.31T = 100$ in Figure 2.4 (c). At both times, a plot of the cell energy (discussed shortly) is also given. From the energy plots, it is clear that after 100 seconds, the breather has not spread or distorted significantly. We have also included the numerically computed values of the total energy H. After 100 seconds, we see that the change in H is negligible, with $\Delta H/H = 0.00084$. The asymptotic estimate of H given by (2.50) is 0.1159, which is a little lower than the numerically obtained values. This is to be expected, since in deriving (2.50), we ignored $\mathcal{O}(\varepsilon^2)$ terms, which make a small contribution. In Figure 2.5, we have shown a montage of snapshots of the breather at times $t = 0, 5T, 10T, 15T, 20T$ and $25T$. From this, we see that the breather does not spread or diminish in amplitude over this time interval.

(a) Profile at $t = 0$.

(b) Plot of e_n, $H = 0.1189$.

(c) Profile at $32.34T = 100$.

(d) Plot of e_n, $H = 0.1190$.
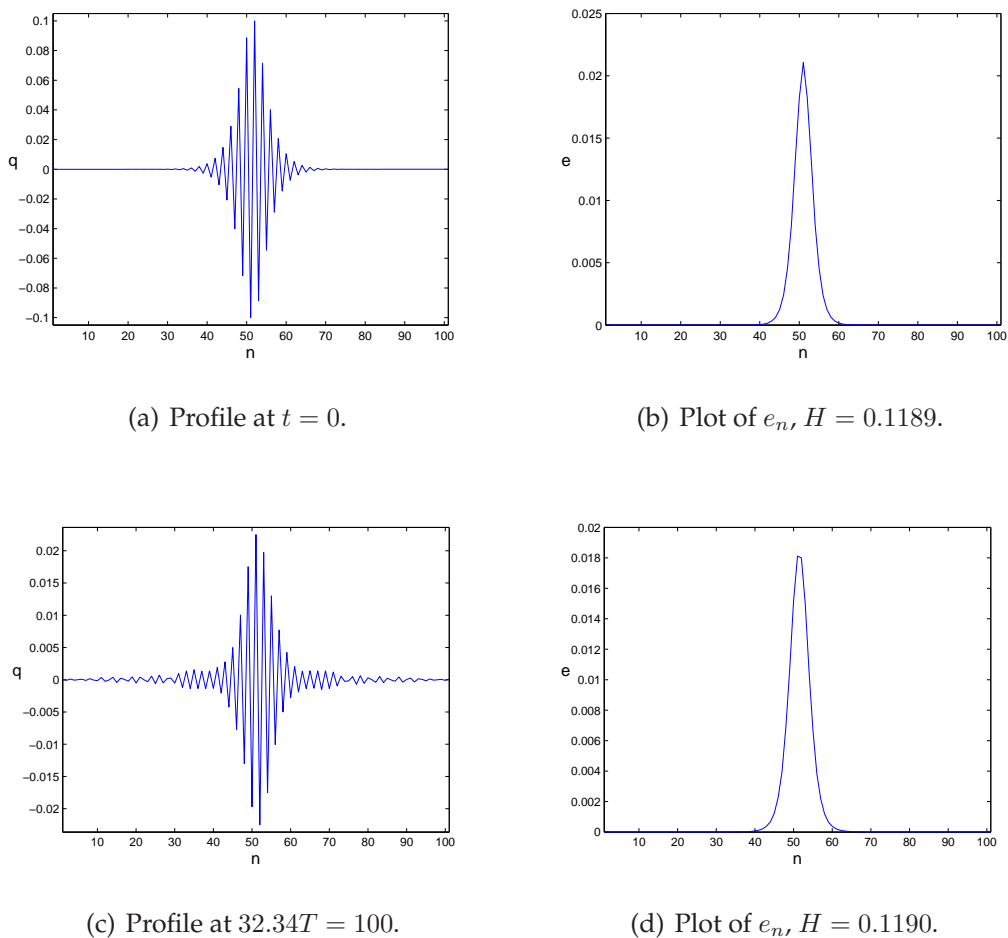
Figure 2.4: Stationary breather, wavenumber $p = \pi$.

We now present a simulation of a moving breather. For this, we set wavenumber $p = \pi/2$, for which $v = -\cos(p/2) = -1/\sqrt{2}$ units per second. The remaining parameters are chosen as follows: $a = 0.1$, $b = 2.0$, $N = 101$, $A = 1.0$ and $\varepsilon = 0.1$, which satisfy the existence inequality (2.31). In this case, the breather frequency is $\Omega = 1.4353$, and so the oscillation period is $T = 4.3779$.

We do not show the initial profile of the breather this time, though we have shown the profile at times $t = 50$ and $t = 91.76$ in Figures 2.6 (a) and 2.6 (c) respectively. In the first of these, we see that the breather has moved to the left and has almost reached the left-hand edge of the chain. A little while later, it disappears from this side and reappears from the right-hand edge (see Figure 2.6 (c)). This is due to the periodic boundary conditions.
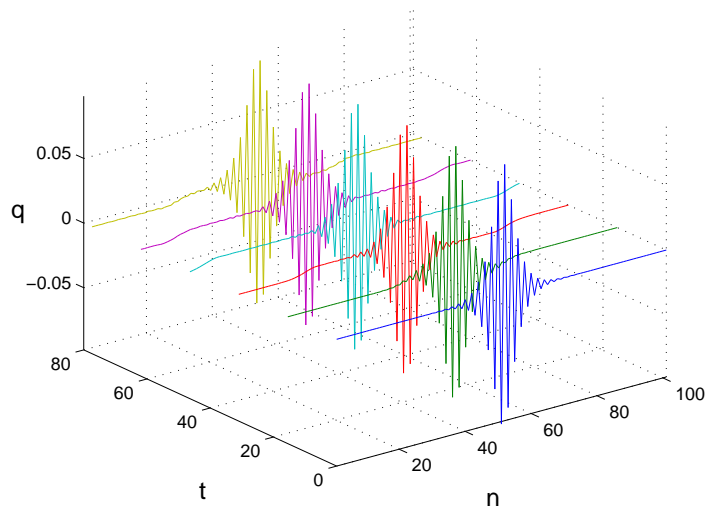
Figure 2.5: Snapshots of a stationary breather at times $t = 0, 5T, 10T, 15T, 20T$ and $25T$, $T = 3.0955$.

Since the breather's exact position is hard to determine from plots of the breather profile, measuring the velocity of the breather accurately is difficult. We find that this is better achieved using a plot of the cell energy e_n, where

$$e_n = \tfrac{1}{2}p_n^2 + V(q_{n+1} - q_n), \tag{2.59}$$

and $H = \sum_{n=1}^{N} e_n$ from (2.2). As we are dealing with a solitary waveform (that is, a localised disturbance whose amplitude decays to zero as $n \to \pm\infty$), the energy associated with the wave is also localised. Hence in order to track the position of the breather (and thus determine its velocity), we may equally use the location of the maximum value of e_n at each value of t. Using this method, we find from Figure 2.6 (d) that the average velocity of the breather is -0.703 units per second. Hence the percentage difference between the analytical and numerical velocities is -0.58%.

In Figure 2.6, we have included the numerically computed values of the energy H. Again, we see that there is only a tiny change in the computed value over the entire duration, with $\Delta H/H = -0.00083$. There is also a close match with the asymptotic estimate for H, which turns out to be 0.1161. In Figure 2.7,
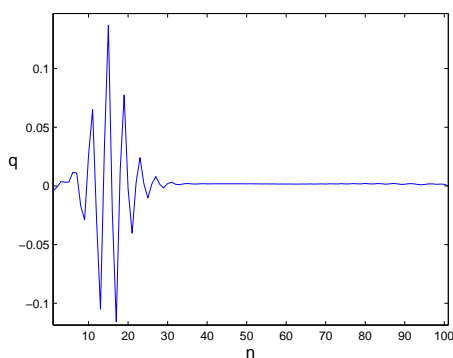
(a) Profile at $t = 50$.
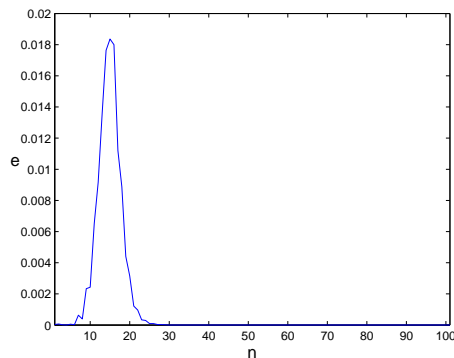
(b) Plot of e_n, $H = 0.1199$.
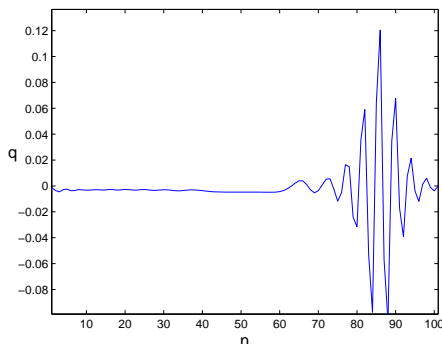
(c) Profile at $t = 91.76$.
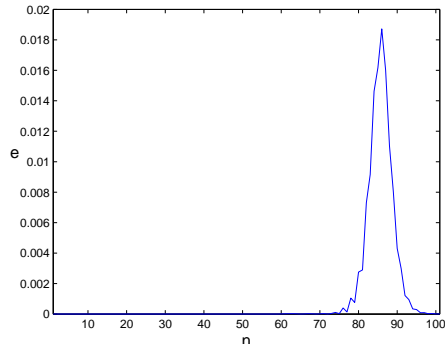
(d) Plot of e_n, $H = 0.1198$.

Figure 2.6: Moving breather, wavenumber $p = \pi/2$.

we have shown the breather at various stages of its motion as it travels left-wards through the chain. The last snapshot at $t = 142.86$ shows the breather as it has just completed one whole circuit and returned to its initial position.

We also use our numerical scheme to further test the existence inequality (2.31). In Section 2.2.4, we showed that a necessary condition for breather existence in the FPU chain is that $3b > 4a^2$. In addition to this, for $a \neq 0$, the wavenumber p must be greater than the minimum wavenumber $p_{\min}$ given by (2.33). It is natural to question what happens as wavenumber $p \to p_{\min}^+$, that is, when the existence condition (2.31) is only just satisfied. We now show that the breather becomes wider as p approaches this threshold.
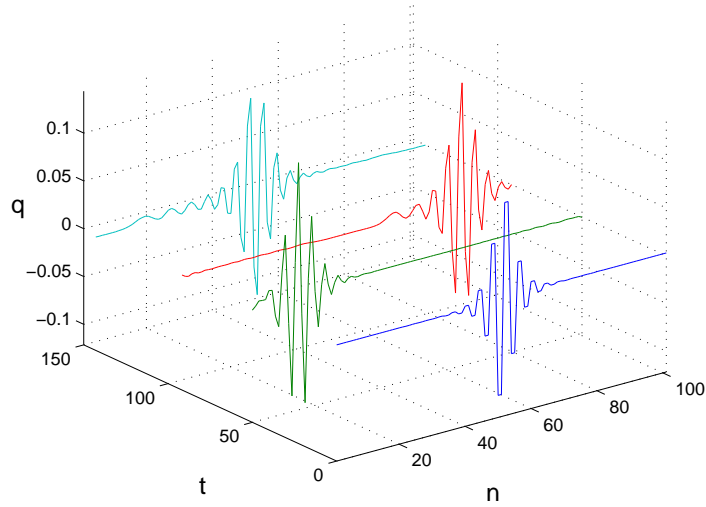
Figure 2.7: Snapshots of a moving breather at times $t = 0, 50, 91.76$ and 142.86.

In order to quantify this, we introduce the notion of a breather's width. If we consider the envelope of the breather given by (2.41), the envelope half-width L_{hw} is measured at half the maximum amplitude of the breather, which is εA. In other words, L_{hw} satisfies

$$2\varepsilon A\,\mathrm{sech}\left(\varepsilon A\sqrt{\frac{Q}{2P}}L_{\mathrm{hw}}\right) = \varepsilon A \quad \Longrightarrow \quad L_{\mathrm{hw}} = \frac{1}{\varepsilon A}\sqrt{\frac{2P}{Q}}\,\mathrm{sech}^{-1}\left(\frac{1}{2}\right). \tag{2.60}$$

The full width of the breather L_{fw} is simply twice the half-width, that is, $L_{\mathrm{fw}} = 2L_{\mathrm{hw}}$. This is illustrated in Figure 2.8. Rewriting the term $\sqrt{Q/2P}$ as

$$\sqrt{\frac{Q}{2P}} = \sqrt{6b - 4a^2 - 4a^2\mathrm{cosec}^2\left(\frac{p}{2}\right)}, \tag{2.61}$$

we see that $\sqrt{Q/2P}$ decreases as p decreases, hence the width of the breather L_{fw} increases as $p \to p_{\mathrm{min}}^{+}$. We can use our numerical program to verify this. If we choose $a = 1$ and $b = 2$, then from (2.33) it follows that $p_{\mathrm{min}} = \pi/2$. In Figure 2.9, we show the initial profiles of two breathers which correspond to two different wavenumbers. For both, we have set $a = 1.0$, $b = 2.0$, $N = 101$, $A = 1.0$ and $\varepsilon = 0.1$. In Figure 2.9 (a), we set $p = \pi$, and in Figure 2.9 (b) we set $p = 1.7$, which is much closer to the threshold value of $\pi/2 \approx 1.57$. As expected,
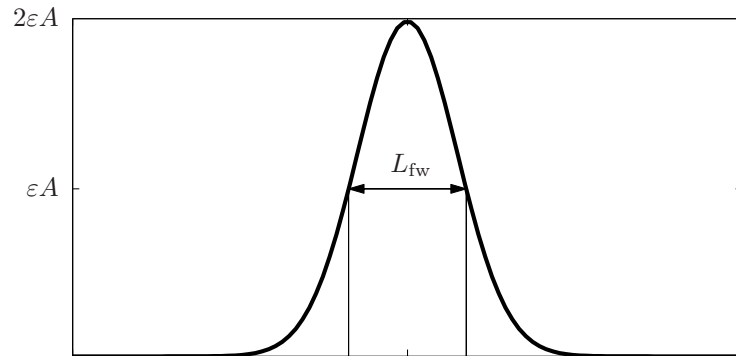
Figure 2.8: Full width L_{fw} of a breather in one dimension.

(a) $p = \pi$.

(b) $p = 1.7$.
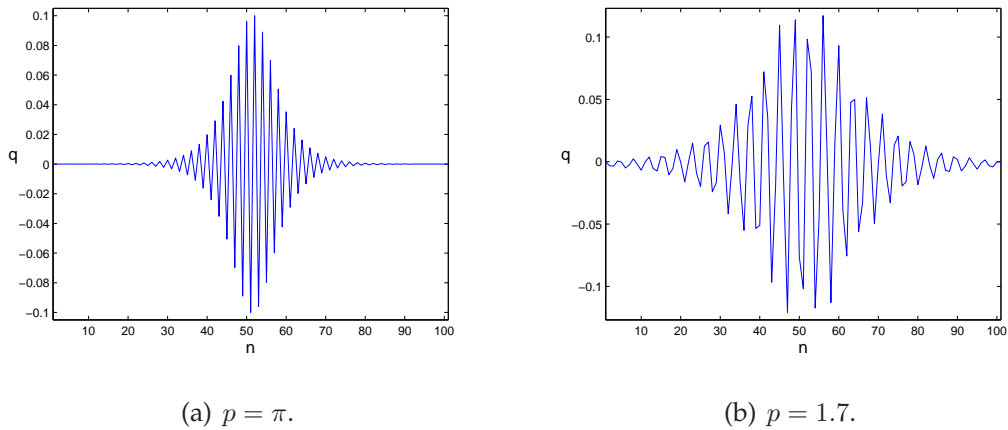
Figure 2.9: Widening of breather profile as $p \to p_{\min}^+ = \pi/2$.

the breather is much wider for $p = 1.7$ than for $p = \pi$. Using the definition (2.60), for $p = \pi$ we find that $L_{\text{fw}} = 13.17$, while for $p = 1.7$ we find $L_{\text{fw}} = 27.57$, which is therefore more than twice as wide.

2.4 The limit of small wavenumber: $p \to 0$

2.4.1 Preliminary results

In this section we show that the FPU lattice can support waveforms more complex than bright or dark breathers or travelling kinks. These more complex waveforms arise when we consider small wavenumbers p (we quantify what we mean by "small" more precisely in Section 2.4.3). Since we consider arbitrarily small wavenumbers p, most of this section is concerned with the case of the quartic lattice, that is, $b > 0$, $a = 0$. Recalling the comments following (2.33) in Section 2.2.4, this is because for the quartic lattice, the existence inequality (2.31) is satisfied for all $p \in (0, 2\pi)$. Hence, only in the case $a = 0$ can we justifiably consider the limit $p \to 0$. However, in Section 2.4.2, we will also note the behaviour of kinks in the lattice with cubic nonlinearity in the potential energy, (that is, $a > 0$, $b = 0$). This is to demonstrate that behaviour in the lattice with quartic potential is quite distinct and unusual when compared with that observed in the lattice with a cubic potential.

Firstly, we show that for the quartic lattice ($a = 0$, $b > 0$), the solution (2.35) reduces to a kink in the limit $p \to 0$. We use the asymptotic analysis of Section 2.2 and the solution for $\phi_n(t)$ in (2.35) to find an exact formula for the kink. Considering only the leading-order expansion for $\phi_n(t)$, we note that as $p \to 0$, $\cos(p/2) \to 1$, and also from (2.36), $\Omega \to 0$ and hence $\cos(\Omega t + pn) \to 1$. Overall, when $p \ll \varepsilon \ll 1$, we have

$$\phi_n(t) = 2\varepsilon A \operatorname{sech}\left[A\sqrt{\frac{Q}{2P}}(\varepsilon n + \varepsilon t)\right] + \mathcal{O}(\varepsilon^3). \tag{2.62}$$

Since ϕ_n is slowly varying in n, (2.8) can be replaced by $q_n = \int^n \phi_k \, dk$, and so (2.62) gives

$$q_n(t) = 4\sqrt{\frac{2P}{Q}} \arctan\left[\exp(\varepsilon A\sqrt{\frac{Q}{2P}}(n + t))\right], \tag{2.63}$$

which describes a kink travelling leftwards through the chain whose speed to leading order is unity. Using (2.63) and (2.9), we find that the amplitude of the

kink is given by

$$q_\infty = 2\pi \sqrt{\frac{2P}{Q}} = \frac{2\pi}{\sqrt{6b}}. \tag{2.64}$$

So we see that in the limit $p \to 0$, the bright breather solution given in (2.35) reduces to q_n as given in (2.63) which describes a travelling kink.

We use our numerical simulation to test whether kinks are observed in the lattice for very small wavenumbers p. We run our simulation for the parameter values $p = 0.01$, $a = 0.0$, $b = 2.0$, $N = 101$, $A = 1.0$ and $\varepsilon = 0.1$. In Figure 2.10, we show the kink at intervals of 10 seconds as it moves leftwards through the chain. For instance, by the time $t = 30$, we see that the kink is close to the left-hand edge of the chain. From (2.24), for very small wavenumbers we expect
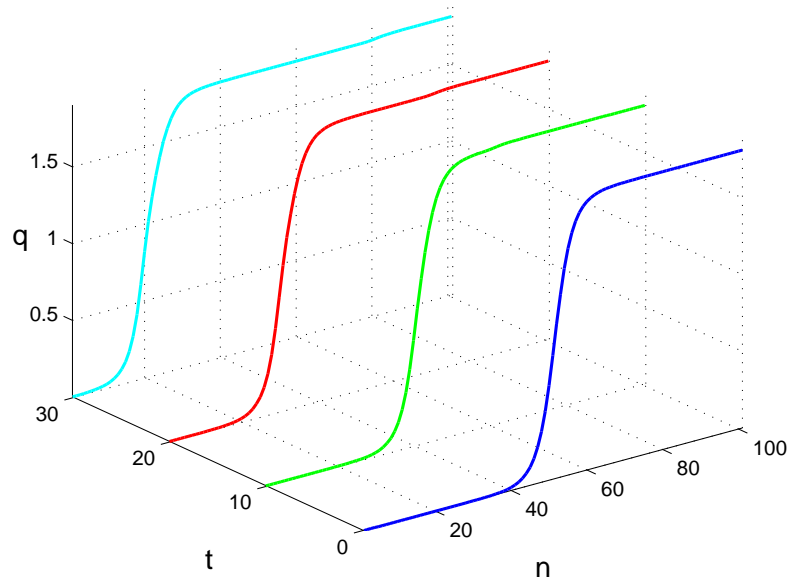
Figure 2.10: Kink for wavenumber $p \to 0$: $a = 0$, $b = 2$ and $p = 0.01$.

the speed of the kink to be very close to unity. Using the method described in Section 2.3, we measure the velocity of the kink and find it to be -1.03 units per second. Hence there is a 3% difference between the theoretical and observed values of -1 and -1.03 units per second respectively. We also measure the height of the kink to be 1.8, which is in close agreement (a difference of -0.6%)

with the calculated value of 1.81 given by (2.64).

The calculation presented in (2.64) gives the amplitude of the kink for the small wavenumber limit $p \to 0$. Later in Section 2.4.3 we will present details of the calculation of q_∞ for the more general case $p = \mathcal{O}(\varepsilon)$. Firstly, we summarise some known properties of kinks in the FPU lattice.

2.4.2 Travelling kinks in the classical continuum limit

In this section, we consider the FPU lattice with either a cubic or a quartic potential. We saw in the previous section that for very small wavenumbers ($p \ll \varepsilon \ll 1$), the breather solution of the quartic FPU lattice reduces to a travelling wave which has the form of a kink. However, kink solutions can be determined directly from the equations of motion (2.7) provided the parameters a and b are chosen appropriately. The discrete lattice equations are not solvable exactly, hence they must be approximated in some way before analytic expressions for solutions can be found. This is done by the method of continuum approximation (in which the discrete index n in (2.7) is replaced by a continuous variable), which we discussed in Section 1.7.2. Moreover, in Section 1.7.2, we saw that there are many different ways in which (2.7) can be approximated by a PDE. Each of these has its own merits and drawbacks. As might be expected, more accurate approximations to (2.7) result in PDEs which are complicated, and for which analytic solutions are thus difficult to obtain.

In fact, Wattis [134] applies quasi-continuum techniques to find travelling kink solutions in a variety of FPU lattice models, to different degrees of accuracy. We do not reproduce details of the calculations here. Instead, we summarise those results which are relevant to the current work. We are concerned with kink solutions in the two special cases of lattices with a symmetric quartic potential ($a = 0$, $b \neq 0$) and an asymmetric cubic potential ($a \neq 0$, $b = 0$).

The lattice with a cubic potential

In the simplest approximation (that is, the standard continuum approxima-
tion, see Section 1.7.2) the lattice (2.7) is governed by the partial differential
equation

$$\phi_{tt} = \phi_{xx} + \tfrac{1}{12}\phi_{xxxx} + a(\phi^2)_{xx}. \tag{2.65}$$

This is the Boussinesq equation, which has a travelling wave solution in the
form of a pulse for ϕ

$$\phi_{2s}(z) = \frac{3(c^2 - 1)}{2a}\mathrm{sech}^2\left(z\sqrt{3(c^2 - 1)}\right), \tag{2.66}$$

where $z = x - ct$ (taking care not to confuse this with the variable Z as defined
in (2.24)), and c is the velocity of the travelling wave. This gives rise to a kink
travelling wave in the variable q which has a kink-amplitude and energy given
by

$$q_\infty^{(2s)} = \frac{\sqrt{3(c^2 - 1)}}{a}, \qquad H_{2s} = \frac{\sqrt{3}(c^2 - 1)^{3/2}(9c^2 + 1)}{10a^2}. \tag{2.67}$$

If, as described in Section 1.7.2, we use the $(0, 2)$ Padé approximation of the
operator $\Lambda(\mathbf{D})$, (which we shall refer to as the improved approximation), then
we obtain a different PDE approximation of (2.7), namely

$$\phi_{tt} = \phi_{xx} + \tfrac{1}{12}\phi_{xxtt} + a(\phi^2)_{xx}. \tag{2.68}$$

This supports a travelling pulse for ϕ of the form

$$\phi_{2i}(z) = \frac{3(c^2 - 1)}{2a}\mathrm{sech}^2\left(\frac{z\sqrt{3(c^2 - 1)}}{c}\right). \tag{2.69}$$

From this, we find slightly more accurate estimates for the kink-amplitude and
energy, namely

$$q_\infty^{(2i)} = \frac{c\sqrt{3(c^2 - 1)}}{a}, \qquad H_{2i} = \frac{c^3\sqrt{3}(c^2 - 1)^{3/2}}{a^2}. \tag{2.70}$$

We note that these have the same behaviour as $c \to 1$ as those generated from
the standard continuum approximation. In particular for both, we observe that

(a) Kink height q_∞.

(b) Kink energy H.

Figure 2.11: Height and energy of kinks in a chain with cubic potential, $(a = 2, b = 0)$ (see equations (2.67) and (2.70)).

as $c \to 1^+$, $q_\infty \to 0^+$ and $H \to 0^+$. Also both approximations yield similar behaviour for large values of c. That is, as $c \to \infty$ we have $q_\infty \to \infty$ and $H \to \infty$. The properties for both the standard and improved continuum approximations are illustrated in Figure 2.11, which shows plots of the kink-amplitude q_∞ in Figure 2.11 (a) and the energy H in Figure 2.11 (b), against the velocity c. In both plots, the upper curve corresponds to the improved continuum approximation. This behaviour is as expected and contrasts with the lattice with a quartic term and no cubic term in the interaction potential as we shall now see.

The lattice with a quartic potential

In this case the standard continuum approximation of (2.7) gives the modified Boussinesq equation,

$$\phi_{tt} = \phi_{xx} + \tfrac{1}{12}\phi_{xxxx} + b(\phi^3)_{xx}, \tag{2.71}$$

which in the ϕ variables gives rise to the pulse solution

$$\phi_{3s}(z) = \sqrt{\frac{2(c^2 - 1)}{b}} \operatorname{sech}\left(2z\sqrt{3(c^2 - 1)}\right). \tag{2.72}$$

Following the transformation back to the q variables we again have a travelling kink with kink-amplitude and energy

$$q_\infty^{(3s)} = \frac{\pi}{\sqrt{6b}}, \qquad H_{3s} = \frac{(5c^2 + 1)}{3b}\sqrt{\frac{c^2 - 1}{3}}. \tag{2.73}$$

Note that H_{3s} has the expected behaviour of $H \to \infty$ as $c \to \infty$ and $H \to 0^+$ as $c \to 1^+$. However, $q_\infty^{(3s)}$ does not share these properties as it is independent of the speed c. Partly this is due to the expression (2.72) being a poor approximation to the waveform of the travelling pulse solution.

If instead we use the $(0, 2)$ Padé approximation of the operator $\Lambda(\mathbf{D})$, we obtain the improved approximation to (2.7)

$$\phi_{tt} = \phi_{xx} + \tfrac{1}{12}\phi_{xxtt} + b(\phi^3)_{xx}, \tag{2.74}$$

which supports a pulse solution of form

$$\phi_{3i}(z) = \sqrt{\frac{2(c^2 - 1)}{b}}\,\text{sech}\left(\frac{2z\sqrt{3(c^2 - 1)}}{c}\right). \tag{2.75}$$

From this, we find more accurate expressions for the kink-amplitude and energy than those in (2.73), namely

$$q_\infty^{(3i)} = \frac{\pi c}{\sqrt{6b}}, \qquad H_{3i} = \frac{2c^3}{b}\sqrt{\frac{c^2 - 1}{3}}. \tag{2.76}$$

In (2.76), we note that H_{3i} shares similar properties with H_{3s}. However, $q_\infty^{(3i)}$ now satisfies the condition $q_\infty^{(3i)} \to \infty$ as $c \to \infty$, but as $c \to 1^+$, $q_\infty^{(3i)} \to \pi/\sqrt{6b} \neq 0$. The amplitude q_∞ and energy H of the kink solutions for the quartic potential is plotted in Figure 2.12. Again, the upper curve corresponds to the improved continuum approximation.

Thus for quartic systems which are initiated with boundary data of the form

$$\begin{aligned} q_n &\to q_\infty &&\text{as} && n \to \infty \\ q_n &\to 0 &&\text{as} && n \to -\infty, \end{aligned} \tag{2.77}$$

with $q_\infty > \pi/\sqrt{6b}$ we expect the large-time evolution of the system to be governed by a kink of amplitude q_∞, which travels at a speed approximately equal

(a) Kink height q_∞.

(b) Kink energy H.

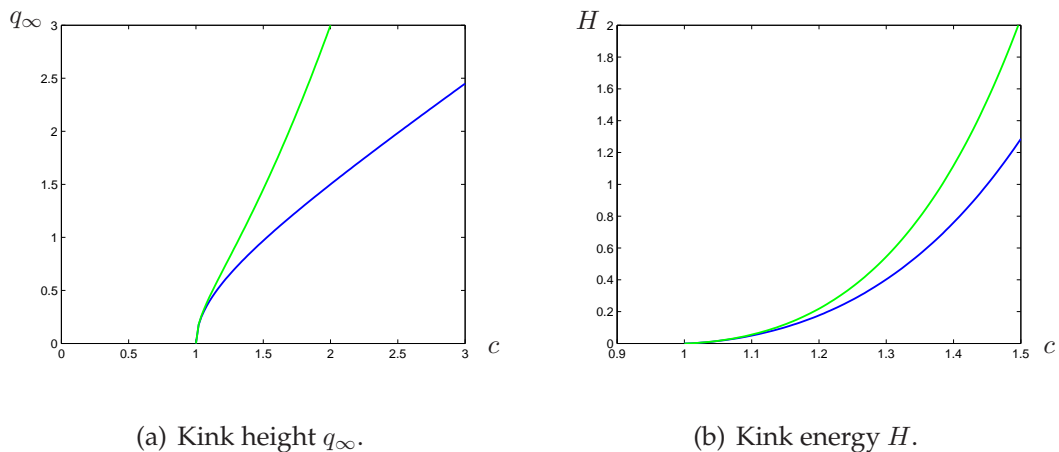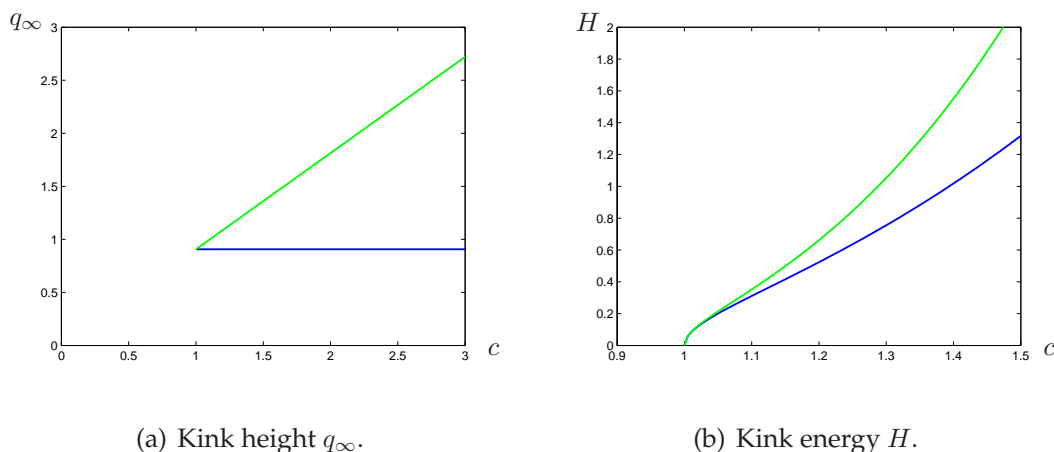**Figure 2.12:** Height and energy of kinks in a chain with quartic potential, $(a = 0, b = 2)$ (see equations (2.73) and (2.76)).

to $q_\infty \sqrt{6b}/\pi$. However, for a system which is initiated with boundary data of the form (2.77) with $q_\infty < \pi/\sqrt{6b}$, there is no travelling kink of this amplitude which can be an attractor for the large-time dynamics. This leaves the open problem of what (if any) coherent structures would be observed at large times in a system with such initial data. For convenience, we will hereupon define $q_\infty^{(c)}$ by $q_\infty^{(c)} := \pi/\sqrt{6b}$.

2.4.3 Combinations of breathers and kinks in the FPU chain

We return to the moving breather modes for which asymptotic approximations were calculated in Section 2.2.5. In this section, we are concerned with small wavenumbers, $(p \ll 1)$. Recalling our comments at the start of Section 2.4.1, we therefore confine our attention to the quartic FPU lattice $(a = 0, b > 0)$ throughout this section.

We show that, in the $q_n(t)$ variables, the moving breather mode appears to be a combination of a kink and a breather, and we analyse the relative importance of each component. From (2.35), the amplitude of the breather component is $\mathcal{O}(\varepsilon)$. We now calculate the size of the kink component q_∞, which is given by the sum in (2.9). We are unable to find an exact expression for q_∞ for general

small p, but we can find q_∞ to leading order. We will see that q_∞ depends upon the relative sizes of p and ε. Note from (2.30) that $\sqrt{Q/2P} = \sqrt{6b}$, since $a = 0$.

From the definition of q_∞, (2.9), and the solution for ϕ_n (2.35), we have

$$q_\infty = \sum_{n=-\infty}^{\infty} \phi_n \sim \sum_{n=-\infty}^{\infty} \frac{2\varepsilon A \cos(pn + \Omega t - s)}{\cosh[\varepsilon A \sqrt{6b}(n - n_0 - vt)]}, \tag{2.78}$$

where n_0 and s represent arbitrary shifts in the waveform of the envelope and the phase of the carrier wave. Replacing the sum by an integral (since the summand is slowly varying in n due to $\varepsilon \ll 1$ and $p \ll 1$) we obtain

$$q_\infty \sim \frac{2\pi}{\sqrt{6b}} \operatorname{sech}\left(\frac{\pi p}{2\varepsilon A \sqrt{6b}}\right) \cos\left((pn_0 - s) + (pv + \Omega)t\right). \tag{2.79}$$

using formula 3.981.3 of [63].

We note that somewhat puzzlingly, the estimate for q_∞ (2.79) appears to time-dependent, though it evolves over an extremely long time-scale, since for small p and small ε, we have

$$pv + \Omega \sim \tfrac{1}{12}p\left(p^2 + 9b\varepsilon^2 A^2\right). \tag{2.80}$$

by (2.36) and $v = -\cos(p/2)$. Thus if, for example, $p = \mathcal{O}(\varepsilon)$ then q_∞ evolves over a timescale of $t = \mathcal{O}(\varepsilon^{-3})$. If we are concerned with the evolution over timescales up to $\mathcal{O}(\varepsilon^{-2})$, then (2.79) can be treated as time-independent.

Clearly from (2.79), the size of q_∞ depends upon the relative magnitudes of p and ε. For instance, if $p \gg \varepsilon$ then the amplitude of the kink is small. Indeed as p approaches $\mathcal{O}(1)$, the amplitude of the kink becomes exponentially small in ε, and hence in this regime, the amplitude of the breather dominates that of the kink. However, if $p \ll \varepsilon$ or $p \sim \varepsilon$, then the amplitude of the kink is $\mathcal{O}(1)$.

We also note from (2.79) that (i) the amplitude q_∞ is maximised when $s = pn_0$, that is, when the maximum of the envelope $n = n_0$ coincides with a maximum of the carrier wave $\cos(pn + \Omega t - s)$; (ii) there is a one-parameter family of breathers with accompanying zero kink-amplitude, that is, for $s = pn_0 + \pi/2$ the amplitude of the kink component vanishes, leaving a pure breather.

We mention in passing that in the limit $p \to 0$, (2.79) agrees with the preliminary result (2.64), both giving a kink height of $2\pi/\sqrt{6b}$. We show a plot of q_∞

(2.79) against wavenumber p for two different values of ε in Figure 2.13. The upper curve corresponds to $\varepsilon = 0.025$, and the lower to $\varepsilon = 0.01$. The remaining parameters in (2.79) are set as $n_0 = 0$, $s = 0$, $A = 1$ and $b = 2$ in both plots. Note that the curves have the same value in the limit $p \to 0$, that is, $2\pi/\sqrt{6b} \approx 1.81$.
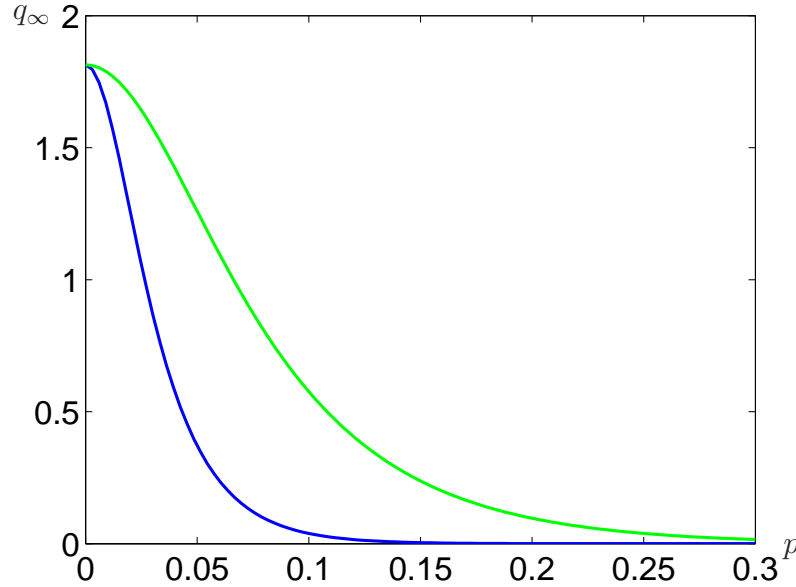
Figure 2.13: Plot of q_∞ given by (2.79) against wavenumber p. The upper and lower curves correspond to $\varepsilon = 0.025$ and $\varepsilon = 0.01$ respectively.

There is an intermediate regime in which $p \ll 1$ and $\varepsilon \ll 1$ in which kink and breather have comparable amplitudes. As we reduce p, it is at this magnitude that coupled breather-kinks (which we term *breathing-kinks* for convenience) become apparent. To determine the magnitude of this wavenumber, we first note that the amplitude of the breather is ε. The amplitude of the kink as given by (2.79) then satisfies

$$q_\infty \sim \frac{4\pi}{\sqrt{6b}} \exp\left(\frac{-\pi p}{2\varepsilon A\sqrt{6b}}\right) \sim \varepsilon, \tag{2.81}$$

from which we deduce that

$$p \sim \frac{2\varepsilon A\sqrt{6b}}{\pi} \log\left(\frac{4\pi}{\varepsilon\sqrt{6b}}\right). \tag{2.82}$$

Hence for $p = \mathcal{O}(\varepsilon \log(1/\varepsilon))$, the breather and kink components have comparable amplitudes, and we have $\varepsilon \ll p \ll 1$.

The most natural range to study further is $p = \mathcal{O}(\varepsilon)$ which differs only slightly from (2.82). We calculate the energy H to leading order. Since $p \sim \varepsilon$, we write $p = \kappa\varepsilon$, where $\kappa = \mathcal{O}(1)$. The total energy, H, is given by (2.2). To simplify the ensuing calculations, we use θ and ψ to denote $pn + \Omega t$ and $\varepsilon A \sqrt{Q/2P}(n + \cos(p/2)t)$ respectively (where ψ is not to be confused with the quantity introduced in (2.10)). After differentiating $q_n(t)$ (2.41) with respect to t, and substituting for $\dot{q}_n$ and ϕ_n in (2.2), we have

$$H \sim \sum_{n=-\infty}^{\infty} \tfrac{1}{2}\varepsilon^2 A^2 \mathrm{sech}^2\psi \left\{ 4\cos^2\theta + \Omega^2 \left[\sin\theta + \cot\left(\frac{p}{2}\right)\cos\theta \right]^2 \right\}. \qquad (2.83)$$

Since $p = \kappa\varepsilon$, it follows that $\cot(p/2) \sim 2/\varepsilon\kappa$ and that $\Omega \sim 2\sin(p/2) \sim \varepsilon\kappa$. Also, we have that $\psi = \varepsilon A\sqrt{6b}(n + t)$ and $\theta = \varepsilon\kappa(n + t) = \kappa\psi/A\sqrt{6b}$. Thus, retaining terms to leading order only, we find that (2.83) becomes

$$H \sim \frac{4\varepsilon A}{\sqrt{6b}} \int_{-\infty}^{\infty} \cos^2\left(\frac{\kappa\psi}{A\sqrt{6b}}\right) \mathrm{sech}^2\psi \, d\psi, \qquad (2.84)$$

where the sum in (2.83) has been replaced by an integral. Applying formula 3.982.1 of [63], we then have an estimate for the energy for wavenumbers $p = \mathcal{O}(\varepsilon)$

$$H \sim \frac{4\varepsilon A}{\sqrt{6b}} + \frac{2\kappa\varepsilon\pi}{3b\sinh\left(\frac{\kappa}{A\sqrt{6b}}\right)} = \mathcal{O}(\varepsilon). \qquad (2.85)$$

2.4.4 Numerical results

We have run numerical simulations of the system with small wavenumbers to investigate the behaviour of breathing-kinks. To illustrate their stability we present the results of a lattice of size $N = 400$, simulated for a time of $T = 2400$ time units. The nonlinear interaction potential has $a = 0$, $b = 2$ and we set $\varepsilon = 0.01$, $p = 0.075$ and $A = 1$. The results are displayed in Figure 2.14.

A snapshot is shown every other time that the wave passes the centre of the lattice (since the lattice has size $N = 400$, and the velocity of the wave is very close to unity, this occurs every 800 seconds). The wave moves to the
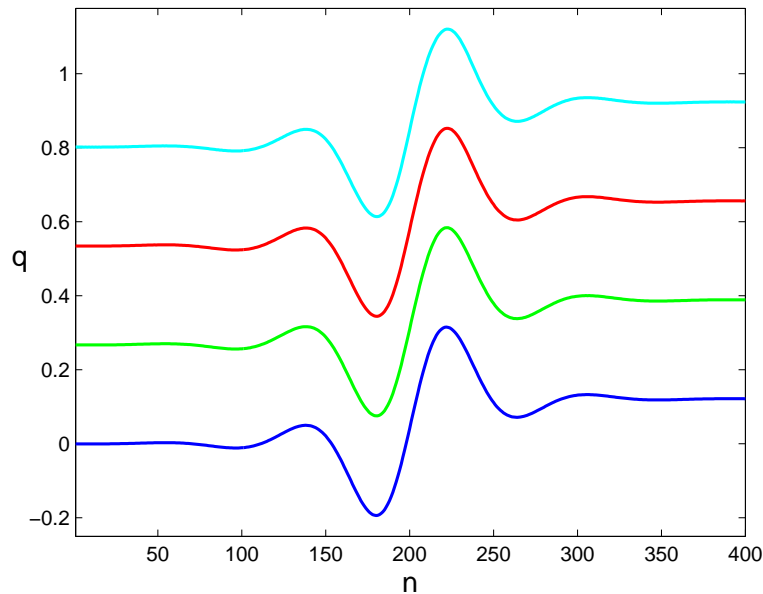
Figure 2.14: Breathing-kink with $q_\infty < q_\infty^{(c)}$ displayed every 800 time units from $t = 0$ to $t = 2400$.

left, so that every circuit, the lattice site displacements $q_n(t)$ register a raise of $q_\infty \approx 0.12$ (recall that we are using periodic boundary conditions). Whilst each individual snapshot of the wave in Figure 2.14 clearly shows both "breather" and "kink" characteristics of the waveform, from the montage of results, the wave actually appears to have the form of a travelling wave. This is because for small p, the phase velocity ($\omega/p = 1 - p^2/24 + \mathcal{O}(p^4)$) and the envelope velocity ($v = 1 - p^2/8 + \mathcal{O}(p^4)$) are almost identical. Any internal breathing in the wave occurs on the timescale $\mathcal{O}(1/p^2)$ which is too long to observe in the simulations we have carried out. With the parameter values as in Figure 2.14, we estimate that it would take a simulation of length in excess of $t = 100/p^2$ (that is, $t \approx 20000$) to observe any possible internal oscillation (i.e. proper breathing) of this mode. The simulation illustrated above, however, confirms that the mode is extremely long-lived and satisfies boundary conditions which are inaccessible to traditional kink travelling wave solutions of FPU lattices with quartic interaction potentials (see the closing comments of Section 2.4.2). Lastly, we

mention that the leading-order estimate for q_∞ given by (2.79) for the parameter values used in this simulation gives a value of 0.1208, which is very close to the measured value 0.12.

Whilst the above example shows that breathing-kinks exist with $q_\infty < q_\infty^{(c)}$, that is, in the range of amplitudes where traditional travelling kinks are forbidden (see Section 2.4.2), we now examine breathing-kinks in the range $q_\infty^{(c)} < q_\infty < 2q_\infty^{(c)}$. In this latter parameter range, both breathing-kinks and traditional kinks exist. We therefore investigate numerically the stability of breathing-kinks, since for example, it is possible that the mode could decompose into a supersonic ($c > 1$) classical (monotone) kink and a subsonic ($c < 1$) classical breather. Figure 2.15 shows the results of such a simulation. For this, we have set $a = 0$, $b = 2$, $\varepsilon = 0.01$, $A = 1$ and $p = 0.025$. Of course, since this corresponds to an even smaller wavenumber than the previous example, the expected time for breathing to be observed is once again beyond a straightforward numerical simulation (requiring an integration in excess of $t = 10^5$). The wave moves to the left, and is depicted in Figure 2.15 at times $t = 0$, 550 and 1250 seconds. During these intervals, it makes a complete circuit (or thereabouts) of the lattice. The vertical displacement is adjusted by q_∞ to allow easy comparison of the waveform. We therefore see that the mode is a travelling wave of permanent form over this timescale. Again, we remark that the observed value of q_∞ is approximately 1.05, whereas the theoretical value given by (2.79) is 1.058, which is in close agreement.

In this section we have demonstrated that in the quartic FPU lattice, traditional kink travelling wave solutions must have an amplitude of $q_\infty > q_\infty^{(c)} := \pi/\sqrt{6b}$ (see the right-hand side of Figure 2.16), and travel at supersonic speeds, ($c > 1$). We have then shown that for small wavenumbers p, our breather modes give rise to waves which share features of both travelling kinks and breathers, and in particular can exist with kink amplitudes in the range $0 < q_\infty < 2q_\infty^{(c)}$ (see the left-hand side of Figure 2.16). These combined breathing-kinks travel subsonically, that is, at speeds less than unity.
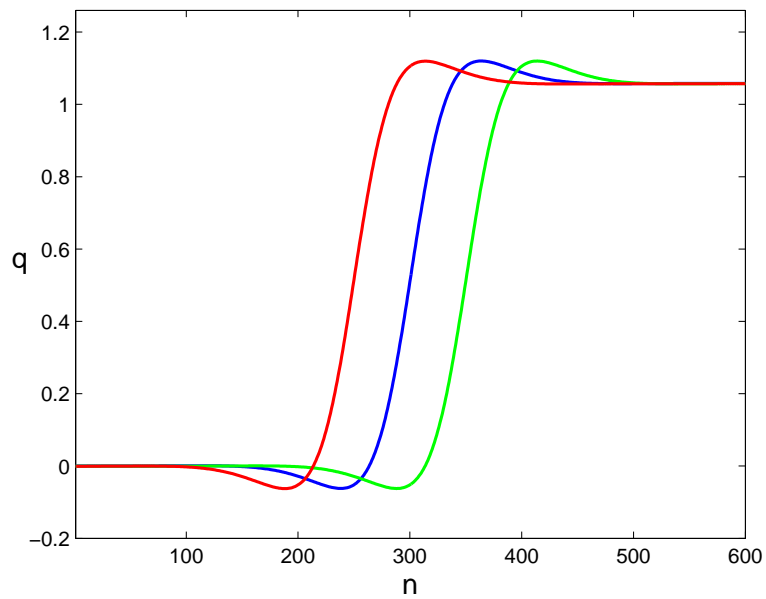
Figure 2.15: Breathing-kink with $q_\infty^{(c)} < q_\infty < 2q_\infty^{(c)}$ displayed approximately every 600 seconds.
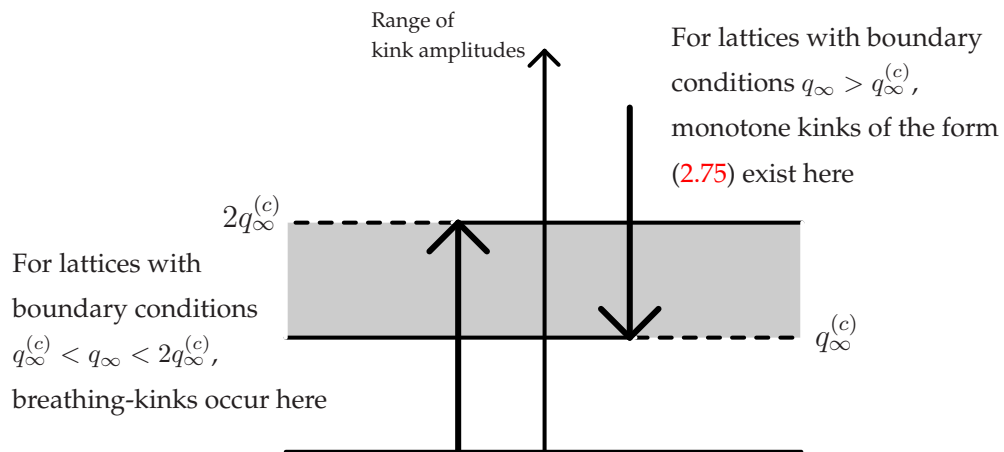
Figure 2.16: Types of waveform which may occur in the quartic FPU chain, depending upon the size of q_∞. Note that $q_\infty^{(c)} := \pi/\sqrt{6b}$.

Thus for lattices with boundary conditions (2.77) in the range $0 < q_\infty < q_\infty^{(c)}$ we have a waveform which may be observed in the large time limit. Also for lattices with boundary conditions in the range $q_\infty^{(c)} < q_\infty < 2q_\infty^{(c)}$ there is now the possibility of two types of kink solution – namely the traditional monotone travelling wave, and the breathing-kink. This corresponds to the shaded band in Figure 2.16. Equation (2.79) gives an asymptotic estimate for the relationship between q_∞ and p (when $p \ll 1$) which any breathing-kink must satisfy. This relationship is illustrated in Figure 2.13.

2.5 Discussion

In this chapter, using asymptotic methods, we have reduced the equations of motion for an FPU lattice with a polynomial potential V to a nonlinear Schrödinger (NLS) equation. Requiring the NLS equation to have localised soliton solutions leads to the identification of a region of parameter space in which the FPU lattice can support breathers. This is a region in which the coefficient of the quartic nonlinearity must exceed the square of the cubic coefficient. There is then a range of wavenumbers for which breather modes exist. The inequality (2.31) generalises an existence condition for stationary breathers obtained by James (see Section 2.1.2), to also include moving breathers.

Conversely when localised modes do not exist, dark soliton solutions of the NLS lead to dark breathers in the FPU lattice, as already noted by other authors (see Flytzanis *et al.* [57]). The calculation of the breather shape given by (2.35) is technically cumbersome since equations from $\mathcal{O}(\varepsilon)$ up to $\mathcal{O}(\varepsilon^4)$ must be solved just to obtain the leading order $\mathcal{O}(\varepsilon)$ solution for the breather.

Numerical simulations in Section 2.3 verified the inequality (2.31), since we observed bright breather solutions for the appropriate parameter values. We have also noted that when there are both cubic and quartic anharmonicities present in the interaction potential, the bright breather solution ceases to exist as the wavenumber is reduced. This is due to the width of the envelope function

diverging at some critical wave number given by (2.33). This gives rise to a maximum velocity for breathers, that is, rather than existing at all speeds from zero up to the speed of sound, there is an upper limit on the speed, namely (2.42).

In Section 2.4, by considering small wavenumbers, we found waveforms supported by the lattice that are more complex than breathers. We have termed these "breathing-kinks" because although they appear to have the form of travelling waves, a snapshot looks like a combination of a breather and a kink. We have shown that the symmetric FPU lattice (with only a quartic nonlinearity, no cubic component) supports traditional monotone travelling kinks only above a critical amplitude $q_\infty^{(c)}$, whereas breathing-kinks have kink amplitudes in the range $0 < q_\infty < 2q_\infty^{(c)}$. The type of waveform exhibited ultimately is determined by the order of magnitude of q_∞, which depends in turn upon the relative magnitudes of p and ε. We found that in the limit $p \to 0$, the kink dominates and the breather component has vanishingly small amplitude. For $\mathcal{O}(1)$ wavenumbers, the amplitude of the breather dominates that of the kink. Numerical simulations presented in Section 2.4 confirmed that breathing-kinks propagate as travelling waves for long periods of time with unit speed, and elementary analysis with wavenumbers p of the same order as the amplitude of the breather (ε) suggests that this should not fail before $t = \mathcal{O}(\varepsilon^{-2})$.

The asymptotic methods we have used are similar to those used by Flytzanis *et al.* [57], Remoissenet [102] and Wattis [136], with the exception that the initial solution ansatz which we make is different to that previously used. We believe the treatment given here is simpler than that given by Flytzanis *et al.* [57] since we analyse the ϕ-equation (2.7) rather than the q-equation (2.1). Our analysis also yields the first correction term as well as the leading order behaviour.

Whilst Flytzanis *et al.* [57] find approximations to travelling breathers in this system and the shape of the breathing-kinks, their solution ansatz assumes the existence of both an oscillatory and a slowly varying component with similar amplitudes.

Also, our approach makes no assumption about the existence of moving breathing-kinks, rather they arise naturally from the analysis. Our ansatz (2.14) has only an oscillatory term ($\phi_n \sim \varepsilon \mathrm{e}^{\mathrm{i}\omega t + \mathrm{i}pn} F + \mathcal{O}(\varepsilon^2) + \text{c.c.}$). The existence of a slowly varying component (which has the form of a kink) then arises naturally. The amplitude of this resultant mode is then determined as part of the problem, and whilst an amplitude of $\mathcal{O}(\varepsilon)$ is possible, we find that amplitudes may lie anywhere from $\mathcal{O}(1)$ to exponentially small in ε.

In contrast, the ansatz of Flytzanis *et al.* [57] postulates the existence of both kink and breather components ($q_n \sim \varepsilon F_{10} + \varepsilon \mathrm{e}^{\mathrm{i}\omega t + \mathrm{i}pn} F_{11} + \mathcal{O}(\varepsilon^2) + \text{c.c.}$), implicitly assuming that their amplitudes have the same order of magnitude.

We mention that whilst such combined breathing-kink modes have been observed in numerical simulations before (see Huang *et al.* [67], Wang [133], Gaididei *et al.* [60] and Bickham *et al.* [17], for example), such a general theory giving their size, shape and speed has, until now, been lacking. A précis of the work in this chapter can be found in Butt & Wattis [24].

In this chapter, using the semi-discrete multiple-scale method, we have made considerable progress on a discrete system for which exact analytic solutions are not known. However, recalling the discussion in Section 1.7.3, we note that we have not yet commented on the validity of this method. This is an active area of research. Most notably for us, a rigorous justification of this method (which is more precise than estimating errors) has been presented recently by Giannoulis & Mielke [61]. Their results can be applied directly to our analytic work on breathers in the FPU chain, though they actually consider a much broader class of waveforms than this. They show that an ansatz of the form (2.14) is justified by proving that solutions of the discrete lattice (2.7) which are initially approximated by the leading-order form of (2.14), where F is a solution of the nonlinear Schrödinger equation (2.29), remain in this form for times up to $t = \mathcal{O}(1/\varepsilon^2)$. In other words, if the approximate solution $\phi_n(0) \sim \varepsilon \mathrm{e}^{\mathrm{i}pn} F(Z, 0) + \text{c.c.}$ (where F solves the NLS equation (2.29)) is close to the exact breather solution at $t = 0$,

then $\phi_n(t) \sim \varepsilon \mathrm{e}^{\mathrm{i}\omega t + \mathrm{i}pn} F(Z, T) + \mathrm{c.c.}$ is also close to the exact breather solution for $t \in [0, t_0/\varepsilon^2]$ for some t_0. The notion of "close" in this context is made precise by specifying a norm in a suitable Banach space. More recently, these results have been extended to include spring-mass systems with general interaction potentials and mth neighbour interactions where m is finite (see Giannoulis & Mielke [62]).

Chapter 3

A two-dimensional square Fermi-Pasta-Ulam lattice

In the last chapter, we considered discrete breathers in a one-dimensional chain. The remainder of this thesis is concerned with discrete breathers in various two-dimensional lattices. Before proceeding further, we review some known results on breathers in higher-dimensional systems.

3.1 Introduction

In this chapter, we discuss the effects of lattice dimension upon the existence and properties of discrete breathers. A large body of early analytical and numerical work seemed to suggest that the dimensionality of a system has no major effect upon breather existence. For example, Takeno [124] uses lattice Green's functions to find approximations to breather solutions in one-, two- and three-dimensional lattices. Later, Takeno [122] uses a similar method to find the profile and properties of localised modes in general d-dimensional lattices.

Other authors present numerically-obtained breather solutions in two-dimensional lattices. For example, Burlakov *et al.* [22] find stationary breather solutions in a two-dimensional square lattice with cubic and quartic nonlinearity. Also, using a numerical procedure derived from the rotating-wave approximation,

Bonart *et al.* [20] show simulations of localised excitations in one, two- and three-dimensional scalar lattices (that is, lattices with one degree of freedom at each site). The stability of these modes is also investigated. However, as with all such early approximate work, one cannot say that the observed waveforms genuinely correspond to exact breather solutions in those systems.

A rigorous analysis of the origins and features of localised excitations in lattices is presented in a series of papers by Flach *et al.* [51, 55]. They argue that the theory for one-dimensional systems discussed in [51, 55] holds irrespective of lattice dimension. Therefore Flach *et al.* [54] conjecture the existence of localised excitations in lattices of arbitrary dimension. This conjecture was confirmed by Mackay and Aubry [84], who outlined how their proof of existence using the anti-continuum method could be extended to establish breather existence in lattices of any dimension.

While some fundamental properties such as the existence of breathers are essentially unaffected by lattice dimension, other properties do depend strongly upon this, for instance, the energy properties of breathers. Intuitively, one might expect the energy of breathers to go to zero with amplitude. However, this may not be so, depending upon the lattice dimension. In fact, breather energies have a positive lower bound if the lattice dimension is greater than or equal to a certain critical value d_c. In other words, the energy of any breather solution must exceed some excitation threshold, as we now explain.

In Section 1.4, we mentioned attempts to link discrete breather solutions of a nonlinear system to plane wave solutions of the linearised equations of motion. In particular, we considered the emergence of discrete breathers through a bifurcation of band-edge plane waves. So far, this has been proved only for certain one-dimensional lattices (see James [69]), and numerical work supports the conjecture in others (Sandusky & Page [109]). Assuming this conjecture to be true, Flach [49] calculates the critical energy E_c at which this bifurcation occurs. The quantity E_c represents the minimum energy of discrete breathers in the lattice. One might expect $E_c = 0$ as occurs in one-dimensional lattices, where

discrete breathers of arbitrarily small energy can be found (see Section 11, Flach & Willis [52]). However, in higher dimensions it is possible that $E_c > 0$. Then no breathers with energies E in the range $0 < E < E_c$ exist.

For instance, Flach *et al.* [56] consider $d-$dimensional hypercubic lattices of N sites, and calculate the bifurcation energy $E_c \sim N^{1-2/d}$. Clearly, for an infinite lattice, as $N \to \infty$, different limiting values of E_c are obtained depending on the dimension d of the lattice. Thus for $d < 2$, the energy of small amplitude breathers tends to zero in the limit of large system size. Hence, breathers of arbitrarily small energy can be found. However, for $d \geq 2$, the energy of small amplitude breathers is nonzero in the limit of infinite lattice size. In other words, breather energies do not approach zero even as the amplitude tends to zero, and hence there exists a positive lower bound on the energy of discrete breathers. In this case, $d_c = 2$.

Kastner [71] obtains different results by considering an alternative class of interaction potentials. In calculating E_c, Flach [49] assumes the on-site and nearest-neighbour interaction potentials to be infinitely differentiable. Kastner [71] obtains estimates for the energy E_c in the degenerate case where the interaction and on-site potentials are not smooth but only twice continuously differentiable (that is, C^2 but not C^3). In this unusual case, it can be shown that the bifurcation energy $E_c \sim N^{1-4/d}$. Hence, in this case, $d_c = 4$, since in the limit $N \to \infty$, for $d < 4$, such systems can support breathers of arbitrarily small energy. However, for $d \geq 4$, there exists a positive lower bound on the energy of discrete breathers.

Both these sets of results obtained by Flach *et al.* [56] and Kastner [71] rely upon the conjecture that discrete breathers bifurcate from band-edge plane waves. The existence of energy threshold phenomena has since been proved rigorously using variational methods for lattices of the nonlinear Schrödinger type (see Weinstein [137]).

We also mention an interesting series of papers by Marin, Eilbeck and Russell who investigate breather mobility in two-dimensional lattices of various

geometries. Their work is motivated by the observation by Russell [106] of dark lines or "tracks" along crystal directions in white mica. A highly readable account of the track forming (or "recording") process is given by Marin *et al.* [90], who also posit that breather modes are responsible for track-creation.

Marin *et al.* [89] test this hypothesis by numerically simulating the hexagonal Potassium planes within mica. Their results suggest that moving breathers do exist, and that the lattice exhibits a strong directional preference whereby breathers travel only along lattice directions. Breathers are easily generated in the lattice by imparting an initial velocity to a few consecutive atoms. After an initial transient (wherein a small amount of energy is radiated), a robust breather, slightly elongated in shape, emerges and travels with almost no further change in shape. The breather is stable against lateral spreading, with perhaps one or two atoms oscillating in the direction perpendicular to the line of travel. Along the breather path, typically no more than three or four consecutive atoms oscillate. The initial velocities can be directed as much as $\pm 15°$ from a lattice direction, and a moving breather still emerges along the crystal axis. Larger deflections (around $\pm 30°$) result in two breathers, each moving along the nearest lattice axes. However, it is not possible to generate breathers which travel in directions other than these.

Similar results (termed "quasi-one-dimensional" effects, see Russell & Collins [107]) are obtained by Marin *et al.* [91] in a later study on two- and three-dimensional lattices with different geometries.

In this section, we have reviewed some of the rigorous results known for discrete breathers in higher-dimensional lattices. Much of this is concerned with abstract properties of breathers in such systems, and not with breather profiles or approximations. While such work has been extensive for one-dimensional systems (see Kivshar & Malomed [75] for a review), we are not aware of many recent analytic studies carried out on higher-dimensional breathers (we have already discussed some of the limitations of early work based on methods such as the rotating-wave approximation in Section 1.7.1). There are some notable

exceptions, for instance, Tamga *et al.* [128] apply analytic methods to find discrete breathers in a two-dimensional sine-Gordon lattice. We will have more to say on this paper in Section 3.8. Also, we have already mentioned the work of Ovchinnikov & Flach [95] in Section 1.7, who present a class of two- and three-dimensional Hamiltonian lattices for which exact solutions can be found. However, these models are admittedly somewhat artificial.

3.1.1 Overview

In this chapter, using analytic methods, we aim to find a leading-order asymptotic form for a restricted class of breather solutions in a two-dimensional Fermi-Pasta-Ulam lattice. To begin with, we proceed in much the same way as in Chapter 2, and we apply the semi-discrete multiple-scale method to determine approximations to small amplitude breathers with a slowly varying envelope.

There are several important differences between the analysis that was carried out for the one-dimensional FPU chain in Chapter 2 and that which is presented in this chapter. As one would expect, the analysis proves to be considerably more complicated. Recalling the analysis of Chapter 2, we were able to reduce the governing equations to a one-dimensional nonlinear Schrödinger equation. Formulae for bright soliton solutions of this equation are known, giving the form of the breather envelope. Thereafter, a straightforward substitution back into the breather ansatz enabled us to construct a leading-order formula for breather solutions in the chain.

Moreover, reduction to the NLS equation could be completed successfully, even for moving breathers, and for lattices with asymmetric potentials. We were therefore able to produce a single formula (2.35), giving the form to second-order of moving breathers in lattices with asymmetric potentials.

For the two-dimensional FPU lattice, this is no longer the case; no such single formula can be obtained. In fact, in Section 3.3, we find that we are able to reduce the lattice equations to a (cubic) two-dimensional NLS equation (that is, with cubic nonlinear term) only for two special cases; firstly, for lattices

with symmetric interaction potential, in which case the reduction can be performed for moving breathers. In this case, we find an ellipticity criterion for the wavenumbers of the carrier wave. Secondly, a cubic NLS equation can be derived for lattices with asymmetric interaction potential, provided we confine our attention to stationary breathers only.

For each of these cases, a different two-dimensional NLS equation (and hence a different leading-order breather form) is generated. As such, the analysis in this chapter may appear somewhat fragmented. To remedy this, we have emphasised clearly which formulae and results apply where any confusion might arise.

In addition, we find more serious limitations of a third-order analysis of the two-dimensional FPU lattice. In Section 3.4, we explain that the cubic NLS equation exhibits behaviour that is unrealistic within the context of discrete systems. Hence, the NLS equations obtained in Section 3.3 do not fully describe the evolution of a breather envelope.

Specifically, the cubic NLS equation over $\mathbb{R}^2$ does not support stable soliton solutions, only unstable *Townes* solitons. When subjected to small perturbations, these may blow up (the amplitude diverges within a finite time), or disperse completely. However, it is known that unstable Townes solitons may be stabilised by including higher-order effects in the model. In Section 3.5 we extend our asymptotic analysis to incorporate higher-order dispersive and nonlinear terms. We show that the two-dimensional FPU lattice equations reduce to a generalised nonlinear Schrödinger equation which includes terms known to stabilise Townes solitons. We carry out extensive numerical simulations (presented in Section 3.7), demonstrating the stability and long-lived nature of breathers in the two-dimensional FPU system.

We also obtain asymptotic estimates for the breather energy in Section 3.6, verifying the expected threshold phenomena described in this section. That is, the breather energy is always greater than some positive lower bound, and in particular does not tend to zero in the limit of small amplitude. We find that the

energy threshold is maximised for stationary breathers, and becomes arbitrarily small as the boundary of the elliptic domain is approached.

In Section 3.8, we review the progress made in this tentative multiple-scale approach to finding breathers in two-dimensional systems. Some of the principal difficulties that have arisen are discussed, and we outline the ways in which these may be overcome. An abridged version of the results obtained in this chapter can be found in Butt & Wattis, [26].

3.2 Derivation of model equations

The two-dimensional square electrical transmission lattice (SETL) comprises a network of repeating unit sections, each consisting of two identical linear inductors and a nonlinear capacitor. The arrangement is illustrated in Figure 3.1. We define lattice sites by the locations of capacitors. Fixing an arbitrary node to be the site $(0,0)$ and using the basis vectors $\mathbf{i} = [1,0]^T$ and $\mathbf{j} = [0,1]^T$, it is clear what is meant by site (m,n) in the lattice. The area surrounding the (m,n)th capacitor is illustrated in greater detail in Figure 3.2. The variable $V_{m,n}(t)$ denotes the voltage across the (m,n)th capacitor and $Q_{m,n}(t)$ denotes the charge stored by the (m,n)th capacitor. Also, $I_{m,n}(t)$ denotes the current through the (m,n)th inductor that lies parallel to the basis vector $\mathbf{i}$, and $J_{m,n}(t)$ denotes the current through the (m,n)th inductor that lies parallel to the vector $\mathbf{j}$.

First, we derive the equations governing voltage $V_{m,n}$, currents $I_{m,n}$ and $J_{m,n}$, and charge $Q_{m,n}$ in the lattice. Considering the section of the lattice shown in Figure 3.2 and applying Kirchoff's law, the difference in shunt voltage between the sites (m,n) and $(m+1,n)$ is given by

$$V_{m+1,n} - V_{m,n} = -L\frac{dI_{m,n}}{dt}, \tag{3.1}$$

while the difference in shunt voltage between the sites (m,n) and $(m,n+1)$ is given by

$$V_{m,n+1} - V_{m,n} = -L\frac{dJ_{m,n}}{dt}, \tag{3.2}$$
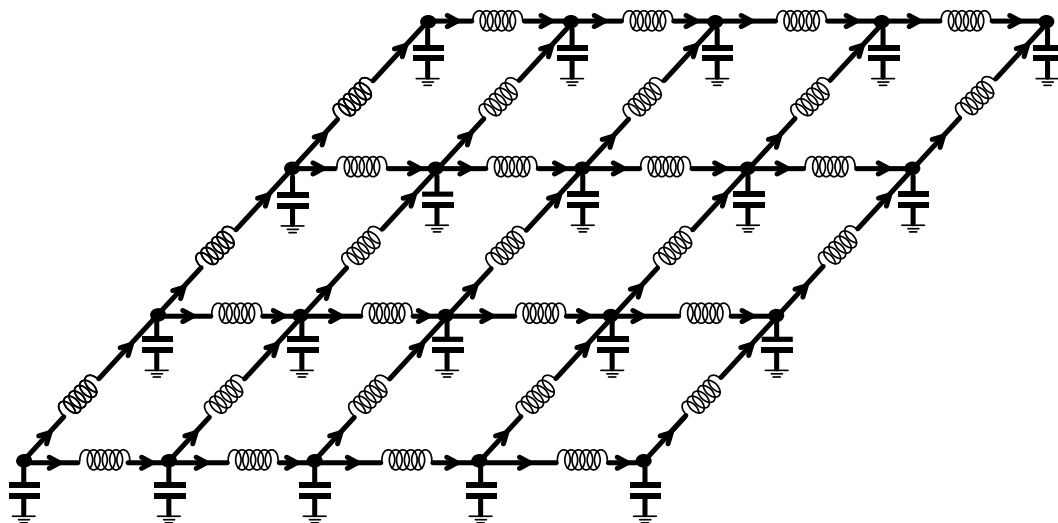
Figure 3.1: The 2D square electrical transmission lattice (SETL).
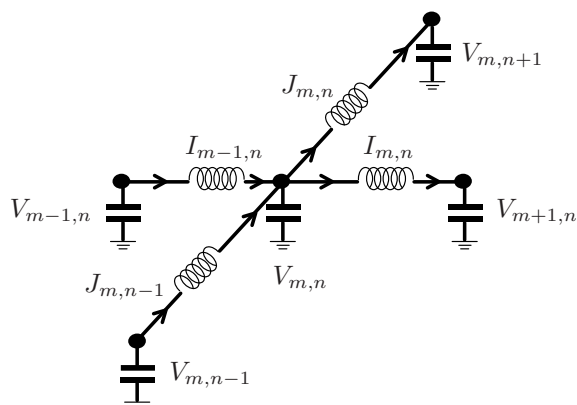
Figure 3.2: Enlarged view of the SETL at site (m, n).

where the inductance L is a constant. Since the total charge is conserved, we also have

$$I_{m-1,n} + J_{m,n-1} - I_{m,n} - J_{m,n} = \frac{\mathrm{d}Q_{m,n}}{\mathrm{d}t}. \tag{3.3}$$

We differentiate (3.3) with respect to time, and use (3.1) and (3.2) to substitute for $\dot{I}_{m-1,n}$, $\dot{J}_{m,n-1}$, $\dot{I}_{m,n}$ and $\dot{J}_{m,n}$ (it is straightforward to find expressions for $\dot{I}_{m-1,n}$ and $\dot{J}_{m,n-1}$ from (3.1) and (3.2)). Proceeding thus, we find that

$$L\frac{\mathrm{d}^2 Q_{m,n}}{\mathrm{d}t^2} = (V_{m+1,n} - 2V_{m,n} + V_{m-1,n}) + (V_{m,n+1} - 2V_{m,n} + V_{m,n-1}), \quad m,\, n \in \mathbb{Z}. \tag{3.4}$$

For the sake of brevity, we employ notation that shortens the appearance of many equations such as (3.4). We use δ_k^2 to denote the centred second-difference of quantities indexed by k. For higher-dimensional lattices, it is necessary to introduce several such indices. Equation (3.4) may thus be rewritten

$$L\frac{\mathrm{d}^2 Q_{m,n}}{\mathrm{d}t^2} = (\delta_m^2 + \delta_n^2)V_{m,n}, \tag{3.5}$$

where we shall sometimes refer to δ_m^2 and δ_n^2 as the "horizontal" and "vertical" second-difference operators respectively. Explicitly, these operators are defined by

$$\delta_m^2 A_{m,n} = A_{m+1,n} - 2A_{m,n} + A_{m-1,n}$$
$$\text{and } \delta_n^2 A_{m,n} = A_{m,n+1} - 2A_{m,n} + A_{m,n-1}, \tag{3.6}$$

where $A_{m,n}$ is an arbitrary quantity referenced by two indices.

Equation (3.5) represents a system of equations in two unknown quantities, $Q_{m,n}$ and $V_{m,n}$. To close the system (3.5), we need to express $Q_{m,n}$ as a function of $V_{m,n}$ or $V_{m,n}$ as a function of $Q_{m,n}$. The first of these is easier to do, though as we shall see, the latter route leads to a more useful formulation.

The nonlinear capacitance is a function of the voltage, and for small voltages, the capacitance-voltage relationship can be approximated by a polynomial expansion

$$C(V_{m,n}) = C_0(1 + 2\tilde{a}V_{m,n} + 3\tilde{b}V_{m,n}^2 + 4\tilde{c}V_{m,n}^3 + 5\tilde{d}V_{m,n}^4), \tag{3.7}$$

where C_0, $\tilde{a}$, $\tilde{b}$, $\tilde{c}$ and $\tilde{d}$ are constants. Since the capacitance $C_{m,n}$ is defined by $C_{m,n} = \mathrm{d}Q_{m,n}/\mathrm{d}V_{m,n}$, it follows upon integrating (3.7) that

$$Q_{m,n} = C_0(V_{m,n} + \tilde{a}V_{m,n}^2 + \tilde{b}V_{m,n}^3 + \tilde{c}V_{m,n}^4 + \tilde{d}V_{m,n}^5). \tag{3.8}$$

Hence (3.5) becomes

$$(\delta_m^2 + \delta_n^2)V_{m,n} = LC_0\frac{\mathrm{d}^2}{\mathrm{d}t^2}(V_{m,n} + \tilde{a}V_{m,n}^2 + \tilde{b}V_{m,n}^3 + \tilde{c}V_{m,n}^4 + \tilde{d}V_{m,n}^5). \tag{3.9}$$

By choosing a suitable timescale, we may put $LC_0 = 1$ without loss of generality.

Though we have reformulated (3.5) in terms of a single unknown quantity $V_{m,n}$ in (3.9), it is advantageous to rewrite (3.9) in terms of the charge $Q_{m,n}$ instead. The reason for this is that (3.9) then takes on a form more familiar from our work on one-dimensional FPU lattice equations (see equation (2.7) of Chapter 2). To do this, $V_{m,n}$ must first be found in terms of $Q_{m,n}$. The right-hand side of equation (3.8) is a quintic polynomial in $V_{m,n}$ which must be inverted to give $V_{m,n}$ in terms of $Q_{m,n}$. Since we are interested only in leading order solutions to (3.9), we approximate the expression for $V_{m,n}$ by a quintic polynomial in $Q_{m,n}$. Hence we assume the following expansion for $V_{m,n}$

$$V_{m,n} = V(Q_{m,n}) \sim \frac{Q_{m,n}}{C_0} + \frac{a'Q_{m,n}^2}{C_0^2} + \frac{b'Q_{m,n}^3}{C_0^3} + \frac{c'Q_{m,n}^4}{C_0^4} + \frac{d'Q_{m,n}^5}{C_0^5}, \tag{3.10}$$

where a', b', c' and d' are combinations of $\tilde{a}$, $\tilde{b}$, $\tilde{c}$ and $\tilde{d}$ obtained by substituting the expansion for $V_{m,n}$ (3.10) into (3.8) and matching coefficients of corresponding powers of $Q_{m,n}$. Proceeding so, we find that

$$a' = -\tilde{a},$$
$$b' = -\tilde{b} + 2\tilde{a}^2,$$
$$c' = -\tilde{c} - 5\tilde{a}(\tilde{a}^2 - \tilde{b}),$$
$$d' = -\tilde{d} + 6\tilde{a}\tilde{c} - 21\tilde{a}^2\tilde{b} + 3\tilde{b}^2 + 14\tilde{a}^4. \tag{3.11}$$

Finally, substituting (3.10) into (3.9) enables the latter to be expressed in terms of $Q_{m,n}$ alone, giving the following equation governing charge $Q_{m,n}$ in the lattice

$$\frac{\mathrm{d}^2Q_{m,n}}{\mathrm{d}t^2} = (\delta_m^2 + \delta_n^2)[Q_{m,n} + aQ_{m,n}^2 + bQ_{m,n}^3 + cQ_{m,n}^4 + dQ_{m,n}^5], \tag{3.12}$$

where $m, n \in \mathbb{Z}$, and $a = a'/C_0$, $b = b'/C_0^2$, $c = c'/C_0^3$ and $d = d'/C_0^4$.

Equation (3.12) is a two-dimensional analogue of the one-dimensional Fermi-Pasta-Ulam equation (2.7) derived in Chapter 2. It may be verified that the lattice equations (3.12) can be derived from the Hamiltonian $\widetilde{H}$ defined by

$$\widetilde{H} = \sum_{m,n} \tfrac{1}{2}(P_{m+1,n} - P_{m,n})^2 + \tfrac{1}{2}(P_{m,n+1} - P_{m,n})^2 + \Upsilon(Q_{m,n}), \tag{3.13}$$

where $\Upsilon(Q_{m,n})$ satisfies $\Upsilon'(Q_{m,n}) = V(Q_{m,n})$ given by (3.10), and $P_{m,n}$ and $Q_{m,n}$ are canonically conjugate momenta and displacement variables of the system, satisfying

$$\frac{\mathrm{d}Q_{m,n}}{\mathrm{d}t} = -\left(\delta_m^2 + \delta_n^2\right)P_{m,n}, \qquad \frac{\mathrm{d}P_{m,n}}{\mathrm{d}t} = -\Upsilon'(Q_{m,n}). \tag{3.14}$$

The Hamiltonian (3.13) for the two-dimensional system is analogous to the Hamiltonian (2.10) of the one-dimensional system. However, we have been unable to find a Hamiltonian of the two-dimensional system which is analogous to the one-dimensional form (2.2).

In the one-dimensional case, the first Hamiltonian form (2.2) represents the total mechanical energy of the chain, and in Section 2.2.2, we showed that it is numerically the same as the second Hamiltonian form (2.10). Returning to the two-dimensional system (3.12), it is natural to ask whether the corresponding Hamiltonian $\widetilde{H}$ (3.13) represents some physical quantity associated with the system. In light of the calculations presented in Section 2.2.2, one might suspect that the Hamiltonian $\widetilde{H}$ is related to the total electrical energy of the system depicted in Figure 3.1. We will pursue this question in greater detail in Section 3.6.1.

For now, we give an expression for the total electrical energy, which we denote E. Taking care to avoid double-counting, the electrical energy in one single unit of the lattice (see Figure 3.2), denoted $e_{m,n}$ is

$$e_{m,n} = \tfrac{1}{2}C(V_{m,n})V_{m,n}^2 + \tfrac{1}{2}L\left(I_{m,n}^2 + J_{m,n}^2\right). \tag{3.15}$$

The total electrical energy E in the lattice is therefore

$$E = \sum_{m,n} e_{m,n} = \sum_{m,n} \tfrac{1}{2}C(V_{m,n})V_{m,n}^2 + \tfrac{1}{2}L\left(I_{m,n}^2 + J_{m,n}^2\right). \tag{3.16}$$

The SETL is a lossless network, and so the total electrical energy E is a conserved quantity. We obtain leading-order estimates for the energy of breathers in the lattice in Section 3.6.

3.3 Asymptotic analysis

3.3.1 Preliminaries

We seek breather solutions of the system of equations (3.12). As in the one-dimensional case, no explicit analytic formulae can be found for breather solutions, and so asymptotic methods are used to determine an approximate analytic form for small-amplitude breathers with slowly varying envelope. We apply the semi-discrete multiple-scale method, and introduce new variables defined by

$$X = \varepsilon m, \quad Y = \varepsilon n, \quad \tau = \varepsilon t \quad \text{and} \quad T = \varepsilon^2 t. \tag{3.17}$$

We look for solutions of (3.12) of the form

$$
\begin{aligned}
Q_{m,n}(t) &= \varepsilon e^{i\psi} F(X,Y,\tau,T) + \varepsilon^2 G_0(X,Y,\tau,T) + \varepsilon^2 e^{i\psi} G_1(X,Y,\tau,T) \\
&\quad + \varepsilon^2 e^{2i\psi} G_2(X,Y,\tau,T) + \varepsilon^3 H_0(X,Y,\tau,T) + \varepsilon^3 e^{i\psi} H_1(X,Y,\tau,T) \\
&\quad + \varepsilon^3 e^{2i\psi} H_2(X,Y,\tau,T) + \varepsilon^3 e^{3i\psi} H_3(X,Y,\tau,T) + \varepsilon^4 I_0(X,Y,\tau,T) \\
&\quad + \varepsilon^4 e^{i\psi} I_1(X,Y,\tau,T) + \varepsilon^4 e^{2i\psi} I_2(X,Y,\tau,T) + \varepsilon^4 e^{3i\psi} I_3(X,Y,\tau,T) \\
&\quad + \varepsilon^4 e^{4i\psi} I_4(X,Y,\tau,T) + \varepsilon^5 J_0(X,Y,\tau,T) + \varepsilon^5 e^{i\psi} J_1(X,Y,\tau,T) \\
&\quad + \cdots + \text{c.c.,}
\end{aligned}
\tag{3.18}
$$

where the phase of the carrier wave ψ is given by $km + ln + \omega t$, and $\mathbf{k} = [k, l]^T$ and ω are its wavevector and temporal frequency respectively. We substitute the ansatz (3.18) into the governing equations (3.12) and equate coefficients of each harmonic frequency at each order of ε. This yields the following equations

$\mathcal{O}(\varepsilon e^{i\psi})$:

$$\omega^2 F = 4\sin^2\left(\frac{k}{2}\right) F + 4\sin^2\left(\frac{l}{2}\right) F, \tag{3.19}$$

$\mathcal{O}(\varepsilon^2 e^{i\psi})$:

$$\omega F_\tau = \sin(k)F_X + \sin(l)F_Y, \tag{3.20}$$

$\mathcal{O}(\varepsilon^2 e^{2i\psi})$:

$$\omega^2 G_2 = [\sin^2 k + \sin^2 l]G_2 + a[\sin^2 k + \sin^2 l]F^2, \tag{3.21}$$

$\mathcal{O}(\varepsilon^3 e^{i\psi})$:

$$\begin{aligned}
2i\omega F_T + F_{\tau\tau} = {} & \cos(k)F_{XX} + \cos(l)F_{YY} \\
& - 8a\left[\sin^2\left(\frac{k}{2}\right) + \sin^2\left(\frac{l}{2}\right)\right][F(G_0 + \overline{G}_0) + \overline{F}G_2] \\
& - 12b\left[\sin^2\left(\frac{k}{2}\right) + \sin^2\left(\frac{l}{2}\right)\right]|F|^2 F,
\end{aligned} \tag{3.22}$$

$\mathcal{O}(\varepsilon^3 e^{3i\psi})$:

$$9\omega^2 H_3 = 4\left[\sin^2\left(\frac{3k}{2}\right) + \sin^2\left(\frac{3l}{2}\right)\right](H_3 + bF^3), \tag{3.23}$$

$\mathcal{O}(\varepsilon^4 e^0)$:

$$G_{0\tau\tau} = G_{0XX} + G_{0YY} + a\left(|F|^2\right)_{XX} + a\left(|F|^2\right)_{YY}. \tag{3.24}$$

A quick inspection of equations (3.19)–(3.24) reveals that (3.19) is the dispersion relation for the system (3.12). Since we are interested only in solutions for which $F \neq 0$, F can be cancelled from (3.19), giving the dispersion relation for the system

$$\omega^2 = 4\sin^2\left(\frac{k}{2}\right) + 4\sin^2\left(\frac{l}{2}\right). \tag{3.25}$$

This is discussed in further detail in Section 3.3.2. Equation (3.20) gives the relationship between the temporal and spatial derivatives of F, and from it we deduce that F is a travelling wave of the form

$$F(X, Y, \tau, T) \equiv F(Z, W, T), \tag{3.26}$$

where $Z = X - u\tau$, $W = Y - v\tau$. The horizontal and vertical velocities u and v of the travelling disturbance F are

$$u = -\frac{\sin k}{w} \quad \text{and} \quad v = -\frac{\sin l}{w}. \tag{3.27}$$

Equation (3.25), together with (3.27), enables the elimination of terms involving G_1 from (3.22) in the same manner as shown in Section 2.2.3 (see equations (2.19) and (2.26) from therein). Hence these terms have not been shown in (3.22).

We denote the angle of propagation of the envelope F through the lattice by Ψ, that is, the angle between the line of travel of F and the vector $\mathbf{i} = [1,0]^T$ (not to be confused with ψ, which denotes the phase of the carrier wave in (3.18)). The angle Ψ is given by $\tan^{-1}(v/u) = \tan^{-1}(\sin l / \sin k)$, using (3.27). Following our discussion of the work of Eilbeck *et al.* in Section 3.1 regarding the permitted directions of travel within two-dimensional lattices, we will investigate whether any such restrictions arise in either our analytic or numerical work. For now, we note that the velocities u and v (and hence also Ψ) are functions of the wavevector $\mathbf{k} = [k,l]^T$. At this stage, we have found no restrictions upon k or l, and hence we can say only that $(k,l) \in \mathcal{T}^2$, where $\mathcal{T}^2 = [0, 2\pi] \times [0, 2\pi]$. However, we shall see in the following that for *all* cases that we consider, there are indeed constraints on k and l which affect the velocities u and v.

Returning to (3.22), we expect this equation to reduce to a version of the nonlinear Schrödinger equation in F (as occurred in the one-dimensional FPU analysis, see Section 2.2.3). Before this can be done however, clearly the quantities G_0 and G_2 must be found in terms of F. The latter is found easily from the algebraic equation (3.21). However, in general, the partial differential equation (3.24) cannot be solved for G_0, save for two special cases. These two cases are detailed in Sections 3.3.3 and 3.3.5.

Firstly, we discuss the properties of the dispersion relation (3.25) for the system in greater detail.

3.3.2   The dispersion relation for the SETL

In this section, we consider the dispersion relation for the system, given by (3.25). A contour plot of ω against k and l is shown in Figure 3.3. It is found that w is periodic in k and l, with period 2π in both directions. The function w is minimised at the points $(0,0)$, $(2\pi, 0)$, $(2\pi, 2\pi)$ and $(0, 2\pi)$, where it assumes the value zero. It is maximised at the point (π, π) (marked at the centre of Figure 3.3), where it takes the value $w = 2\sqrt{2}$. We will denote the wavevector $[\pi, \pi]^T$ by $\mathbf{k_1}$. Note from (3.27) that for the wavevector $\mathbf{k_1}$, the horizontal and

vertical velocities u and v are both zero. In other words, $\mathbf{k_1}$ corresponds to stationary modes. Recalling the closing comments of Section 3.3.1, we remark that in general, the analysis becomes simpler if we consider stationary breathers. In fact, for some of the following analysis, (see Sections 3.3.5 and 3.5), reduction to an NLS equation is possible only if we restrict our attention to stationary breathers. In other words, the significance of the wavevector $\mathbf{k_1}$ in Figure 3.3 is clear; analysis that might otherwise prove to be intractably difficult at a general point in (k, l)-parameter space can often still be carried for $\mathbf{k_1}$.
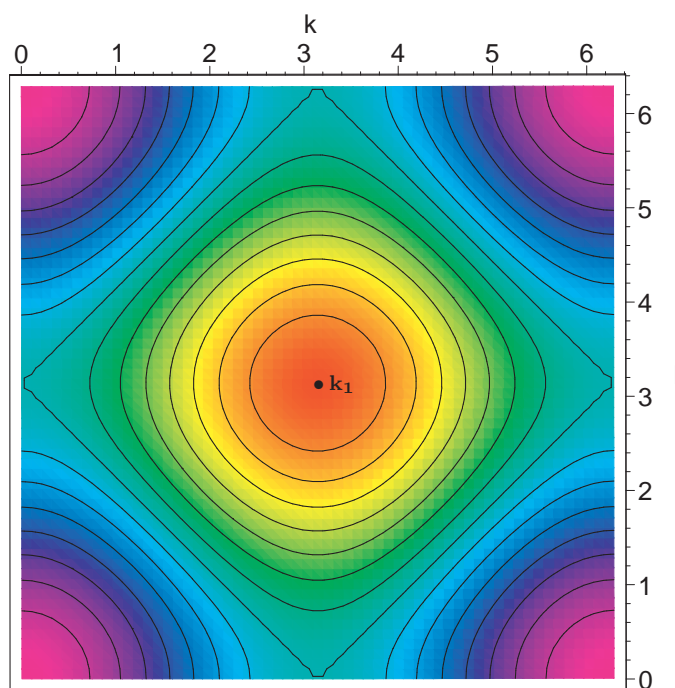
Figure 3.3: Contour plot of ω, showing $\mathbf{k_1} = [\pi, \pi]^T$.

3.3.3 Lattices with a symmetric potential

By a symmetric interaction potential, we mean one for which $\Upsilon'(-Q) = -\Upsilon'(Q)$, that is, one for which $\Upsilon'(Q)$ has odd symmetry and $\Upsilon(Q)$ is even. This corresponds to $a = c = 0$ in (3.10) and (3.12), and $\Upsilon(Q)$ has only fourth-order and sixth-order nonlinear terms in addition to the harmonic term. In this case, it is immediately clear that $G_0 = G_2 = 0$, since a vibration controlled by

a symmetric potential cannot generate any even harmonics (see for example, Chapter 7.1 of Main [86]).

Inspecting (3.22), it remains to find the temporal derivative $F_{\tau\tau}$ in terms of F_{ZZ}, F_{ZW} and F_{WW} before (3.22) can be cast into a standard form. This is done using (3.26) and (3.27), from which we find that

$$F_{\tau\tau} = u^2 F_{ZZ} + 2uv F_{ZW} + v^2 F_{WW}. \tag{3.28}$$

Substituting this into (3.22), we obtain

$$2i\omega F_T + [u^2 - \cos k]F_{ZZ} + [v^2 - \cos l]F_{WW} + 2uv F_{ZW} + 3b\omega^2 |F|^2 F = 0. \tag{3.29}$$

Equation (3.29) is a two-dimensional NLS equation with cubic nonlinearity. The presence of mixed derivative terms of the form F_{ZW} in (3.29) complicates matters. The equation can be reduced to a standard form by eliminating the mixed term F_{ZW}. This is done by introducing new variables ξ and η defined by

$$\xi = \frac{Z}{\sqrt{u^2 - \cos k}} \quad \text{and}$$
$$\eta = \frac{-uvZ + [u^2 - \cos k]W}{\sqrt{(u^2 - \cos k)[\cos k \cos l - u^2 \cos l - v^2 \cos k]}}. \tag{3.30}$$

Applying the above transformation maps (3.29) to a new equation in the variables ξ, η and T, namely

$$2i\omega F_T + \nabla^2 F + 3b\omega^2 |F|^2 F = 0, \tag{3.31}$$

where the Laplacian operator in (3.31) is defined by $\nabla^2 F = F_{\xi\xi} + F_{\eta\eta}$. To motivate the choice of variables ξ and η in (3.30), we mention that in practice, one considers variables defined by $\xi = Z$ and $\eta = -\widehat{A}Z + \widehat{B}W$, where $\widehat{A}$ and $\widehat{B}$ are constants to be determined. Rewriting (3.29) in the variables ξ and η, $\widehat{A}$ and $\widehat{B}$ are chosen so that terms of the form $F_{\xi\eta}$ are eliminated. A further rescaling may be necessary to ensure that the coefficients of $F_{\xi\xi}$ and $F_{\eta\eta}$ are identical.

Equation (3.31) is a canonical two-dimensional cubic NLS equation (3.39), of which we shall have much more to say in Section 3.4. For now, we remark that in this special case (namely, a two-dimensional square FPU lattice with

symmetric potential), we have been able to reduce the equations (3.19)–(3.24) to a cubic two-dimensional NLS equation in the variable F as required. Since the differential operator in (3.31) is isotropic, we seek radially symmetric soliton solutions of the form $F = e^{i\lambda T}\phi(r)$ where $r^2 = \xi^2 + \eta^2$. Approximations to $\phi(r)$ can be generated using the method outlined in Appendix B. Once a formula for F is known, it can be substituted into the ansatz (3.18) giving an expression for the form of a breather in a lattice with symmetric potential. This is presented in Section 3.6.3.

3.3.4 Determining the domain of ellipticity

The two-dimensional NLS equation admits different types of solution depending on whether the equation is elliptic or hyperbolic. We discuss this further in Section 3.4. We shall confine our attention to elliptic NLS equations. By definition, the equation (3.29) is elliptic when $u^2 v^2 < (u^2 - \cos k)(v^2 - \cos l)$. We aim to determine the region $\mathcal{D}$ of (k, l)-parameter space (which is the two-torus $\mathcal{T}^2 = [0, 2\pi] \times [0, 2\pi]$) in which this inequality is satisfied. As we now show, it is possible to determine this region exactly.

Substituting for u, v and ω from (3.25) and (3.27), the criterion for ellipticity becomes

$$\sin^4\left(\tfrac{1}{2}k\right)\left[1 - 2\sin^2\left(\tfrac{1}{2}l\right)\right] + \sin^4\left(\tfrac{1}{2}l\right)\left[1 - 2\sin^2\left(\tfrac{1}{2}k\right)\right] < 0. \qquad (3.32)$$

Since the function on the left-hand side of (3.32) is symmetric in k and l about π, it is only necessary to consider one-quarter of the two-torus $\mathcal{T}^2$, namely the subspace $[0, \pi] \times [0, \pi]$.

Defining θ and σ by $\theta = \sin^2(\tfrac{1}{2}k)$ and $\sigma = \sin^2(\tfrac{1}{2}l)$, then $0 \leq \theta \leq 1$, $0 \leq \sigma \leq 1$, and the condition for ellipticity (3.32) becomes

$$\theta^2(1 - 2\sigma) + \sigma^2(1 - 2\theta) < 0. \qquad (3.33)$$

Substituting $\theta = \rho\cos\zeta$, $\sigma = \rho\sin\zeta$, into (3.33) leads to the inequality

$$\rho > \frac{1}{2\cos\zeta\sin\zeta(\cos\zeta + \sin\zeta)}. \qquad (3.34)$$

It is straightforward to show that $\pi/8 \leq \zeta \leq 3\pi/8$, (since $0 \leq \theta \leq 1$, $0 \leq \sigma \leq 1$). The inequality (3.34) defines in parametric form the curve in (ρ, ζ)-space which constitutes the boundary of the region where the equation (3.29) is elliptic; this boundary is shown in Figure 3.4(a). Reverting back to the variables θ and σ, the boundary of the region of ellipticity of (3.29) in (θ, σ)-space can be found; $\mathcal{D}$ is the shaded area shown in Figure 3.4(b). Reverting back to k and l variables, we find the curve in (k, l)-space which corresponds to the one shown in Figure 3.4(b). This forms the boundary of the domain of ellipticity $\mathcal{D}$ in (k, l)-space, illustrated in Figure 3.4(c) (shaded). Hence, if we are to consider elliptic NLS equations, then (k, l) cannot be an arbitrary point in $\mathcal{T}^2$, rather, (k, l) must lie inside the region $\mathcal{D}$. We remark that some of our numerical work involves points that lie very close to the boundary of $\mathcal{D}$; the effects of this are discussed in Section 3.7.5.

Permitted directions of travel within the lattice

The velocities u and v and hence the angle of travel Ψ are functions of the wavevector $\mathbf{k} = [k, l]^T$ (see equations (3.26) and (3.27), and the comments following). Bearing in mind the numerical work of Eilbeck *et al.* described in Section 3.1, we would like to determine whether the constraints upon (k, l) shown in Figure 3.4 also restrict the range of values that can be assumed by the angle Ψ. We now show that there are no such restrictions, namely, that Ψ can take any value in the interval $[0, 2\pi)$. To simplify matters, we consider a subspace of $\mathcal{D}'$ of $\mathcal{D}$, where $\mathcal{D}' = [\pi/2, 3\pi/2] \times [\pi/2, 3\pi/2]$, shown in Figure 3.5. If $\mathcal{D}'$ is partitioned into four quadrants, then it is easily verified that in any one of the four quadrants, the sign of the velocity u remains the same throughout (that is, it remains either positive or negative throughout any single quadrant). The same is true of the velocity v. The signs assumed by u and v in $\mathcal{D}'$ are summarised in Figure 3.5(b).

From Figure 3.5(b), focusing on the top-right quadrant of $\mathcal{D}'$ for a moment, it may therefore be deduced that wavevectors here correspond to an angle Ψ
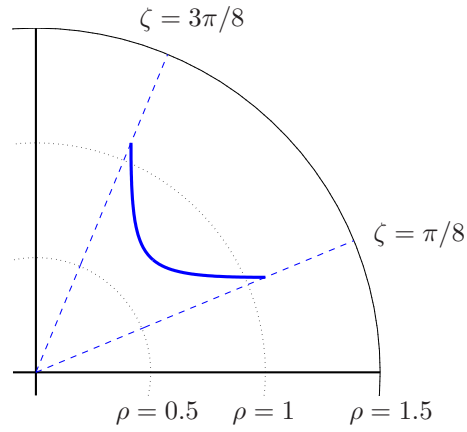
(a) Boundary of the region of ellipticity in (ρ, ζ)-space.
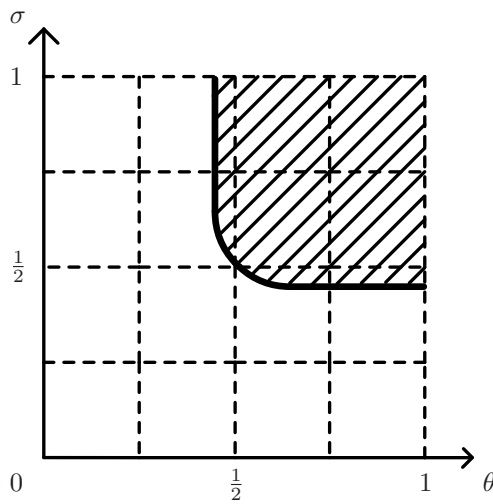
(b) The region of ellipticity shown in (θ, σ)-space.
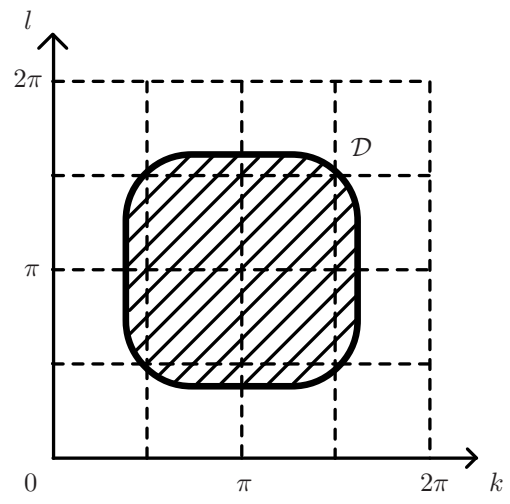
(c) The domain $\mathcal{D}$ in (k, l)-space.

Figure 3.4: The domain $\mathcal{D}$ in which the NLS equation (3.29) is elliptic.

(a) $(\mathrm{sgn}(\sin k), \mathrm{sgn}(\sin l))$.

(b) $(\mathrm{sgn}(u), \mathrm{sgn}(v))$.
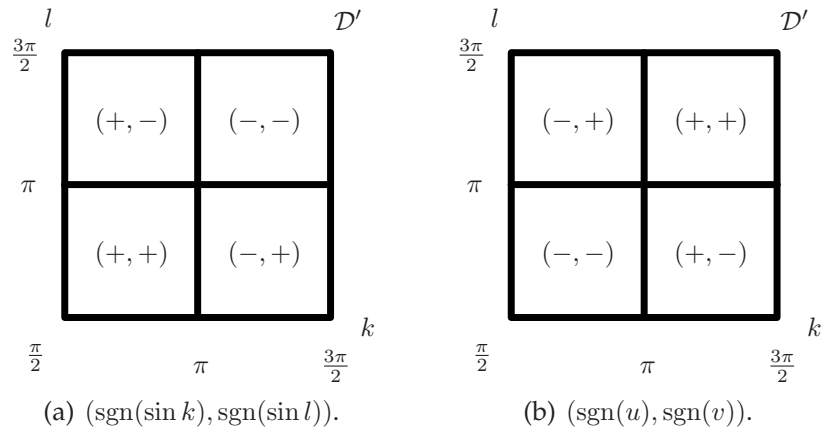
Figure 3.5: Signs of velocities u and v in $\mathcal{D}'$.

which must lie in $[0, \pi/2)$. In fact, we now show that there is some (k, l) in this quadrant which corresponds to *any* angle in $[0, \pi/2)$.

For instance, suppose we start at the point $(k, l) = (7\pi/6, 7\pi/6)$, where $\sin l = \sin k = -1/2$, so that $\Psi = \pi/4$. If we now let $k \to \pi^+$, then $1/\sin k \to -\infty$. Hence, $\tan \Psi \to \infty$, and so $\Psi \to \pi/2$ from below. Alternatively, ψ can also be arbitrarily small; if instead we let $l \to \pi^+$, then $\tan \Psi \to 0$ and therefore $\Psi \to 0$ from above. In this way, a suitable point $(k, l) \in \mathcal{D}$ may be chosen which corresponds to any angle $\Psi \in [0, \pi/2)$. Applying an identical argument in each of the other quadrants of $\mathcal{D}'$, we conclude that Ψ may assume any value in the interval $[0, 2\pi)$.

3.3.5 Lattices with an asymmetric potential

In this section, we consider more general lattices for which the potential function V may be asymmetric. In this case, the terms a and c in (3.10) and (3.12) are not necessarily zero. Clearly, in order to reduce (3.22) to an NLS equation in F alone, it is first necessary to find expressions for G_0 and G_2 in terms of F. The term G_2 is found easily; it is obtained by solving a simple algebraic equation, (3.21). However, the partial differential equation for G_0 (3.24) is more difficult to solve.

Since G_0 is a higher-order correction term to the leading order quantity F, we assume that it travels at the same velocity as F. Hence, $G_0(X, Y, \tau, T) \equiv G_0(Z, W, T)$. Eliminating the term $G_{0\tau\tau}$ and rewriting (3.24) in terms of the variables Z and W therefore yields

$$(u^2 - 1)G_{0ZZ} + (v^2 - 1)G_{0WW} + 2uvG_{0ZW} = a(|F|^2)_{ZZ} + a(|F|^2)_{WW}. \quad (3.35)$$

Unfortunately, there is no straightforward asymptotic procedure for determining solutions of this partial differential equation for arbitrary u and v (that is, for general $(k, l) \in \mathcal{D}$). In fact (recalling the comments made in Section 3.3.2), it is possible to obtain G_0 analytically only when u and v are both zero; in other words, for $\mathbf{k} = \mathbf{k_1} = [\pi, \pi]^T$ (illustrated in Figure 3.3), where the breather envelope F is stationary. When $u = v = 0$, (3.35) reduces to $\nabla^2 G_0 = -a\nabla^2 |F|^2$ and hence $G_0 = -a|F|^2$, where the operator ∇^2 defined by $\nabla^2_{(Z,W)} \equiv \partial_{ZZ} + \partial_{WW}$ is equivalent to $\nabla^2_{(X,Y)} \equiv \partial_{XX} + \partial_{YY}$. From (3.21), clearly $G_2 = 0$.

Substituting for $G_0 = -a|F|^2$ in (3.22) gives

$$2i\omega F_T + \nabla^2 F + \omega^2(3b - 4a^2)|F|^2 F = 0, \quad (3.36)$$

where $\omega = 2\sqrt{2}$. Hence, provided we consider only stationary breathers, we see that it is possible to reduce the lattice equations (3.19)–(3.24) with asymmetric potential to a two-dimensional cubic NLS equation in $F(X, Y, T)$. As with (3.31), in Appendix B we seek radially symmetric soliton solutions to (3.36) of the form $F = e^{i\lambda T}\phi(r)$ where $r^2 = X^2 + Y^2$. This will enable us to produce an analytic approximation for the form of stationary breather solutions in lattices with asymmetric potentials, which we give in Section 3.6.2.

3.4 Blow-up in nonlinear Schrödinger equations: a brief review

We have seen that it is possible to reduce the lattice equations (3.12) to a two-dimensional NLS equation (with cubic nonlinearity) in F for the two cases

considered in Sections 3.3.3 and 3.3.5, where F determines the form of the envelope of a breather solution. At this point, one might consider proceeding as in the one-dimensional case (see Chapter 2), and using a soliton solution for F to substitute back into the ansatz (3.18). This in turn would give a leading-order analytic form for the charge $Q_{m,n}$. Unfortunately, this approach cannot be used directly for the two-dimensional case, because the two-dimensional cubic nonlinear Schrödinger equation does not support stable soliton solutions. In this section, we review some properties of generalised higher-order nonlinear Schrödinger equations, some of which do support stable soliton solutions.

3.4.1   Structural properties

Firstly, we summarise some of the structural properties of the d-dimensional nonlinear Schrödinger equation with general power nonlinearity,

$$\mathrm{i}F_T + D\nabla^2 F + B|F|^{2\sigma}F = 0, \tag{3.37}$$

where $F(\mathbf{x}, T) \in \mathbb{C}$, with $\mathbf{x} = [x_1, \ldots, x_d]^T \in \mathbb{R}^d$ and $T \in [0, \infty)$. The operator $\nabla^2 = \partial_{x_1}^2 + \cdots + \partial_{x_d}^2$. The NLS equation (3.37) is generic. It arises as the evolution equation for the envelope of a wavepacket propagating in weakly dispersive nonlinear media. Consequently, the NLS equation (3.37) occurs in a wide variety of different physical settings, ranging from deep-water gravity waves (Yuen & Lake [138]), to nonlinear optics (Chiao *et al.* [32], Anderson *et al.* [4]), to plasma physics (Zakharov [140]).

Several important conservation laws are known for solutions of the NLS equation. These follow from the symmetries (that is, invariance under certain transformations) of an action integral associated with the NLS equation, upon applying Noether's theorem. An in-depth account of the derivation of conservation laws for the NLS equation is given by Rasmussen & Rypdal (Section 2, [99]) and Sulem & Sulem (Chapter 2, [120]). Two important conserved quantities of solutions of (3.37) are the Hamiltonian $\mathcal{H}$, and the power $\mathcal{N}$, given by

$$\mathcal{H} = \iint \left\{ D|\nabla F|^2 - \frac{B}{\sigma+1}|F|^{2\sigma+2} \right\} \mathrm{d}\mathbf{x} \quad \text{and} \quad \mathcal{N} = \iint |F|^2 \, \mathrm{d}\mathbf{x}. \tag{3.38}$$

There are two cases for (3.37) that one may consider, depending upon the sign of the product DB. When $DB > 0$, (3.37) is known as the *focusing* NLS equation. This case is also known as the anomalous dispersion regime. When $DB < 0$, (3.37) is known as the *defocusing* NLS equation, also referred to as the normal dispersion regime. It is known that solutions of the defocusing NLS equation exist for all time (see Fibich [47], Section 2). That is, they are said to exist globally, for all $T \in [0, \infty)$. Some useful theorems regarding global existence of solutions of certain NLS equations are presented by Strauss (Chapter 3, [119]). However, in this case, it is also known that (3.37) admits no localised solutions (see Davydova *et al.* [38]). In particular, the defocusing $(DB < 0)$ NLS equation does not admit soliton solutions. Since we are interested only in soliton solutions of (3.39), we will concern ourselves primarily with the focusing $(DB > 0)$ NLS equation.

It is known that solutions of the focusing NLS equation with smooth initial conditions can become singular in a finite time. That is, the amplitude of a wavepacket becomes infinite within a time $T^* > 0$, where $T^* \in \mathbb{R}$. The solution is said to exist locally. This phenomenon is known generally as *blow up*, though it is also referred to as *self-focusing* within the context of optics, or *wave collapse* within the context of plasma physics. The blow-up properties of the focusing NLS equation (3.37) depend critically upon the dimensionality d and the nonlinear power σ. There are three broad cases that we may consider:

(i) In the *subcritical* case, $(\sigma D < 2)$, dispersive effects always dominate, and focusing singularities do not form.

(ii) In the *critical* case, $(\sigma D = 2)$, solutions can become singular within a finite time. For this case, there is a very fine balance between nonlinear and dispersive effects. Consequently, small perturbing terms can have a large effect upon blow-up, even leading to the prevention of collapse.

(iii) In the *supercritical* case, $(\sigma D > 2)$, there is a large class of smooth initial conditions for which singularities form. For this case, nonlinearity

dominates over dispersion, hence, perturbing terms have little effect upon blow-up.

For the NLS equations obtained in Sections 3.3.3 and 3.3.5, comparing with (3.37), we have $\sigma = 1, d = 2$, implying that we are in the critical case $\sigma D = 2$. Hence, the rest of this section will be concerned only with the critical nonlinear Schrödinger (CNLS) equation,

$$iF_T + D\nabla^2 F + B|F|^2 F = 0, \tag{3.39}$$

where $F(\xi, \eta, T) \in \mathbb{C}$, and the operator $\nabla^2 = \partial_{\xi\xi} + \partial_{\eta\eta}$.

Of central importance is the establishment of conditions under which the formation of a singularity either occurs or is prevented. Conservation laws of the NLS equation (such as those given in (3.38)), are vital tools with which the blow-up properties of the NLS equation (3.37) can be analysed. A well-known result is that $\mathcal{H} < 0$ is a sufficient condition for blow-up. The proof of this requires the invariance of $\mathcal{H}$, the "uncertainty principle," and the variance identity (we shall return to the last of these shortly). A necessary condition for blow-up in the CNLS is also known. Namely, the initial power $\mathcal{N}_0 = \mathcal{N}(0)$ must exceed some critical threshold $\mathcal{N}_c$ ($\mathcal{N}_0 > \mathcal{N}_c$) in order for blow-up to occur. The threshold $\mathcal{N}_c$ is a number that depends only upon the dimension, and typically, for $B = D = 1$, $\mathcal{N}_c \approx 1.862$. Formal proofs for both of these results are given by, for example, Rasmussen & Rypdal (Sections 4 and 5 of [99]), Sulem & Sulem (Chapter 5, [120]), and Fibich & Papanicolaou (Section 2, [47]).

3.4.2   Townes solitons

It is well known that in one-dimensional systems, the competing effects of nonlinearity and dispersion in (3.37) may balance each other, giving rise to long-lived solitonic structures (see Section 2.2.4). This is not so for the CNLS equation (3.39), for which there exists a very fine balance between focusing and dispersive effects. The CNLS supports a one-parameter family of radially symmetric soliton solutions of the form $F(\mathbf{x}, T) = e^{i\lambda T} R(r)$, where the profile

$R(r) \in \mathbb{R}$ satisfies the nonlinear eigenvalue problem

$$- \lambda R + D\nabla^2 R + BR^3 = 0, \tag{3.40}$$

where $r = |\mathbf{x}| = \sqrt{\xi^2 + \eta^2}$ and $\lambda > 0$. The solution with the lowest power amongst all of these (also known as the *ground state* solution) is known as the *Townes* soliton (see Chiao *et al.* [32]).

The Townes soliton possesses exactly the critical power required for blow-up, that is, it has power $\mathcal{N} = \mathcal{N}_c$. Also, its Hamiltonian $\mathcal{H} = 0$. Clearly, the Townes soliton is highly unstable since a tiny perturbation could give $\mathcal{H} < 0$ or $\mathcal{N} > \mathcal{N}_c$, leading to blow-up.

An exact analytic formula for the Townes soliton solution of (3.39) is not known, and so we apply the *Rayleigh-Ritz* variational method (see for example, Chapter 8.3 of Spencer *et al.* [118]) to generate an approximate formula. Details of this calculation are given in Appendix B.I. There, we seek approximate solutions to the nonlinear eigenvalue problem (3.40) of the form $R(r) = \alpha \, \mathrm{sech}(\beta r)$, where the variational parameters α and β are determined in terms of the parameters that occur in (3.40), namely, λ, D and B. Using this method, we find that

$$\alpha = \sqrt{\frac{12\lambda\ln2}{B(4\ln2 - 1)}} \quad \text{and} \quad \beta = \sqrt{\frac{6\lambda\ln2}{D(2\ln2 + 1)}}, \tag{3.41}$$

and thus an approximate form for the Townes soliton solution of (3.39) is

$$
\begin{aligned}
F &= \alpha \exp(\mathrm{i}\lambda T)\mathrm{sech}(\beta r) \\
&= \sqrt{\frac{12\lambda\log 2}{B(4\log 2 - 1)}} \, \exp(\mathrm{i}\lambda T) \, \mathrm{sech}\left(\sqrt{\frac{6\lambda\log 2}{D(2\log 2 + 1)}}\sqrt{\xi^2 + \eta^2}\right).
\end{aligned} \tag{3.42}
$$

The approximate formula (3.42) for soliton solutions of the two-dimensional NLS equation should be compared with the exact expression for bright solitons of the one-dimensional NLS equation (2.34). In (3.42), the quantity λ represents the temporal frequency at which the soliton solution of (3.39) oscillates, and α is the amplitude of the soliton. From (3.41), we see that the two are related; this is to be expected, since (3.42) is the solution of a nonlinear wave equation. Specifically, the frequency varies as amplitude squared, or equivalently, $\alpha \sim \sqrt{\lambda}$. From

(2.34), we see that the amplitude and temporal frequency of soliton solutions of the one-dimensional NLS equation are related in the same manner. We will return to these scalings in our discussion of the breather energy in Section 3.6.

3.4.3 Stable soliton solutions of generalised nonlinear Schrödinger equations

The CNLS equation (3.39) exhibits behaviour that is impossible in the context of our spatially discrete system: in a discrete system, the focusing of all the system's energy at a single point will not lead to blow-up, and the amplitude would not diverge. In Section 3.7 we present numerical simulations which suggest that long-lived breather modes *are* supported by the scalar two-dimensional Fermi-Pasta-Ulam lattice. We therefore conclude that the cubic two-dimensional NLS equation does not completely capture the full dynamics of the two-dimensional Fermi-Pasta-Ulam lattice.

In physical systems, blow-up cannot proceed indefinitely. That is to say, the amplitude of a wavepacket cannot grow to infinity. When blow-up arises in an evolution equation, it indicates a failure of the model of the system under consideration, or equivalently, that the assumptions made in deriving the model are not valid.

In applications, blow-up is prevented by a variety of mechanisms, for example, by dissipation, or damping, or by higher-order effects. We discuss specific models which incorporate higher-order effects shortly. Useful summaries of mechanisms for the suppression of collapse are given by Rasmussen & Rypdal [99], and more recently by Kivshar & Pelinovsky (Section 2, [77]). For lattice models such as ours, quasi-continuum methods approximate discreteness by a continuous variable. Discrete differences are then replaced by derivatives, where depending upon the accuracy of the model, higher-order derivatives may be retained in the resulting Taylor expansions. As pointed out by Kivshar & Pelinovsky [77], since higher-order dispersive and nonlinear effects can have a critical effect upon self-focusing, these must also be included in the model.

Returning to the two-dimensional FPU lattice, in particular, we are interested in *collapse-arresting*, whereby the blowing-up of a localised solution is prevented by some mechanism. However, this in itself is not enough to guarantee the existence of robust soliton solutions, since it does not preclude the possibility of decay through dispersion or dissipation. Hence, in addition, it is essential to check for *soliton regularisation* or *soliton management*, which ensures that robustness follows collapse inhibition (see Bergé, [14]). In fact, it is known that unstable Townes soliton solutions of the two-dimensional cubic NLS equation may be stabilised through a variety of mechanisms (Schjødt-Eriksen *et al.* [112], Abdullaev *et al.* [1], and Montesinos *et al.* [93] present a few such examples). However, we concern ourselves only with those mechanisms which are relevant and applicable to lattice models.

For example, it is shown by Karpman [70] that an additional higher-order dispersive term can have a stabilising effect. Specifically, the generalised two-dimensional NLS equation with higher order dispersion

$$\mathrm{i}F_T + D\nabla^2 F + B|F|^2 F + P\nabla^4 F = 0, \tag{3.43}$$

can support stable soliton solutions when $PD < 0$. Of greatest relevance to us is a result of Davydova *et al.* [38], who establish the existence of stable solitons for a generalised two-dimensional NLS equation which incorporates higher-order dispersion and an additional quintic nonlinear term, namely

$$\mathrm{i}F_T + D\nabla^2 F + B|F|^2 F + P\nabla^4 F + K|F|^4 F = 0. \tag{3.44}$$

The possibility of stable soliton solutions is investigated in both the anomalous $(BD > 0)$ and normal $(BD < 0)$ dispersive regimes. It is found that stable soliton solutions exist in both regimes.

Both the above results are established using a variational method, sometimes referred to as the method of constrained minimisation, first introduced by Pohožaev [98], though an updated account is given by Kuznetsov *et al.* [82], and also by Bergé (Section 2, [15]). In this method, one seeks localised standing wave solutions of the form $\mathrm{e}^{\mathrm{i}\lambda T}\phi(\mathbf{x})$ ($\lambda > 0$) of the NLS equation in question,

which leads to a nonlinear eigenvalue problem for $\phi(\mathbf{x})$ (as in Section 3.4.2). We define an action integral $\mathcal{S}(\phi) = \mathcal{H}(\phi) + \lambda \mathcal{N}(\phi)$, where $\mathcal{H}$ is the Hamiltonian for the NLS equation. It is easily verified that the corresponding Euler-Lagrange equation $\delta\{\mathcal{H} + \lambda \mathcal{N}\} = 0$ is none other than the nonlinear eigenvalue equation in $\phi(\mathbf{x})$. In other words, soliton solutions of the NLS equation are obtained as extrema (actually expected to be minima) of the action $\mathcal{S}$, or equivalently, as extrema of $\mathcal{H}$ subject to the constraint that the power $\mathcal{N}$ is constant. A common approach to identify minima of $\mathcal{S}$ follows a procedure developed by Derrick [39]. Application of this procedure also reveals conditions for the existence of soliton solutions.

Once the existence of soliton solutions has been proved, their stability properties must then be established. It is shown (see Kuznetsov *et al.* [82], for instance) that the action integral $\mathcal{S}(\phi) = \mathcal{H}(\phi) + \lambda \mathcal{N}(\phi)$ constitutes an appropriate Lyapunov function (up to some constant quantity rendering it positive definite). Soliton stability follows upon applying Lyapunov's theorem. However, this approach to soliton stability in NLS systems has its limitations; a more suitable approach is that of *orbital* stability (a thorough account of this is given by Bergé, Section 2, [15]).

A useful tool for analysing the blow-up properties of localised waves is the variance identity, also known as the virial theorem. One defines an effective "beam" radius r_{eff},

$$r_{\text{eff}}^2(T) = \frac{1}{\mathcal{N}} \iint |\mathbf{x}|^2 |F(\mathbf{x}, T)|^2 \, \mathrm{d}^2\mathbf{x}. \tag{3.45}$$

The virial theorem gives the time evolution of the beam width. By differentiating r_{eff}^2 given by (3.45) with respect to time, we determine whether the radius of a soliton grows without limit (soliton dispersal) or decreases to zero (blow-up) as time evolves. In particular, the effect of the individual equation parameters on soliton stability becomes clear. In fact, by analysing $\ddot{r}_{\text{eff}}^2$ for (3.44), Davydova *et al.* [38] show that the term proportional to PK is the dominant term, and provided $PK > 0$, this corresponds to a defocusing term. In other words, if $PK > 0$, the dominant term provides a "repulsive force" which prevents

collapse in both regimes. Hence stable soliton solutions can be found in the parameter regime $PK > 0$ for both anomalous and normal cases.

As we shall see in Section 3.5, the higher-order NLS equation (3.44) studied by Davydova *et al.* is directly relevant to our analysis of the two-dimensional FPU lattice. Approximations to soliton solutions of (3.44) of the form $F = \alpha \exp(i\lambda T)\text{sech}(\beta r)$ can be generated in the same way that is done for the cubic CNLS equation (3.39) (see Section 3.4.2 and Appendix B.I). Details of this calculation are given in Appendix B.II. When P and K are small compared to B and D in (3.44) (as is the case for the two-dimensional FPU lattice, see Section 3.5), we expect the inclusion of these terms to have only a small effect on the variational parameters α and β obtained by the third-order procedure, (3.41). Hence, when an analytic formula for Townes solitons is required, we will use the third-order approximation given by (3.42), instead of the fifth-order approximation given by (B.15) and (B.16).

3.5 Higher-order asymptotic analysis

In the light of comments made in Section 3.4.3, we extend our analysis of (3.12) to fifth-order and reduce the lattice equations (3.12) to a generalised nonlinear Schrödinger equation which also includes higher-order terms. The principal task is to determine whether the new terms are stabilising, and in particular, whether the generalised NLS equation admits stable soliton solutions for the breather envelope F.

As we saw in Section 3.3, a third-order analysis of moving breathers in lattices with asymmetric potentials in not analytically solvable. At third-order, we were able to perform a reduction to a nonlinear Schrödinger equation in two cases; for moving breathers in lattices with symmetric potentials (see Section 3.3.3) and for stationary breathers in lattices with asymmetric potentials (see Section 3.3.5).

Unsurprisingly, at fifth-order, the analysis is much more involved, and so we consider only lattices with symmetric potentials. Hence, as in Section 3.3.3,

we have $a = c = 0$ in (3.12). This means that no second or fourth harmonic terms are generated by the nonlinearity. Hence, we can use a much simpler ansatz, of the form

$$Q_{m,n}(t) = \varepsilon e^{i\psi} F(X, Y, \tau, T) + \varepsilon^3 e^{3i\psi} H_3(X, Y, \tau, T) + \cdots + \text{c.c.,} \qquad (3.46)$$

where the phase $\psi = km + ln + wt$. In this case, in addition to the equations (3.25), (3.26), (3.27), (3.29) and (3.23), we also have the following equation at fifth-order

$\mathcal{O}(\varepsilon^5 e^{i\psi})$:

$$
\begin{aligned}
F_{TT} =& \tfrac{1}{12} \cos(k) F_{XXXX} + \tfrac{1}{12} \cos(l) F_{YYYY} \\
&+ 3b \cos(k)[F^2 \overline{F}_{XX} + 2F\overline{F}F_{XX} + 4FF_X\overline{F}_X + 2\overline{F}F_X^2] \\
&+ 3b \cos(l)[F^2 \overline{F}_{YY} + 2F\overline{F}F_{YY} + 4FF_Y\overline{F}_Y + 2\overline{F}F_Y^2] \\
&- 3b\omega^2 \overline{F}^2 H_3 - 10d\omega^2 |F|^4 F.
\end{aligned}
\qquad (3.47)
$$

Unfortunately, this equation proves too difficult to handle in general. However, the analysis becomes manageable if we consider stationary breathers only. In other words, the following analysis is carried out for the wavevector $\mathbf{k_1} = [\pi, \pi]^T$ in $\mathcal{D}$. Since we seek stationary breathers, only one further timescale $T = \varepsilon^2 t$ is required, and the simplified ansatz (3.46) takes the form

$$Q_{m,n}(t) = \varepsilon e^{i\psi} F(X, Y, T) + \varepsilon^3 e^{3i\psi} H_3(X, Y, T) + \cdots + \text{c.c.,} \qquad (3.48)$$

where $\exp(i\psi) = \exp(i\pi m + i\pi n + i\omega t) = (-1)^{m+n} \exp(i\omega t)$. Substituting the ansatz (3.48) into equations (3.12) yields the following equations.

$\mathcal{O}(\varepsilon e^{i\psi})$:

$$\omega^2 = 8 \Rightarrow \omega = 2\sqrt{2}, \qquad (3.49)$$

$\mathcal{O}(\varepsilon^3 e^{i\psi})$:

$$2i\omega F_T + F_{XX} + F_{YY} + 3b\omega^2 |F|^2 F = 0, \qquad (3.50)$$

$\mathcal{O}(\varepsilon^3 e^{3i\psi})$:

$$9\omega^2 H_3 = 8H_3 + 8bF^3 \Rightarrow H_3 = \tfrac{1}{8}bF^3, \qquad (3.51)$$

$\mathcal{O}(\varepsilon^5 \mathrm{e}^{\mathrm{i}\psi})$:

$$F_{TT} = -\tfrac{1}{12}F_{XXXX} - \tfrac{1}{12}F_{YYYY} - 3b\nabla^2(|F|^2 F) - 3b\omega^2\overline{F}^2 H_3 - 10d\omega^2 F^3\overline{F}^2, \quad (3.52)$$

since in (3.47) the terms in square brackets on the right-hand side are simply $(|F|^2 F)_{XX}$ and $(|F|^2 F)_{YY}$.

In order to obtain a higher-order generalised NLS equation, we combine the higher-order equation (3.52) with the cubic two-dimensional NLS equation (3.50). If we are to arrive at an NLS equation of a form similar to those discussed in Section 3.4, the temporal derivative F_{TT} in (3.52) must be eliminated. This is done by differentiating (3.50) with respect to T, which gives F_{TT} in terms of spatial derivatives of F. Thus, differentiating (3.50) gives

$$\begin{aligned} 2\mathrm{i}\omega F_{TT} &= -F_{XXT} - F_{YYT} - 3b\omega^2(|F|^2 F)_T = 0 \\ &= -F_{TXX} - F_{TYY} - 3b\omega^2(2|F|^2 F_T + F^2\overline{F}_T). \end{aligned} \quad (3.53)$$

Using (3.50) again gives

$$\begin{aligned} F_{TT} = {}&- \tfrac{1}{32}\nabla^4 F - \tfrac{3}{4}b\nabla^2(|F|^2 F) - 54b^2|F|^4 F \\ &- \tfrac{3}{2}b|F|^2\nabla^2 F - \tfrac{3}{4}bF^2\nabla^2\overline{F}. \end{aligned} \quad (3.54)$$

Equation (3.54) allows for the term F_{TT} on the left-hand side of (3.52) to be replaced, and from (3.51), we have $H_3 = bF^3/8$. The resulting fifth-order equation can then be added to the third-order NLS equation (3.50). Overall, we arrive at the following equation for F

$$4\sqrt{2}\,\mathrm{i}F_T + \nabla^2 F + 24b|F|^2 F + \varepsilon^2\left[\tfrac{5}{96}\nabla^4 F - (51b^2 - 80d)|F|^4 F\right]$$
$$-\tfrac{1}{6}\varepsilon^2 F_{XXYY} + \tfrac{9}{4}b\varepsilon^2\nabla^2(|F|^2 F) - \tfrac{3}{4}b\varepsilon^2(2|F|^2\nabla^2 F + F^2\nabla^2\overline{F}) = 0. \quad (3.55)$$

In other words, if we seek stationary breather solutions in lattices with symmetric potentials of the form (3.10), then the lattice equations (3.12) reduce to the generalised two-dimensional NLS equation (3.55) for the breather envelope F.

Clearly, we would like to know whether (3.55) supports stable soliton solutions. We are aware of many papers which determine the (non)stability of

solitons in perturbed NLS equations (see for example, Section 3.4.3). However, to the best of our knowledge, equation (3.55) has not been studied in the literature before. We note the similarity between it and the perturbed NLS equation (3.44) studied by Davydova *et al.* [38]. Indeed, the first line of (3.55) is identical to the two-dimensional NLS equation (3.44), and hence includes known stabilising terms. However, (3.55) also has several additional terms, including anisotropic dispersive terms. The (de)stabilising effects of these upon Townes solitons are as yet unknown to us.

At the time of writing, we have been unable to find a variational formulation for (3.55), hence Pohožaev's constrained minimisation technique for determining soliton existence and stability (see Section 3.4.3) cannot be applied directly.

In fact, given the complexity of (3.55), a more suitable approach might be to apply the modulation theory for perturbed NLS equations, covered in depth by Fibich & Papanicolaou [46, 47]. This approach reduces a perturbed NLS equation to a simpler set of equations from which one can (in principle) determine the effect of small perturbations upon self-focusing. Fibich & Papanicolaou [46, 47] consider several classes of common perturbing terms, and show that depending upon the type of perturbation terms present, one of several different outcomes can result. For instance, blow-up may occur, or on the other hand, it may be prevented completely. In addition, one might find a solitary wave solution which undergoes small oscillations in radial width. Analysis of (3.55) using one of the above methods is the subject of future work. We return to this matter in Section 3.8.

For now, we rely on Davydova's criteria for soliton existence (see Section 3.4.3). Hence, anomalous dispersion in (3.55) corresponds to $b > 0$ and the condition $PK > 0$ becomes $80d > 51b^2$. Numerical simulations presented in Section 3.7 suggest that long-lived stationary breather solutions *are* supported by lattices with symmetric potentials. This implies that the additional terms in (3.55) do have a stabilising effect upon Townes solitons. At this point, it would be useful to determine formulae for approximations to soliton solutions of (3.55), as was

done in Section 3.4.2. This could then be substituted into the breather ansatz (3.18), giving its leading-order form in this case. However, as noted at the end of Section 3.4.3, if we seek soliton solutions of the form $F = \alpha \exp(i\lambda T)\mathrm{sech}(\beta r)$ for higher-order NLS equations, then typically, the correction terms have only an asymptotically small effect on the variational parameters α and β. In fact, simulations using a fifth-order formula for Townes solitons given by (B.15) and (B.16) (see Appendix B.II) show no significant improvement upon the results obtained using the third-order formula (3.42). Hence, in finding leading-order formulae for stationary breather solutions in lattices with symmetric potentials, we will use the third-order formula for the envelope, given by (3.42).

For more general cases (that is, moving breathers and asymmetric potentials), the resulting NLS equations feature yet more perturbative terms, and their stability properties are still harder to establish. As we show in Section 3.7, numerical work suggests that breathers are long-lived in both these cases, again implying that the NLS equations corresponding to these cases do support stabilised Townes solitons. This is covered in greater depth in Section 3.7. For the same reasons as outlined above, we will use the third-order formula (3.42) for the breather envelope F when finding a leading-order analytic form for breather solutions in these cases.

3.6 Approximate analytic forms for breather solutions

In this section, we use the third-order formula (3.42) for soliton solutions of (3.39) to find expressions for breather solutions in all cases where we have successfully performed a reduction to the NLS equation. Care must be taken when applying this formula for the breather envelope F, because for both of the cases that we have considered (Sections 3.3.3 and 3.3.5), the values of B and D in (3.42) are not the same, and also the form of r^2 may also differ (see Section 3.4.2). In order to prevent any possible confusion, we present formulae for each case separately, starting with the simplest first (namely, lattices with

an asymmetric potential). These formulae are then used to find asymptotic estimates for the breather energy, and also to generate initial data for numerical simulations (see Section 3.7.2). First, we discuss the calculation of the energy E of breathers in the two-dimensional SETL, given by (3.16).

3.6.1   Asymptotic estimates for breather energy

The two-dimensional SETL is a lossless network, and so the total electrical energy is conserved. We derive leading-order estimates for the total electrical energy, which we denote $E^{(0)}$. Accordingly, we use leading-order expressions for each of the quantities in (3.16). It follows from (3.7) that $C(V_{m,n}) \sim C_0$, and from (3.10) that $V_{m,n} \sim Q_{m,n}/C_0$. Substituting this into (3.16), the first term of the summand $e_{m,n}$ is simply $Q_{m,n}^2/(2C_0)$. To leading-order, the energy of the lattice $E^{(0)}$ is therefore given by

$$E^{(0)} \sim \sum_{m,n} e_{m,n}^{(0)} = \sum_{m,n} \frac{Q_{m,n}^2}{2C_0} + \frac{L}{2}(I_{m,n}^2 + J_{m,n}^2). \tag{3.56}$$

We use leading-order expressions for the charge $Q_{m,n}$ obtained later in this section to substitute for the terms in the summand in (3.56). It remains to find leading-order expressions for the currents $I_{m,n}$ and $J_{m,n}$. These can be obtained from the expressions for $Q_{m,n}$ by using the relationship between voltage and current in equations (3.1) and (3.2). Using the fact that $V_{m,n} \sim Q_{m,n}/C_0$, and substituting into equations (3.1) and (3.2), these become

$$Q_{m+1,n} - Q_{m,n} \sim -\frac{dI_{m,n}}{dt}, \tag{3.57}$$

$$Q_{m,n+1} - Q_{m,n} \sim -\frac{dJ_{m,n}}{dt}, \tag{3.58}$$

where as explained in Section 3.2, we have put $LC_0 = 1$. The currents $I_{m,n}$ and $J_{m,n}$ are obtained by inserting the leading-order expression for $Q_{m,n}$ into equations (3.57) and (3.58) and then integrating with respect to time.

Before finding explicit formulae for the breather energy, we return to the relationship between the Hamiltonian $\widetilde{H}$ for the system (3.13), and the leading-order electrical energy $E^{(0)}$ given by (3.56) (see the closing comments of Section 3.2). The dominant contribution to the energy stored in the capacitors is $\Upsilon(Q_{m,n}) = Q_{m,n}^2/2$. Comparing the resulting expression for $\widetilde{H}$ (3.13) with $E^{(0)}$ (3.56), we see that it necessary to establish a link between the currents $I_{m,n}$ and $J_{m,n}$ and the generalised momenta $P_{m,n}$. Applying Hamilton's equations (the second equation in (3.14)) gives $\mathrm{d}P_{m,n}/\mathrm{d}t = -Q_{m,n}$. Also, equation (3.57) relates the charge $Q_{m,n}$ to the current $I_{m,n}$. Replacing $Q_{m,n}$ by $-\mathrm{d}P_{m,n}/\mathrm{d}t$ in (3.57) and then integrating gives $I_{m,n} = P_{m+1,n} - P_{m,n}$. Using (3.58) in an identical manner gives $J_{m,n} = P_{m,n+1} - P_{m,n}$. Therefore, $LI_{m,n}^2 = (1/C_0)(P_{m+1,n} - P_{m,n})^2$ and $LJ_{m,n}^2 = (1/C_0)(P_{m,n+1} - P_{m,n})^2$, and so $E^{(0)} = (1/C_0)\widetilde{H}$.

3.6.2 Lattices with an asymmetric potential

For lattices with an asymmetric potential (see Section 3.3.5), the equations (3.12) reduce to the NLS equation (3.36). Recalling the discussion in Section 3.4.2, we seek soliton solutions of the form $F = \mathrm{e}^{\mathrm{i}\lambda T}\phi(r)$, where $r^2 = X^2 + Y^2$. Comparing (3.36) with (3.39), we see that $D = \sqrt{2}/8$ and $B = \sqrt{2}(3b - 4a^2)$. Note that our analysis for asymmetric lattices was carried out only for the point $(k, l) = (\pi, \pi) \in \mathcal{D}$, at which $\omega = 2\sqrt{2}$, and $u = v = 0$, that is, for stationary breathers. Soliton solutions for F are given by (3.42). Since we also know that $G_0 = -a|F|^2$ and $G_2 = 0$, we can then determine the stationary breather solution to second-order by substituting for these in the breather ansatz (3.18). Overall, we have

$$Q_{m,n}(t) = 2\varepsilon\alpha\cos[\pi m + \pi n + (\omega + \varepsilon^2\lambda)t]\operatorname{sech}(\beta r) - 2a\varepsilon^2\alpha^2\operatorname{sech}^2(\beta r) + \mathcal{O}(\varepsilon^3),$$
(3.59)

where α and β are given by (3.41) with the values of B and D above, and $r = \sqrt{X^2 + Y^2} = \varepsilon\sqrt{m^2 + n^2}$. Surprisingly the presence of the quadratic nonlinearity ($a \neq 0$) in (3.59) does not generate any second harmonic term ($G_2 = 0$), but does cause a small shift of the oscillation to lower Q values.

Breather energy

We calculate the leading-order energy $E^{(0)}$ of stationary breathers in lattices with an asymmetric potential. It is convenient to rewrite the leading-order expression for $Q_{m,n}$ given by (3.59) in the form

$$Q_{m,n} \sim 2\varepsilon\alpha \cos\Theta \operatorname{sech}(\beta r), \tag{3.60}$$

where $\Theta = \pi m + \pi n + \Omega t$ describes the phase of the carrier wave, $\Omega = \omega + \varepsilon^2\lambda$ is the breather frequency including the first correction term, λ parametrises the amplitude of the breather (see Section 3.4.2), α and β are as explained above, and $r = \sqrt{X^2 + Y^2} = \varepsilon\sqrt{m^2 + n^2}$ is a scaled distance from the centre of the breather. We turn our attention to the currents $I_{m,n}$ and $J_{m,n}$.

Substituting the expression for $Q_{m,n}$ (3.60) into the right hand side of (3.57) and integrating with respect to t gives the current $I_{m,n}$

$$I_{m,n} \sim -\frac{4\varepsilon\alpha}{\omega} \sin\Theta \operatorname{sech}(\beta r), \tag{3.61}$$

where we have taken the constant of integration to be zero, and $\Omega \sim \omega$ to leading order. Similarly, substituting for $Q_{m,n}$ given by (3.60) in (3.58) and integrating gives the following expression for the current $J_{m,n}$

$$J_{m,n} \sim -\frac{4\varepsilon\alpha}{\omega} \sin\Theta \operatorname{sech}(\beta r). \tag{3.62}$$

Substituting the expressions for $Q_{m,n}$, $I_{m,n}$ and $J_{m,n}$ given by (3.60), (3.61) and (3.62) respectively into (3.56) gives an expression for the total energy $E^{(0)}$

$$E^{(0)} \sim \sum_{m,n} \frac{2\varepsilon^2\alpha^2}{C_0} \cos^2\Theta \operatorname{sech}^2(\beta r) + \frac{16L\varepsilon^2\alpha^2}{\omega^2} \sin^2\Theta \operatorname{sech}^2(\beta r). \tag{3.63}$$

Using the fact that $(k, l) = (\pi, \pi)$, $\omega^2 = 8$ and $LC_0 = 1$ (or equivalently, $L = 1/C_0$), the sum in (3.63) simplifies considerably, becoming

$$E^{(0)} \sim \sum_{m,n} \frac{2\varepsilon^2\alpha^2}{C_0} \operatorname{sech}^2(\beta r). \tag{3.64}$$

Since the variables $X = \varepsilon m$ and $Y = \varepsilon n$ vary slowly with m, n, so does $r = \varepsilon\sqrt{m^2 + n^2}$ and we can justifiably replace the sum in (3.64) by an integral. Hence,

we find that the energy $E^{(0)}$ is given by

$$E^{(0)} \sim \frac{2\alpha^2}{C_0} \iint \mathrm{sech}^2(\beta\sqrt{X^2 + Y^2})\,\mathrm{d}X\mathrm{d}Y,$$

$$= \frac{4\pi \log 2}{C_0}\frac{\alpha^2}{\beta^2} = \frac{8\pi D \log 2(2\log 2 + 1)}{BC_0(4\log 2 - 1)}, \tag{3.65}$$

after substituting for α and β from (3.41). Substituting further for $B = \sqrt{2}(3b - 4a^2)$ and $D = \sqrt{2}/8$, (3.65) becomes

$$E^{(0)} \sim \frac{\pi \log 2(2\log 2 + 1)}{C_0(4\log 2 - 1)(3b - 4a^2)}, \tag{3.66}$$

which can be approximated by $E^{(0)} \approx 2.935/(3b - 4a^2)C_0$.

Note that this leading-order expression is independent of breather amplitude (parametrised by λ), illustrating the threshold energy property for breathers in two-dimensional systems. That is, no matter how small the amplitude of a breather ($2\varepsilon\alpha$), the energy required to create it is an $\mathcal{O}(1)$ quantity, confirming the observations of Flach *et al.* [56] discussed in Section 3.1.

3.6.3   Lattices with a symmetric potential

For lattices with a symmetric potential, the equations (3.12) reduce to the NLS equation (3.31), and we seek soliton solutions of the form $F = \mathrm{e}^{\mathrm{i}\lambda T}\phi(r)$, where $r^2 = \xi^2 + \eta^2$. Comparing (3.31) with (3.39), we see that $D = 1/2\omega(k, l)$ and $B = 3b\omega(k, l)/2$, where $\omega(k, l)$ is given by (3.25), and $(k, l) \in \mathcal{D}$. In this case, u and v may be nonzero, corresponding to moving breathers. Soliton solutions for F given by (3.42) are substituted into the breather ansatz (3.18), giving at leading-order

$$Q_{m,n}(t) = 2\varepsilon\alpha \cos[km + ln + (\omega + \varepsilon^2\lambda)t]\,\mathrm{sech}(\beta r) + \mathcal{O}(\varepsilon^3), \tag{3.67}$$

where α and β are given in (3.41) with the above values for B and D. Also, in terms of the original variables Z and W, from (3.30) we have

$$r^2 = \xi^2 + \eta^2 = \frac{[v^2 - \cos l]Z^2 + [u^2 - \cos k]W^2 - 2uvZW}{\cos k \cos l - u^2 \cos l - v^2 \cos k}, \tag{3.68}$$

where $Z = \varepsilon(m - ut)$, $W = \varepsilon(n - vt)$, and u, v and ω are given by (3.27) and (3.25) respectively.

Breather energy

We calculate the leading-order energy $E^{(0)}$ of moving breathers in lattices with a symmetric potential, whose form is given by (3.67). We rewrite this as

$$Q_{m,n} \sim 2\varepsilon\alpha \cos\Phi \operatorname{sech}(\beta r), \tag{3.69}$$

where this time $\Phi = km + ln + \Omega t$ is the phase of the carrier wave, $(k,l) \in \mathcal{D}$, $\Omega = \omega + \varepsilon^2\lambda$ is the breather frequency, and α, β and r are as described immediately above. Note that $\Phi = km + ln + \Omega t$ is distinct from $\Theta = \pi m + \pi n + \Omega t$ and $\psi = km + lm + \omega t$, which appear in (3.60) and (3.18) respectively.

Again, the first term of the summand in (3.56) is simply $Q_{m,n}^2/(2C_0)$, and the current $I_{m,n}$ is determined by (3.57). The expression for $Q_{m,n}$ (3.69) is substituted into (3.57). However, considering the expression for r given by (3.68), this time the left-hand side of (3.57) cannot be directly integrated with respect to time. To overcome this, we note that in (3.69), the variable r varies slowly in time compared to the phase of the oscillatory component $\Phi = km + ln + \Omega t$. Integration by parts of (3.57) using (3.69) (and $\int f'(t)g(\varepsilon t)\mathrm{d}t = [f(t)g(\varepsilon t)] - \varepsilon \int f(t)g'(\varepsilon t)\mathrm{d}t$) then implies that to leading order we have

$$I_{m,n} \sim -\frac{2\varepsilon\alpha}{\omega}\operatorname{sech}(\beta r)[(\cos k - 1)\sin\Phi + \sin k \cos\Phi]. \tag{3.70}$$

Similarly, using (3.58), the current $J_{m,n}$ is given by

$$J_{m,n} \sim -\frac{2\varepsilon\alpha}{\omega}\operatorname{sech}(\beta r)[(\cos l - 1)\sin\Phi + \sin l \cos\Phi]. \tag{3.71}$$

Substituting the expressions for $Q_{m,n}$, $I_{m,n}$ and $J_{m,n}$ given by (3.69), (3.70) and (3.71) respectively into (3.56) gives the total energy $E^{(0)}$

$$\begin{aligned}
E^{(0)} \sim \sum_{m,n} &\frac{2\varepsilon^2\alpha^2}{C_0}\cos^2\Phi \operatorname{sech}^2(\beta r) \\
&+ \frac{2L\varepsilon^2\alpha^2}{\omega^2}\operatorname{sech}^2(\beta r)\left[\{(\cos k - 1)\sin\Phi + \sin k \cos\Phi\}^2\right. \\
&\left.+ \{(\cos l - 1)\sin\Phi + \sin l \cos\Phi\}^2\right].
\end{aligned} \tag{3.72}$$

Unfortunately, the summand on the right-hand side of (3.72) does not simplify greatly, and therefore subsequent sums (and integrals) become too difficult to

evaluate exactly. We overcome this by approximating the expression in square brackets. Specifically, using the fact that r varies slowly with m and n, we take the average value of $\cos^2 \Phi$ and $\sin^2 \Phi$, which is $\frac{1}{2}$, whilst the average value of $\sin \Phi \cos \Phi$ is zero. The expression within square brackets simplifies to $\omega^2/2$, hence overall, (3.72) becomes

$$E^{(0)} \sim \sum_{m,n} \frac{\varepsilon^2 \alpha^2}{C_0} \operatorname{sech}^2(\beta r) + \frac{\varepsilon^2 \alpha^2}{C_0} \operatorname{sech}^2(\beta r)$$
$$= \sum_{m,n} \frac{2\varepsilon^2 \alpha^2}{C_0} \operatorname{sech}^2(\beta r). \tag{3.73}$$

This expression has the same form as that obtained for the energy of a breather in a lattice with asymmetric potential (see equation (3.64) of Section 3.6.2). The first line in (3.73) shows the individual contributions to the summand made by the capacitors and inductors of a lattice unit; on average, these amounts are both equal. This is to be expected; it is the electrical analogue of the equipartition of energy between kinetic and potential energy in a mechanical system (for instance, as exhibited by a simple harmonic oscillator).

We replace the double sum in (3.73) by a double integral over all space. For this case, the definition of r is given by (3.68), and so the expression for $E^{(0)}$ is more complex than that obtained in (3.65) for asymmetric potentials. In particular, the envelope of the breather is not in general radially symmetric. The resulting integral is easier to evaluate in ξ and η variables. Hence, after evaluating the Jacobian associated with the transformation from (m, n) to (ξ, η) variables, we have

$$E^{(0)} \sim \frac{2\alpha^2}{C_0} \sqrt{\cos k \cos l - u^2 \cos l - v^2 \cos k} \iint \operatorname{sech}^2(\beta\sqrt{\xi^2 + \eta^2}) \, \mathrm{d}\xi \mathrm{d}\eta. \tag{3.74}$$

The integral on the right-hand side can be evaluated, giving (after substituting for $u = -\sin k/\omega$ and $v = -\sin l/\omega$ inside the radical)

$$E^{(0)} \sim \frac{4\pi\alpha^2 \log 2}{\beta^2 C_0 \omega} \sqrt{\omega^2 \cos k \cos l - \cos k \sin^2 l - \cos l \sin^2 k}. \tag{3.75}$$

After substituting for α and β in terms of B and D (which are $1/2\omega(k,l)$ and $3b\omega(k,l)/2$ respectively), the expression for $E^{(0)}$ in (3.75) becomes

$$E^{(0)} \sim \frac{8\pi(1 + 2\log 2)\log 2}{3\, b\, C_0\, \omega^3(4\log 2 - 1)} \sqrt{\omega^2 \cos k \cos l - \cos k \sin^2 l - \cos l \sin^2 k}. \tag{3.76}$$

The expression for the breather energy (3.76) is independent of the breather amplitude since from (3.41), the ratio α/β is independent of the envelope parameter λ. Hence, as with asymmetric potentials, the energy of moving breathers in lattices with symmetric potentials does not tend to zero as the breather amplitude becomes very small. This demonstrates that there is a minimum threshold energy required to create moving breathers. Although this threshold does not depend on the amplitude, it does depend upon the wavenumbers k and l.

A plot of the expression (3.76) in Figure 3.6 (for $b = 1$) shows that it is strictly positive in the region of ellipticity $\mathcal{D}$ (see Figure 3.4). It has a maximum at $(k, l) = (\pi, \pi)$, (which corresponds to stationary breathers), and decays to zero at the edge of the domain of ellipticity $\mathcal{D}$. Thus the energy threshold for moving breathers is *lower* than that for stationary breathers. The threshold becomes small as the boundary of the domain of ellipticity is approached.

As a check, we mention that if we put $k = l = \pi$ in (3.76), the resulting expression for $E^{(0)}$ reduces to the expression obtained in (3.66) if we put $a = 0$ in the latter, as expected.
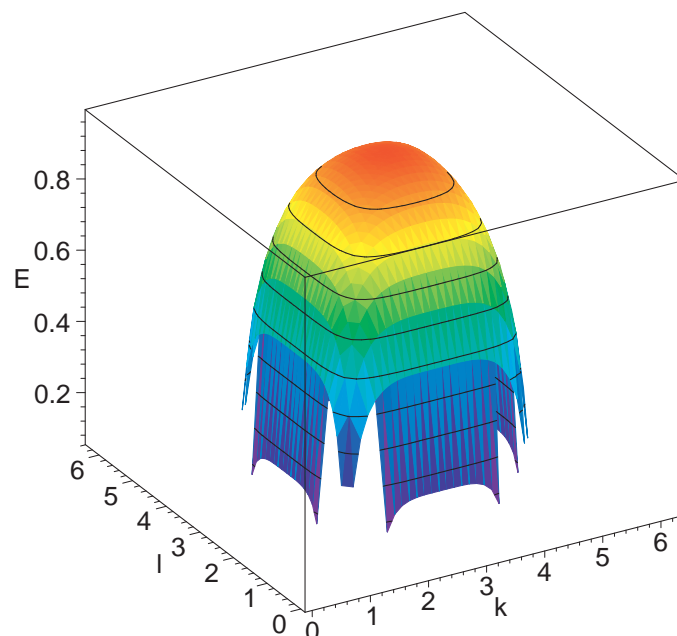

Figure 3.6: Plot of $E^{(0)}$ for lattices with a symmetric potential.

3.7 Numerical results

3.7.1 Preliminaries

In this section, the equations governing charge $Q_{m,n}$ in the lattice, (3.12), are solved numerically. Equations (3.12) comprise an infinite set of coupled second-order nonlinear ordinary differential equations. In order to solve these numerically, we consider these equations defined on a finite square lattice of $N \times N$ sites. To allow for computation within reasonable times, typically we consider lattices for which $N \leq 50$. Firstly, the system of N^2 second-order ordinary differential equations (3.12) is converted to an equivalent system of $2N^2$ first-order equations. This is done by introducing the variable $R_{m,n}$, where $R_{m,n} = dQ_{m,n}/dt$. Equations (3.12) are thus equivalent to

$$\frac{dQ_{m,n}}{dt} = R_{m,n}, \quad \text{and}$$

$$\frac{dR_{m,n}}{dt} = (\delta_m^2 + \delta_n^2)[Q_{m,n} + aQ_{m,n}^2 + bQ_{m,n}^3 + cQ_{m,n}^4 + dQ_{m,n}^5],$$
$$m, \, n = 1, 2, \ldots, N, \qquad (3.77)$$

where the second-difference operators δ_m^2 and δ_n^2 are defined in (3.6). The numerical algorithm used to solve the first-order system (3.77) is based on a fourth-order Runge-Kutta scheme, implemented by MATLAB (see for example, Redfern & Campbell, [101]).

We present the results of numerical simulations carried out for a broad range of parameter values. In particular, we show the results of simulations of stationary and moving breathers in lattices with symmetric and asymmetric potentials. We also show a simulated collision between two breathers.

Since from (3.27) the breather velocity $\mathbf{v} = [u, v]^T$ depends entirely upon the wavevector $\mathbf{k}$, it follows that we obtain moving breathers by choosing the wavevector $[k, l]^T$ such that $(k, l) \in \mathcal{D}$ (depicted in Figure 3.4(c)) and $(k, l) \neq (\pi, \pi)$ (see Section 3.3.2).

We summarise this in Figure 3.7 by showing the points in $\mathcal{D}$ for which we solve the lattice equations (3.77) numerically. These points correspond to the wavevectors $\mathbf{k_1} = [\pi, \pi]^T$, $\mathbf{k_a} = [\pi/2, \pi]^T$, $\mathbf{k_b} = [3\pi/4, 3\pi/4]^T$ and $\mathbf{k_c} = [3\pi/4, 2.881]^T$.

In Sections 3.7.4–3.7.7, we present numerical simulations of stationary and moving breathers in lattices with symmetric potentials, that is $a = c = 0$. Systems with asymmetric potentials ($a, c \neq 0$) are covered in Section 3.7.8.
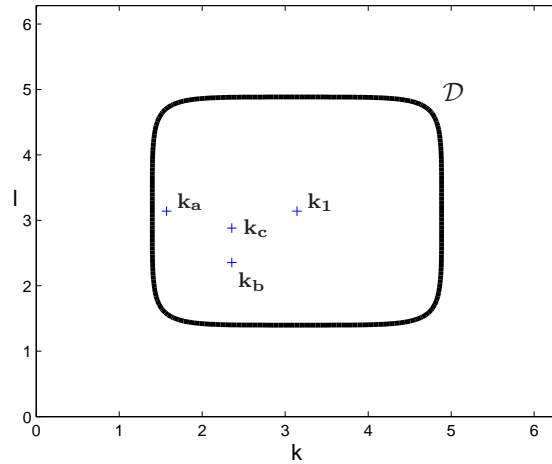

Figure 3.7: Wavevectors in $\mathcal{D}$ for which breathers are simulated.

3.7.2   Initial data and boundary conditions

We generate initial data by using the analytic expressions for breather solutions given in Section 3.6. The relevant function is found in terms of the original discrete variables m and n and then shifted by approximately $N/2$ units in both horizontal and vertical directions, so that it is centred on the $N \times N$ lattice.

We impose periodic boundary conditions in both the horizontal and vertical directions in the lattice. The planar two-dimensional arrangement in Figure 3.1 thus becomes in effect a two-torus. These boundary conditions allow for long-time simulations of moving breathers, by ensuring that disturbances moving

horizontally to the right (left) through the lattice disappear from the far right-
(left-) hand edge and reemerge from the left- (right-) hand edge. A similar effect
is observed for disturbances travelling in the vertical direction.

Selecting the site (1,1) to lie at the bottom left-hand corner of the square
arrangement in Figure 3.8, the remaining lattice sites are labelled with a coordi-
nate pair (m, n) denoting their relative horizontal and vertical positions. That
is, site (m, n) denotes the site which lies in the mth column across and in the nth
row up from site (1,1).

From (3.77), we see that the charge $Q_{m,n}$ stored on each capacitor depends
on the charge stored on the capacitors located at the four nearest neighbour-
ing sites; namely, the capacitors located at either side and also above and be-
low. This is depicted in Figure 3.8 (looking at the lattice from above), where the
solid circles represent capacitors located at lattice sites, and the lines represent
inductors that connect capacitors. Whilst it is clear that equations (3.77) are de-
fined at interior lattice sites, sites along the boundary are missing at least one
neighbour (two neighbours are missing for each of the corner sites). To impose
periodic boundary conditions, we introduce fictitious points (represented by
hollow circles) adjacent to the lattice boundaries as follows, where $1 \leq m \leq N$
and $1 \leq n \leq N$ (this is summarised in Figure 3.8);

$$Q_{N+1,n} = Q_{1,n}, \quad Q_{m,N+1} = Q_{m,1}, \quad Q_{0,n} = Q_{N,n}, \quad Q_{m,0} = Q_{m,N},$$
$$R_{N+1,n} = R_{1,n}, \quad R_{m,N+1} = R_{m,1}, \quad R_{0,n} = R_{N,n}, \quad R_{m,0} = R_{m,N}. \quad (3.78)$$

3.7.3 Numerical computation of breather energy

The SETL is a lossless network, and therefore we expect the total electrical
energy to be conserved. To check the accuracy of our numerical solutions, we
compute the leading-order energy $E^{(0)}$, given by (3.56). We express the sum-
mand $e_{m,n}^{(0)}$ in (3.56) in terms of the output variables of the numerical solver,
which are $Q_{m,n}$ and $R_{m,n}$. Clearly, this is trivial for the first term of $e_{m,n}^{(0)}$. It re-
mains to find the currents $I_{m,n}$ and $J_{m,n}$ in terms of $Q_{m,n}$ and $R_{m,n}$. The details
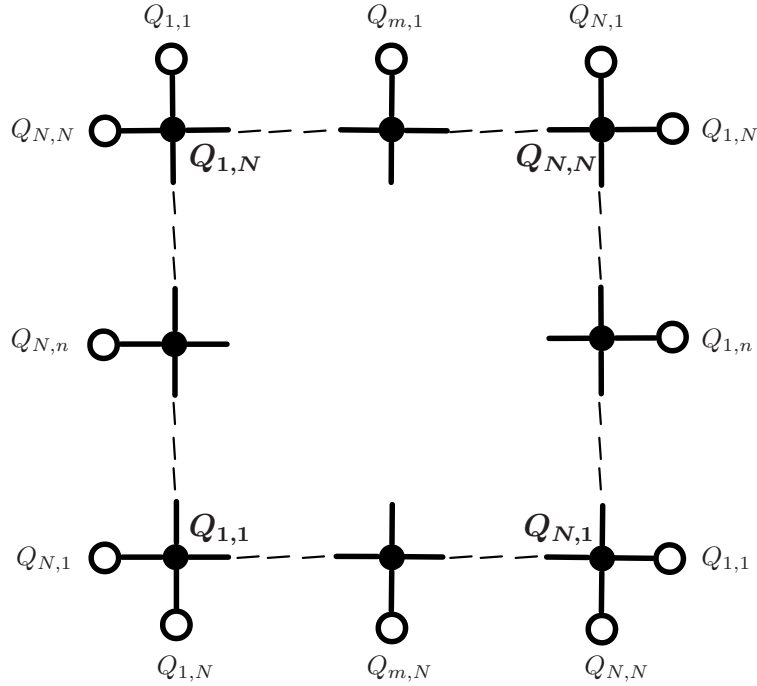
Figure 3.8: Periodic boundary conditions for the two-dimensional SETL.

are slightly different depending upon whether the lattice interaction potential is symmetric or asymmetric.

Lattices with an asymmetric potential

Firstly, we find the current $I_{m,n}$ in terms of $Q_{m,n}$ and $R_{m,n}$. Using the leading-order expression for a stationary breather in (3.60), differentiating with respect to time t gives

$$\dot{Q}_{m,n} = R_{m,n} = -2\varepsilon\alpha\omega \sin\Theta \operatorname{sech}(\beta r). \tag{3.79}$$

Comparing (3.79) with the expression for the current $I_{m,n}$ (3.61), we see that the current $I_{m,n}$ is simply

$$I_{m,n} = \frac{2}{\omega^2} R_{m,n}. \tag{3.80}$$

Similarly, comparing the expression for the current $J_{m,n}$ (3.62) with (3.79) gives

$$J_{m,n} = \frac{2}{\omega^2} R_{m,n}. \tag{3.81}$$

Substituting the expressions for $I_{m,n}$ and $J_{m,n}$ given by (3.80) and (3.81) respectively into the sum $E^{(0)}$ (3.56) gives

$$E^{(0)} = \sum_{m,n} \frac{1}{16C_0}[R^2_{m,n} + \omega^2 Q^2_{m,n}], \tag{3.82}$$

which expresses $E^{(0)}$ as a combination of $Q_{m,n}$ and $R_{m,n}$ as required. The quantity on the right-hand side of (3.82) is summed over the entire lattice for simulations of lattices with asymmetric potentials. We check whether this quantity is conserved, and also whether it matches with the asymptotic estimate given by (3.66) in Section 3.6.2.

Lattices with a symmetric potential

Once again, the first term in the summand (3.56) is trivially found in terms of $Q_{m,n}$. To substitute for the currents $I_{m,n}$ and $J_{m,n}$, we differentiate (3.69). Retaining leading-order terms only, we have that

$$\dot{Q}_{m,n} = R_{m,n} = -2\varepsilon\alpha\omega \sin\Phi \operatorname{sech}(\beta r). \tag{3.83}$$

Using (3.69) and (3.83), the currents $I_{m,n}$ and $J_{m,n}$ given by (3.70) and (3.71) respectively can be expressed in terms of $Q_{m,n}$ and $R_{m,n}$ as follows

$$I_{m,n} = \frac{\cos k - 1}{\omega^2}R_{m,n} - \frac{\sin k}{\omega}Q_{m,n},$$

$$J_{m,n} = \frac{\cos l - 1}{\omega^2}R_{m,n} - \frac{\sin l}{\omega}Q_{m,n}. \tag{3.84}$$

The expressions for $I_{m,n}$ and $J_{m,n}$ given by (3.84) are then substituted into the sum (3.56) to give an overall expression for $E^{(0)}$ in terms of $Q_{m,n}$ and $R_{m,n}$ as follows

$$E^{(0)} = \sum_{m,n} \frac{Q^2_{m,n}}{2C_0} +$$

$$+ \frac{1}{2C_0\omega^4}\left[(\cos k - 1)^2 R^2_{m,n} - 2\omega\sin k(\cos k - 1)Q_{m,n}R_{m,n} + \omega^2\sin^2(k)Q^2_{m,n}\right]$$

$$+ \frac{1}{2C_0\omega^4}\left[(\cos l - 1)^2 R^2_{m,n} - 2\omega\sin l(\cos l - 1)Q_{m,n}R_{m,n} + \omega^2\sin^2(l)Q^2_{m,n}\right]$$

$$\tag{3.85}$$

It may be verified that when $k = l = \pi$, the expression (3.85) reduces to that obtained for asymmetric potentials in (3.82) when we put $a = 0$ in the latter. We sum the right-hand side of (3.85) for simulations of lattices with asymmetric potentials.

Effective breather width

Although we may compute the expressions for $E^{(0)}$ in (3.82) and (3.85) to check that the total energy in the lattice is conserved, this in itself does not tell us much about the preservation (or distortion) of the breather form. To do this, we define breather widths in the m and n directions, the sum of which we denote $\mathcal{W}_{\mathrm{br}}$, given by

$$\mathcal{W}_{\mathrm{br}}^2 = \frac{r_{20}}{E^{(0)}} + \frac{r_{02}}{E^{(0)}} - \left(\frac{r_{10}}{E^{(0)}} \right)^2 - \left(\frac{r_{01}}{E^{(0)}} \right)^2, \tag{3.86}$$

where r_{10}, r_{01}, r_{20} and r_{02} are defined by

$$r_{10} = \sum_{m,n} m e_{m,n} \qquad r_{20} = \sum_{m,n} m^2 e_{m,n}$$

$$r_{01} = \sum_{m,n} n e_{m,n} \qquad r_{02} = \sum_{m,n} n^2 e_{m,n}$$

We will use this measure to quantify the distortion suffered by the breather if it becomes clear that its profile undergoes appreciable degradation over time. In addition to these tools, we will also observe and record other physical properties (for example, the breather velocity) of the breather to check whether they match with the theoretical values predicted by the analysis of Section 3.3.

3.7.4 Stationary breather in a lattice with symmetric potential

Firstly, we seek stationary breathers in the anomalous dispersion regime. From (3.55) in Section 3.5, this corresponds to $b > 0$. We also impose $k = l = \pi$ so that the velocities u and v are both zero, corresponding to $\mathbf{k} = \mathbf{k_1}$ in Figure 3.7. Following the discussion in Section 3.5, stable solitons are expected when $PK > 0$; since $P = 5\varepsilon^2/96$, this inequality corresponds to $K > 0$, or $51b^2 < 80d$. As an example, we set $b = d = 1$. The remaining parameters are the lattice size $N = 31$, $\varepsilon = 0.2$ and $\lambda = 1$.

The variational parameters (3.41) are calculated as $\alpha = 1.0517$ and $\beta = 3.1399$. The breather frequency is $\omega + \lambda\varepsilon^2 = 2.868$, and hence the period of oscillation is $T = 2.190$. Figure 3.9 (a) shows the initial profile of the breather, located at the lattice centre (as is the case for all our simulations). At time $t = 0$, we calculate that the breather energy $E^{(0)} = 0.9772$. Also, we find that the breather width $\mathcal{W}_{\mathrm{br}} = 2.22$.

We also show the breather after it has completed thirty complete oscillations in Figure 3.9 (c). We observe from this that the breather is a long-lived mode, which remains highly localised with almost no spreading in any direction, even after long times. We find that at $t = 30T$, $\mathcal{W}_{\mathrm{br}} = 2.03$, implying that the breather undergoes a slight narrowing over thirty complete cycles, with $\Delta\mathcal{W}_{\mathrm{br}}/\mathcal{W}_{\mathrm{br}} = -0.086$. Also, we find that $E^{(0)} = 0.9905$, which shows that the computed energy remains almost constant as expected; in particular, $\Delta E^{(0)}/E^{(0)} = 0.014$. The asymptotic estimate of the breather energy $E^{(0)}$ given by (3.76) is 0.9772, which shows good agreement with the numerically obtained value. The plots of the cell energy $e_{m,n}$ shown in Figures 3.9 (b) and 3.9 (d) confirm that the breather preserves its form with negligible spreading after thirty oscillations.
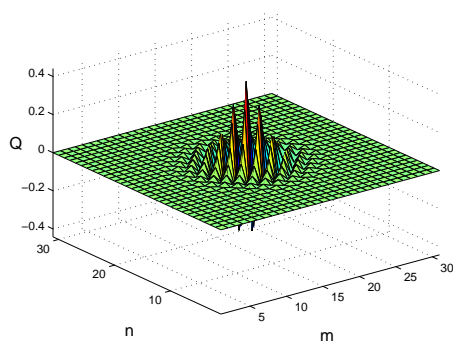
(a) Profile at $t = 0$.
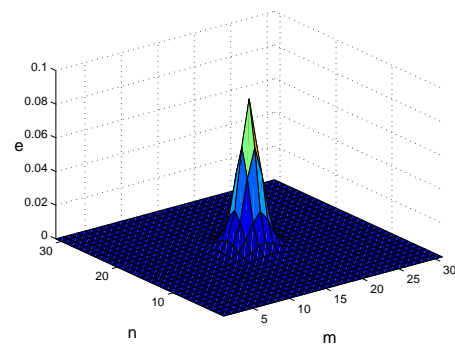
(b) Plot of $e_{m,n}$, $E^{(0)} = 0.9772$.
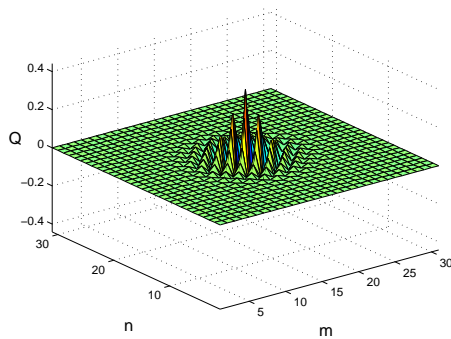
(c) Profile at $30T = 65.7$.
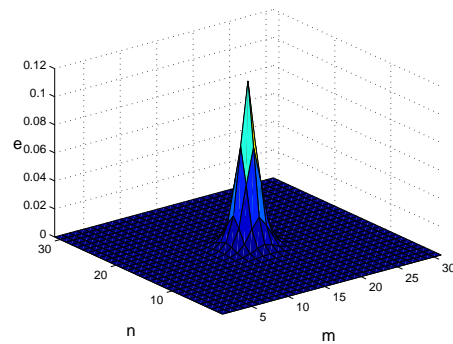
(d) Plot of $e_{m,n}$, $E^{(0)} = 0.9905$.

Figure 3.9: Stationary breather in a lattice with symmetric potential.

3.7.5 Breather moving along a lattice direction $(\Psi = 0°)$

We now present a simulation of a breather which travels along the lattice direction parallel to the $m-$axis (or equivalently, the basis vector **i**). We choose wavevector $\mathbf{k} = \mathbf{k_a} = [\pi/2, \pi]^T$, shown in Figure 3.7. For this choice of k and l we find that $u = -1/\sqrt{6} \approx -0.40823$ and $v = 0$; hence the calculated angle of travel is $\Psi = 0°$. Also, we calculate the breather frequency $\omega = \sqrt{6}$ and period $T = \sqrt{2/3}\,\pi \approx 2.565$.

The remaining parameters are chosen as follows; $b = d = 1$, $N = 31$, $\varepsilon = 0.1$ and $\lambda = 1$. It turns out that the variational parameters α and β are 1.1301 and 2.9220 respectively. The initial profile of the breather (at the centre of the lattice) is shown in Figure 3.10 (a), where the orientation of the carrier wave can be seen clearly. Clearly, the breather envelope is not radially symmetric, rather, it is sharply elongated in the n-direction. This is because, in (k, l)-parameter space, the wavevector $\mathbf{k_a}$ to which this simulated breather corresponds lies extremely close to the boundary of the region of ellipticity $\mathcal{D}$, shown in Figure 3.7. In the expression for r^2 given by (3.68), substituting $k = \pi/2$ and $l = \pi$ gives $r^2 = 6Z^2 + W^2$. From this, it is clear that the level curves of a travelling wave function of r^2 are elongated in the direction of the n-axis.

Figure 3.10 shows the breather at various stages as it travels through the lattice. Clearly, this is a long-lived mode, not suffering major degradation even after sixty seconds or more. The breather also leaves behind very little radiation during its near complete circuit of the lattice. The computed values of the energy $E^{(0)}$ (given in the captions of Figure 3.10) barely fluctuate throughout the simulation. The asymptotic estimate of $E^{(0)}$ given by (3.76) is 0.5319, which is very close to the numerical values.

Figure 3.10 (b) shows the breather as it approaches the left hand edge of the lattice. It is not possible to read the exact position of the breather from a plot of $Q_{m,n}(t)$ with great precision, since the breather is spread over a number of lattice sites. Nevertheless, one may observe that by $t = 9T = 23.086$, the breather has traversed approximately 9 sites. The theoretical value for the velocity is

calculated as -0.40823 units per second, by which time the breather should have travelled 9.4 units, which is in good agreement with the measured value. Figure 3.10 (c) shows the breather disappearing from the left hand edge and reappearing from the right, which is a consequence of the periodic boundary conditions in place. After approximately sixty seconds, the breather has completed nearly a full circuit, remaining localised with very little spreading, leaving only a little radiation in its wake (see Figure 3.10 (d)). However, we observe from Figure 3.10 (d) that the amplitude of the breather appears to have diminished very slightly. In fact, the breather width at $t = 0$ is found to be $\mathcal{W}_{\mathrm{br}} = 3.63$, whereas at $t = 24.83T$, we find that $\mathcal{W}_{\mathrm{br}} = 4.71$. Clearly, the breather has spread slightly, which is consistent with the observed emission of radiation as it propagates. It is not clear from these simulations whether the shedding of radiation is due to a short-term transient effect as the approximate initial conditions adjust to the true shape of a travelling breather, or whether the breather will continue to lose energy as it moves through the lattice.

From the plot of the breather profile in Figure 3.10 (d), we record that the breather has travelled a total of 24 units parallel to the basis vector $\mathbf{i}$, and so the measured velocity is -0.38 units per second, which is slightly lower than the expected value. Again, this is to be expected, given the comments immediately above.
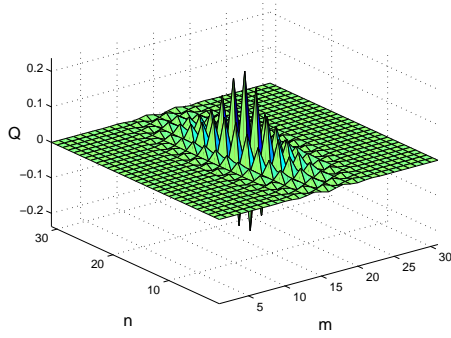
(a) Profile at $t = 0$, $E^{(0)} = 0.5358$.
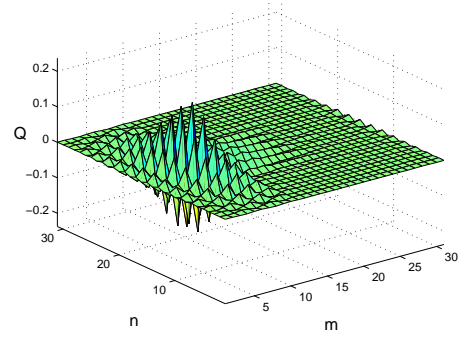
(b) Profile at $9T$, $E^{(0)}=0.5357$.
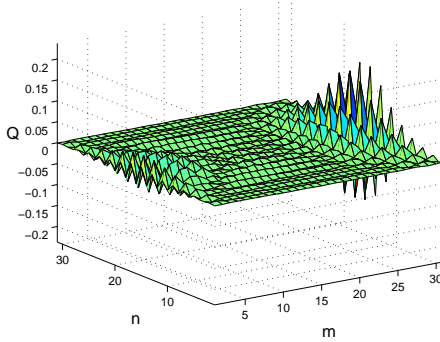
(c) Profile at $t = 17.41T$, $E^{(0)} = 0.5360$.
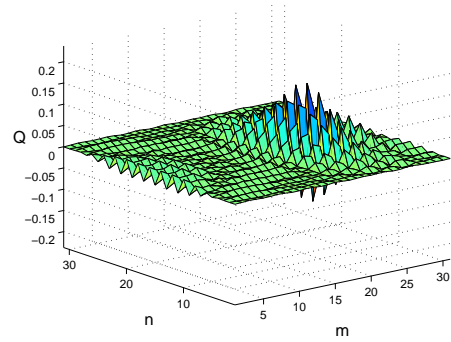
(d) Profile at $t = 24.83T$, $E^{(0)} = 0.5359$.

Figure 3.10: Breather moving along a lattice direction, $\Psi = 0°$.

3.7.6   Breather moving at $\Psi = 45°$

We now show that is it possible to simulate breathers moving in directions other than $\Psi = 0°$ (as in Section 3.7.5). Recall from (3.27) that the angle of propagation of the envelope Ψ is given by $\tan^{-1}(\sin(l)/\sin(k))$. We investigate the direction $\Psi = 45°$, and so we set $k = l$. Noting the extremely elongated breathers of Section 3.7.5, we choose a point in (k, l)-parameter space that is not too near the boundary of ellipticity. Hence, we select $k = l = 3\pi/4$, which corresponds to the wavevector $\mathbf{k_b}$ in Figure 3.7. The horizontal and vertical velocities are therefore both -0.2706 units per second. Also, the breather frequency is $\omega = 2.6131$ and hence the period of oscillation is $T = 2.3953$. The remaining parameters are

$b = d = 1$, $N = 31$, $\varepsilon = 0.1$ and $\lambda = 1$. We find that the variational parameters are $\alpha = 1.0941$ and $\beta = 3.0180$.

Although it is not easy to track the position of a moving breather accurately from a plot of the breather profile $Q_{m,n}$, a much greater level of accuracy can be attained if we plot the cell energy $e_{m,n}$. Since breathers are spatially localised waveforms, it follows that their energy is also localised. Typically, a plot of the cell energy yields a single smooth peak, the centre of which gives the breather position. In practise, even greater accuracy can be achieved through the use of a plot of $e_{m,n}^3$ since this is more sharply peaked than $e_{m,n}$.

The breather starts at the centre of the lattice (not shown), and is shown at later times $t = 20$, 40, 60 and 80 seconds in Figure 3.11. Overall, it can be seen that the breather remains a localised coherent structure even after 80 seconds, without any obvious degradation as it completes a whole loop. The energy is also given at each of these times. This remains virtually constant throughout the motion. The numerically computed value is also very close to the estimate (3.76) obtained through the asymptotic analysis, which is $E^{(0)} = 0.8894$.

To measure the velocity of the breather, we record the horizontal and vertical displacements travelled by the breather at intervals of 20 seconds, and record these in Table 3.1. The calculated average horizontal and vertical velocities are also recorded therein. By way of illustration, we show plots of the energy $e_{m,n}$ and $e_{m,n}^3$ in Figure 3.11 (e) and Figure 3.11 (f). The breather position is easiest to read off when either of these plots are viewed from above (not shown). From Table 3.1, we have $\tan \Psi = 1$ and hence $\Psi = 45°$. The final computed value for the velocities is -0.2625 units per second, which is very close to the theoretical prediction of -0.2706 units per second (a relative error of 3%).
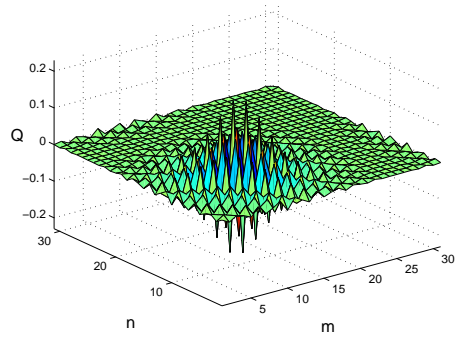
(a) Profile at $t = 20$, $E^{(0)} = 0.8911$.
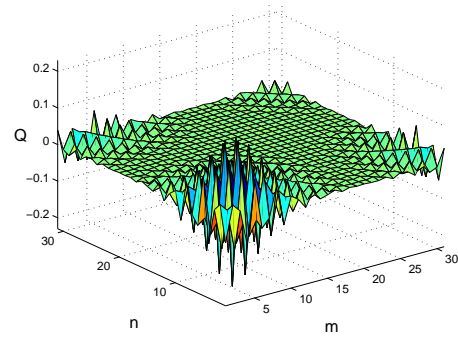
(b) Profile at $t = 40$, $E^{(0)} = 0.8900$.
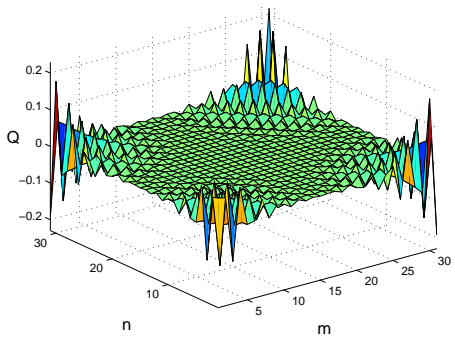
(c) Profile at $t = 60$, $E^{(0)} = 0.8880$.
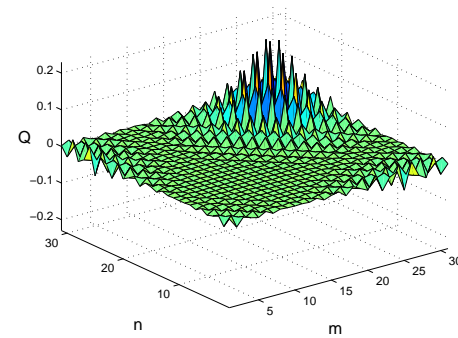
(d) Profile at $t = 80$, $E^{(0)} = 0.8870$.
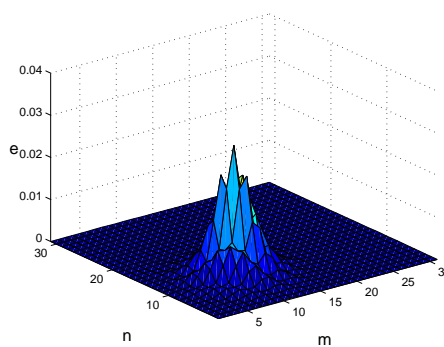
(e) Plot of $e_{m,n}$ at $t = 20$.
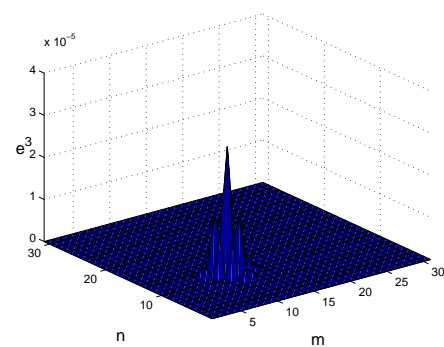
(f) Plot of $e_{m,n}^3$ at $t = 20$.

Figure 3.11: Breather moving at $\Psi = 45°$.

Time (s)	Horizontal displacement	Vertical displacement	Average horizontal velocity (units s^{-1})	Average vertical velocity (units s^{-1})
20	-5	-5	-0.25	-0.25
40	-10.5	-10.5	-0.2625	-0.2625
60	-15.5	-15.5	-0.2583	-0.2583
80	-21	-21	-0.2625	-0.2625

Table 3.1: Summary of breather motion ($\Psi = 45°$).

3.7.7 Breather moving at $\Psi = 20°$

We recall the work of Marin *et al.* described in Section 3.1, whom observed that breathers could travel through the lattice only along directions of symmetry. A natural question to consider is whether our scalar (one-component) two-dimensional system supports breathers that move in directions which are not axes of symmetry of the lattice. From the asymptotic analysis of Section 3.3.4, we conclude that there is no restriction upon the direction in which breathers may travel through the lattice, that is, Ψ may take any value in the interval $[0, 2\pi)$.

We would like to test this conjecture in our numerical work. We have tried propagating breathers in a wide range of directions, including at an angle $\Psi = 20°$ to the m-axis. The results of this are shown in Figure 3.12. To preclude waveforms that are severely elongated, we avoid values of (k, l) which are too close to the boundary of the elliptic domain $\mathcal{D}$. Thus we initiate the numerical scheme with $k = 3\pi/4$ and $l = 2.881$ radians; this corresponds to the wavevector $\mathbf{k_c}$ shown in Figure 3.7. It may be checked that for this choice of wavenumbers, the theoretical values for u and v are -0.2609 and -0.0950 respectively, giving an angle of travel $\Psi = 20°$. Also, the breather has frequency $\omega = 2.710$ and so the time period for an oscillation is $T = 2.318$. Once more, we set $b = d = 1$, $N = 31$, $\varepsilon = 0.1$ and $\lambda = 1$. The variational parameters turn out to be $\alpha = 1.0743$ and $\beta = 3.0737$. The breather is initially located at the centre of the lattice (not

Time (s)	Horizontal displacement	Vertical displacement	Average horizontal velocity (units s^{-1})	Average vertical velocity (units s^{-1})	tan Ψ	Ψ
40	-10	-3.5	-0.25	-0.0875	0.35	19.29°
75	-18.5	-7	-0.2466	-0.0933	0.3783	20.72°
120	-30	-11	-0.25	-0.0917	0.3667	20.14°
160	-41.5	-15.5	-0.2594	-0.0969	0.3737	20.48°

Table 3.2: Summary of breather motion ($\Psi = 20°$).

shown).

Figure 3.12 shows the breather at times $t = 40, 75, 120$ and 160 seconds. Clearly the breather moves through the lattice and preserves its form remarkably well, leaving behind very little radiation as it moves, nor spreading noticeably in any direction. We also include the computed energy at each of these times in Figure 3.12. The energy remains almost constant throughout, with the relative difference between the first and last computed values being $\Delta E^{(0)}/E^{(0)} = -0.015$. The asymptotic estimate for the breather energy given by (3.76) is $E^{(0)} = 0.9248$.

The motion of the breather is summarised in Table 3.2. The final measurement for the average velocities u and v are -0.2594 and -0.0969 units per second respectively, yielding relative errors of 1% and 2%. The direction of travel is measured to lie at $20.48°$ to the m-axis, which is very close to the expected angle $\Psi = 20°$.

Though we do not show all the results we have obtained here, we have successfully propagated breathers in a range of different angles, which supports the conjecture that breathers can travel in any direction through the lattice.
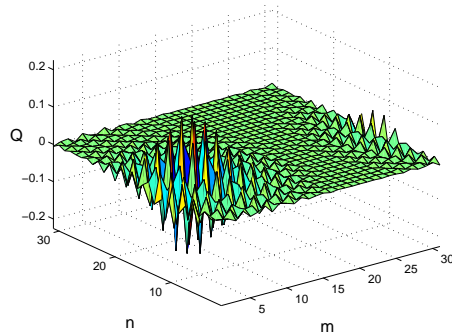
(a) Profile at $t = 40$, $E^{(0)} = 0.9260$.
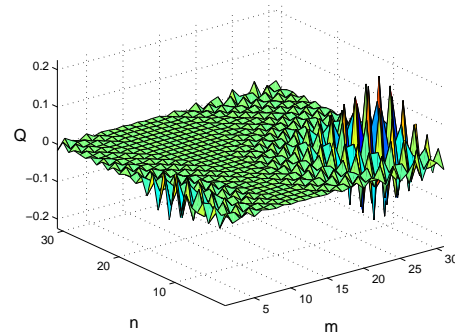
(b) Profile at $t = 75$, $E^{(0)} = 0.9218$.
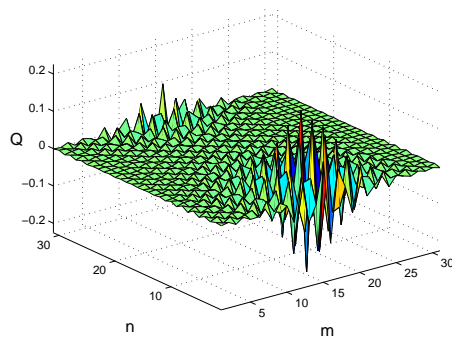
(c) Profile at $t = 120$, $E^{(0)} = 0.9210$.
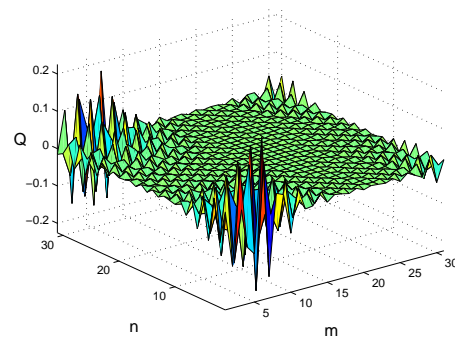
(d) Profile at $t = 160$, $E^{(0)} = 0.9140$.

Figure 3.12: Breather moving at $\Psi = 20°$.

3.7.8 Stationary breather in a lattice with asymmetric potential

The above numerical results all feature lattices with symmetric potentials, namely, those for which $a = c = 0$ so that $V(-Q) = -V(Q)$ in (3.10). We now present results of a simulation for which the potential function is asymmetric. In this case, initial data is generated using the results of Section 3.6.2. Also, from (3.36) in Section 3.3.5, we see that anomalous dispersion corresponds to $3b > 4a^2$. As an example, we set $a = 1$ and $b = 2$. Also, $c = 0$ and $d = 1$. The remaining parameters are assigned the values $N = 41$, $\varepsilon = 0.1$ and $\lambda = 1$. The breather frequency is $\omega = 2.8284$, and the period is $T = 2.2214$. The variational parameters are computed to be $\alpha = 1.2880$ and $\beta = 3.1399$.

The breather is initially situated at the centre of the lattice (not shown), at which time the energy $E^{(0)} = 1.4657$. The breather width, given by (3.86), is found to be $\mathcal{W}_{\mathrm{br}} = 4.45$ at time $t = 0$. The breather is shown after it has completed ten and thirty oscillations in Figure 3.13. The numerically computed energy is shown at each of these times in Figure 3.13. Note that the energy $E^{(0)}$ remains more or less unchanged, and even after thirty oscillations, $\Delta E^{(0)}/E^{(0)} = 0.014$. From the plots of the cell energy $e_{m,n}$ shown in figures 3.13 (b) and 3.13 (d), we observe that the breather remains localised with very little loss of form, even after almost seventy seconds. As with static breathers in a lattice with symmetric potential (see Section 3.7.4), very little energy is shed in the form of radiation. At $t = 30T$, we find that $\mathcal{W}_{\mathrm{br}} = 4.35$, and so the relative difference between the first and last measured values of the effective breather width is $\Delta \mathcal{W}_{\mathrm{br}}/\mathcal{W}_{\mathrm{br}} = -0.022$, reflecting a tiny contraction. Also, the asymptotic estimate for the breather energy given by (3.66) is $E^{(0)} = 1.4658$, which is in good agreement with the numerically computed value.
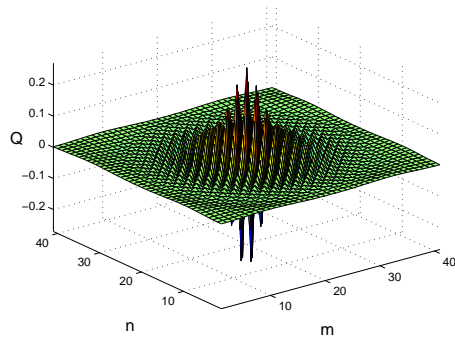
(a) Profile at $t = 10T = 22.21$.
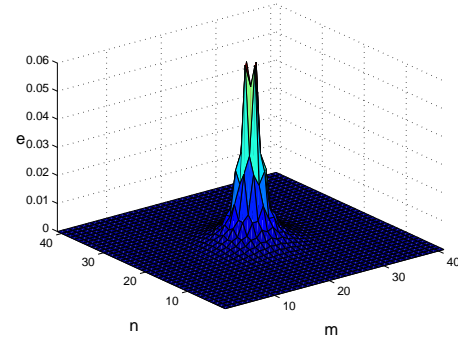
(b) Plot of $e_{m,n}$, $E^{(0)} = 1.4907$.
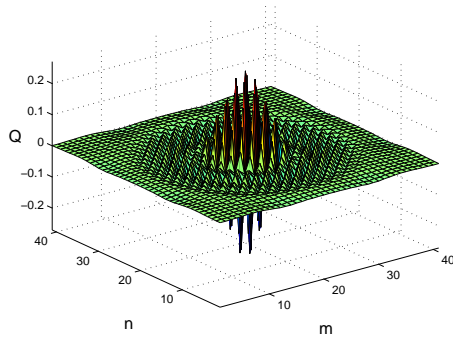
(c) Profile at $t = 30T = 66.64$.
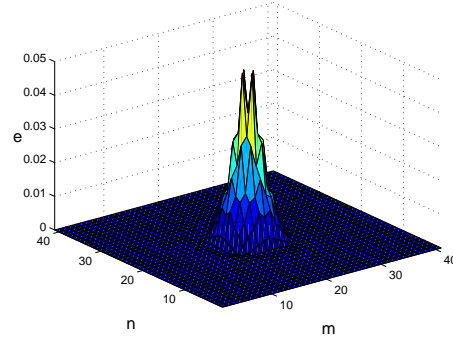
(d) Plot of $e_{m,n}$, $E^{(0)} = 1.4864$.

Figure 3.13: Stationary breather in a lattice with an asymmetric potential.

3.7.9 Breather collisions

Thus far, all the numerical results that we have presented have been concerned with the evolution of a single breather over time. In this section, we simulate a collision between two breather modes. In doing so, we aim to gain insight into the stability and robustness of breathers. To make it possible to follow the progress of the simulation on a lattice of size $N = 31$, we choose to initiate a collision between two breathers moving in opposite directions. In general though, one could consider a greater number of breathers, each travelling in different directions through the lattice.

Amongst other things, we aim to find whether the breathers regain their

form following a collision, whether individual velocities are altered significantly, whether breather stability depends upon the relative orientation of incoming breather paths, and other properties besides these.

In Figure 3.14, we show the evolution of two breathers which move towards one another and interact as they collide. We also show the two breathers at later times. One breather is initially located towards the left-hand edge of the lattice, at the grid point $(7.5, 15)$. A second breather begins near the right-hand edge of the lattice, at the point $(22.5, 15)$. In order to ensure that the breathers move towards one another parallel to the m-axis, we choose $k_L = 5\pi/4$, $l_L = \pi$, and $k_R = 3\pi/4$, $l_R = \pi$; hence $\omega = 2.7229$ and $T = 2.3075$. It may be checked that the corresponding velocities of the left-hand and right-hand breather are 0.2597 and -0.2597 units per second respectively. The initial configuration of the lattice is shown in Figure 3.14 (a). The breathers then approach one another and undergo a complicated interaction as they collide. This result of this interaction is shown at an early stage in Figure 3.14 (b) and at a slightly later stage in Figure 3.14 (c).

They then pass through one another and begin to separate. This is seen clearly in Figure 3.14 (d), where the breathers can be recognised as two visibly distinct structures in the lattice. Comparing Figure 3.14 (a) and Figure 3.14 (d), it is also apparent that both breathers emerge having undergone little overall change. We note that some energy is clearly shed during the collision, but this is to be expected since the FPU system is in general known to be nonintegrable. Though we do not include a tabulated record of measurements here, we find that the velocities of both breathers are preserved almost exactly even after collision. The overall picture becomes complicated for much longer times because of the periodic boundary conditions that are imposed on the lattice. (This means that breathers emerging from the first collision will collide again at the boundary).

Again, though we have not presented the results here, other simulations of colliding breathers which are initially located at different places in the lattice and move along different paths to those detailed above give similar results.
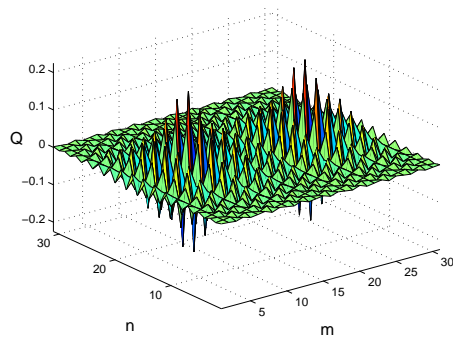
(a) Profile at $t = 0$
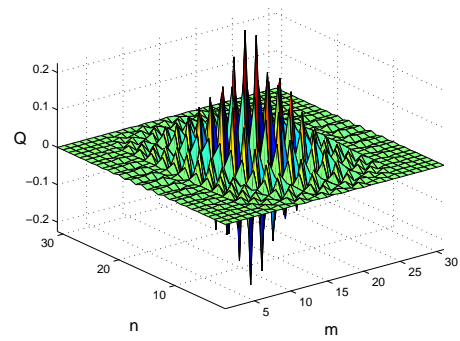
(b) Profile at $t = 26.51$.
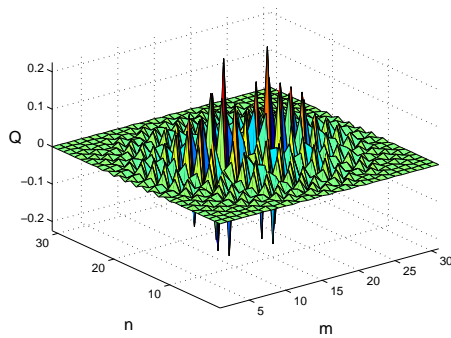
(c) Profile at $t = 45.89$.
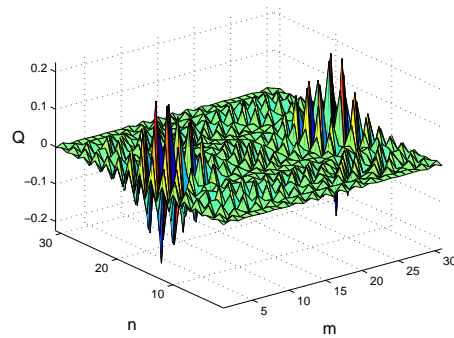
(d) Profile at $t = 70.80$.

Figure 3.14: Colliding breathers interact and separate.

Namely, after a complex interaction during which a small quantity of energy is lost, both breathers emerge and regain their forms. After they have separated completely, they continue to move at the velocities with which they were travelling initially.

3.8 Discussion

In this section, we have applied analytic methods to find approximations to discrete breathers in a two-dimensional square FPU lattice, governed by (3.12). In essence, the semi-discrete multiple-scale method reduces the governing equations for the lattice to a partial differential equation for the breather envelope. In one-dimensional lattices such as those considered in Chapter 2, few difficulties arise, since the resulting partial differential equation (the one-dimensional NLS equation), is essentially well-behaved. Specifically, it is integrable, and explicit formulae for soliton solutions are known.

In contrast, we showed in Section 3.3 that a similar reduction of (3.12) to a two-dimensional cubic NLS equation is more complicated, and can be done only for selected cases. In Section 3.3.3, we considered moving breathers in lattices with symmetric interaction potentials, and we found an ellipticity criterion for the wavenumbers of the carrier wave. For lattices with asymmetric potentials (see Section 3.3.5), reduction to the two-dimensional cubic NLS equation could be performed only for stationary breathers.

Unfortunately, a third-order analysis of this kind is inconclusive, since the two-dimensional cubic NLS equation does not support stable soliton solutions for the form of the breather envelope, only unstable Townes solitons. These are marginally stable, and either blow up or disperse completely when perturbed. Hence, the two-dimensional cubic NLS equation does not completely capture the actual dynamics of the two-dimensional FPU lattice. The phenomenon of blow-up is discussed at length in Section 3.4. We have shown that these problems may be overcome by including higher-order effects. Our motivation comes from a review (see Section 3.4.3) of results available for generalised NLS equations which incorporate higher-order nonlinearity and dispersion.

The NLS equation (3.39) is generic, in that it describes the envelope of a wavepacket in many models which take into account nonlinearity and dispersion at the lowest orders. However, the derivation of higher-order equations yields many possible perturbations, not all of which have been considered in

the literature. Generality of the cubic two-dimensional NLS equation is lost when higher-order terms are included. For some perturbations it is known that blow-up is suppressed, and stable solitons exist.

In Section 3.5, we derived a higher-order NLS equation (3.55) by applying a fifth-order multiple-scale analysis to the two-dimensional Fermi-Pasta-Ulam equations (3.12). Unfortunately the equation (3.55) has several perturbing terms, and as far as we are aware, only some of the perturbing terms have been studied previously in the literature. The analysis of (3.55), namely the rigorous determination of which parameter values support stable soliton solutions, is left for future work. As discussed in Section 3.4.3, if a variational formulation can be found for (3.55), then the methods of Pohožaev [98] can be used to analyse its properties. We suspect that a variational formulation for (3.55) exists, since one can be found for similarly complicated generalised NLS equations (see Zakharov & Kuznetsov, [141]).

On the other hand, we mentioned in Section 3.5 that the modulation theory described by Fibich and Papanicolaou [46, 47] might be better suited for an equation of this complexity. An advantage of this method is that it applies to a broad class of perturbing terms. One reduces the perturbed NLS equation to a much simpler system of modulation equations which do not involve the "transverse" variables (in our case, the spatial variables $\mathbf{x} = [\xi, \eta]^T$). The effect of small perturbations upon self-focusing in the critical nonlinear Schrödinger equation is easier to determine from the modulation equations.

Of course, numerical analysis of the modified NLS equation is another possible approach, but then one may as well bypass analysis of the continuum equation (3.55), and instead numerically solve the lattice equations (3.12) to begin with.

There are other possibilities that may be pursued in addition. We mention the work of Tamga *et al.* [128], who apply a simple one-term multiple-scale expansion to a two-dimensional lattice. They show that the lattice equations can be reduced to a cubic two-dimensional NLS equation at third order, which they

recognise "cannot be used to predict the time evolution" of nonlinear localised modes. Rather than pursuing soliton solutions, they instead consider modulational instability of their NLS equation, and (aided by numerical simulations), show that localised modes exist in the regions where a uniform solution is unstable. As pointed out by Marin *et al.* [89], the drawback to this approach is that the observed "nonlinear localised modes" cannot reliably be identified as discrete breathers. The authors of [128] thus describe the modes as "breathing solitary waves," rather than discrete breathers.

One of our aims has been to find criteria for the existence of breathers in the two-dimensional Fermi-Pasta-Ulam equation. From our fifth-order analysis in Section 3.5, we found various conditions on the lattice interaction parameters a, b, c, d, and on the form of the carrier wavenumbers k and l. These results have been supplemented and supported by numerical simulations. Several interesting breather properties are presented in the numerical results of Section 3.7. Firstly, we note that stationary and moving breathers appear to be long-lived modes of the lattice; their profiles do not change over time and they shed very little energy as they evolve. We have shown this to be true for a range of different parameter values, including asymmetric as well as symmetric potentials. The fact that breather modes are observed to reform following collisions supports the claim that these modes are robust structures.

One of the more surprising results that emerges from the numerics is that there appears to be no restriction upon the direction in which breathers can travel in the lattice, in contrast to the scenario reported by Marin *et al.* [89, 90] for two-component two-dimensional lattices. We have found, for instance, breathers which move at $20°$ to the lattice, suffering no appreciable distortion or spreading, even after relatively long times. In fact, we have obtained breathers moving at many other angles not parallel to the lattice axes, though we have not presented results of those simulations here. Breathers which move along lattice directions are elongated in the direction perpendicular to their motion. Previous work on the two-dimensional lattice analysed here has focused on other types of excitation. In [42], Eilbeck found highly accurate numerical approxi-

mations to the shape of travelling solitary plane waves. These were also found to travel at any angle to the lattice, and showed a more subtle angle-dependence in their amplitude-speed characteristics, which was explained using high-order quasi-continuum expansions by Wattis [135].

In Section 3.6 we derived asymptotic estimates for the energy of breathers. This has the expected form that the energy does *not* vanish as the amplitude becomes arbitrarily small. Rather, there is a threshold energy required to create a breather, in agreement with the results of Flach *et al.* [56]. We have provided formulae for these energy thresholds in Sections 3.6.2 and 3.6.3. Contrary to what one might expect, the energy threshold for moving breathers is *smaller* than that for stationary breathers. It is independent of the breather amplitude, but is dependent on the wavenumbers, and becomes vanishingly small as one approaches the boundary of the domain of ellipticity.

Chapter 4

A two-dimensional hexagonal Fermi-Pasta-Ulam lattice

4.1   Introduction

The previous chapter was concerned with a two-dimensional square lattice. As well as possessing translational symmetry, the square lattice considered in Chapter 3 possesses axes of rotational symmetry. Formally, the lattice in Chapter 3 has C_4 (or square) rotational symmetry, which we now explain. Suppose we rotate the lattice about an axis perpendicular to the plane, which passes through any lattice site. Then a rotation through any multiple of the angle $2\pi/4 = \pi/2$ maps the lattice back onto itself. Equivalently, such an axis is said to be a "four-fold" axis, and its multiplicity is equal to 4. A comprehensive group-theoretic approach to describing the full symmetry properties of two- and three-dimensional lattices is detailed by Boardman *et al.* (see Chapters 1 and 4 of [19]).

In this chapter, we consider a hexagonal electrical transmission lattice (HETL). This two-dimensional network possesses C_6 (or hexagonal) rotational symmetry. That is, rotation through any multiple of the angle $2\pi/6 = \pi/3$ maps the lattice back onto itself. The HETL is shown in Figure 4.1, pictured from a point vertically above the plane of the lattice. Before we comment on the compo-
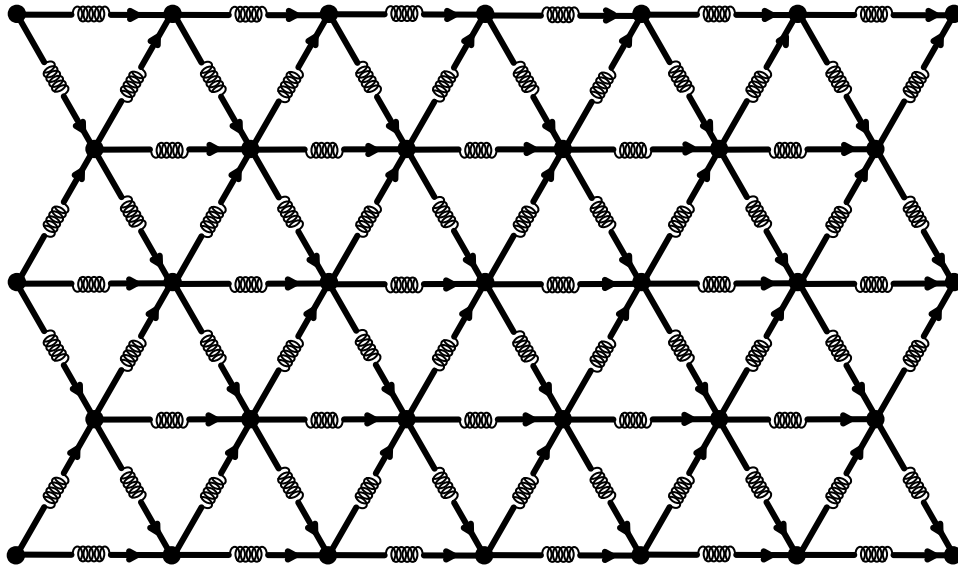
Figure 4.1: The 2D hexagonal electrical transmission lattice (HETL).

sition of the HETL, we mention that geometrically, it consists of a repeating array of hexagons, with nodes at the vertices and centre of each hexagon. As such, we note that the HETL appears to be an arrangement of tessellating triangles, and not hexagons. One is entitled to enquire why such an arrangement is not referred to instead as a "triangular" lattice, and why say, the description "hexagonal" isn't reserved for lattices in which every site possesses three nearest neighbours (such as that shown in Figure 4.2). In this work, we adopt the convention that the descriptions "hexagonal" and "triangular" refer to a lattice's symmetry properties and not to the repeating geometrical shapes which comprise the array. The lattice depicted in Figure 4.1 possesses C_6 rotational symmetry, hence, it is "hexagonal." Likewise, the lattice shown in Figure 4.2 possesses C_3 rotational symmetry, and so it is "triangular." As a note of caution, we emphasise that not all authors follow this convention.

4.1.1 Overview

In this chapter, we apply analytic methods to find approximations to breathers in a two-dimensional Fermi-Pasta-Ulam lattice with hexagonal rotational sym-
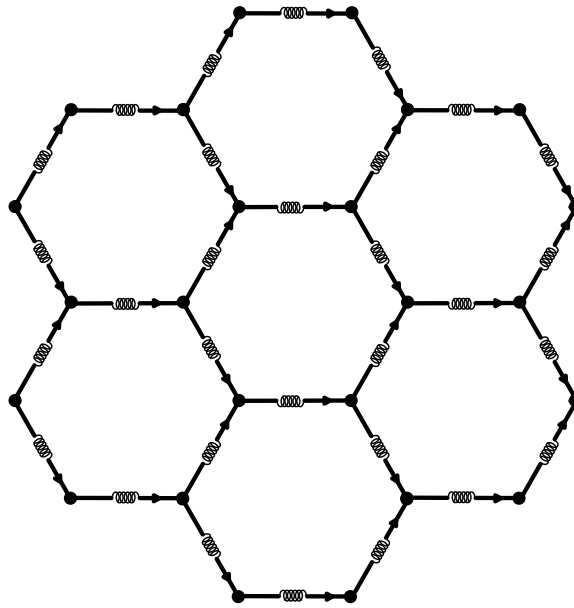
Figure 4.2: A "triangular" (C_3 rotationally symmetric) lattice.

metry. We restrict our attention to breathers of small amplitude which have a slowly varying envelope. We aim to investigate how the rotational symmetry of the hexagonal lattice impacts upon the properties of discrete breathers found therein, and in particular whether breather properties for the hexagonal lattice differ greatly from those found for breathers in the square lattice.

As such, we follow essentially the same steps as in Chapter 3, and it is instructive to contrast corresponding results of this and the previous chapter throughout. Speculating for a moment, one might expect the analysis for the hexagonal lattice to be more involved, since geometrically, it is a more complicated arrangement after all. However, one might also reasonably expect the different rotational symmetry properties of the hexagonal lattice to result in a system of equations of greater structural simplicity than those obtained for the square lattice.

We derive the equations of motion and demonstrate a Hamiltonian formalism in Section 4.2. In Section 4.3, we present two cases for which the hexagonal FPU lattice equations can be reduced to a two-dimensional NLS equation with

cubic nonlinearity. We consider lattices with a symmetric interaction potential, in which case reduction to a cubic NLS equation can be performed for moving breathers. We find an ellipticity criterion for the wavenumbers of the carrier wave. A reduction to a cubic NLS equation can also be carried out for lattices with an asymmetric potential, provided we consider only stationary breathers. We find that the hexagonal lattice differs from the square lattice in regard to the generation of second and third harmonics.

As we know from Section 3.4, the cubic NLS equation does not fully describe the evolution of the breather envelope, since it admits only unstable Townes solitons. Hence in Section 4.4, we extend our asymptotic analysis to higher order and find a generalised NLS equation which incorporates known stabilising terms. This equation is similar to the generalised NLS equation obtained for the square lattice, except that here, the perturbing terms are isotropic. Our analytic work is supplemented by numerical simulations presented in Section 4.5, which suggest that long-lived stationary and moving breather modes are supported by the system.

In Section 4.3, we obtain leading-order analytic estimates for the breather energy, and show that as expected, there is a minimum energy below which breathers cannot exist in the hexagonal FPU lattice. As before, we find that the energy threshold is dependent upon the wavevector of the carrier wave. It is maximised for stationary breathers, but becomes arbitrarily small near the boundary of the elliptic domain. In Section 4.6, we discuss the results obtained in this chapter.

The theoretical methods used in this chapter closely follow those of the previous chapter, and hence it is necessary to employ some key formulae from therein. To avoid continual references to the previous chapter, we have reproduced several essential formulae and results where appropriate, in order that both chapters may be read more or less independently.

4.2 Derivation of model equations

We aim to derive the equations governing the charge at each capacitor in the HETL. The first task is to decide upon a scheme to index all of the nodes, at which the capacitors are located. This depends upon the choice of basis vectors for the lattice. For the SETL, a natural choice for a basis pair was $\{\mathbf{i}, \mathbf{j}\}$, where $\mathbf{i} = [1, 0]^T$ and $\mathbf{j} = [0, 1]^T$ (see Section 3.2). For the HETL, we are presented with a number of possibilities, one of which is shown in Figure 4.3, along with the corresponding node labelling, centred about the site (m, n). The lattice basis vectors in this case are $\mathbf{i}' = \mathbf{i} = [1, 0]^T$ and $\mathbf{j}' = [-\frac{1}{2}, \frac{\sqrt{3}}{2}]^T$.
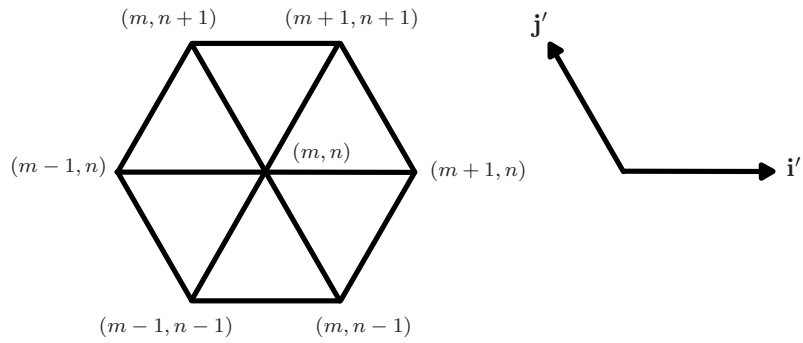
Figure 4.3: An alternative choice of basis $\{\mathbf{i}', \mathbf{j}'\}$ for the HETL.

However, we instead introduce a rectangular lattice with basis vectors $\mathcal{B} = \{\mathbf{i}', \mathbf{j}'\}$, where $\mathbf{i}' = \mathbf{i} = [1, 0]^T$ and $\mathbf{j}' = [0, h]^T$, illustrated in Figure 4.4. We use only half of the (m, n) indices, namely, those for which the sum $m + n$ is even. We choose an origin with coordinates $(0, 0)$. The position of the site (m, n) is then $m\mathbf{i}' + n\mathbf{j}'$. Clearly for this choice of basis and general h, the hexagonal units which comprise the array are not regular. This is remedied by choosing an appropriate scaling for the lattice in the vertical direction, namely $h = \sqrt{3}$. Consequently, we introduce the scaling factor h in various expressions throughout the analysis (in particular, see equations (4.16) and (4.17)).

We describe the composition of the HETL. At every node lies a nonlinear
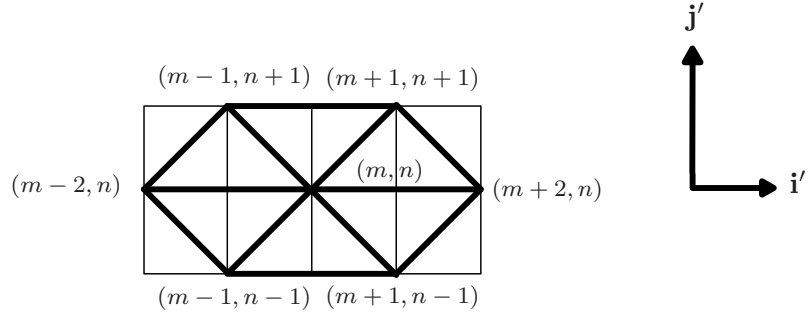
Figure 4.4: Labelling of nodes in the HETL with basis $\mathcal{B} = \{\mathbf{i'}, \mathbf{j'}\}$.

capacitor (not shown in Figure 4.1), and also between every node and each of its six nearest neighbours is a linear inductor. An enlarged view of the area surrounding the $(m, n)th$ capacitor is shown in Figure 4.5, where the capacitor is visible. As before, $V_{m,n}$ denotes the voltage across the (m, n)th capacitor and $Q_{m,n}$ denotes the total charge stored on the (m, n)th capacitor. Also, $I_{m,n}$, $J_{m,n}$ and $K_{m,n}$ are the currents through the (m, n)th inductors which lie in the direction parallel to the vectors $\mathbf{e_i} = [2, 0]^T$, $\mathbf{e_j} = [1, -\sqrt{3}]^T$ and $\mathbf{e_k} = [1, \sqrt{3}]^T$ respectively, as illustrated in Figure 4.5.

The equations relating current, charge and voltage in the lattice can now be derived. Applying Kirchoff's law as before, we have that

$$V_{m+2,n} - V_{m,n} = -L\frac{\mathrm{d}I_{m,n}}{\mathrm{d}t}, \tag{4.1}$$

$$V_{m+1,n-1} - V_{m,n} = -L\frac{\mathrm{d}J_{m,n}}{\mathrm{d}t}, \tag{4.2}$$

$$\text{and} \quad V_{m+1,n+1} - V_{m,n} = -L\frac{\mathrm{d}K_{m,n}}{\mathrm{d}t}, \tag{4.3}$$

where the inductance L is constant. Conservation of total charge gives

$$I_{m-2,n} - I_{m,n} + J_{m-1,n+1} - J_{m,n} + K_{m-1,n-1} - K_{m,n} = \frac{\mathrm{d}Q_{m,n}}{\mathrm{d}t}. \tag{4.4}$$

Differentiating (4.4) with respect to time, and then using (4.1), (4.2) and (4.3) to
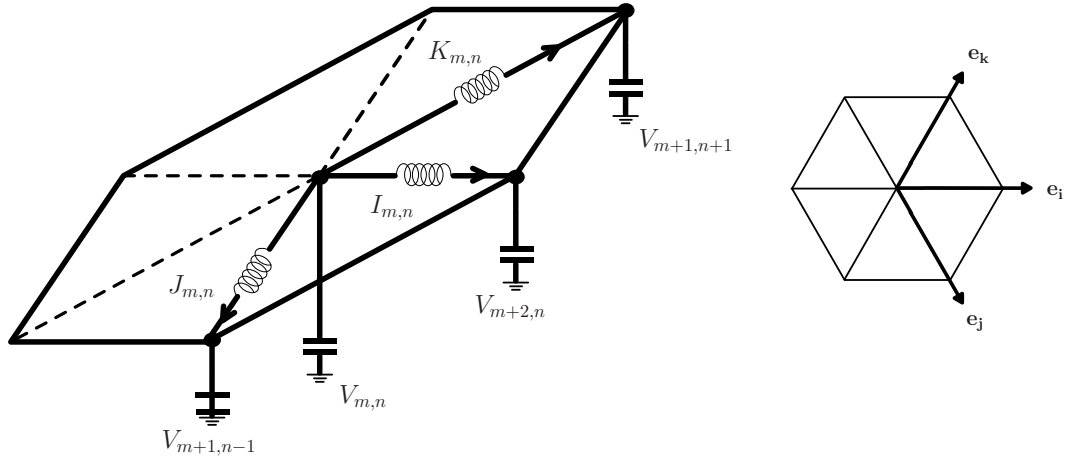
Figure 4.5: Enlarged view of the HETL at site (m, n).

find $\dot{I}_{m-2,n}$, $\dot{J}_{m-1,n+1}$ and $\dot{K}_{m-1,n-1}$, after substituting we arrive at

$$
\begin{aligned}
L\ddot{Q}_{m,n} = \; & (V_{m+2,n} - V_{m,n} + V_{m-2,n}) \\
& + (V_{m+1,n-1} - V_{m,n} + V_{m-1,n+1}) \\
& + (V_{m+1,n+1} - V_{m,n} + V_{m-1,n-1}).
\end{aligned}
\tag{4.5}
$$

Equation (4.5) may be written in the abbreviated form

$$
L\ddot{Q}_{m,n} = (\delta_I^2 + \delta_J^2 + \delta_K^2)V_{m,n},
\tag{4.6}
$$

where the centred second-difference operators on the right-hand side of (4.6) are defined by

$$
\delta_I^2 A_{m,n} = A_{m+2,n} - 2A_{m,n} + A_{m-2,n},
\tag{4.7}
$$

$$
\delta_J^2 A_{m,n} = A_{m+1,n-1} - 2A_{m,n} + A_{m-1,n+1},
\tag{4.8}
$$

$$
\text{and} \quad \delta_K^2 A_{m,n} = A_{m+1,n+1} - 2A_{m,n} + A_{m-1,n-1},
\tag{4.9}
$$

and $A_{m,n}$ is an arbitrary quantity referenced by two indices. In other words, δ_I^2, δ_J^2 and δ_K^2 are centred second-difference operators in the directions of $\mathbf{e_i}$, $\mathbf{e_j}$ and $\mathbf{e_k}$ respectively, as shown in Figure 4.5. As before, we would like to reformulate

(4.6) in terms of a single quantity, namely, charge. This is done by using the expansion (3.10), which gives $V_{m,n}$ in terms of $Q_{m,n}$. We have reproduced this for convenience

$$V_{m,n} = V(Q_{m,n}) \sim \frac{Q_{m,n}}{C_0} + \frac{a'Q_{m,n}^2}{C_0^2} + \frac{b'Q_{m,n}^3}{C_0^3} + \frac{c'Q_{m,n}^4}{C_0^4} + \frac{d'Q_{m,n}^5}{C_0^5}, \tag{4.10}$$

where a', b', c' and d' are known in terms of the parameters $\tilde{a}$, $\tilde{b}$, $\tilde{c}$ and $\tilde{d}$ which express the nonlinear capacitance $C(V_{m,n})$ as a function of $V_{m,n}$ (see equations (3.7) and (3.11)). The expansion for $V_{m,n}$ (4.10) is substituted into the HETL equations (4.6), giving a set of equations in terms of the charge $Q_{m,n}$ alone. We set $LC_0 = 1$ without loss of generality, giving

$$\frac{\mathrm{d}^2 Q_{m,n}}{\mathrm{d}t^2} = (\delta_I^2 + \delta_J^2 + \delta_K^2) \left[Q_{m,n} + a Q_{m,n}^2 + b Q_{m,n}^3 + c Q_{m,n}^4 + d Q_{m,n}^5 \right], \tag{4.11}$$

where $m, n \in \mathbb{Z}$, and $a = a'/C_0$, $b = b'/C_0^2$, $c = c'/C_0^3$ and $d = d'/C_0^4$. Thus we have shown that the equation governing charge in the HETL (4.11) is a two-dimensional analogue of the one-dimensional Fermi-Pasta-Ulam equation (2.7).

It is found that the lattice equations (4.11) can be derived from the Hamiltonian $\widetilde{H}$ given by

$$\widetilde{H} = \sum_{m,n} \frac{1}{2}(P_{m+2,n} - P_{m,n})^2 + \frac{1}{2}(P_{m+1,n-1} - P_{m,n})^2$$
$$+ \frac{1}{2}(P_{m+1,n+1} - P_{m,n})^2 + \Upsilon(Q_{m,n}), \tag{4.12}$$

where $\Upsilon(Q_{m,n})$ satisfies $\Upsilon'(Q_{m,n}) = V(Q_{m,n})$ given in (4.10). Also, $P_{m,n}$ and $Q_{m,n}$ are canonically conjugate momenta and displacement variables of the system satisfying

$$\frac{\mathrm{d}Q_{m,n}}{\mathrm{d}t} = -(\delta_I^2 + \delta_J^2 + \delta_K^2)P_{m,n}, \qquad \frac{\mathrm{d}P_{m,n}}{\mathrm{d}t} = -\Upsilon'(Q_{m,n}). \tag{4.13}$$

The Hamiltonian (4.12) for the HETL is analogous to the Hamiltonian (2.10) of the one-dimensional FPU system. Again, we have been unable to find a two-dimensional analogue of (2.2) for the HETL. Recalling the discussion in Sections 2.2.2 and 3.6.1, one might expect the Hamiltonian $\widetilde{H}$ given in (4.12) to be related to the total electrical energy of the HETL. In Section 4.3.1, we show that $\widetilde{H}$ is a

constant multiple of $E^{(0)}$, which is the electrical energy of the lattice calculated to leading-order.

The electrical energy $e_{m,n}$ in one single unit of the lattice is (see Figure 4.5)

$$e_{m,n} = \tfrac{1}{2}C(V_{m,n})V_{m,n}^2 + \tfrac{1}{2}L\left(I_{m,n}^2 + J_{m,n}^2 + K_{m,n}^2\right),\qquad(4.14)$$

and hence the total electrical energy of the HETL, which we denote E, is

$$E = \sum_{m,n} e_{m,n} = \sum_{m,n} \tfrac{1}{2}C(V_{m,n})V_{m,n}^2 + \tfrac{1}{2}L\left(I_{m,n}^2 + J_{m,n}^2 + K_{m,n}^2\right).\qquad(4.15)$$

The total electrical energy E is conserved, since the HETL is a lossless network. We obtain leading-order estimates for the energy of breathers in the HETL in Section 4.3.

4.3 Asymptotic analysis

4.3.1 Preliminaries

We apply the semi-discrete multiple-scale method to determine an approximate analytic form for small amplitude breather solutions of (4.11), with slowly varying envelope. We introduce new variables defined by

$$X = \varepsilon m, \quad Y = \varepsilon h n, \quad \tau = \varepsilon t \quad \text{and} \quad T = \varepsilon^2 t.\qquad(4.16)$$

In comparing (4.16) with (3.17), we note the presence of the additional scaling factor h in the definition of Y (see the comments made in Section 4.2). We seek solutions of (4.11) of the form

$$
\begin{aligned}
Q_{m,n}(t) = {}& \varepsilon e^{i\psi} F(X,Y,\tau,T) + \varepsilon^2 G_0(X,Y,\tau,T) + \varepsilon^2 e^{i\psi} G_1(X,Y,\tau,T) \\
& + \varepsilon^2 e^{2i\psi} G_2(X,Y,\tau,T) + \varepsilon^3 H_0(X,Y,\tau,T) + \varepsilon^3 e^{i\psi} H_1(X,Y,\tau,T) \\
& + \varepsilon^3 e^{2i\psi} H_2(X,Y,\tau,T) + \varepsilon^3 e^{3i\psi} H_3(X,Y,\tau,T) + \varepsilon^4 e^{i\psi} I_1(X,Y,\tau,T) \\
& + \varepsilon^4 e^{2i\psi} I_2(X,Y,\tau,T) + \varepsilon^4 e^{3i\psi} I_3(X,Y,\tau,T) + \varepsilon^4 e^{4i\psi} I_4(X,Y,\tau,T) \\
& + \varepsilon^5 e^{i\psi} J_1(X,Y,\tau,T) + \cdots + \text{c.c.},
\end{aligned}\qquad(4.17)
$$

where the phase ψ of the carrier wave is given by $km + lhn + \omega t$ (once again noting the presence of the extra factor h), and $\mathbf{k} = [k, l]^T$ and ω are its wavevector and temporal frequency respectively. We substitute the ansatz (4.17) into the lattice equations (4.11) and equate coefficients of each harmonic frequency at each order of ε. This yields the following system of equations (after much simplification):

$\mathcal{O}(\varepsilon e^{i\psi})$:

$$\omega^2 F = 4\sin^2(k)F + 4\sin^2\left(\frac{k + lh}{2}\right)F + 4\sin^2\left(\frac{k - lh}{2}\right)F, \qquad (4.18)$$

$\mathcal{O}(\varepsilon^2 e^{i\psi})$:

$$\omega F_\tau = 2\sin k[2\cos k + \cos(lh)]F_X + 2h\cos k \sin(lh)F_Y, \qquad (4.19)$$

$\mathcal{O}(\varepsilon^2 e^{2i\psi})$:

$$\omega^2 G_2 = [\sin^2(2k) + \sin^2(k + lh) + \sin^2(k - lh)](G_2 + aF^2), \qquad (4.20)$$

$\mathcal{O}(\varepsilon^3 e^{i\psi})$:

$$\begin{aligned}
2i\omega F_T = &- F_{\tau\tau} + [4\cos(2k) + 2\cos k \cos(lh)]F_{XX} + 2h^2 \cos k \cos(lh)F_{YY} \\
&- 4h\sin k \sin(lh)F_{XY} \\
&- 8a\left[\sin^2(k) + \sin^2\left(\frac{k + lh}{2}\right) + \sin^2\left(\frac{k - lh}{2}\right)\right][F(G_0 + \overline{G}_0) + \overline{F}G_2] \\
&- 12b\left[\sin^2(k) + \sin^2\left(\frac{k + lh}{2}\right) + \sin^2\left(\frac{k - lh}{2}\right)\right]|F|^2 F, \qquad (4.21)
\end{aligned}$$

$\mathcal{O}(\varepsilon^3 e^{3i\psi})$:

$$\begin{aligned}
9\omega^2 H_3 = &\, 4\left[\sin^2(3k) + \sin^2\left(\frac{3k + 3lh}{2}\right) + \sin^2\left(\frac{3k - 3lh}{2}\right)\right]H_3 \\
&+ 8a\left[\sin^2(3k) + \sin^2\left(\frac{3k + 3lh}{2}\right) + \sin^2\left(\frac{3k - 3lh}{2}\right)\right]FG_2 \\
&+ 4b\left[\sin^2(3k) + \sin^2\left(\frac{3k + 3lh}{2}\right) + \sin^2\left(\frac{3k - 3lh}{2}\right)\right]F^3, \qquad (4.22)
\end{aligned}$$

$\mathcal{O}(\varepsilon^4 e^0)$:

$$G_{0\tau\tau} = 6\,G_{0XX} + 2h^2 G_{0YY} + a\left[6\left(|F|^2\right)_{XX} + 2h^2\left(|F|^2\right)_{YY}\right]. \qquad (4.23)$$

Each of these equations should be compared with its counterpart from Section 3.3.1.

Clearly, equations (4.18)–(4.23) are more complicated than equations (3.19)–(3.24), though each equation plays a similar role. Hence, (4.18) is the dispersion relation for the system (4.11). Since we are interested only in solutions for which $F \neq 0$, (4.18) yields

$$\omega^2 = 4\sin^2(k) + 4\sin^2\left(\frac{k+lh}{2}\right) + 4\sin^2\left(\frac{k-lh}{2}\right), \qquad (4.24)$$

which does not simplify significantly. From equation (4.19), we determine the velocity of the travelling wave F, finding that

$$F(X, Y, \tau, T) \equiv F(Z, W, T), \qquad (4.25)$$

where $Z = X - u\tau$ and $W = Y - v\tau$, and the horizontal and vertical velocity components u and v are found to be

$$u = \frac{-2\sin k[2\cos(k) + \cos(lh)]}{\omega} \quad \text{and} \quad v = \frac{-2h\cos(k)\sin(lh)}{\omega}. \qquad (4.26)$$

Equation (4.26), along with (4.24) enables the elimination of terms involving G_1 from (4.21) which are not shown. We use Ψ to denote the angle at which the envelope F propagates through the lattice (not to be confused with ψ, which denotes the phase of the carrier wave in (4.17)). It is measured from the direction of the basis vector $\mathbf{e_i}$ to the line of travel. The angle Ψ is given by $\tan^{-1}(v/u)$, which unlike before (see Section 3.3.1) does not simplify greatly. The angle of travel depends upon the velocities u and v, which in turn depend upon the wavevector $\mathbf{k} = [k, l]^T$. For both cases that we consider (namely, symmetric and asymmetric interaction potentials), we shall find constraints upon the wavenumbers k and l which affect the velocity components u and v. However, recalling the results on permitted directions of travel presented in Section 3.3.4, as one might expect, we find that Ψ can still take any value in the interval $[0, 2\pi)$.

In all cases, our priority is to reduce (4.21) to a nonlinear Schrödinger (NLS) equation in F. From this, a soliton solution for the form of the breather envelope F can be found and substituted into the ansatz (4.17). This then gives a leading-order analytic form for breather solutions. Before this can be done,

the quantities G_0 and G_2 in (4.21) must be found in terms of F. As for the SETL, it is straightforward to determine G_2 from the algebraic equation (4.20). However, the partial differential equation (4.23) for G_0 can be solved for two special cases only. Namely, we consider symmetric potentials, in which case the reduction of (4.21) to an NLS equation can be completed even for moving breathers, and also asymmetric potentials, provided we confine our attention to stationary breathers only. These two cases are considered in Sections 4.3.3 and 4.3.5 respectively. In Sections 4.3.3 and 4.3.5, we use the formulae for breather solutions to obtain estimates for the breather energy, which we now discuss.

Asymptotic estimates for breather energy

Since the HETL is a lossless network, the total electrical energy E given by (4.15) is conserved. We derive leading-order estimates for the electrical energy, which we denote $E^{(0)}$. Hence, we use leading-order expressions for each of the terms in the terms in the summand of (4.15). From (4.10), it follows that $V_{m,n} \sim Q_{m,n}/C_0$ to leading order, and so the first term in the summand of (4.15) is $Q_{m,n}^2/(2C_0)$. To leading-order, the energy of the HETL, $E^{(0)}$, is therefore

$$E^{(0)} = \sum_{m,n} e_{m,n}^{(0)} = \sum_{m,n} \frac{Q_{m,n}^2}{2C_0} + \frac{L}{2}\left(I_{m,n}^2 + J_{m,n}^2 + K_{m,n}^2\right). \tag{4.27}$$

It remains to find leading-order expressions for the currents $I_{m,n}$, $J_{m,n}$ and $K_{m,n}$, which can then be substituted into (4.27). These are obtained from equations (4.1)–(4.3), which upon substitution of $V_{m,n} \sim Q_{m,n}/C_0$ become

$$Q_{m+2,n} - Q_{m,n} = -\frac{\mathrm{d}I_{m,n}}{\mathrm{d}t}, \tag{4.28}$$

$$Q_{m+1,n-1} - Q_{m,n} = -\frac{\mathrm{d}J_{m,n}}{\mathrm{d}t}, \tag{4.29}$$

$$\text{and} \quad Q_{m+1,n+1} - Q_{m,n} = -\frac{\mathrm{d}K_{m,n}}{\mathrm{d}t}, \tag{4.30}$$

where $LC_0 = 1$. The currents are determined by substituting the expression for the breather $Q_{m,n}$ into (4.28)–(4.30) and then integrating with respect to time.

Firstly, using equations (4.28)–(4.30), we establish a relationship between the Hamiltonian $\widetilde{H}$ for the system (4.12), and the leading-order electrical energy $E^{(0)}$ given by (4.27) (see the comments following equation (4.12)). The dominant contribution to the energy stored in the capacitors is $\Upsilon(Q_{m,n}) = Q_{m,n}^2/2$. Comparing the resulting expression for $\widetilde{H}$ (4.12) with $E^{(0)}$ (4.27), we see that it remains to establish a link between the currents $I_{m,n}$, $J_{m,n}$ and $K_{m,n}$ and the generalised momenta $P_{m,n}$. From Hamilton's equations (the second equation in (4.13)), we have $dP_{m,n}/dt = -Q_{m,n}$. Also, equation (4.28) relates the charge $Q_{m,n}$ to the current $I_{m,n}$. We substitute for $Q_{m,n}$ by $-dP_{m,n}/dt$ in (4.28) and then integrate, giving $I_{m,n} = P_{m+2,n} - P_{m,n}$ (where we have taken the constant of integration to be zero). Similarly, we find from (4.29) and (4.30) that $J_{m,n} = P_{m+1,n-1} - P_{m,n}$ and $K_{m,n} = P_{m+1,n+1} - P_{m,n}$. Therefore, $LI_{m,n}^2 = (1/C_0)(P_{m+2,n} - P_{m,n})^2$, $LJ_{m,n}^2 = (1/C_0)(P_{m+1,n-1} - P_{m,n})^2$ and $LK_{m,n}^2 = (1/C_0)(P_{m+1,n+1} - P_{m,n})^2$. Hence, we find $E^{(0)} = (1/C_0)\widetilde{H}$, as for the SETL (see Section 3.6.1).

Before proceeding any further, the dispersion relation given by (4.24) merits further discussion.

4.3.2 The dispersion relation for the HETL

In this section, we analyse the dispersion relation (4.24) for the system (4.11). A contour plot of ω against k and l is shown in Figure 4.6. It is found that w is periodic in both k and l, with period 2π along the k-direction, and $2\pi/h$ in the l-direction. In other words, we consider k and l such that $(k,l) \in \mathcal{T}^2 = [0, 2\pi] \times [0, 2\pi/h]$.

The function ω is minimised, and assumes the value zero, at the centre of the circular patterns in Figure 4.6. It is maximised at the centre of the triangular structures, where $\omega = 3$. Of course, it is ambiguous to refer to a triangle's centre without first specifying *which* centre (circumcentre, orthocentre, centroid *etc.*) is meant. However, the contour plot of ω shown in Figure 4.7 allows for a closer analysis of the geometry of the pattern in Figure 4.6. From this, one deduces that the triangles in Figure 4.6 are equilateral, for which the various centres are
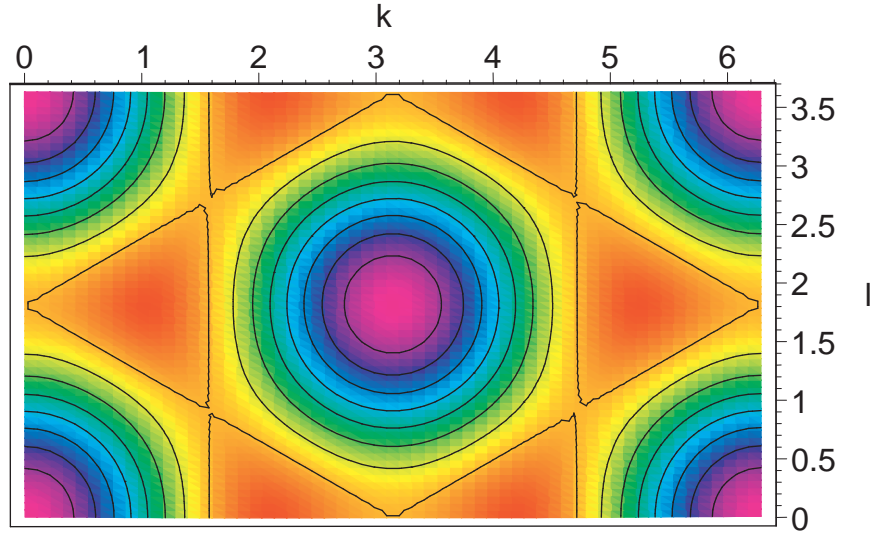
Figure 4.6: Plot of w against k and l.

coincident. Further, we determine the coordinates of other significant points shown in Figure 4.7, as well as the length of the equilateral triangles, which is found to be π/h. The circles in Figure 4.7 mark the points in (k, l)-space at which w attains its minimum value, zero. These points are located at $(0, 0)$, $(2\pi, 0)$, $(2\pi, 2\pi/h)$, $(0, 2\pi/h)$ and $(\pi, \pi/h)$ (see Figure 4.7). The crosses mark points at which ω is maximised and assumes the value $\omega = 3$. The wavevectors corresponding to these points are denoted $\mathbf{k_1}, \ldots, \mathbf{k_6}$, where

$$\begin{aligned}
\mathbf{k_1} &= [\pi/3, \pi/h]^T, & \mathbf{k_4} &= [5\pi/3, \pi/h]^T, \\
\mathbf{k_2} &= [2\pi/3, 0]^T, & \mathbf{k_5} &= [4\pi/3, 2\pi/h]^T, \\
\mathbf{k_3} &= [4\pi/3, 0]^T, & \mathbf{k_6} &= [2\pi/3, 2\pi/h]^T.
\end{aligned}$$

The dispersion relation for the system (4.11) should be compared with that obtained for the SETL in Section 3.3.2, along with the corresponding contour plot (Figure 3.3). Recall from Section 3.3.2 that for the SETL, the point (π, π) in (k, l)-space at which ω (3.25) was maximised played a special role. Namely, at this point, the velocity components u and v were both found to be zero, and consequently, the analysis at this point became simpler in all cases (see Sec-
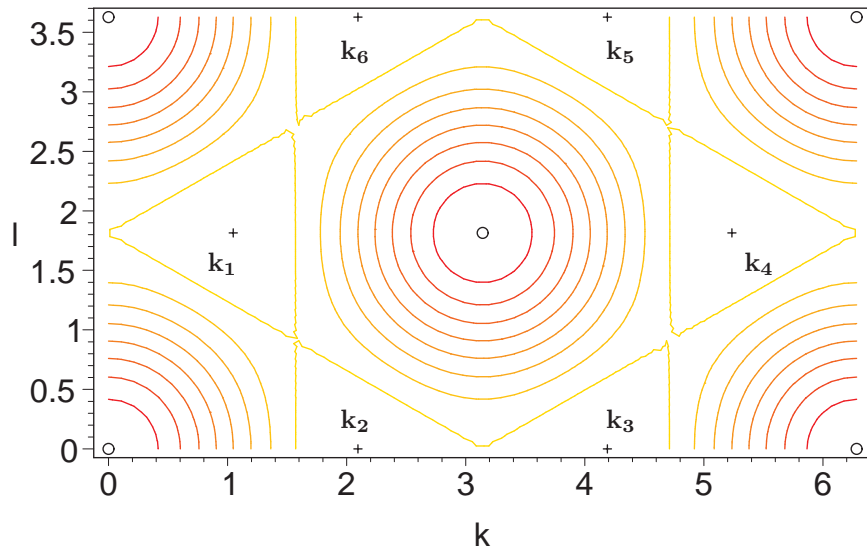
Figure 4.7: Contour plot of w.

tions 3.3.5 and 3.5). For the HETL, there are now six such points, reflecting the lattice's hexagonal symmetry. It may be verified using (4.26) that the velocity components u and v are both zero for each of the wavevectors $\{\mathbf{k_1}, \ldots, \mathbf{k_6}\}$. In sections 4.3.5 and 4.4, our analysis shall focus exclusively on the points corresponding to these wavevectors.

4.3.3 Lattices with a symmetric potential

In this section, we consider lattices with a symmetric interaction potential, namely, those which satisfy $\Upsilon'(-Q) = -\Upsilon'(Q)$. In other words, $\Upsilon'(Q)$ has odd symmetry and $\Upsilon(Q)$ is even. This corresponds to $a = c = 0$ in (4.10) and (4.11). Since there are no even harmonics for vibrations controlled by symmetric potentials, it follows that G_0 and G_2 are both zero. In (4.21), the term $F_{\tau\tau}$ is substituted for using (4.25), from which it is found that

$$F_{\tau\tau} = u^2 F_{ZZ} + 2uv F_{ZW} + v^2 F_{WW}. \tag{4.31}$$

Substituting thus gives an NLS equation in F at third-order,

$$2\mathrm{i}\omega F_T + \left[u^2 - 4\cos(2k) - 2\cos k \cos(lh)\right] F_{ZZ} + \left[v^2 - 2h^2 \cos k \cos(lh)\right] F_{WW}$$
$$+ \left[2uv + 4h \sin k \sin(lh)\right] F_{ZW} + 3b\omega^2 |F|^2 F = 0, \tag{4.32}$$

where the velocities u and v are given in (4.26). By applying an appropriate transformation of variables, we eliminate the mixed term F_{ZW} in (4.32), and thus reduce the equation to a standard form. It so happens that none of the subsequent expressions simplify greatly, and therefore in order to avoid unnecessary clutter, we rewrite (4.32) as

$$2\mathrm{i}\omega F_T + D_1 F_{ZZ} + D_2 F_{WW} + D_3 F_{ZW} + 3b\omega^2 |F|^2 F = 0, \tag{4.33}$$

where $D_1 = u^2 - 4\cos(2k) - 2\cos k \cos(lh)$, $D_2 = v^2 - 2h^2 \cos k \cos(lh)$ and $D_3 = 2uv + 4h \sin k \sin(lh)$. A suitable transformation is

$$\xi = \frac{hZ}{\sqrt{D_1}} \quad \text{and} \quad \eta = \frac{h(2D_1 W - D_3 Z)}{\sqrt{D_1(4D_1 D_2 - D_3^2)}}, \tag{4.34}$$

upon which (4.33) becomes

$$2\mathrm{i}\omega F_T + 3\nabla^2 F + 3b\omega^2 |F|^2 F = 0, \tag{4.35}$$

where the differential operator $\nabla^2 F \equiv F_{\xi\xi} + F_{\eta\eta}$ is isotropic in the (ξ, η) variables. The new variables ξ and η are chosen in the manner suggested in Section 3.3.3. Equation (4.35) has the same form as (3.39), with $D = 3/2\omega$ and $B = 3b\omega/2$. Formulae for approximations to Townes soliton solutions of (4.35) are given by (3.42) with these values for B and D. The resulting expression for the envelope F is then substituted into the breather ansatz (4.17), yielding a leading-order analytic expression for the breather

$$Q_{m,n}(t) = 2\varepsilon\alpha \cos[km + lhn + (\omega + \varepsilon^2\lambda)t] \operatorname{sech}(\beta r) + \mathcal{O}(\varepsilon^3), \tag{4.36}$$

where α and β are determined from (3.41) using $D = 3/2\omega$, $B = 3b\omega/2$. Further, $r = \sqrt{\xi^2 + \eta^2}$ is found in terms of the physical discrete variables m and n by

inverting the transformations (4.34) and reverting back to the variables Z and W, using

$$r^2 = \xi^2 + \eta^2 = \frac{4h^2(D_2 Z^2 + D_1 W^2 - D_3 ZW)}{4D_1 D_2 - D_3^2}. \tag{4.37}$$

The terms D_1, D_2 and D_3 are found from (4.33), $Z = \varepsilon(m - ut)$ and $W = \varepsilon(hn - vt)$ in terms of the discrete variables m and n, the velocities u and v are given by (4.26), and ω is given in (4.24).

4.3.4 Determining the domain of ellipticity

We confine our attention to elliptic NLS equations, as we did for the square lattice (see Section 3.3.4). We seek to determine the region $\mathcal{D}$ of (k, l)-parameter space (that is, the two-torus $\mathcal{T}^2 = [(0, 2\pi)] \times [0, 2\pi/h]$) where the NLS equation (4.32) is elliptic. By definition, this equation is elliptic when $D_3^2 < 4D_1 D_2$, where D_1, D_2 and D_3 are known combinations of the wavenumbers k and l, given in (4.33). Unlike the square lattice (see Section 3.3.4), we have not been able to find analytically the region $\mathcal{D}$ in (k, l)-parameter space where this inequality is satisfied. However, the region $\mathcal{D}$ can be determined numerically using Maple (see for example, Redfern [100]). In order to do this, we define a function $e(k, l)$ by $e(k, l) = 4D_1(k, l) \cdot D_2(k, l) - D_3(k, l)^2$. Clearly, we are concerned with the region(s) of (k, l)-space for which $e(k, l) > 0$. This can be found from a contour plot of $e(k, l)$, shown in Figure 4.8. Again, the hexagonal symmetry properties of the HETL are reflected clearly in the function $e(k, l)$. The six maxima (at which $e(k, l) = 36$) lie at the (red) centres of the concentric closed curves in Figure 4.8. The maxima of $e(k, l)$ coincide with the six maxima of $\omega(k, l)$ shown in Figure 4.7, namely, at the points in $\mathcal{T}^2$ which correspond to the wavevectors $\{\mathbf{k_1}, \ldots, \mathbf{k_6}\}$. We mention in passing that $e(k, l)$ is minimised ($e(k, l) = -48$) at the six midpoints of the line segments which connect adjacent maxima, that is, at the centres of the (purple) rectangle-like regions.

The contour plot of $e(k, l)$ in Figure 4.9 shows the subset of $\mathcal{T}^2$ for which $e(k, l) = 0$, and the function $e(k, l)$ is strictly positive within the interior of the six closed curves. In other words, the closed curves form the boundary of the
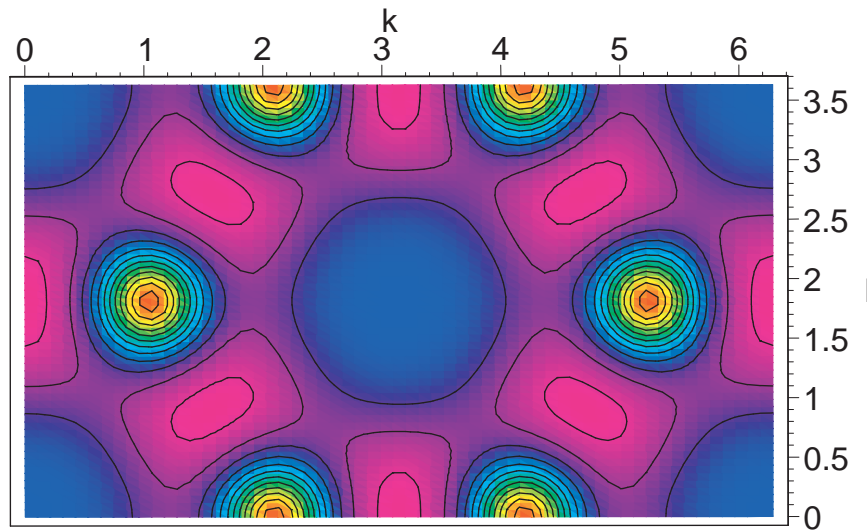
Figure 4.8: Plot of $e(k, l)$ viewed from above the (k, l)-plane.

region $\mathcal{D}$, and the NLS equation (4.32) is elliptic within the interior of these closed curves. For the hexagonal lattice therefore, $\mathcal{D}$ is a disconnected subset comprising six hexagonally-arranged local neighbourhoods around each of the points corresponding to $\{\mathbf{k_1}, \ldots, \mathbf{k_6}\}$. These subdomains have been labelled $\{\mathcal{D}_1, \ldots, \mathcal{D}_6\}$ in Figure 4.9, where $\mathcal{D} = \mathcal{D}_1 \cup \ldots \cup \mathcal{D}_6$. This should be compared with the corresponding domain for the SETL determined in Section 3.3.4, which comprised a single connected subset of the two-torus $[0, 2\pi] \times [0, 2\pi]$.

Permitted directions of travel within the lattice

The angle of travel $\Psi = \tan^{-1}(v/u)$ depends upon the velocity components u and v, which in turn depend upon the wavevector $\mathbf{k} = (k, l)$ (see equation (4.26)). Bearing in mind the restrictions upon the wavevector obtained in this section, we would like to determine whether this leads to any restrictions upon the values assumed by the angle of travel Ψ. In Section 3.3.4, using our formulae for u, v and Ψ, we were able to demonstrate that there are no such constraints upon Ψ in the SETL. In fact, the same is true for the HETL, for which it can be shown that Ψ may assume any value in the interval $[0, 2\pi)$. The argument takes exactly the same form as before, though the details for the HETL are messy, and
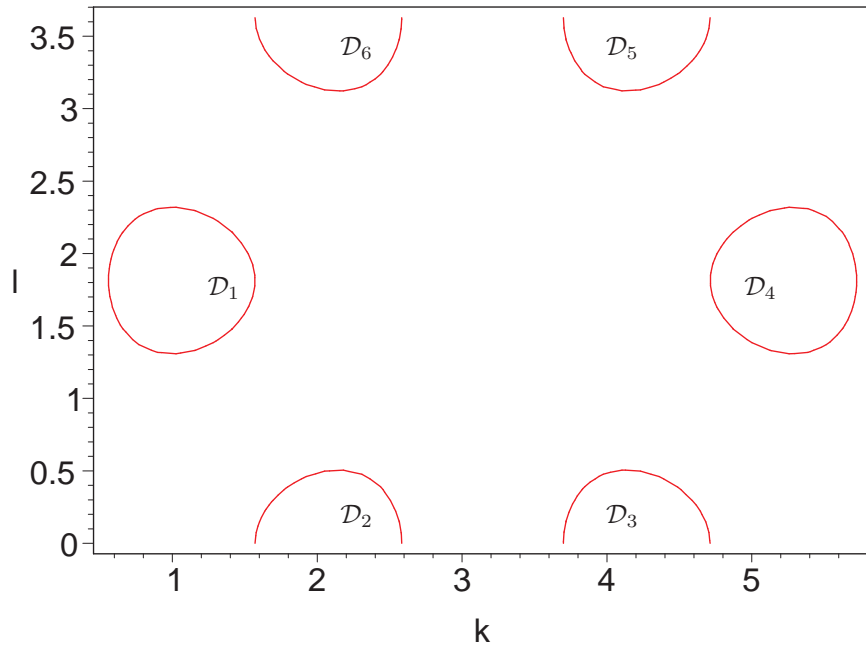
Figure 4.9: The domain $\mathcal{D} = \mathcal{D}_1 \cup \ldots \cup \mathcal{D}_6$ in which the NLS equation (4.32) is elliptic.

so we do not include them here.

Breather energy

We calculate the leading-order energy $E^{(0)}$ of moving breathers in lattices with a symmetric potential using the breather formula given by (4.36), which for convenience we rewrite as

$$Q_{m,n}(t) \sim 2\varepsilon\alpha \cos \Phi \, \text{sech}(\beta r), \tag{4.38}$$

where $\Phi = km + lhn + \Omega t$ is the phase of the carrier wave, $(k, l) \in \mathcal{D}$, $\Omega = \omega + \varepsilon^2 \lambda$ is the breather frequency including the first correction term, and λ parametrises the breather amplitude (see Section 3.4.2). Also, α, β and r^2 are as described in Section 4.3.3. Note that $\Phi = km + lhn + \Omega t$ is distinct from $\psi = km + lhn + \omega t$, which appears in (4.17). The expression (4.38) is substituted into (4.27).

We now find expressions for the currents $I_{m,n}$, $J_{m,n}$ and $K_{m,n}$, as explained at the end of Section 4.3.1. The current $I_{m,n}$ is obtained by substituting the expression for $Q_{m,n}$ (4.38) into (4.28) and integrating with respect to time. Given the

complexity of the expression for r given by (4.37), the left-hand side of (4.28) is not easily integrated with respect to time. However, in (4.38), the variable r varies slowly in time compared to the oscillatory component Φ. Hence, as explained in Section 3.6.3, integration by parts gives (to leading-order)

$$I_{m,n} \sim \frac{2\varepsilon\alpha}{\omega} \left[1 - \cos(2k)\right] \sin \Phi \operatorname{sech}(\beta r) - \frac{2\varepsilon\alpha}{\omega} \sin(2k) \cos \Phi \operatorname{sech}(\beta r), \quad (4.39)$$

where we have taken the constant of integration to be zero, and $\Omega \sim \omega$ to leading order. Similarly, substituting for $Q_{m,n}$ in equations (4.29) and (4.30) and integrating, it is found that

$$J_{m,n} \sim \frac{2\varepsilon\alpha}{\omega} \left[1 - \cos(k - lh)\right] \sin \Phi \operatorname{sech}(\beta r) - \frac{2\varepsilon\alpha}{\omega} \sin(k - lh) \cos \Phi \operatorname{sech}(\beta r),$$
$$(4.40)$$

$$K_{m,n} \sim \frac{2\varepsilon\alpha}{\omega} \left[1 - \cos(k + lh)\right] \sin \Phi \operatorname{sech}(\beta r) - \frac{2\varepsilon\alpha}{\omega} \sin(k + lh) \cos \Phi \operatorname{sech}(\beta r).$$
$$(4.41)$$

Hence substituting for $Q_{m,n}$, $I_{m,n}$, $J_{m,n}$ and $K_{m,n}$ using (4.38) and (4.39)–(4.41), the overall sum (4.27) for $E^{(0)}$ becomes

$$\begin{aligned} E^{(0)} \sim \sum_{m,n} &\frac{2\varepsilon^2\alpha^2}{C_0} \cos^2 \Phi \operatorname{sech}^2(\beta r) \\ &+ \frac{2L\varepsilon^2\alpha^2}{\omega^2} \operatorname{sech}^2(\beta r) \left\{ \left[(1 - \cos(2k)) \sin \Phi - \sin(2k) \cos \Phi\right]^2 \right. \\ &+ \left[(1 - \cos(k - lh)) \sin \Phi - \sin(k - lh) \cos \Phi\right]^2 \\ &+ \left. \left[(1 - \cos(k + lh)) \sin \Phi - \sin(k + lh) \cos \Phi\right]^2 \right\}. \end{aligned} \quad (4.42)$$

Since the variables $X = \varepsilon m$ and $Y = \varepsilon h n$ vary slowly with m and n, so does r^2, and so we replace the sum in (4.42) by an integral. The summand in (4.42) is rather complicated, making the resulting integral difficult to evaluate exactly. To simplify the summand, using the fact that r varies slowly with m and n, we approximate the term in square brackets by taking the average values of $\cos^2 \Phi$, $\sin^2 \Phi$ and $\sin \Phi \cos \Phi$, which are $\frac{1}{2}$, $\frac{1}{2}$ and 0 respectively. Hence the sum (4.42) becomes

$$E^{(0)} \sim \sum_{m,n} \frac{2\varepsilon^2\alpha^2}{C_0} \operatorname{sech}^2(\beta r). \quad (4.43)$$

We mention that the average energy stored by the capacitor (given by the first term in the summand in (4.42)) is equal to the average energy stored by the three inductors in a single unit, as one would expect. Again, this represents the electrical analogue of the equipartition between kinetic and potential energy in mechanical systems.

Replacing the double sum (4.43) by an integral over all space, we note from the definition of r that the function $\text{sech}(\beta r)$ is not in general radially symmetric. We work in (ξ, η)-space to facilitate evaluation of this integral. Hence, after evaluating the Jacobian associated with the transformation from (m, n) to (ξ, η) coordinates, we have that

$$
\begin{aligned}
E^{(0)} &\sim \sum_{m,n} \frac{2\varepsilon^2 \alpha^2}{C_0} \text{sech}^2(\beta r) \\
&= \frac{\alpha^2}{h^3 C_0} \sqrt{4D_1 D_2 - D_3^2} \iint \text{sech}(\beta \sqrt{\xi^2 + \eta^2}) \, \mathrm{d}\xi \mathrm{d}\eta.
\end{aligned}
\tag{4.44}
$$

Evaluating the integral on the right-hand side of (4.44) gives

$$
E^{(0)} \sim \frac{2\pi \log 2}{h^3 C_0} \frac{\alpha^2}{\beta^2} \sqrt{4D_1 D_2 - D_3^2}.
\tag{4.45}
$$

Substituting for α and β in terms of $D = 3/2\omega(k, l)$ and $B = 3b\omega(k, l)/2$ (see Section 4.3.3) we find that (4.45) becomes

$$
E^{(0)} \sim \frac{4\pi \log 2(2 \log 2 + 1)}{3\, h^3\, C_0\, b\, \omega^2 (4 \log 2 - 1)} \sqrt{4D_1 D_2 - D_3^2}.
\tag{4.46}
$$

It is evident from (4.46) that the leading-order energy $E^{(0)}$ is independent of the breather amplitude, again confirming the existence of a minimum energy of moving breathers in the two-dimensional HETL with symmetric potential. However, the threshold energy does depend upon the wavenumbers k and l.

A plot of the expression (4.46), shown in Figure 4.10, has features similar to the corresponding plot for the SETL, which is depicted in Figure 3.6. We see that $E^{(0)}$, given by (4.46), is strictly positive in the region of ellipticity $\mathcal{D}$, and is maximised (attaining the same value) at each of the points corresponding to wavevectors $\{\mathbf{k_1}, \ldots, \mathbf{k_6}\}$, that is, at the points which correspond to stationary breathers. It decays to zero towards the boundary of the elliptic domain

$\mathcal{D}$ (see Figure 4.9). Hence, just as we found for the SETL in Section 3.6.3, the energy threshold for moving breathers is lower than for stationary breathers. The threshold becomes arbitrarily small near the boundary of the domain of ellipticity.
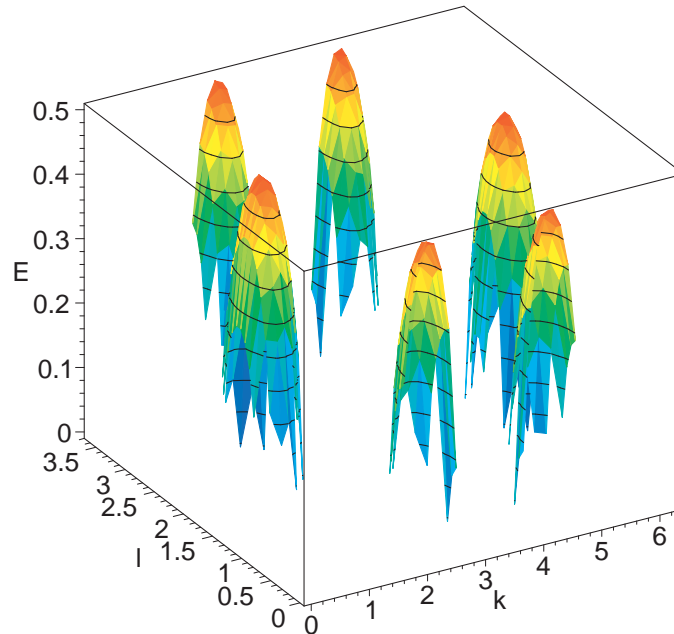
Figure 4.10: Plot of $E^{(0)}$ for lattices with a symmetric potential.

4.3.5 Lattices with an asymmetric potential

In this section, we consider the more general scenario for which the potential $\Upsilon'(Q)$ may be asymmetric. In this case, the terms a and c in (4.10) and (4.11) are not necessarily zero. Clearly if (4.21) is to be reduced to an NLS equation in F, the terms G_0 and G_2 must be found in terms of F. It is a straightforward task to find G_2 in terms of F, since it is given by a simple algebraic equation (4.20). In order to find G_0, the partial differential equation (4.23) must be solved. The term G_0 is a higher order correction term to the leading order term F, and hence we assume that it travels at the same velocity as F. In other words, $G_0(X, Y, \tau, T) \equiv G_0(Z, W, T)$. Eliminating the term $G_{0\tau\tau}$ and rewriting

(4.23) in terms of the variables Z and W, this equation becomes

$$(u^2 - 6)G_{0ZZ} + (v^2 - 2h^2)G_{0WW} + 2vcG_{0ZW} = 6a|F|^2_{ZZ} + 2ah^2|F|^2_{WW}. \quad (4.47)$$

For general k and l, it is difficult to solve for G_0 explicitly. We focus on points in the (k, l) plane for which (4.47) can be solved. As expected (in the light of comments made at the end of Section 4.3.2), equation (4.47) simplifies greatly if we consider any of the wavevectors $\{\mathbf{k_1}, \ldots, \mathbf{k_6}\}$. For all of these wavevectors, the velocities u and v become zero, and so (4.47) becomes $\nabla^2 G_0 = -a\nabla^2|F|^2$, where the operator ∇^2 defined by $\nabla^2_{(Z,W)} \equiv \partial_{ZZ} + \partial_{WW}$ is equivalent to $\nabla^2_{(X,Y)} \equiv \partial_{XX} + \partial_{YY}$. It follows that $G_0 = -a|F|^2$ for all of these wavevectors.

It may also be verified that the remaining equations (4.18)–(4.23) are identical no matter which of the wavevectors $\{\mathbf{k_1}, \ldots, \mathbf{k_6}\}$ is taken. That is to say, it is not necessary to specify which of the wavevectors $\{\mathbf{k_1}, \ldots, \mathbf{k_6}\}$ we are referring to, since the analysis for any of these is completely identical. Thus, (4.18) gives $\omega = 3$, and from (4.20) it is found that $G_2 = aF^2/3$. Interestingly, comparing this with the corresponding result for the SETL (see Section 3.3.5), G_0 is found to be exactly the same for both the SETL and HETL, though unlike before, G_2 is now found to be nonzero.

Substituting these expressions for G_0 and G_2 in (4.21) gives the following NLS equation for asymmetric potentials for any of the wavevectors $\{\mathbf{k_1}, \ldots, \mathbf{k_6}\}$

$$2i\omega F_T + 3\nabla^2 F + \omega^2(3b - \tfrac{10}{3}a^2)|F|^2 F = 0, \quad (4.48)$$

which is similar to its counterpart for the SETL (see equation (3.36)). Equation (4.48) has the same form as (3.39), with $D = 3/2\omega = 1/2$ and (after simplifying) $B = (9b - 10a^2)/2$. The anomalous dispersive regime thus corresponds to $b > 10a^2/9$. Again, we note that this describes a different region of (a, b)-parameter space to the corresponding regime for the SETL (see Section 3.7.8). Using the results of Section 3.4.2, soliton solutions of (4.48) are given by (3.42), this time with $D = 1/2$ and $B = (9b - 10a^2)/2$, and also $r^2 = X^2 + Y^2$. Substituting the solution for F into the lattice ansatz (4.17), along with the known expressions for G_0 and G_2 gives the following second-order formula for stationary breathers

in lattices with an asymmetric potential

$$
\begin{aligned}
Q_{m,n}(t) =\, & 2\varepsilon\alpha\cos[km + lhn + (\omega + \varepsilon^2\lambda)t]\,\mathrm{sech}(\beta r) \\
& + \tfrac{2}{3}a\varepsilon^2\alpha^2\mathrm{sech}^2(\beta r)\big\{\cos[2km + 2lhn + (2\omega + 2\varepsilon^2\lambda)t] - 3\big\} + \mathcal{O}(\varepsilon^3),
\end{aligned}
\tag{4.49}
$$

where α, β are determined from (3.41) using the values of B and D described immediately above, $r = \sqrt{X^2 + Y^2}$, and $X = \varepsilon m$ and $Y = \varepsilon hn$ in terms of the original discrete variables m and n.

Breather energy

We calculate the leading-order energy $E^{(0)}$ of stationary breathers in lattices with an asymmetric potential. In this case, stationary breathers are given by (4.49), which we rewrite in the form

$$
Q_{m,n}(t) \sim 2\varepsilon\alpha\cos\Theta\,\mathrm{sech}(\beta r),
\tag{4.50}
$$

where $\Theta = km + lhn + \Omega t$ is the phase of the carrier wave, (k, l) corresponds to one of $\{\mathbf{k_1}, \ldots, \mathbf{k_6}\}$, $\Omega = \omega + \varepsilon^2\lambda$ is the breather frequency, and $w = 3$. Also α, β and $r^2 = X^2 + Y^2$ are as described above. We remark that $\Theta = km + lhn + \Omega t$ is distinct from Φ introduced in (4.38), since for the former, (k, l) corresponds to one of $\{\mathbf{k_1}, \ldots, \mathbf{k_6}\}$, whereas for the latter, (k, l) can be any point in $\mathcal{D}$.

The expression for $Q_{m,n}$ given by (4.50) is substituted into (4.27). The currents $I_{m,n}$, $J_{m,n}$ and $K_{m,n}$ are obtained by substituting (4.50) into equations (4.28)–(4.30) and integrating with respect to time, taking the constant of integration to be zero. Also, the breather frequency $\Omega \sim \omega$ to leading order. Thus we find

$$
I_{m,n} \sim \frac{3\varepsilon\alpha}{\omega}\sin\Theta\,\mathrm{sech}(\beta r) - \frac{\sqrt{3}\varepsilon\alpha}{\omega}\cos\Theta\,\mathrm{sech}(\beta r),
\tag{4.51}
$$

$$
J_{m,n} \sim \frac{3\varepsilon\alpha}{\omega}\sin\Theta\,\mathrm{sech}(\beta r) + \frac{\sqrt{3}\varepsilon\alpha}{\omega}\cos\Theta\,\mathrm{sech}(\beta r),
\tag{4.52}
$$

$$
K_{m,n} \sim \frac{3\varepsilon\alpha}{\omega}\sin\Theta\,\mathrm{sech}(\beta r) + \frac{\sqrt{3}\varepsilon\alpha}{\omega}\cos\Theta\,\mathrm{sech}(\beta r).
\tag{4.53}
$$

Substituting for $Q_{m,n}$, $I_{m,n}$, $J_{m,n}$ and $K_{m,n}$ in (4.27) using (4.50) and (4.51)–(4.53) gives a leading-order expression for the total energy $E^{(0)}$

$$E^{(0)} \sim \sum_{m,n} \frac{2\varepsilon^2 \alpha^2}{C_0} \cos^2 \Theta \, \mathrm{sech}^2(\beta r)$$
$$+ \frac{Lh^2}{2\omega^2} \varepsilon^2 \alpha^2 \left[3h^2 \sin^2 \Theta + 2h \sin \Theta \cos \Theta + 3 \cos^2 \Theta \right] \mathrm{sech}^2(\beta r) \quad (4.54)$$

Unfortunately, the summand in (4.54) does not simplify much further, and hence we approximate the term in square brackets by taking the average values of $\cos^2 \Theta$ and $\sin^2 \Theta$ (both equal $\frac{1}{2}$), whilst the average value of $\sin \Theta \cos \Theta$ is 0. Proceeding thus, the expression for $E^{(0)}$ (4.54) becomes

$$E^{(0)} \sim \sum_{m,n} \frac{2\varepsilon^2 \alpha^2}{C_0} \mathrm{sech}^2(\beta r). \quad (4.55)$$

We replace the double sum (4.55) by an integral over space, giving

$$E^{(0)} \sim \frac{2\alpha^2}{hC_0} \iint \mathrm{sech}^2(\beta \sqrt{X^2 + Y^2}) \, \mathrm{d}X \mathrm{d}Y, \quad (4.56)$$

(noting the extra factor of h in the denominator, compared to (3.65)). Evaluating the integral in (4.56) gives

$$E^{(0)} \sim \frac{4\pi \log 2}{hC_0} \frac{\alpha^2}{\beta^2} = \frac{8\pi D \log 2 (2 \log 2 + 1)}{BC_0 h (4 \log 2 - 1)}, \quad (4.57)$$

where $D = 1/2$ and $B = (9b - 10a^2)/2$ as explained above. Evaluating (4.57) numerically, we find that $E^{(0)} \approx 13.5401/(9b - 10a^2)C_0$. Again, we find that this estimate for energy is independent of the breather amplitude λ, demonstrating the energy threshold properties of the two-dimensional HETL; namely, the activation energy required to create a breather in the HETL is an $\mathcal{O}(1)$ quantity, irrespective of the smallness of its amplitude ($2\varepsilon\alpha$).

We mention that if we put $a = 0$ in the expression (4.57) for $E^{(0)}$ for stationary breathers in lattices with an asymmetric potential, it reduces to the expression (4.46) obtained for lattices with a symmetric potential when (k, l) corresponds to one of $\{\mathbf{k_1}, \dots, \mathbf{k_6}\}$ in the latter, as expected.

4.4 Higher-order asymptotic analysis

As discussed extensively in Section 3.4, it is known that the two-dimensional cubic NLS equations derived in Sections 4.3.3 and 4.3.5 do not completely describe the evolution of the breather envelope, since the cubic NLS equation exhibits blow-up, which is not physically realistic within the context of discrete systems. We explained in Section 3.4.3 that higher-order dispersive and nonlinear effects play an important role in the dynamics of quasi-continuum models such as (4.11), and therefore must also be incorporated.

Acting upon this, in this section we extend our analysis of the lattice equations (4.11) to fifth-order, and derive a generalised NLS equation which includes higher-order dispersive and nonlinear terms. It then remains to determine whether this generalised NLS equation supports stable soliton solutions for the form of the breather envelope F. As for the SETL, we expect to find several additional perturbing terms. What is of interest is whether the perturbing terms for the HETL are any simpler than those obtained for the SETL (see equation (3.55) of Section 3.5).

As one might expect, the fifth-order analysis is extremely complicated, and so we consider only lattices with symmetric potentials, namely, those for which $a = c = 0$ in (4.10) and (4.11). Since no second or fourth harmonic terms are generated by the nonlinearity, we also use a much simpler ansatz, namely

$$Q_{m,n}(t) = \varepsilon \mathrm{e}^{\mathrm{i}\psi} F(X, Y, \tau, T) + \varepsilon^3 \mathrm{e}^{3\mathrm{i}\psi} H_3(X, Y, \tau, T) + \cdots + \text{c.c.,} \qquad (4.58)$$

where the phase $\psi = km + lhn + \omega t$. In this case, in addition to the equations (4.24), (4.25), (4.26), (4.32) and (4.22), we also have the following equation at fifth-order:

$\mathcal{O}(\varepsilon^5 \mathrm{e}^{\mathrm{i}\psi})$:

$$F_{TT} = \frac{1}{6}\left[8\cos(2k) + \cos k\cos(lh)\right]F_{XXXX}$$

$$+ h^2\cos k\cos(lh)F_{XXYY} + \frac{h^4}{6}\cos k\cos(lh)F_{YYYY}$$

$$- \frac{2h}{3}\sin k\sin(lh)F_{XXXY} - \frac{2h^3}{3}\sin k\sin(lh)F_{XYYY}$$

$$+ 6b\left[2\cos(2k) + \cos k\cos(lh)\right](|F|^2F)_{XX} + 6bh^2\cos k\cos(lh)(|F|^2F)_{YY}$$

$$- 12b\sin k\sin(lh)\left[2hFF_X\overline{F}_Y + 2hFF_Y\overline{F}_X + 2h\overline{F}F_XF_Y + hF^2\overline{F}_{XY} + 2hF\overline{F}F_{XY}\right]$$

$$- 3b\omega^2\overline{F}^2H_3 - 10\omega^2d|F|^4F. \tag{4.59}$$

Clearly, this equation is still rather complicated, so we simplify matters by restricting our attention to stationary breathers. Accordingly, only one extra timescale $T = \varepsilon^2 t$ is required, and we fix the wavenumbers k and l to correspond to one of the wavevectors $\{\mathbf{k_1}, \ldots, \mathbf{k_6}\}$. Hence the simplified ansatz becomes

$$Q_{m,n}(t) = \varepsilon\mathrm{e}^{\mathrm{i}\psi}F(X,Y,T) + \varepsilon^3\mathrm{e}^{3\mathrm{i}\psi}H_3(X,Y,T) + \cdots + \mathrm{c.c.}, \tag{4.60}$$

where the phase ψ is as before, except that (k,l) corresponds to one of $\{\mathbf{k_1}, \ldots, \mathbf{k_6}\}$. Substituting the ansatz (4.60) into the lattice equations (4.11) yields the following set of equations:

$\mathcal{O}(\varepsilon\mathrm{e}^{\mathrm{i}\psi})$:

$$\omega^2 = 9 \quad \Rightarrow \quad \omega = 3, \tag{4.61}$$

$\mathcal{O}(\varepsilon^3\mathrm{e}^{\mathrm{i}\psi})$:

$$2\mathrm{i}\omega F_T + 3\nabla^2 F + 3b\omega^2|F|^2F = 0, \tag{4.62}$$

$\mathcal{O}(\varepsilon^3\mathrm{e}^{3\mathrm{i}\psi})$:

$$H_3 = 0, \tag{4.63}$$

$\mathcal{O}(\varepsilon^5\mathrm{e}^{\mathrm{i}\psi})$:

$$F_{TT} = -\tfrac{3}{4}\nabla^4 F - 9b\nabla^2(|F|^2F) - 10\omega^2d|F|^4F. \tag{4.64}$$

It may be verified that exactly the same set of equations (4.61)–(4.64) results, irrespective of which of the wavevectors $\{\mathbf{k_1}, \ldots, \mathbf{k_6}\}$ is chosen. Interestingly, it emerges from (4.63) that for the HETL, $H_3 = 0$, unlike for the SETL (see Section 3.5), where H_3 was found to be nonzero. This result should be compared with the remarks on G_2 (see Section 4.3.5), which is zero for square lattices with asymmetric potentials, but nonzero for hexagonal lattices.

Also, recalling the opening comments of this section, we note that all differentials on the right-hand side of (4.64) are isotropic. This is a direct consequence of the hexagonal symmetry of the HETL. In comparison, the differential operator in the corresponding equation (3.52) for the SETL was found to be anisotropic.

In order to obtain a higher-order NLS equation, we combine the higher-order equation (4.64) with the cubic two-dimensional NLS equation (4.62). Firstly, the term F_{TT} on the left-hand side of (4.64) is eliminated. This is done by differentiating (4.62) with respect to T and substituting. We find that

$$F_{TT} = -\frac{9}{4\omega^2}\nabla^4 F - \frac{9b}{4}\nabla^2(|F|^2 F) - \frac{27}{4}b^2\omega^2|F|^4 F - \frac{9b}{2}|F|^2\nabla^2 F - \frac{9b}{4}F^2\nabla^2\overline{F}. \quad (4.65)$$

Substituting for F_{TT} in (4.64) using (4.65), and then adding the resulting fifth-order equation to the third-order NLS equation (4.62), gives overall

$$6\mathrm{i}F_T + 3\nabla^2 F + 27b|F|^2 F + \frac{\varepsilon^2}{2}\nabla^4 F + \frac{9\varepsilon^2}{4}(40d - 27b^2)|F|^4 F$$
$$+ \frac{27b\varepsilon^2}{4}\nabla^2(|F|^2 F) - \frac{9b\varepsilon^2}{2}|F|^2\nabla^2 F - \frac{9b\varepsilon^2}{4}F^2\nabla^2\overline{F} = 0. \quad (4.66)$$

Hence, if we confine our attention to stationary breathers and symmetric potentials, we find that the equations for the HETL (4.11) reduce to the generalised NLS equation (4.66) for the breather envelope F. Equation (4.66) should be compared with its counterpart for the SETL, which is equation (3.55). Clearly, (4.66) is isotropic, unlike (3.55). Other than this, the terms present in both equations are identical, occurring only with different coefficients. To the best of our knowledge, (4.66) has not been studied in the literature before. We note that (4.66) is similar to the perturbed NLS equation (3.44) considered by Davydova *et al.* [38], and therefore includes known stabilising terms. We have been unable

to find a variational formulation of (4.66), and therefore we cannot determine its stability properties using the methods outlined in Section 3.4.3. Alternative methods have been discussed in Sections 3.5 and 3.8.

For now, we rely on Davydova's criteria for soliton existence, discussed in Section 3.4.3. Anomalous dispersion corresponds to $b > 0$, and the condition $PK > 0$ becomes $40d > 27b^2$. Hence, it is in this parameter regime that we seek breathers solutions of the HETL for the numerical work in Section 4.5. As we shall see in Section 4.5, numerical simulations show that long-lived breather solutions are supported by the two-dimensional hexagonal FPU lattice, which suggests that the additional perturbing terms in (4.66) have a stabilising effect upon Townes solitons.

4.5 Numerical results

4.5.1 Preliminaries

In this section, we solve the equations governing charge $Q_{m,n}$ in the lattice numerically. The lattice equations (4.11) form a system of infinitely many coupled second-order nonlinear ordinary differential equations. To allow for numerical solution of this system, we consider the equations defined upon a finite lattice. We use MATLAB to implement a numerical algorithm based on a fourth-order Runge-Kutta scheme. Firstly, by introducing the variable $R_{m,n}$, defined by $R_{m,n} = \mathrm{d}Q_{m,n}/\mathrm{d}t$, the system of second-order ordinary differential equations (4.11) is converted to an equivalent system of first-order differential equations,

$$\frac{\mathrm{d}Q_{m,n}}{\mathrm{d}t} = R_{m,n},$$

$$\frac{\mathrm{d}R_{m,n}}{\mathrm{d}t} = (\delta_I^2 + \delta_J^2 + \delta_K^2)\left[Q_{m,n} + aQ_{m,n}^2 + bQ_{m,n}^3 + cQ_{m,n}^4 + dQ_{m,n}^5\right], \qquad (4.67)$$

where the second-difference operators δ_I^2, δ_J^2 and δ_K^2 are defined in (4.7)–(4.9).

We present the results of simulations for a range of parameter values. From (4.26), the breather $\mathbf{v} = (u, v)$ depends upon the wavevector $\mathbf{k} = [k, l]^T$, and hence we obtain moving breathers by choosing $(k, l) \in D$ (see Figure 4.9) and $[k, l]^T \notin \{\mathbf{k_1}, \ldots, \mathbf{k_6}\}$ (see Section 4.3.2). In Figure 4.11, we show the points in $\mathcal{D}_1 \subset \mathcal{D}$ (see Figure 4.9 and Section 4.3.4) for which we solve the lattice equations (4.67) numerically. These points correspond to the wavevectors $\mathbf{k_1} = [\pi/3, \pi/h]^T$, $\mathbf{k_a} = [1.4, \pi/h]^T$, $\mathbf{k_b} = [0.79, 1.7324]^T$ and $\mathbf{k_c} = [0.8, 1.9987]^T$.

We present simulations of stationary and moving breathers in lattices with symmetric potentials (that is, $a = c = 0$ in (4.67)) in Sections 4.5.4–4.5.7. Numerical results for systems with asymmetric potentials ($a, c \neq 0$) are presented in Section 4.5.8.

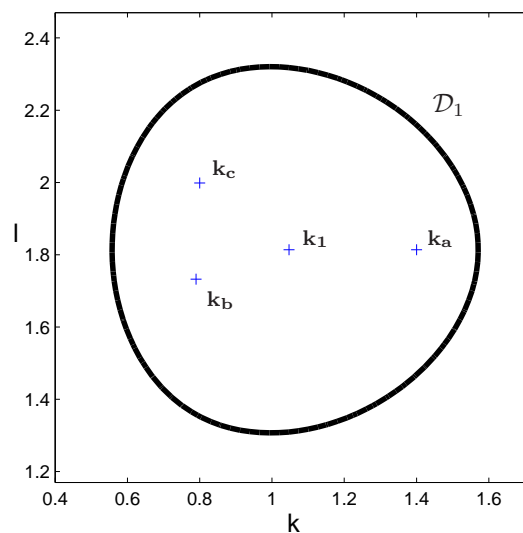**Figure 4.11:** Wavevectors in $\mathcal{D}_1 \subset \mathcal{D}$ for which breathers are simulated.

4.5.2   Initial data and boundary conditions

We generate initial data by using the analytic expressions for breather solutions derived in Section 4.3. The formulae for $Q_{m,n}$ and $R_{m,n}$ are found in terms of the original discrete variables m and n, and then shifted in both the horizon-

tal and vertical directions so that initially the breather lies at the centre of the finite lattice.

We impose periodic boundary conditions for the lattice in both the horizontal and vertical directions, so that the flat two-dimensional arrangement in Figure 4.1 is effectively a two-torus. This is implemented so that for long-time simulations of moving breathers, waveforms which approach any edge of the lattice reappear from the opposite edge. Setting up periodic boundary conditions for the HETL to this effect is far more complicated than for the SETL (see Section 3.7.2).

An illustration of a small finite lattice is shown in Figure 4.12. Care must be taken to ensure that the truncated finite lattice (that is, the two-torus) retains the same translational invariance as the original infinite lattice. The dots represent capacitors located at lattice sites, and the lines represent inter-connecting inductors. For the sake of clarity, the inductors connecting the capacitors at the center of each hexagon to its six nearest neighbours are not shown (see Figure 4.1). It is not necessary that the lattice should be "square," meaning that the lattice could comprise $M \times N$ lattice sites, with $M \neq N$. However, typically, we consider $M = N$ as in Figure 4.12, since the numerical routines become considerably simpler to encode when the lattice *is* square. We will usually consider lattices with $N \leq 50$.

We select the site $(1, 1)$ to lie at the bottom left-hand corner of the arrangement in Figure 4.12, which has coordinate position (1,1). The remaining lattice sites are labelled according to scheme described in Section 4.2, that is, using the lattice basis $\mathcal{B} = \{\mathbf{i}', \mathbf{j}'\}$ where $\mathbf{i}' = [1, 0]^T$ and $\mathbf{j}' = [0, h]^T$.

From equations (4.67), the charge $Q_{m,n}$ stored on each capacitor depends upon the charge stored on the capacitors located at its six neighbouring sites. These are located at the two nearest neighbouring sites in each of the directions parallel to the vectors $\mathbf{e_i}$, $\mathbf{e_j}$ and $\mathbf{e_k}$ (see Figure 4.5). Clearly from Figure 4.12, for the finite lattice, not all lattice sites possess six nearest neighbours. We see
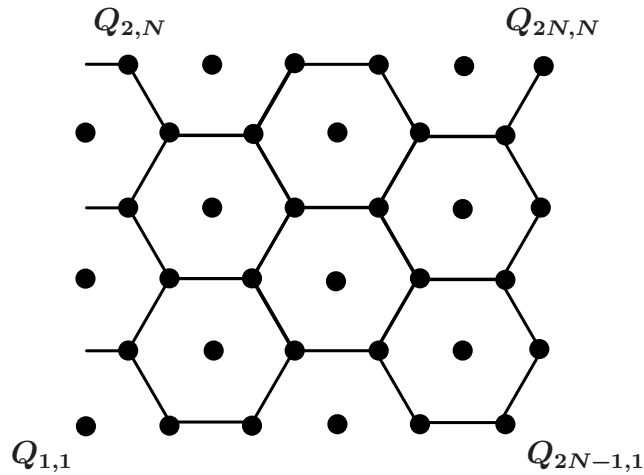
Figure 4.12: Periodic boundary conditions for the two-dimensional HETL.

from this that equations (4.67) are defined at interior lattice sites, but sites along the boundaries and corners are missing between one and four neighbours. We introduce fictitious point along the boundaries and corners where necessary to effect periodic boundary conditions. The full details are rather complicated, though the underlying principle is exactly the same as before (see Section 3.7.2), and so we have not included the details here.

4.5.3 Numerical computation of breather energy

Since the HETL is a lossless network, we expect the total energy E to be conserved. We check the accuracy of our numerical scheme by computing the leading-order energy $E^{(0)}$, given by (4.27). To do this, we express the summand $e^{(0)}_{m,n}$ in terms of the output variables of the numerical routine, namely $Q_{m,n}$ and $R_{m,n}$. The first term of $e^{(0)}_{m,n}$ is already given in terms of $Q_{m,n}$. It remains to find the currents $I_{m,n}$, $J_{m,n}$ and $K_{m,n}$ in terms of $Q_{m,n}$ and $R_{m,n}$. The actual details of this depend upon whether the interaction potential is symmetric or asymmetric.

Lattices with a symmetric potential

First, we find the current $I_{m,n}$ in terms of $Q_{m,n}$ and $R_{m,n}$. Differentiating the leading-order expression for the breather given by (4.38), we have (retaining leading-order terms only)

$$\dot{Q}_{m,n} = R_{m,n} \sim -2\varepsilon\alpha\omega \sin\Phi \operatorname{sech}(\beta r), \tag{4.68}$$

where α, β and r^2 are as defined in Section 4.3.3. Comparing the analytic expression (4.39) for the current $I_{m,n}$ with the expressions for $Q_{m,n}$ (4.38) and $R_{m,n}$ (4.68), we see that

$$I_{m,n} = \frac{\cos(2k) - 1}{\omega^2} R_{m,n} - \frac{\sin(2k)}{\omega} Q_{m,n}. \tag{4.69}$$

Similarly, comparing the expressions (4.40) and (4.41) for the currents $J_{m,n}$ and $K_{m,n}$ respectively with equations (4.38) and (4.68), we find that

$$J_{m,n} = \frac{\cos(k - lh) - 1}{\omega^2} R_{m,n} - \frac{\sin(k - lh)}{\omega} Q_{m,n}, \tag{4.70}$$

$$K_{m,n} = \frac{\cos(k + lh) - 1}{\omega^2} R_{m,n} - \frac{\sin(k + lh)}{\omega} Q_{m,n}. \tag{4.71}$$

The expressions for $I_{m,n}$, $J_{m,n}$ and $K_{m,n}$ given by equations (4.69)–(4.71) are then substituted into the sum (4.27), giving an overall expression for $E^{(0)}$ in terms of $Q_{m,n}$ and $R_{m,n}$. The resulting expression does not simplify greatly, so we do not reproduce it here. We check whether this sum is conserved for simulations of lattices with symmetric potentials, and also whether it matches with the asymptotic estimate given by (4.46).

Lattices with an asymmetric potential

Differentiating the leading-order expression (4.50) for the charge $Q_{m,n}$ in lattices with an asymmetric potential gives

$$\dot{Q}_{m,n} = R_{m,n} \sim -2\varepsilon\alpha\omega \sin\Theta \operatorname{sech}(\beta r). \tag{4.72}$$

Using (4.50) and (4.72), the current $I_{m,n}$ which is given by (4.51) can be expressed in terms of $Q_{m,n}$ and $R_{m,n}$,

$$I_{m,n} \sim -\frac{\sqrt{3}}{2\omega} \left[\frac{\sqrt{3} R_{m,n}}{\omega} + Q_{m,n} \right]. \tag{4.73}$$

Similarly, from equations (4.52) and (4.53), we also have

$$J_{m,n} = K_{m,n} \sim -\frac{\sqrt{3}}{2\omega} \left[\frac{\sqrt{3}R_{m,n}}{\omega} - Q_{m,n} \right]. \tag{4.74}$$

Inserting the expressions for $I_{m,n}$, $J_{m,n}$ and $K_{m,n}$ given by equations (4.73) and (4.74) respectively into (4.27) becomes after simplification

$$E^{(0)} \sim \sum_{m,n} \frac{1}{72C_0} \left[45Q_{m,n}^2 + 3R_{m,n}^2 - 2\sqrt{3}Q_{m,n}R_{m,n} \right], \tag{4.75}$$

which is the required expression giving $E^{(0)}$ as a combination of $Q_{m,n}$ and $R_{m,n}$. The quantity on the right-hand side of (4.75) is summed over the entire lattice for simulations of lattices with an asymmetric potential. It may be verified that if we put $a = 0$ in the expression (4.75) for $E^{(0)}$, it matches the estimate obtained for symmetric potentials when (k, l) corresponds to one of $\{\mathbf{k_1}, \ldots, \mathbf{k_6}\}$ in the latter.

Effective breather width

Numerical computation of the energy as described above allows us to check that the total lattice energy is conserved, but does not indicate whether a breather changes shape significantly with time. To remedy this, we define a measure of breather width $\mathcal{W}_{\mathrm{br}}$ in the same manner as in Section 3.7.3,

$$\mathcal{W}_{\mathrm{br}}^2 = \frac{r_{20}}{E^{(0)}} + \frac{r_{02}}{E^{(0)}} - \left(\frac{r_{10}}{E^{(0)}} \right)^2 - \left(\frac{r_{01}}{E^{(0)}} \right)^2, \tag{4.76}$$

though the form of r_{10}, r_{01}, r_{20} and r_{02} is slightly different (note the presence of an additional factor h)

$$r_{10} = \sum_{m,n} m e_{m,n} \qquad r_{20} = \sum_{m,n} m^2 e_{m,n}$$

$$r_{01} = \sum_{m,n} hn e_{m,n} \qquad r_{02} = \sum_{m,n} h^2 n^2 e_{m,n}$$

The quantity $\mathcal{W}_{\mathrm{br}}$ gives a measure of the degree of distortion suffered by a breather over time.

4.5.4 Stationary breather in a lattice with symmetric potential

We seek stationary breather solutions in the anomalous dispersion regime. From (4.66), this corresponds to $b > 0$. The horizontal and vertical velocities u and v respectively are zero when (k, l) corresponds to one of $\{\mathbf{k_1}, \dots, \mathbf{k_6}\}$; we set $k = \pi/3$ and $l = \pi/h$, corresponding to $\mathbf{k_1}$ in Figure 4.11. Following the discussion in Section 4.4, we expect to find stable soliton solutions when $PK > 0$. From (4.66), $P = \varepsilon^2/2$, hence this inequality becomes $40d > 27b^2$. For instance, this is satisfied when $b = d = 1$. The following values are chosen for the remaining parameters: $N = 30$, $\varepsilon = 0.2$ and $\lambda = 1$.

The variational parameters (3.41) are calculated as $\alpha = 1.0212$, $\beta = 1.8670$. The breather frequency is $\omega + \varepsilon^2\lambda = 3.040$, and therefore the period of oscillation is $T = 2.0668$. In Figure 4.13 (a), the initial profile of the breather is shown, located at the centre of the lattice (this is the case for all our simulations). At time $t = 0$, we find that the breather energy $E^{(0)} = 0.7606$, and the breather width $\mathcal{W}_{\mathrm{br}} = 3.74$.

In Figure 4.13 (c) we show the breather after it has completed 30 full oscillations. Plots of the cell energy $e_{m,n}$ at $t = 0$ and $t = 30T$ are presented in Figures 4.13 (b) and 4.13 (d). We note that after thirty oscillations, the breather has shed a small amount of energy, which manifests itself as background noise throughout the lattice. Accordingly, the breather appears a little distorted in shape compared to its initial profile in Figure 4.13 (a), though not greatly so. In particular, at $t = 30T$, we find that $\mathcal{W}_{\mathrm{br}} = 4.21$, and so $\Delta\mathcal{W}_{\mathrm{br}}/\mathcal{W}_{\mathrm{br}} = 0.13$. Clearly, after thirty cycles, the breather has not preserved its form as well as was recorded for the SETL, described in Section 3.7.4. It should also be noted that the calculated energy of the breather at $t = 30T$ is 0.7087, giving $\Delta E^{(0)}/E^{(0)} = -0.0682$, which marks a significantly greater fluctuation in the calculated values of $E^{(0)}$ than obtained in Section 3.7.4. The asymptotic estimate for $E^{(0)}$ given by (4.46) is 0.7523, which is in close agreement with the numerically obtained value.
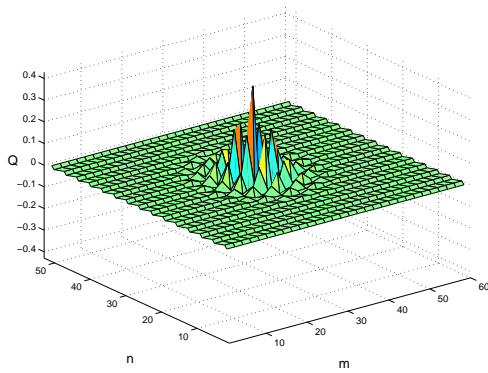
(a) Profile at $t = 0$.
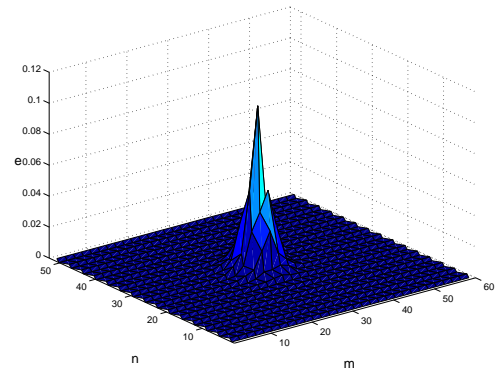
(b) Plot of $e_{m,n}$, $E^{(0)} = 0.7606$.
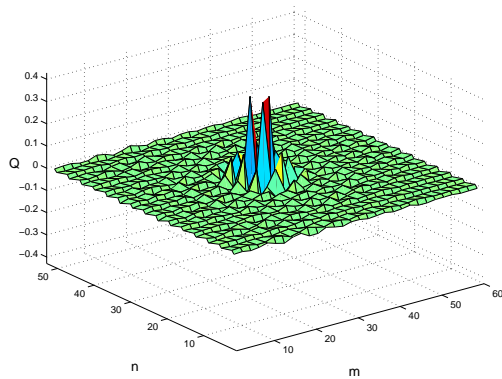
(c) Profile at $t = 30T = 62.82$.
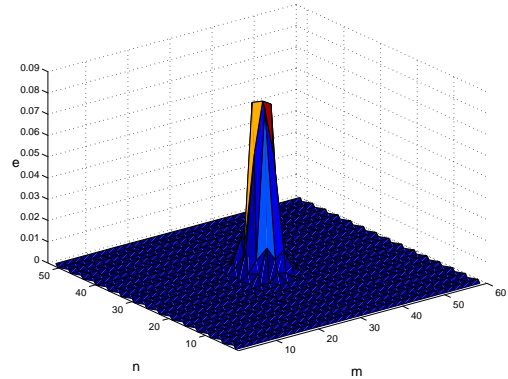
(d) Plot of $e_{m,n}$, $E^{(0)} = 0.7087$.

Figure 4.13: Stationary breather in a lattice with symmetric potential.
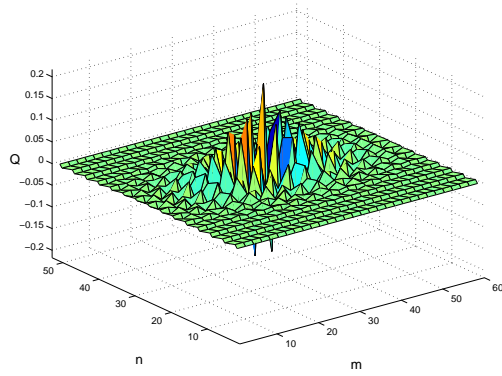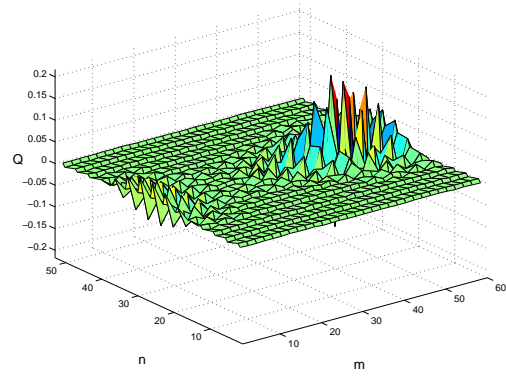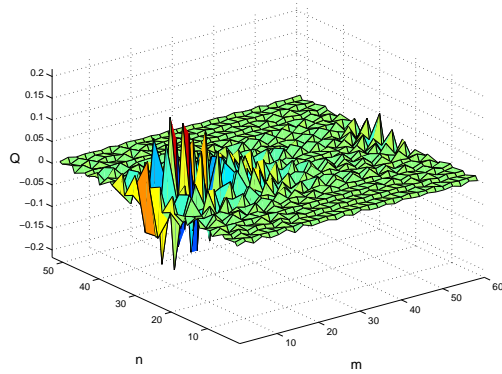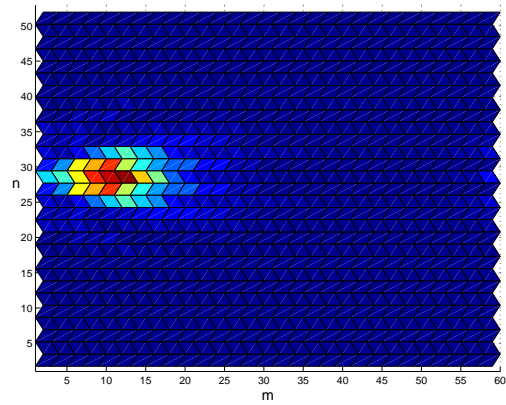
4.5.5 Breather moving along a lattice direction ($\Psi = 0°$)

In Figure 4.14, we show a simulation of a breather moving along a lattice direction parallel to the m-axis, that is, $\Psi = 0°$. The angle of direction of travel Ψ satisfies $\tan \Psi = v/u$. We choose wavevector $\mathbf{k} = \mathbf{k_a} = [1.4, \pi/h]^T$ shown in Figure 4.11, so that $u = 0.4445$ and $v = 0$ and thus $\Psi = 0°$. It turns out that the breather frequency $\omega = 2.9265$, and hence the period $T = 2.1470$. Also, the variational parameters are $\alpha = 1.0339$ and $\beta = 1.8440$. The remaining parameters are set as follows; $b = 1$, $d = 1$, $N = 30$, $\varepsilon = 0.1$ and $\lambda = 1$.

The initial profile of the breather is shown in Figure 4.14 (a), and at this time, the calculated energy is $E^{(0)} = 0.5537$. It may be observed that the breather is not radially symmetric. In fact, it is slightly elongated in the direction parallel to the m-axis, that is, parallel to the direction of motion. This is because the point corresponding to the wavevector $[1.4, \pi/h]^T$ in (k, l)-parameter space is near the boundary of the region of ellipticity $\mathcal{D}_1$ in Figure 4.9.

The breather is shown in Figure 4.14 (b) at a later stage at $t = 21.58T = 46.3513$, at which time we find that $E^{(0)} = 0.5562$. By this time, the breather has reached the right-hand edge of the lattice. Owing to the periodic boundary conditions, it is seen to disappear from this end and reemerge from the left-hand side. This is shown in Figure 4.14 (c), for which $t = 46.59T = 100$. At this time, the breather has almost completely reappeared on the left-hand side, and we find that $E^{(0)} = 0.5696$. This is clearly a long-lived mode, though the breather form distorts noticeably as it travels, as well as leaving behind a small amount of energy in its path (visible in Figures 4.14 (b) and 4.14 (c)). Overall though, the breather remains localised, without spreading greatly. We also note that the computed energy changes very little, with $\Delta E^{(0)}/E^{(0)} = 0.0287$, which is much smaller than for the previous simulation. The asymptotic estimate for the energy of moving breathers (4.46) gives $E^{(0)} = 0.5522$.

We would also like to check whether the velocity of the breather as measured from Figure 4.14 matches with the theoretical velocity u, which is 0.4445 units per second. This is easier to determine from a plot of the energy $e_{m,n}$,

(a) Profile at $t = 0$, $E^{(0)} = 0.5537$.

(b) Profile at $21.58T$, $E^{(0)} = 0.5562$.

(c) Profile at $t = 46.59T$, $E^{(0)} = 0.5696$.

(d) Plot of $e_{m,n}$.

Figure 4.14: Breather moving along a lattice direction, $\Psi = 0°$.

which is shown in Figure 4.14 (d), viewed from directly above the plane of the lattice. From this plot, we record the final position of the breather, and then determine the total distance travelled, which is 42 units to the right. Hence the measured velocity is 0.42 units per second. This value is 5.5% lower than the theoretical value. This is consistent with the observation that a small amount of energy was shed during travel.

4.5.6   Breather moving at $\Psi = 210°$

We now show that it is possible to simulate breathers moving in directions other than $\Psi = 0°$. In this section, we aim to simulate a breather moving at $\Psi = 210°$. Recalling the results of the previous simulation in Section 4.5.5, we note that although k and l can be chosen such that (k, l) lies anywhere within the elliptic domain $\mathcal{D}$, selecting (k, l) to lie too near the boundary of $\mathcal{D}$ results in a sharply elongated breather, which as we have seen, may yield poorer results than expected. On the other hand, wavevectors very close to any of $\{\mathbf{k_1}, \ldots, \mathbf{k_6}\}$ (which correspond to stationary breathers), lead to breather modes with very low speeds (see equation (4.26)). This necessitates excessively long running times, since very slowly moving breathers do not traverse appreciable distances over intermediate times. In practice then, we aim to determine "optimal" wavenumbers k and l; that is, wavenumbers which on the one hand do not lead to a severely elongated breather envelope, and on the other, yield velocities of a magnitude which result in measurable displacements over reasonable times. Unfortunately, unlike the SETL, the expressions for the quantities u, v, $\tan \Psi = v/u$ and $\sqrt{u^2 + v^2}$ do not simplify greatly, and therefore the task of selecting suitable k and l which result in a measurable velocity with a required direction is rather tedious.

We set $k = 0.79$ and $l = 1.7324$, which corresponds to $\mathbf{k_b}$ in Figure 4.11. It may be verified that $u = -0.1999$ and $v = -0.1154$ units per second, leading to $\Psi = \arctan(0.5774) = 210°$ as required. Also, we have that $\omega = 2.9675$ and hence $T = 2.1174$. The remaining parameters are $b = 1$, $d = 1$, $N = 30$, $\varepsilon = 0.1$ and $\lambda = 1$. The variational parameters α and β are 1.0267 and 1.8568 respectively. The breather is shown at times $t = 25, 50, 75$ and 100 seconds in Figure 4.15. It may be observed that the breather does not deform significantly as it travels, nor does it radiate much energy. The initial energy is computed to be $E^{(0)} = 0.6306$, and at $t = 100$, the energy is 0.6275. Thus we have $\Delta E^{(0)}/E^{(0)} = -0.005$, and hence the energy does not fluctuate greatly. The asymptotic estimate for the energy is $E^{(0)} = 0.6184$, which is close to the numerically computed values.
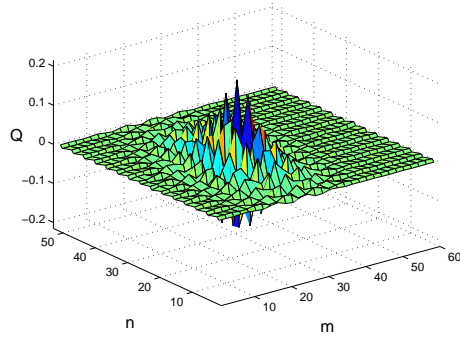
(a) Profile at $t = 25$, $E^{(0)} = 0.6295$.
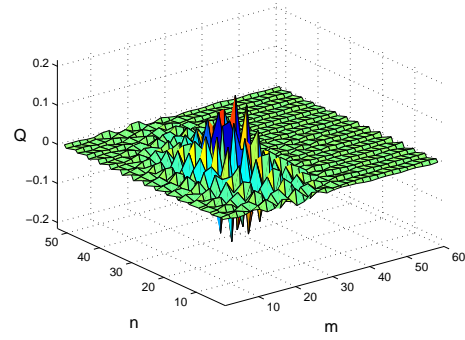
(b) Profile at $t = 50$, $E^{(0)} = 0.6292$.
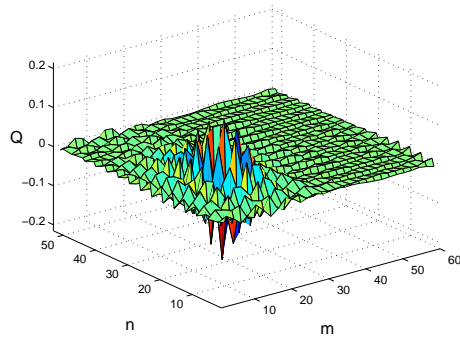
(c) Profile at $t = 75$, $E^{(0)} = 0.6235$.
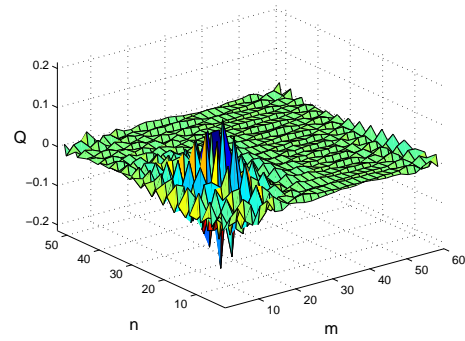
(d) Profile at $t = 100$, $E^{(0)} = 0.6275$.

Figure 4.15: Breather moving at $\Psi = 210°$.

It remains to find the velocity of the breather. For this simulation, we have not shown plots of the energy $e_{m,n}$, rather, the motion of the breather is charted in Table 4.1. The measured displacement, velocities and angle of direction of travel Ψ are recorded therein. As calculated from the last row, the final measured values for the velocities u and v are -0.185 and -0.11 units per second, and hence the overall speed is 0.2152 units per second. The predicted speed (corresponding to $u = -0.1999$ and $v = -0.1154$) is 0.2308 units per second. Hence the measured speed is 6.8% lower than predicted, though the angle of travel is found to be almost identical to the expected value $\Psi = 210°$.

Time (s)	Horizontal displacement	Vertical displacement	Average horizontal velocity (units s^{-1})	Average vertical velocity (units s^{-1})	$\tan \Psi$	Ψ
25	-3.5	-2	-0.14	-0.08	0.5714	209.74°
50	-8	-4.5	-0.16	-0.09	0.5625	209.36°
75	-13	-7.5	-0.1733	-0.1	0.5770	209.99°
100	-18.5	-11	-0.185	-0.11	0.5946	210.74°

Table 4.1: Summary of breather motion ($\Psi = 210°$).

4.5.7 Breather moving at $\Psi = 130°$

We have presented simulations of breathers which move along axes of symmetry of the lattice. In Section 4.3.4, from the results of our asymptotic analysis, we found no constraints upon the permitted directions of travel within the lattice. In other words, the angle of travel Ψ can take any value in the interval $[0, 2\pi)$. In this section, we use our numerical routines to test the conjecture that breathers may move along directions which do not correspond to axes of symmetry of the lattice.

We mention that we have successfully propagated breathers in a range of directions. We show only one such simulated breather in this section, namely, a breather moving at an angle $\Psi = 130°$. We set $k = 0.8$ and $l = 1.9987$, for which it is found that $u = -0.2160$, $v = 0.2575$, and hence $\Psi = \arctan(-1.1918) = 130°$. Also, $\omega = 2.9502$ and so the period $T = 2.1298$. The remaining parameters are $b = 1$, $d = 1$, $N = 30$, $\varepsilon = 0.1$ and $\lambda = 1$. The variational parameters α and β are 1.0297 and 1.8514 respectively. We observe that the breather remains localised without suffering appreciable degradation even after 120 seconds or more, nor is a much radiation left behind in its wake. Initially the energy $E^{(0)}$ is computed as 0.5977, and after 120 seconds, $E^{(0)}$ is 0.5897, giving $\Delta E^{(0)}/E^{(0)} = -0.0133$. The asymptotic estimate for the energy is $E^{(0)} = 0.5965$.

To find the velocity of the breather, we have again recorded its motion at each of the stages depicted in Figure 4.16. The relevant data is presented in

(a) Profile at $t = 30$, $E^{(0)} = 0.5961$.

(b) Profile at $t = 60$, $E^{(0)} = 0.5966$.

(c) Profile at $t = 90$, $E^{(0)} = 0.5939$.

(d) Profile at $t = 120$, $E^{(0)} = 0.5897$.
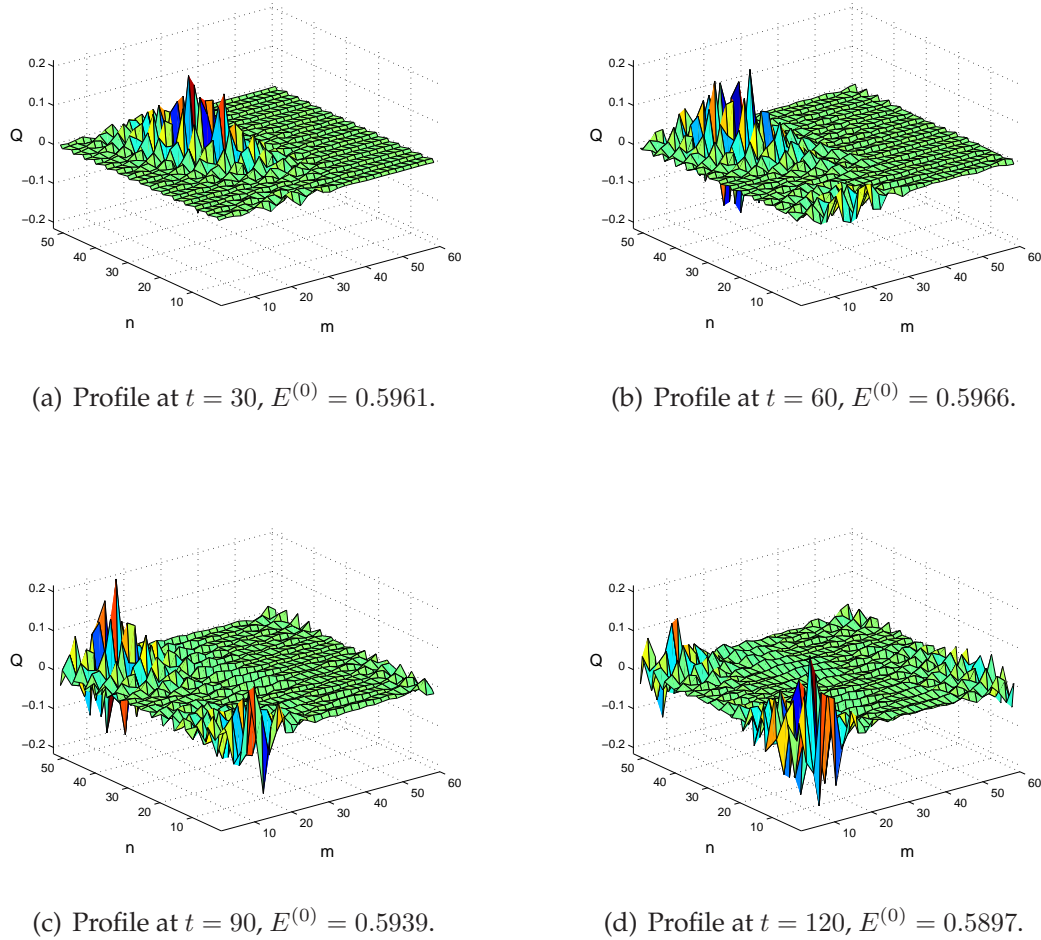
Figure 4.16: Breather moving at $\Psi = 130°$.

Table 4.2. The final measured velocity components of the breather (see the last row of Table 4.2) are $u = -0.2083$ and $v = 0.25$, giving a measured speed of 0.3254 units per second. The predicted velocity components are $u = -0.2160$ and $v = 0.2575$, giving a speed of 0.3361 units per second. Hence the measured speed is 3.2% lower than the expected speed. However, the measured angle of travel is almost exactly the same as the theoretical value $\Psi = 130°$.

4.5.8 Stationary breather in a lattice with asymmetric potential

In Sections 4.5.4–4.5.7, we have shown simulations of lattices with a symmetric potential, namely, those for which $a = c = 0$ in (4.67). We now consider

Time (s)	Horizontal displacement	Vertical displacement	Average horizontal velocity (units s^{-1})	Average vertical velocity (units s^{-1})	$\tan\Psi$	Ψ
30	-6	7	-0.2	0.2333	-1.1667	130.60°
60	-11	13.5	-0.1833	0.225	-1.2273	129.17°
90	-17.5	21.5	-0.1944	0.2389	-1.2286	129.14°
120	-25	30	-0.2083	0.25	-1.2	129.81°

Table 4.2: Summary of breather motion ($\Psi = 130°$).

the more general case for which the interaction potential is asymmetric. Initial data is generated using the formula given (4.49). As discussed in Section 4.3.5, anomalous dispersion corresponds to $b > 10a^2/9$. As an example, we set $a = 1$, $b = 2.5$, $c = 0$ and $d = 1$. Also, recalling the analysis of Section 4.3.5 we choose wavevector $\mathbf{k} = \mathbf{k_1}$, that is $k = \pi/3$ and π/h, which corresponds to a stationary breather. The remaining parameter values are $N = 30$, $\varepsilon = 0.1$ and $\lambda = 1$. The variational parameters are $\alpha = 0.8665$ and $\beta = 1.8670$, and the breather frequency $\omega = 3$, hence $T = 2.0668$.

The breather is shown in Figure 4.17 after 10, 30 and 40 full oscillations. Initially, we find the energy $E^{(0)} = 0.5429$, and the breather width $\mathcal{W}_{br} = 7.46$. The accompanying plots of $e_{m,n}$ demonstrate clearly that the breather preserves its form and remains localised, even after 80 seconds. At $t = 40T$, we find that $\mathcal{W}_{br} = 6.83$, in which case $\Delta\mathcal{W}_{br}/\mathcal{W}_{br} = -0.08$, showing that the breather has contracted very slightly over this time. Also, at $t = 40T$, the numerically computed value of the energy $E^{(0)} = 0.5371$, showing that the energy does not fluctuate significantly. Specifically, we find that $\Delta E^{(0)}/E^{(0)} = -0.01$. The asymptotic estimate of the energy given by (4.57) is 0.5416.
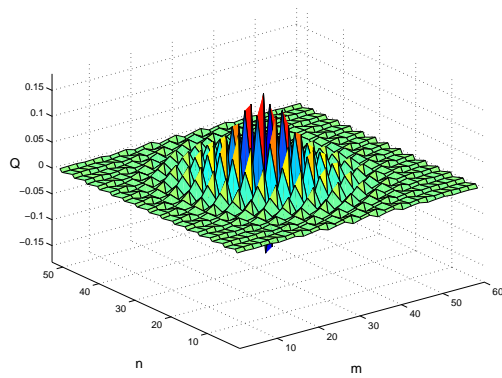
(a) $t = 10T = 20.69$.
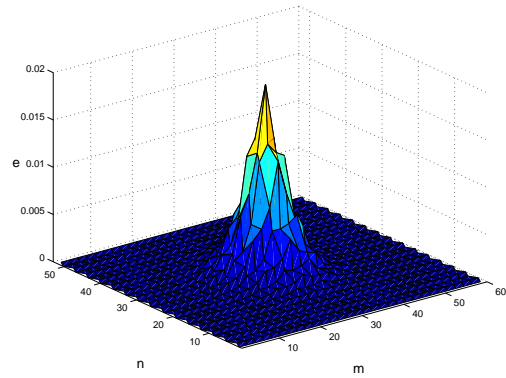
(b) Plot of $e_{m,n}$, $E^{(0)} = 0.5453$.
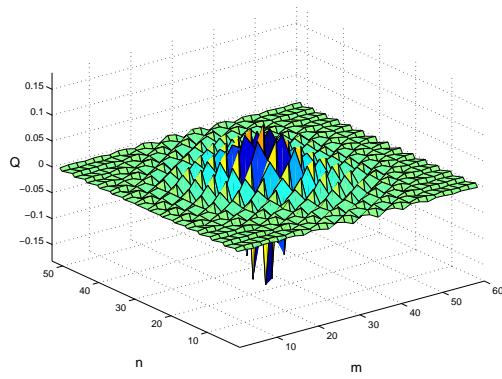
(c) $t = 30T = 41.34$.

(d) Plot of $e_{m,n}$, $E^{(0)} = 0.5425$.
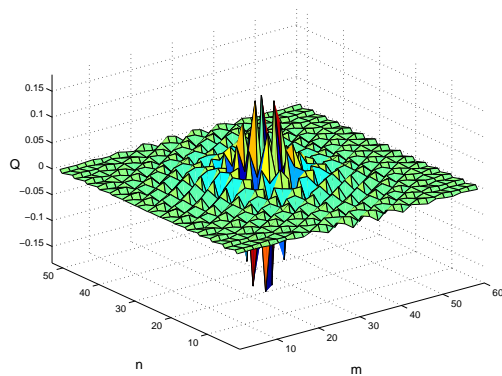
(e) $t = 40T = 82.67$.
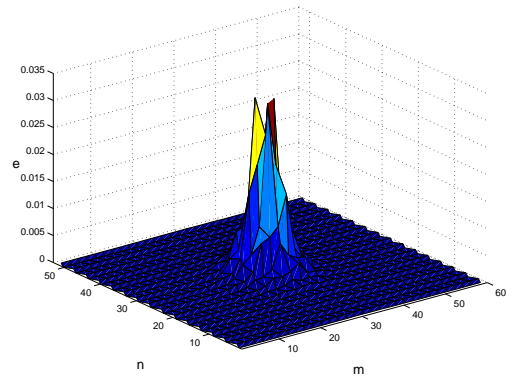
(f) Plot of $e_{m,n}$, $E^{(0)} = 0.5371$.

Figure 4.17: Stationary breather in a lattice with an asymmetric potential.

4.6   Discussion

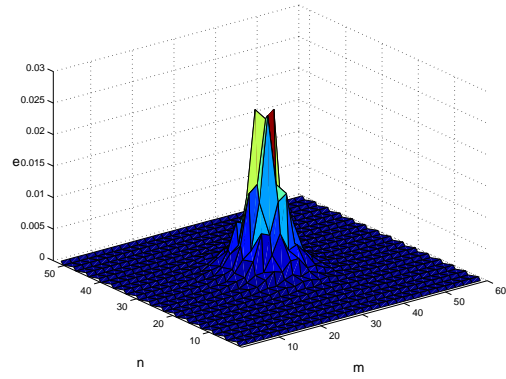In this chapter, we have found approximations to discrete breathers in a two-dimensional hexagonal FPU lattice. We have shown that the lattice equations can be reduced to a cubic NLS equation for two special cases. In Section 4.3.3, we considered moving breathers in lattices with a symmetric interaction potential, in which case an ellipticity criterion for the wavevector was found. Also, in Section 4.3.5, we considered lattices with an asymmetric potential, in which case a reduction could be performed only for stationary breathers. We used formulae for soliton solutions of the NLS equation derived in Section 3.4.2 to generate leading-order forms for breather solutions in both cases. Although the theoretical methods used for the square lattice of Chapter 3 and the hexagonal lattice are similar, several important differences emerge in the course of the analysis. For example, we find that the higher-order correction term G_2 is nonzero in hexagonal lattices with an asymmetric potential, unlike in square lattices, where G_2 is zero. Similarly, we found that the anomalous dispersion regime corresponds to a different region of (a, b)-parameter space.

We also presented asymptotic estimates for the breather energy in Sections 4.3.3 and 4.3.5. As expected, we found a minimum energy required to create breathers in the hexagonal lattice. The threshold energy for moving breathers is smaller than that required for stationary breathers, becoming vanishingly small near the boundary of the elliptic domain.

In Section 4.4, we extended the analysis to fifth-order to derive a higher-order equation which correctly describes the evolution of the breather envelope. We obtained a generalised NLS equation (4.66) with known stabilising terms. This equation is slightly simpler than the corresponding equation (3.55) obtained for the SETL. In particular, the higher-order dispersive terms in (4.66) are isotropic, reflecting the hexagonal rotational symmetry of the lattice. Also, we found that the higher-order correction term H_3 is zero, unlike for the square lattice, where H_3 is nonzero. The stability properties of (4.66) can be established rigorously using methods such as those outlined in Sections 3.5 and 3.8. From

our fifth-order analysis, we determined regions of parameter space in which we expect to find breather solutions. These results are tested and supported by numerical simulation of the lattice, presented in Section 4.5.

In Section 4.5, we showed that the hexagonal FPU lattice supports both long-lived stationary and moving breathers. On the whole, the breather profiles change very little over time, and only a small amount of energy is shed as the breathers propagate. This is true for lattices with symmetric as well as asymmetric interaction potentials. We have successfully propagated long-lived breathers moving in directions which are not axes of symmetry of the lattice (for instance, $\Psi = 130°$). This suggests that there is no restriction upon the angle of travel Ψ, in contrast to the observations reported by Marin *et al.* [89, 90] for two-component lattices (see Section 3.1).

A shortened version of the work in this chapter is presented in Butt & Wattis [25].

Chapter 5

Conclusions

In this thesis, we have discussed discrete breathers, that is, spatially localised time-periodic excitations in translationally invariant lattices. In Chapter 1, we described how the paired effects of nonlinearity and discreteness allow discrete breathers to occur and remain stable against decay though phonon resonances. Breathers occur in a wide range of lattice models, since only relatively weak conditions are required for their existence. The existence of (continuum) breather solutions of partial differential equations is quite rare in comparison. Discrete breathers have attracted a great deal of interest because of their ability to focus or localise vibrational energy. It is thought that breathers act as agents of energy storage and transfer in a broad range of physical settings.

A large body of literature is concerned with the existence and properties of breathers in different lattices. In Chapter 1, we reviewed several seminal papers on discrete breathers, for instance, those which establish existence and stability rigorously. We discussed current active areas of research, concerned with, for example, moving breathers, and the connection with band-edge plane waves. We also described several recent experiments in which breathers have been observed directly.

In Section 1.7, we reviewed several analytic methods used to investigate properties of discrete breathers in lattices. We have used the semi-discrete multiple-scale method (due to Remoissenet [102]) extensively throughout this

thesis. The validity of this method is proved by Giannoulis & Mielke [61, 62].

In Chapter 2, we considered an FPU chain for which the interaction potential is given by a quartic polynomial. We reduced the lattice equation to a nonlinear Schrödinger (NLS) equation for the breather envelope. From this NLS equation, we determined the conditions for which stationary and moving breathers exist in the FPU chain. For stationary breathers, we recover James's inequality $3b > 4a^2$, and for moving breathers, we obtained a generalised version of this inequality.

When the coefficient of the cubic term in the potential is nonzero, we found a critical wavenumber $p_{\min}$ below which breathers cease to exist. This also led an upper bound for the velocity of breathers in the FPU chain, which is lower than the speed of sound. We presented simulations of breathers in the chain, and verified the existence inequality by finding breathers in the appropriate regions of parameter space. When the interaction potential includes a cubic term, we observed that breather solutions widen and diverge as the wavenumber approaches the critical wavenumber $p_{\min}$.

In Section 2.4, we showed that the symmetric FPU chain (which has no cubic component in the potential) supports classical monotone kinks only above a critical amplitude $q_\infty^{(c)}$. It also supports waveforms which are combinations of a breather and a kink (breathing-kinks). We found that the kink amplitude q_∞ of breathing-kinks lies in the range $0 < q_\infty < 2q_\infty^{(c)}$, and depends upon the relative magnitudes of p and ε. This is summarised by equation (2.79). When p is much smaller than ε, the kink amplitude is larger than that of the breather. When $p = \mathcal{O}(1)$ (that is, when p is large compared to ε), the breather amplitude is larger than that of the kink. We determined a region of (ε, p)-parameter space where both breather and kink are of comparable size; this is where breathing-kinks are observed. Numerical simulations showed that breathing-kinks are long-lived modes. They propagate as travelling waves (as expected), moving with unit speed. Lastly, we also explained some of the differences between our approach and that used by Flytzanis *et al.* [57], who consider a similar problem.

In Chapter 3 we applied the semi-discrete multiple-scale method to a two dimensional FPU lattice with square (C_4) symmetry. We were able to reduce the lattice equations to a two-dimensional NLS equation with cubic nonlinearity only for two cases. Namely, for lattices with a symmetric potential, in which case the reduction was possible even for moving breathers. This led to an ellipticity criterion for the wavenumbers of the carrier wave. Secondly, we also considered lattices with an asymmetric potential, for which we found that the reduction to an NLS equation could be performed only for stationary breathers.

In Section 3.4, we reviewed the phenomenon of blow-up in depth, and concluded that a third-order analysis of the two-dimensional FPU lattice is insufficient. The cubic NLS equation supports a family of highly unstable Townes solitons which either blow-up or disperse when perturbed. Hence, this equation does not fully capture the true dynamics of the FPU lattice, in which we would not expect amplitudes to diverge. In Section 3.4.3, we explained that higher-order effects moderate blow-up, resulting in stable solitons. Hence, for lattice models such as ours, the effects of higher-order dispersion and nonlinearity must be taken into account. Acting on this, we derived a generalised fifth-order NLS equation (3.55) which includes various perturbing terms, some of which are known to be stabilising. Other perturbing terms (as far as we are aware) have not yet been studied. A rigorous analysis of (3.55) is left for future work.

We supplemented our analytic work with numerical simulations, which showed that the two-dimensional FPU lattice supports long-lived stationary and moving breathers. These are robust structures, and do not distort or shed much energy as they evolve. We were also able to simulate breathers moving in any direction in the lattice. This stands in contrast to the numerical work of Marin *et al.* [89, 90], who found that breathers can move only along lines of symmetry of two-component lattices.

In Section 3.6, we derived estimates for the energy of breathers, and found that the breather energy does not go to zero with the amplitude. In other words,

we found a threshold energy, below which breathers cannot exist, confirming the results of Flach *et al.* [56] and Kastner [71]. Surprisingly, we found that the energy threshold for moving breathers is smaller than that for stationary breathers, and becomes vanishingly small near the boundary of the elliptic domain.

In Chapter 4, we considered a two-dimensional lattice with hexagonal (C_6) rotational symmetry. We expected the different rotational symmetry properties of the lattice to result in a system of equations of greater structural simplicity than that obtained for the square lattice. We were able to reduce the hexagonal lattice equations to a two-dimensional cubic NLS equation for the same two cases as before, though we obtained significantly different results for the hexagonal lattice. In particular, we found that for asymmetric potentials, the higher-order correction term G_2 is nonzero for the hexagonal lattice, whereas G_2 is zero for the square lattice. The region of (a, b)-parameter space corresponding to the anomalous dispersion regime is also different for the hexagonal and square lattices.

We extended the analysis to fifth-order, and derived a generalised NLS equation (4.66) very similar to the one obtained for the square lattice. The two differ in that the dispersive terms in (4.66) are isotropic, and also the H_3 correction term is zero (unlike the square lattice, where it is nonzero).

Our numerical simulations of the hexagonal lattice suggest that long-lived stationary and moving breather modes are supported by the system. Again, we were able to propagate breathers moving in directions other than axes of symmetry of the lattice. Also, we obtained estimates for the breather energy, and found a minimum threshold requirement for the creation of breathers as expected.

In the course of this thesis, we have identified several problems which require further work. These include the determination of the stability properties

of the generalised NLS equations (3.55) and (4.66) derived for the SETL and HETL respectively. As we discussed in Section 3.4.3, if a variational formulation for these equations exists (we suspect that one does, see Zakharov & Kuznetsov [141]), then Pohožaev's method of constrained minimisation is applicable. On the other hand, the modulation theory of Fibich & Papanicolaou [46, 47] is perhaps better suited for equations of this complexity.

There are also other problems that could be pursued in addition. An obvious candidate for further study is a two-dimensional FPU lattice with triangular (C_3) rotational symmetry, as shown in Figure 4.2. Bearing in mind the results of Chapter 3 and Chapter 4, one would expect to find a higher-order generalised NLS equation similar to (3.55) and (4.66), with perhaps different dispersive terms.

All of the two-dimensional lattices that we have considered in this thesis have been scalar (or one-component) electrical networks, namely, lattices for which there is one degree of freedom at each lattice site. We could consider two-dimensional mechanical spring-mass lattices, for which there are two degrees of freedom at each lattice site (assuming that vibrations are restricted to the lattice plane). We describe such a lattice in Appendix A, where we have outlined a preliminary analysis using the semi-discrete multiple-scale method. Since this is a two-component lattice (that is, there are two unknowns at each site), we obtain coupled systems of equations for the leading-order horizontal and vertical displacements of each particle. Naturally, a similar analysis of two-dimensional spring-mass lattices with hexagonal or triangular symmetry is also possible. Bearing in mind our results for the SETL and HETL, we would expect the resulting systems of equations for hexagonal and triangular spring-mass lattices to be similar to those obtained for the square lattice (A.11) described in Appendix A.

As an intermediate problem, we could consider a one-dimensional analogue of (A.11), namely a spring-mass chain with transverse displacements (see for example, Cadet [27, 28]), unlike Chapter 2, where we considered longitudinal

disturbances only. This would lead to a coupled system of one-dimensional NLS equations for the horizontal and vertical displacements of each particle. In this way, we would avoid the blow-up properties associated with two-dimensional NLS equations. We expect that such a system would provide insights into the two-dimensional spring-mass lattice (A.11) of Appendix A.

We could also apply similar analytic methods to three-dimensional lattices. In this case, we would expect the lattice equations to reduce to a three-dimensional NLS equation at third-order. As discussed in Section 3.4, this also exhibits blow-up. Unlike the two-dimensional (critical) NLS equation, which is finely balanced between nonlinear focusing and dispersive effects, the nonlinear focusing effects dominate when the dimensionality is greater than two. Hence, we suspect that it would be more difficult to find stabilising terms by extending the analysis of a three-dimensional lattice to higher order.

Appendix A

A two-dimensional spring-mass system

In Chapters 3 and 4, we considered small amplitude breathers in different two-dimensional electrical networks, with square and hexagonal rotational symmetry. These are examples of scalar lattices, where there is one degree of freedom at each lattice site.

Here, we consider small amplitude breathers in a two-dimensional spring-mass lattice with square symmetry, depicted in Figure A.1. This comprises a repeating arrangement of identical particles of unit mass, connected by identical nonlinear springs of natural length h. As well as relative FPU-type interactions, we also assume that each particle experiences a nonlinear onsite potential. At equilibrium, the particles are spaced regularly in both the horizontal and vertical directions, with all of the springs unextended. Vibrations are restricted to the plane of the lattice, and hence there are two-degrees of freedom at each lattice site, making this model considerably more complicated than the scalar one-component lattices analysed in Chapter 3 and 4.

We select an arbitrary site to be the site $(0,0)$, and the remaining sites are labelled using the lattice basis vectors $\mathbf{i} = [1, 0]^T$ and $\mathbf{j} = [0, 1]^T$, as in Chapter 3. The particle located at site (m, n) is labelled $P_{m,n}$. At general time t, particle $P_{m,n}$ is displaced from its equilibrium position, as shown in Figure A.2. We
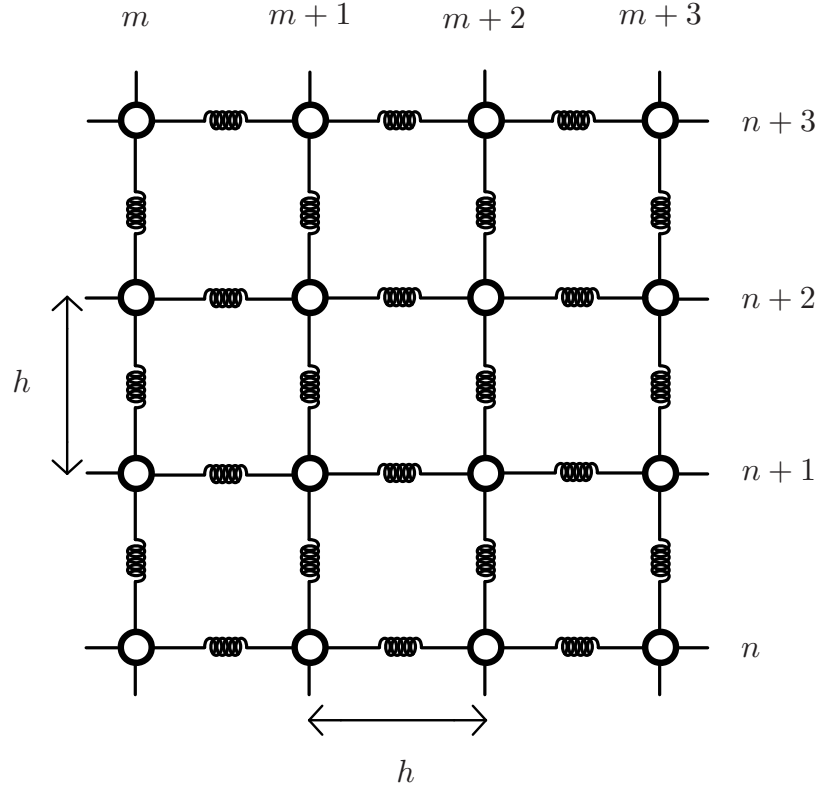
Figure A.1: A two-dimensional square spring-mass lattice.

denote the displacement of particle $P_{m,n}$ from its equilibrium position at time t by $(u_{m,n}(t), v_{m,n}(t))$.

A.I Derivation of model equations

First, we derive the Hamiltonian (total energy) of the lattice. We assume that the elastic potential energy V_s stored by each spring is given by

$$V_s(\phi) = \tfrac{1}{2}\phi^2 + \tfrac{1}{3}a\phi^3 + \tfrac{1}{4}b\phi^4, \tag{A.1}$$

where ϕ is the extension of the spring (see Section 2.2.1). The onsite potential V_o experienced by each particle has the form

$$V_o(r) = \tfrac{1}{2}\,\Omega^2 r^2 + \tfrac{1}{4}\lambda r^4, \tag{A.2}$$
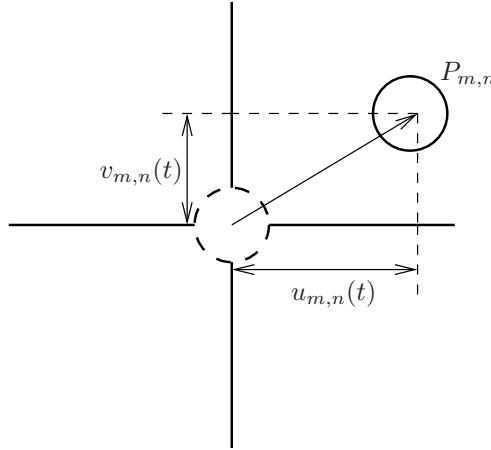
Figure A.2: Particle $P_{m,n}$ at general time t.

where $r = \sqrt{u_{m,n}^2 + v_{m,n}^2}$ is the magnitude of the displacement of each particle from its equilibrium position (see Figure A.2), and Ω and λ are constants.

The total energy of the system H is given by the sum of the kinetic energy of every particle, as well as the energy due to the springs and onsite potential. Taking care to avoid repeat counting, the energy of the spring-mass lattice is therefore

$$H = \sum_{m,n} \tfrac{1}{2}\dot{u}_{m,n}^2 + \tfrac{1}{2}\dot{v}_{m,n}^2 + V_o\left(\sqrt{u_{m,n}^2 + v_{m,n}^2}\right)$$

$$+ V_s\left(\|(u_{m+1,n}, v_{m+1,n}) - (u_{m,n}, v_{m,n})\|\right)$$

$$+ V_s\left(\|(u_{m,n+1}, v_{m,n+1}) - (u_{m,n}, v_{m,n})\|\right), \tag{A.3}$$

where $\|\cdot\|$ denotes distance. Also in (A.3), the second and third lines of the summand represent the potential energy of the springs which connect particle $P_{m,n}$ to particles $P_{m+1,n}$ and $P_{m,n+1}$ respectively. We derive an expression for the total energy H by calculating each of the terms in (A.3) explicitly.

Firstly, we calculate the energy of the spring which connects particle $P_{m,n}$ to particle $P_{m+1,n}$. This spring lies horizontally in the plane of the lattice, to the right of particle $P_{m,n}$, as shown in Figure A.3. The particles have been omitted for the purpose of clarity. At equilibrium, this spring is of total length h, as shown in Figure A.3(a). At later time t, the spring occupies the general position

shown in Figure A.3(b).

(a) At equilibrium.   (b) At later time t.
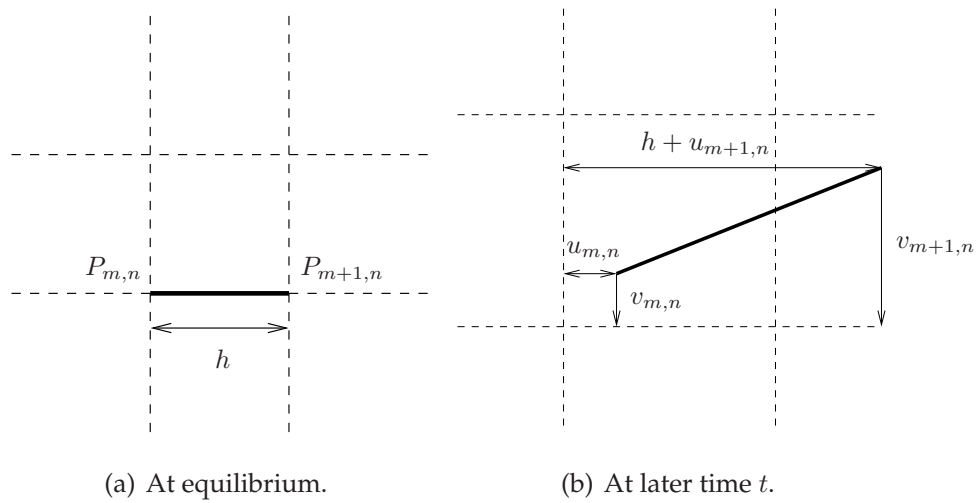
Figure A.3: Spring connecting particles $P_{m,n}$ and $P_{m+1,n}$.

The overall extension of this spring at time t, denoted $\phi_h(t)$, is therefore

$$\phi_h(t) = \left[(h + u_{m+1,n}(t) - u_{m,n}(t))^2 + (v_{m+1,n}(t) - v_{m,n}(t))^2 \right]^{\frac{1}{2}} - h. \qquad \text{(A.4)}$$

Equivalently, denoting $u_{m+1,n}(t) - u_{m,n}(t)$ and $v_{m+1,n}(t) - v_{m,n}(t)$ by $\delta u(t)$ and $\delta v(t)$ respectively, (A.4) can be rewritten as

$$\phi_h(t) = \left[(h + \delta u)^2 + \delta v^2 \right]^{\frac{1}{2}} - h. \qquad \text{(A.5)}$$

The presence of the radical in (A.5) makes further calculations extremely cumbersome. Since we are interested only in small amplitude oscillations, we assume that $\delta u/h$ and $\delta v/h$ are small, and of size $\mathcal{O}(\varepsilon)$. Hence, we expand the expression (A.5) for the extension $\phi_h(t)$ using the Binomial theorem. We aim to reduce the governing equations of motion to a nonlinear Schrödinger system at third-order in ε, and so we retain terms up to fourth-order in the expansion for $\phi_h(t)/h$, giving

$$\frac{\phi_h}{h} = \frac{\delta u}{h} + \frac{\delta v^2}{2h^2} - \frac{\delta u \delta v^2}{2h^3} + \frac{\delta u^2 \delta v^2}{2h^4} - \frac{\delta v^4}{8h^4} + \mathcal{O}(\varepsilon^5). \qquad \text{(A.6)}$$

Substituting (A.6) into (A.1) gives the elastic potential energy stored in the horizontal spring depicted in Figure A.3. We denote the energy of this spring V_h,

where

$$V_h = \left(\frac{\delta u^2}{2} + \frac{\delta u \delta v^2}{2h} + \frac{\delta v^4}{8h^2} - \frac{\delta u^2 \delta v^2}{2h^2} \right) + a \left(\frac{\delta u^3}{3} + \frac{\delta u^2 \delta v^2}{2h} \right) + b \left(\frac{\delta u^4}{4} \right) + \mathcal{O}(\varepsilon^5).$$

(A.7)

In an identical manner, we find that the extension in the spring which connects particle $P_{m,n}$ to particle $P_{m,n+1}$ (lying vertically in the plane of the lattice) is given by

$$\phi_v(t) = \left[(h + \Delta v)^2 + \Delta u^2 \right]^{\frac{1}{2}} - h,$$

(A.8)

where $\Delta u(t) = u_{m,n+1}(t) - u_{m,n}(t)$ and $\Delta v(t) = v_{m,n+1}(t) - v_{m,n}(t)$. Expanding the expression (A.8) for the extension $\phi_v(t)$ and retaining terms to fourth-order gives

$$\frac{\phi_v}{h} = \frac{\Delta v}{h} + \frac{\Delta u^2}{2h^2} - \frac{\Delta v \Delta u^2}{2h^3} + \frac{\Delta v^2 \Delta u^2}{2h^4} - \frac{\Delta u^4}{8h^4} + \mathcal{O}(\varepsilon^5).$$

(A.9)

Substituting the expansion for the extension (A.9) into (A.1) gives the elastic potential energy V_v stored in the spring connecting particle $P_{m,n}$ to particle $P_{m,n+1}$ to fourth-order, where

$$V_v = \left(\frac{\Delta v^2}{2} + \frac{\Delta v \Delta u^2}{2h} + \frac{\Delta u^4}{8h^2} - \frac{\Delta v^2 \Delta u^2}{2h^2} \right) + a \left(\frac{\Delta v^3}{3} + \frac{\Delta v^2 \Delta u^2}{2h} \right) + b \left(\frac{\Delta v^4}{4} \right) + \mathcal{O}(\varepsilon^5).$$

(A.10)

Using equations (A.7) and (A.10), the Hamiltonian H for the spring-mass lattice (A.3) is therefore

$$
\begin{aligned}
H = \sum_{m,n} & \frac{1}{2} \dot{u}_{m,n}^2 + \frac{1}{2} \dot{v}_{m,n}^2 + \frac{\Omega^2}{2} (u_{m,n}^2 + v_{m,n}^2) + \frac{\lambda}{4} (u_{m,n}^2 + v_{m,n}^2)^2 \\
& + \left(\frac{\delta u^2}{2} + \frac{\delta u \delta v^2}{2h} + \frac{\delta v^4}{8h^2} - \frac{\delta u^2 \delta v^2}{2h^2} \right) + \left(\frac{\Delta v^2}{2} + \frac{\Delta v \Delta u^2}{2h} + \frac{\Delta u^4}{8h^2} - \frac{\Delta v^2 \Delta u^2}{2h^2} \right) \\
& + a \left(\frac{\delta u^3}{3} + \frac{\delta u^2 \delta v^2}{2h} \right) + a \left(\frac{\Delta v^3}{3} + \frac{\Delta v^2 \Delta u^2}{2h} \right) \\
& + b \left(\frac{\delta u^4}{4} \right) + b \left(\frac{\Delta v^4}{4} \right) + \mathcal{O}(\varepsilon^5),
\end{aligned}
$$

(A.11)

where $\delta u(t)$, $\delta v(t)$, $\Delta u(t)$ and $\Delta v(t)$ have been defined immediately above.

Applying Hamilton's equations to (A.11) gives the equations of motion for

the spring-mass lattice,

$$
\begin{aligned}
\ddot{u}_{m,n} =\ & -\Omega^2 u_{m,n} - \lambda(u_{m,n}^2 + v_{m,n}^2)u_{m,n} + (u_{m+1,n} - 2u_{m,n} + u_{m-1,n}) \\
& + \frac{1}{2h}\left[(v_{m+1,n} - v_{m,n})^2 - (v_{m,n} - v_{m-1,n})^2\right] \\
& + \frac{1}{h}\left[(v_{m,n+1} - v_{m,n})(u_{m,n+1} - u_{m,n}) - (v_{m,n} - v_{m,n-1})(u_{m,n} - u_{m,n-1})\right] \\
& + \frac{1}{2h^2}\left[(u_{m,n+1} - u_{m,n})^3 - (u_{m,n} - u_{m,n-1})^3\right] \\
& + a\left[(u_{m+1,n} - u_{m,n})^2 - (u_{m,n} - u_{m-1,n})^2\right] \\
& + \frac{ah - 1}{h^2}\left[(v_{m+1,n} - v_{m,n})^2(u_{m+1,n} - u_{m,n}) - (v_{m,n} - v_{m-1,n})^2(u_{m,n} - u_{m-1,n})\right] \\
& + \frac{ah - 1}{h^2}\left[(v_{m,n+1} - v_{m,n})^2(u_{m,n+1} - u_{m,n}) - (v_{m,n} - v_{m,n-1})^2(u_{m,n} - u_{m,n-1})\right] \\
& + b\left[(u_{m+1,n} - u_{m,n})^3 - (u_{m,n} - u_{m-1,n})^3\right],
\end{aligned}
\tag{A.12}
$$

$$
\begin{aligned}
\ddot{v}_{m,n} =\ & -\Omega^2 v_{m,n} - \lambda(u_{m,n}^2 + v_{m,n}^2)v_{m,n} + (v_{m,n+1} - 2v_{m,n} + v_{m,n-1}) \\
& + \frac{1}{2h}\left[(u_{m,n+1} - u_{m,n})^2 - (u_{m,n} - u_{m,n-1})^2\right] \\
& + \frac{1}{h}\left[(v_{m+1,n} - v_{m,n})(u_{m+1,n} - u_{m,n}) - (v_{m,n} - v_{m-1,n})(u_{m,n} - u_{m-1,n})\right] \\
& + \frac{1}{2h^2}\left[(v_{m+1,n} - v_{m,n})^3 - (v_{m,n} - v_{m-1,n})^3\right] \\
& + a\left[(v_{m,n+1} - v_{m,n})^2 - (v_{m,n} - v_{m,n-1})^2\right] \\
& + \frac{ah - 1}{h^2}\left[(u_{m,n+1} - u_{m,n})^2(v_{m,n+1} - v_{m,n}) - (u_{m,n} - u_{m,n-1})^2(v_{m,n} - v_{m,n-1})\right] \\
& + \frac{ah - 1}{h^2}\left[(u_{m+1,n} - u_{m,n})^2(v_{m+1,n} - v_{m,n}) - (u_{m,n} - u_{m-1,n})^2(v_{m,n} - v_{m-1,n})\right] \\
& + b\left[(v_{m,n+1} - v_{m,n})^3 - (v_{m,n} - v_{m,n-1})^3\right].
\end{aligned}
\tag{A.13}
$$

A.II   Asymptotic analysis

We seek small amplitude breather solutions of (A.12) and (A.13), and apply the semi-discrete multiple-scale method. We introduce new variables defined by

$$
X = \varepsilon m, \quad Y = \varepsilon n, \quad \tau = \varepsilon t \quad \text{and} \quad T = \varepsilon^2 t,
\tag{A.14}
$$

and look for solutions for $u_{m,n}(t)$ and $v_{m,n}(t)$ of the form

$$
\begin{aligned}
u_{m,n}(t) = {} & \varepsilon \mathrm{e}^{\mathrm{i}\psi} F(X,Y,\tau,T) + \varepsilon^2 G_0(X,Y,\tau,T) + \varepsilon^2 \mathrm{e}^{\mathrm{i}\psi} G_1(X,Y,\tau,T) \\
& + \varepsilon^2 \mathrm{e}^{2\mathrm{i}\psi} G_2(X,Y,\tau,T) + \varepsilon^3 H_0(X,Y,\tau,T) + \varepsilon^3 \mathrm{e}^{\mathrm{i}\psi} H_1(X,Y,\tau,T) \\
& + \varepsilon^3 \mathrm{e}^{2\mathrm{i}\psi} H_2(X,Y,\tau,T) + \varepsilon^3 \mathrm{e}^{3\mathrm{i}\psi} H_3(X,Y,\tau,T) + \cdots + \text{c.c.,} \qquad \text{(A.15)}
\end{aligned}
$$

$$
\begin{aligned}
v_{m,n}(t) = {} & \varepsilon \mathrm{e}^{\mathrm{i}\psi} P(X,Y,\tau,T) + \varepsilon^2 Q_0(X,Y,\tau,T) + \varepsilon^2 \mathrm{e}^{\mathrm{i}\psi} Q_1(X,Y,\tau,T) \\
& + \varepsilon^2 \mathrm{e}^{2\mathrm{i}\psi} Q_2(X,Y,\tau,T) + \varepsilon^3 R_0(X,Y,\tau,T) + \varepsilon^3 \mathrm{e}^{\mathrm{i}\psi} R_1(X,Y,\tau,T) \\
& + \varepsilon^3 \mathrm{e}^{2\mathrm{i}\psi} R_2(X,Y,\tau,T) + \varepsilon^3 \mathrm{e}^{3\mathrm{i}\psi} R_3(X,Y,\tau,T) + \cdots + \text{c.c.,} \qquad \text{(A.16)}
\end{aligned}
$$

where the phase $\psi = km + ln + \omega t$. We substitute the ansatz (A.15) and (A.16) into the governing equations (A.12) and (A.13), and equate coefficients of each harmonic frequency at each order of ε. This yields the following sets of equations:

$\mathcal{O}(\varepsilon \mathrm{e}^{\mathrm{i}\psi})$:

$$
\omega^2 F = 4\sin^2\left(\frac{k}{2}\right) F + \Omega^2 F, \qquad \text{(A.17)}
$$

$\mathcal{O}(\varepsilon^2)$:

$$
\Omega^2 G_0 = 0 \Rightarrow G_0 = 0, \qquad \text{(A.18)}
$$

$\mathcal{O}(\varepsilon^2 \mathrm{e}^{\mathrm{i}\psi})$:

$$
\omega F_\tau = F_X \sin k, \qquad \text{(A.19)}
$$

$\mathcal{O}(\varepsilon^2 \mathrm{e}^{2\mathrm{i}\psi})$:

$$
\begin{aligned}
4\omega^2 G_2 = {} & 4\sin^2(k) G_2 + \Omega^2 G_2 \\
& + \frac{8\mathrm{i}}{h} \sin^3\left(\frac{k}{2}\right) \cos\left(\frac{k}{2}\right) \left[P^2 + 2haF^2\right] \\
& + \frac{16\mathrm{i}}{h} \sin^3\left(\frac{l}{2}\right) \cos\left(\frac{l}{2}\right) FP, \qquad \text{(A.20)}
\end{aligned}
$$

$\mathcal{O}(\varepsilon^3 e^{i\psi})$:

$$
\begin{aligned}
2i\omega F_T + F_{\tau\tau} + 2i\omega G_{1\tau} &= \cos(k)F_{XX} + 2i\sin(k)G_{1X} \\
&+ \frac{16i}{h}\sin^3\left(\frac{k}{2}\right)\cos\left(\frac{k}{2}\right)\left[\overline{P}Q_2 + 2ah\overline{F}G_2\right] \\
&+ \frac{16i}{h}\sin^3\left(\frac{l}{2}\right)\cos\left(\frac{l}{2}\right)\left[\overline{P}G_2 + \overline{F}Q_2\right] \\
&- \frac{16}{h^2}\sin^4\left(\frac{k}{2}\right)\left[(ah-1)(2FP\overline{P} + P^2\overline{F}) + 3bh^2F^2\overline{F}\right] \\
&- \frac{8}{h^2}\sin^4\left(\frac{l}{2}\right)\left[2(ah-1)(2FP\overline{P} + P^2\overline{F}) + 3F^2\overline{F}\right] \\
&- 3\lambda F^2\overline{F} + \lambda(2FP\overline{P} + P^2\overline{F}).
\end{aligned} \tag{A.21}
$$

The second set of equations is

$\mathcal{O}(\varepsilon e^{i\psi})$:

$$
\omega^2 P = 4\sin^2\left(\frac{l}{2}\right)P + \Omega^2 P, \tag{A.22}
$$

$\mathcal{O}(\varepsilon^2)$:

$$
\Omega^2 Q_0 = 0 \Rightarrow Q_0 = 0, \tag{A.23}
$$

$\mathcal{O}(\varepsilon^2 e^{i\psi})$:

$$
\omega P_\tau = P_Y \sin l, \tag{A.24}
$$

$\mathcal{O}(\varepsilon^2 e^{2i\psi})$:

$$
\begin{aligned}
4\omega^2 Q_2 &= 4\sin^2(l)Q_2 + \Omega^2 Q_2 \\
&+ \frac{8i}{h}\sin^3\left(\frac{l}{2}\right)\cos\left(\frac{l}{2}\right)\left[F^2 + 2ahP^2\right] \\
&+ \frac{16i}{h}\sin^3\left(\frac{k}{2}\right)\cos\left(\frac{k}{2}\right)PF, \tag{A.25}
\end{aligned}
$$

$\mathcal{O}(\varepsilon^3 \mathrm{e}^{\mathrm{i}\psi})$:

$$
\begin{aligned}
2\mathrm{i}\omega P_T + P_{\tau\tau} + 2\mathrm{i}\omega Q_{1\tau} &= \cos(l)P_{YY} + 2\mathrm{i}\sin(l)Q_{1Y} \\
&\quad + \frac{16\mathrm{i}}{h}\sin^3\left(\frac{l}{2}\right)\cos\left(\frac{l}{2}\right)\left[\overline{F}G_2 + 2ah\overline{P}Q_2\right] \\
&\quad + \frac{16\mathrm{i}}{h}\sin^3\left(\frac{k}{2}\right)\cos\left(\frac{k}{2}\right)\left[\overline{F}Q_2 + \overline{P}G_2\right] \\
&\quad - \frac{16}{h^2}\sin^4\left(\frac{l}{2}\right)\left[(ah-1)(2PF\overline{F} + F^2\overline{P}) + 3bh^2P^2\overline{P}\right] \\
&\quad - \frac{8}{h^2}\sin^4\left(\frac{k}{2}\right)\left[2(ah-1)(2PF\overline{F} + F^2\overline{P}) + 3P^2\overline{P}\right] \\
&\quad - 3\lambda P^2\overline{P} + \lambda(2PF\overline{F} + F^2\overline{P}).
\end{aligned}
\tag{A.26}
$$

We do not present a full analysis of the above system of equations here. However, we note these equations are similar in structure to those obtained for the SETL and HETL (see Chapters 3 and 4). Both equations (A.17) and (A.22) give a dispersion relation for the system, leading to a contradiction except in two cases. In the first case, one of F or P is zero, and we may take $P = 0$ without loss of generality. Then (A.21) leads to an NLS equation in F. However, we note that (A.21) contains only derivatives of the form F_{XX}, with no corresponding F_{YY} term (unlike the corresponding equations (3.22) and (4.21) obtained for the SETL and HETL respectively). Hence (A.21) admits only solutions that are localised in one direction ("planar solitons"), but not in both. It could be that the scalings chosen above for the variables X, Y, $u_{m,n}$ and $v_{m,n}$ are incorrect, and that different scalings are applicable.

In the second case, a contradiction in equations (A.17) and (A.22) can be avoided by setting $k = l$, in which case both F and P may be nonzero. Equations (A.21) and (A.26) lead to a pair of coupled NLS equations for F and P. Again, we note that (A.26) includes terms of the form P_{YY}, and no terms of the form P_{XX}, leading to solutions which are localised in the Y direction alone. In addition, the stability properties of this pair of coupled two-dimensional NLS equations are unknown to us, though we note that the results of Bergé *et al.* [16] could prove relevant.

Hence, equations (A.12) and (A.13) require more detailed study, with scal-

ings more general than those used in equations (A.14)–(A.16). Also, a higher-order analysis of the type done for the SETL and HETL (to determine soliton stability) would prove considerably more complicated for this spring-mass system. This is left for future work.

Appendix B

Approximations to Townes solitons

B.I The critical NLS equation

In this section, using the Rayleigh-Ritz variational method (see Chapter 8.3 of Spencer *et al.* [118]), we determine approximations to soliton solutions of the CNLS equation (see equation (3.39) of Section 3.4.2)

$$\mathrm{i}F_T + D\nabla^2 F + B|F|^2 F = 0, \tag{B.1}$$

where $F(\xi, \eta, T) \in \mathbb{C}$, and the operator $\nabla^2 = \partial_{\xi\xi} + \partial_{\eta\eta}$. We look for time-harmonic radially symmetric solutions of (B.1) of the form $F(\mathbf{x}, T) = \mathrm{e}^{\mathrm{i}\lambda T}\phi(r)$, where $r = |\mathbf{x}| = \sqrt{\xi^2 + \eta^2}$ and $\phi(r) \in \mathbb{R}$. Substituting for F in (B.1) leads to the real nonlinear eigenvalue problem

$$-\lambda\phi + D\nabla^2\phi + B\phi^3 = 0. \tag{B.2}$$

As explained in Section 3.4.3, equation (B.2) is the Euler-Lagrange equation corresponding to the action integral $\mathcal{S}(\phi) = \mathcal{H}(\phi) + \lambda\mathcal{N}(\phi)$, which for (B.1) is

$$\mathcal{S}(\phi) = \int \tfrac{1}{2}\lambda|\phi|^2 + \tfrac{1}{2}D|\nabla\phi|^2 - \tfrac{1}{4}B|\phi|^4 d^2\mathbf{r}. \tag{B.3}$$

We use a radially symmetric trial solution of the form $\phi(r) = \alpha\operatorname{sech}(\beta r)$, where α and β are parameters to be determined and $r = \sqrt{\xi^2 + \eta^2}$. Substituting this form for ϕ into (B.3), and evaluating the resulting integral (using Maple to evaluate a few of the trickier integrals) gives an expression for $\mathcal{S}$ in terms of the

variational parameters α and β. After much simplification, it turns out that

$$S(\alpha, \beta) = \frac{D(1 + 2\ln2)}{12}\, \alpha^2 + \frac{1}{24}\frac{\alpha^2}{\beta^2}\left[12\lambda\ln2 - B(4\ln2 - 1)\alpha^2\right]. \qquad \text{(B.4)}$$

The soliton solution of (B.1) corresponds to a stationary point of the action S, and therefore the parameters α and β are determined by the equations

$$\frac{\partial S}{\partial \alpha} = 0, \qquad \frac{\partial S}{\partial \beta} = 0. \qquad \text{(B.5)}$$

The two equalities in (B.5) form a pair of nonlinear simultaneous equations in α and β, which must be solved. After further simplification, it emerges that both equations are in fact linear in α^2 and β^2, and hence solving them is straightforward. Differentiating S with respect to β (the right-hand equation in (B.5)) results in an equation in α^2 alone, which can be solved to give α. The left-hand equation in (B.5) gives a linear equation in β^2 and α^2, which is then easily solved to give β. In this way, the variational parameters α and β are found in terms of the parameters that occur in the nonlinear eigenvalue problem (B.2), λ, B and D. We have

$$\alpha = \sqrt{\frac{12\lambda\ln2}{B(4\ln2 - 1)}} \quad \text{and} \quad \beta = \sqrt{\frac{6\lambda\ln2}{D(2\ln2 + 1)}}. \qquad \text{(B.6)}$$

An approximate form for the Townes soliton solution of (B.1) is therefore

$$F = \alpha \exp(i\lambda T)\operatorname{sech}(\beta r)$$

$$= \sqrt{\frac{12\lambda\log2}{B(4\log2 - 1)}}\, \exp(i\lambda T)\, \operatorname{sech}\left(\sqrt{\frac{6\lambda\log2}{D(2\log2 + 1)}}\sqrt{\xi^2 + \eta^2}\right). \qquad \text{(B.7)}$$

B.II A higher-order NLS equation

In this section, we use the Rayleigh-Ritz procedure to obtain approximations to soliton solutions of the higher-order NLS equation studied by Davydova *et al.* [38] (see equation (3.44) of Section 3.4.3),

$$iF_T + D\nabla^2 F + B|F|^2F + P\nabla^4 F + K|F|^4F = 0, \qquad \text{(B.8)}$$

where the operator ∇^2 is defined above. Seeking solutions of (B.8) of the form $F(\mathbf{x}, T) = e^{i\lambda T}\psi(r)$ as above leads to the nonlinear eigenvalue equation

$$-\lambda\psi + D\nabla^2\psi + B\psi^3 + P\nabla^4\psi + K\psi^5 = 0. \tag{B.9}$$

The action integral $\mathcal{E}(\psi) = \mathcal{H}(\psi) + \lambda\mathcal{N}(\psi)$ corresponding to (B.9) is

$$\mathcal{E}(\psi) = \int \tfrac{1}{2}\lambda|\psi|^2 + \tfrac{1}{2}D|\nabla\psi|^2 - \tfrac{1}{4}B|\psi|^4 - \tfrac{1}{2}P|\nabla^2\psi|^2 - \tfrac{1}{6}K|\psi|^6 d^2\mathbf{r}. \tag{B.10}$$

Using a trial solution of the form $\psi(r) = \widetilde{\alpha}\,\text{sech}(\widetilde{\beta}r)$, and substituting into (B.10) gives the action integral $\mathcal{E}$ in terms of the variational parameters $\widetilde{\alpha}$ and $\widetilde{\beta}$,

$$\mathcal{E}(\widetilde{\alpha}, \widetilde{\beta}) = \frac{D(1 + 2\ln2)}{12}\widetilde{\alpha}^2 - \frac{P}{30}\left[15I_1 + 7\ln2 - 1\right]\widetilde{\alpha}^2\widetilde{\beta}^2$$
$$+ \frac{1}{360}\frac{\widetilde{\alpha}^2}{\widetilde{\beta}^2}\left[180\lambda\ln2 - 15B(4\ln2 - 1)\widetilde{\alpha}^2 - K(32\ln2 - 11)\widetilde{\alpha}^4\right], \tag{B.11}$$

where $I_1 = \int_0^\infty u^{-1}\text{sech}^2(u)\tanh^2(u)\,du \approx 0.384928$. The soliton solution of (B.8) corresponds to an extremum of the action $\mathcal{E}(\widetilde{\alpha}, \widetilde{\beta})$ given by (B.11). Hence the parameters $\widetilde{\alpha}$ and $\widetilde{\beta}$ are determined by the equations

$$\frac{\partial\mathcal{E}}{\partial\widetilde{\alpha}} = 0, \qquad \frac{\partial\mathcal{E}}{\partial\widetilde{\beta}} = 0. \tag{B.12}$$

The resulting simultaneous equations for $\widetilde{\alpha}$ and $\widetilde{\beta}$ given by (B.12) are harder to solve than before, since both equations are nonlinear in $\widetilde{\alpha}^2$ and $\widetilde{\beta}^2$.

However, when P and K in (B.8) are small compared to B and D, we expect the variational parameters generated from (B.12) to be close the parameters given by (B.6). This applies to the nonlinear Schrödinger equation (3.55) derived in Section 3.5, where we see that B and D are $\mathcal{O}(1)$, and P and K are $\mathcal{O}(\varepsilon^2)$. We rewrite $P = \varepsilon^2\widehat{P}$ and $K = \varepsilon^2\widehat{K}$ where $\widehat{P}$ and $\widehat{K}$ are both $\mathcal{O}(1)$. Hence we assume perturbation expansions for solutions of (B.12), where $\widetilde{\alpha}^2$ and $\widetilde{\beta}^2$ assume the form

$$\widetilde{\alpha}^2 \sim \alpha^2 + \alpha_1^2\varepsilon^2 + \alpha_2^2\varepsilon^4 + \alpha_3^2\varepsilon^6 + \cdots, \tag{B.13}$$

$$\widetilde{\beta}^2 \sim \beta^2 + \beta_1^2\varepsilon^2 + \beta_2^2\varepsilon^4 + \beta_3^2\varepsilon^6 + \cdots, \tag{B.14}$$

where α and β are the variational parameters generated for the CNLS, given by (B.6). Substituting the expansions (B.13) and (B.14) into the simultaneous

equations ([B.12](#)), we determine the first correction term for solutions of $\widetilde{\alpha}^2$ and $\widetilde{\beta}^2$, finding that

$$\widetilde{\alpha}^2 = \alpha^2 + \alpha_1^2 \varepsilon^2 + \mathcal{O}(\varepsilon^4), \tag{B.15}$$

$$\widetilde{\beta}^2 = \beta^2 + \beta_1^2 \varepsilon^2 + \mathcal{O}(\varepsilon^4), \tag{B.16}$$

where

$$\alpha_1^2 = \frac{12(\ln 2)^2 \left[15 I_1 + (7\ln 2 - 1)\right]}{(1 + 2\ln 2)^2 (4\ln 2 - 1)} \frac{\lambda^2 \widehat{P}}{D^2 B} - \frac{4(\ln 2)^2 (32\ln 2 - 11)}{5(4\ln 2 - 1)^3} \frac{\lambda^2 \widehat{K}}{B^3}, \tag{B.17}$$

$$\beta_1^2 = \frac{18(\ln 2)^2 \left[15 I_1 + (7\ln 2 - 1)\right]}{(1 + 2\ln 2)^3} \frac{\lambda^2 \widehat{P}}{D^3} + \frac{18(\ln 2)^2 (32\ln 2 - 11)}{5(1 + 2\ln 2)(4\ln 2 - 1)^2} \frac{\lambda^2 \widehat{K}}{D B^2}. \tag{B.18}$$

References

[1] FK Abdullaev, BB Baizakov, and M Salerno. Stable two-dimensional dispersion-managed soliton. *Phys. Rev. B*, 68:066605, 2003.

[2] MJ Ablowitz and JF Ladik. Nonlinear differential-difference equations and Fourier analysis. *J. Math. Phys.*, 17:1011, 1976.

[3] MJ Ablowitz, Dj Kaup, AC Newell, and H Segur. The inverse scattering transform-Fourier analysis for nonlinear problems. *Stud. Appl. Math.*, 53: 249, 1974.

[4] D Anderson, M Bonnedal, and M Lisak. Self-trapped cylindrical laser beams. *Phys. Fluids*, 22:1838, 1979.

[5] PW Anderson. Absence of diffusion in certain random lattices. *Phys. Rev. E*, 109:1492, 1958.

[6] J Archilla, R MacKay, and J Marin. Discrete breathers and Anderson modes: two faces of the same phenomenon? *Physica D*, 134:406, 1999.

[7] S Aubry and G Abramovici. Chaotic trajectories in the standard map: the concept of anti-integrability. *Physica D*, 43:199, 1990.

[8] S Aubry and T Cretegny. Mobility and reactivity of discrete breathers. *Physica D*, 119:34, 1998.

[9] S Aubry, G Kopidakis, and V Kadelburg. Variational proof for hard discrete breathers in some classes of Hamiltonian dynamical systems. *Disc. Cont. Dyn. Sys. B*, 1:271, 2001.

[10] GA Baker and P Graves-Morris. *Padé Approximants*. Addison-Wesley, Reading, Mass., 1981.

[11] D Bambusi. Exponential stability of breathers in hamiltonian networks of weakly coupled oscillators. *Nonlinearity*, 9:433, 1996.

[12] O Bang and M Peyrard. Higher order breathers solutions to a discrete nonlinear Klein-Gordon model. *Physica D*, 81:9, 1995.

[13] HC Berg. Molecular motors: Keeping up with the F_1-ATPase. *Nature*, 394: 324, 1998.

[14] L Bergé. Soliton stability versus collapse. *Phys. Rev. E*, 62:R3071, 2000.

[15] L Bergé. Wave collapse in physics: principles and applications to light and plasma waves. *Phys. Rep.*, 303:259, 1998.

[16] L Bergé, O Bang, JJ Rasmussen, and VK Mezentsev. Self-focusing and solitonlike structures in materials with competing quadratic and cubic nonlinearities. *Phys. Rev. E*, 55:3555, 1997.

[17] SR Bickham, SA Kiselev, and Sievers AJ. Stationary and moving intrinsic localized modes in one-dimensional monatomic lattices with cubic and quartic anharmonicity. *Phys. Rev. B*, 47:14206, 1993.

[18] P Binder and AP Ustinov. Exploration of a rich variety of breather modes in Josephson ladders. *Phys. Rev. E*, 66:016603, 1993.

[19] AD Boardman, DE O'Connor, and PA Young. *Symmetry and its Applications in Science*. McGraw-Hill, UK, 1973.

[20] D Bonart, AP Mayer, and U Schröder. Anharmonic localized surface vibrations in a scalar model. *Phys. Rev. B*, 51:13739, 1995.

[21] WE Boyce and RC DiPrima. *Elementary Differential Equations and Boundary Value Problems, sixth edition*. Wiley, New York, 1997.

[22] VM Burlakov, SA Kisilev, and VN Pyrkov. Computer simulation of intrinsic localized modes in one-dimensional and two-dimensional anharmonic lattices. *Phys. Rev. B*, 42:4921, 1990.

[23] AW Bush. *Perturbation Methods for Engineers and Scientists*. CRC Press, Boca Raton, FL., 1993.

[24] IA Butt and JAD Wattis. Asymptotic analysis of combined breather-kink modes in a Fermi-Pasta-Ulam chain. Submitted, 2006.

[25] IA Butt and JAD Wattis. Discrete breathers in a two-dimensional hexagonal Fermi-Pasta-Ulam lattice. Submitted, 2006.

[26] IA Butt and JAD Wattis. Discrete breathers in a two-dimensional Fermi-Pasta-Ulam lattice. *J. Phys. A: Math. Gen.*, 39:4955, 2006.

[27] S Cadet. Transverse envelope solutions in an atomic chain. *Phys. Lett. A*, 121:77, 1987.

[28] S Cadet. Propagation and interactions of nonlinear shear waves in a discrete lattice. *Wave Motion*, 11:77, 1989.

[29] DK Campbell. Fresh breather. *Nature*, 432:455, November 2004.

[30] DK Campbell, S Flach, and YS Kivshar. Localizing energy through nonlinearity and discreteness. *Physics Today*, pages 43–49, January 2004.

[31] SJ Chapman. *Fortran 90/95 for Scientists and Engineers, second edition*. McGraw-Hill, Boston, Mass., 2004.

[32] RY Chiao, E Garmire, and CH Townes. Self-trapping of optical beams. *Phys. Rev. Lett.*, 13:479, 1964.

[33] C Claude, YS Kivshar, O Kluth, and KH Spatschek. Moving localized modes in nonlinear lattices. *Phys. Rev. B*, 47:142282, 1993.

[34] M Collins. A quasicontinuum approximation for solitons in an atomic chain. *Chem. Phys. Lett.*, 77:342, 1981.

[35] M Collins and S Rice. Some properties of large amplitude motion in an anharmonic chain with nearest neighbor interactions. *J. Chem. Phys.*, 67: 2607, 1982.

[36] T Dauxois, M Peyrard, and A Bishop. Entropy-driven DNA denaturation. *Phys. Rev. E*, 47:R44, 1993.

[37] T Dauxois, M Peyrard, and A Bishop. Dynamics and thermodynamics of a nonlinear model for DNA denaturation. *Phys. Rev. E*, 47:684, 1993.

[38] TA Davydova, AI Yakimenko, and YA Zaliznyak. Two-dimensional solitons and vortices in normal and anomalous dispersive media. *Phys. Rev. E*, 67:026402, 2003.

[39] GH Derrick. Comments on nonlinear wave equations as models for elementary particles. *J. Math. Phys.*, 5:1252, 1964.

[40] R Dodd, JC Eilbeck, J Gibbon, and H Morris. *Solitons and Nonlinear Wave Equations*. Academic Press, London, 1982.

[41] J Edler and P Hamm. Self-trapping of the amide I band in a peptide model crystal. *J. Chem. Phys.*, 117:2415, 2002.

[42] JC Eilbeck. *Numerical studies of solitons on lattices (Nonlinear Coherent Structures in Physics and Biology)*. Springer-Verlag, Berlin, 1991. Lecture Notes in Physics Vol. 393, Eds M Remoissenet and M Peyrard.

[43] HS Eisenberg, Y Silberberg, R Morandotti, AR Boyd, and JS Aitchison. Discrete spatial optical solitons in waveguide arrays. *Phys. Rev. Lett.*, 81: 3383, 1998.

[44] H Fedderson. Localization of vibrational energy in globular protein. *Phys. Lett. A*, 154:391, 1991.

[45] E Fermi, J Pasta, and S Ulam. Studies of nonlinear problems. Los Alamos Scientific Report, 1940, originally unpublished. Later published in Lectures in Applied Mathematics, 15:143, 1974.

[46] G Fibich and G Papanicolaou. A modulation method for self-focusing in the perturbed critical nonlinear Schrödinger equation. *Phys. Lett. A*, 239: 167, 1998.

[47] G Fibich and G Papanicolaou. Self-focusing in the perturbed and unperturbed nonlinear Schrödinger equation in critical dimension. *SIAM J. Appl. Math.*, 60:183, 1999.

[48] S Flach. Existence of localized excitations in nonlinear Hamiltonian lattices. *Phys. Rev. E*, 51:1503, 1995.

[49] S Flach. Tangent bifurcation of band edge plane waves, dynamical symmetry breaking and vibrational localization. *Physica D*, 91:223, 1996.

[50] S Flach and K Kladko. Moving discrete breathers? *Physica D*, 127:61, 1999.

[51] S Flach and CR Willis. Localized excitations in a discrete Klein-Gordon system. *Phys. Lett. A*, 181:232, 1993.

[52] S Flach and CR Willis. Discrete breathers. *Phys. Rep.*, 295:181, 1998.

[53] S Flach and CR Willis. Movability of localized excitations in nonlinear discrete systems: A separatrix problem. *Phys. Rev. Lett.*, 72:1777, 1994.

[54] S Flach, K Kladko, and CR Willis. Localized excitations in two-dimensional lattices. *Phys. Rev. E*, 50:2293, 1994.

[55] S Flach, CR Willis, and E Olbrich. Integrability and localized excitations in nonlinear discrete systems. *Phys. Rev. E*, 49:836, 1994.

[56] S Flach, K Kladko, and RS MacKay. Energy thresholds for discrete breathers in one-, two-, and three-dimensional lattices. *Phys. Rev. Lett.*, 78:1207, 1997.

[57] N Flytzanis, S Pnevmatikos, and M Remoissenet. Kink, breather and asymmetric envelope or dark solitons in nonlinear chains I: monatomic chain. *J. Phys. C: Sol. St. Phys.*, 18:4603, 1985.

[58] J Ford. The Fermi-Pasta-Ulam problem: paradox turns discovery. *Phys. Rep.*, 213:271, 1992.

[59] A Franchini, V Bortolani, and RF Wallis. Theory of intrinsic localized modes in diatomic chains: beyond the rotating wave approximation. *J. Phys.: Condens. Matter*, 14:145, 2002.

[60] Y Gaididei, R Huß, and FG Mertens. Envelope solitary waves on two-dimensional lattices with in-plane displacements. *Euro. Phys. Journ. B*, 6: 257, 1998.

[61] J Giannoulis and A Mielke. The nonlinear Schrödinger equation as a macroscopic limit for an oscillator chain with cubic nonlinearities. *Nonlinearity*, 17:551, 2004.

[62] J Giannoulis and A Mielke. Dispersive evolution of pulses in oscillator chains with general interaction potentials. *Disc. Cont. Dyn. Sys. B*, 6:493, 2006.

[63] IS Gradshteyn and IM Ryzhik. *Table of Integrals, Series and Products, sixth edition*. Academic Press, London, 2000.

[64] K Hori and S Takeno. Moving self-localized modes for the displacement field in a one-dimensional lattice system with quartic anharmonicity. *J. Phys. Soc. Japan*, 61:2186, 1992.

[65] K Hori and S Takeno. Low-frequency and high-frequency moving anharmonic localized modes in a one-dimensional lattice with quartic anharmonicity. *J. Phys. Soc. Japan*, 61:4263, 1992.

[66] X Hu, A A Damjanovic, T Ritz, and K Schulten. Architecture and function of the light harvesting apparatus of purple bacteria. *Proc. Natl. Acad. Sci.*, 95:5935, 1998.

[67] G Huang, Z Shi, and Z Xu. Asymmetric intrinsic localized modes in a

homogeneous lattice with cubic and quartic anharmonicity. *Phys. Rev. B*, 47:14561, 1993.

[68] E Infeld and G Rowlands. *Nonlinear Waves, Solitons and Chaos (second edition)*. Cambridge University Press, Cambridge, United Kingdom, 2000.

[69] G James. Existence of breathers on FPU lattices. *C. R. Acad. Sci. Paris*, 332: 581, 2001.

[70] VI Karpman. Stabilization of soliton instabilities by higher-order dispersion: fourth-order nonlinear Schrödinger-type equations. *Phys. Rev. E*, 53: R1336, 1996.

[71] M Kastner. Energy thresholds for discrete breathers. *Phys. Rev. Lett.*, 92: 104301, 2004.

[72] PG Kevrekidis, IG Kevrekidis, AR Bishop, and ES Titi. Continuum approach to discreteness. *Phys. Rev. E*, 65:046613, 2002.

[73] TWB Kibble and FH Berkshire. *Classical Mechanics*. Imperial College Press, London, 2004.

[74] S Kichenassamy. Breather solutions of nonlinear wave equation. *Commun. Pure and Appl. Math.*, 44:789, 91.

[75] Y Kivshar and B Malomed. Dynamics of solitons in nearly integrable systems. *Rev. Mod. Phys.*, 61:763, 1989.

[76] YS Kivshar and DK Campbell. Peierls-Nabarro potential barrier for highly localized nonlinear modes. *Phys. Rev. E*, 48:3077, 1993.

[77] YS Kivshar and DE Pelinovsky. Self-focusing and transverse instabilities of solitary waves. *Phys. Rep.*, 331:117, 2000.

[78] G Kopidakis and S Aubry. Discrete breathers in realistic models: hydrocarbon structures. *Physica B*, 296:237, 2000.

[79] G Kopidakis, S Aubry, and GP Tsironis. Targeted energy transfer through discrete breathers in nonlinear systems. *Phys. Rev. Lett.*, 87:165501, 2001.

[80] AM Kosevich and AS Kovalev. Selflocalization of vibrations in a one-dimensional anharmonic chain. *Sov. Phys. JETP*, 67:1793, 1974.

[81] N Krylov and NN Bogoliubov. *Introduction to Nonlinear Mechanics*. Princeton University Press, Princeton, 1947.

[82] EA Kuznetsov, AM Rubenchik, and VE Zakharov. Soliton stability in plasmas and hydrodynamics. *Phys. Rep.*, 142:103, 1986.

[83] IM Lifshitz and AM Kosevich. The dynamics of a crystal lattice with defects. *Rep. Prog. Phys.*, 29:217, 1966.

[84] RS MacKay and S Aubry. Proof of existence of breathers for time-reversible or Hamiltonian networks of weakly coupled oscillators. *Nonlinearity*, 7:1623, 1994.

[85] RS MacKay and J-A Sepulchre. Effective Hamiltonian for travelling discrete breathers. *J. Phys. A: Math. Gen.*, 35:3985, 2002.

[86] IG Main. *Vibrations and Waves in Physics, third edition*. Cambridge University Press, Cambridge, 1993.

[87] AA Maradudin. Some effects of point defects on the vibrations of crystal lattices. *Rep. Prog. Phys.*, 28:331, 1965.

[88] AA Maradudin, E Montroll, G Weiss, and I Ipatova. *The Theory of Lattice Dynamics in the Harmonic Approximation, second edition (Solid State Physics, Suppl. 3)*. Academic Press, New York, 1971.

[89] JL Marin, JC Eilbeck, and FM Russell. Localised moving breathers in a 2D hexagonal lattice. *Phys. Lett. A*, 248:225, 1998.

[90] JL Marin, JC Eilbeck, and FM Russell. *2D breathers and applications (Nonlinear Science at the Dawn of the 21st Century)*. Springer, Berlin, 2000. Eds: PL Christiansen and MP Sørensen.

[91] JL Marin, FM Russell, and JC Eilbeck. Breathers in cuprate-like lattices. *Phys. Lett. A*, 281:21, 2001.

[92] SF Mingaleev, YS Kivshar, and RA Sammut. Long-range interaction and nonlinear localized modes in photonic crystal waveguides. *Phys. Rev. E*, 62:5777, 2000.

[93] GD Montesinos, VM Perez-Garcia, and P Torres. Stabilization of solitons of the multidimensional nonlinear Schrödinger equation: matter-wave breathers. *Physica D*, 191:193, 2004.

[94] AA Ovchinnikov. Localized long-lived vibrational states in molecular crystals. *Sov. Phys. JETP*, 30:147, 1970.

[95] AA Ovchinnikov and S Flach. Discrete breathers in systems with homogeneous potentials: analytic solutions. *Phys. Rev. Lett.*, 83:248, 1999.

[96] JB Page. Asymptotic solutions for localized vibrational modes in strongly anharmonic periodic systems. *Phys. Rev. B*, 41:7835, 1990.

[97] M Peyrard and A Bishop. Statistical mechanics of a nonlinear model for DNA denaturation. *Phys. Rev. Lett.*, 62:2755, 1989.

[98] SI Pohožaev. Eigenfunctions of the equation $\Delta u + \lambda f(u) = 0$. *Sov. Math. Dokl.*, 6:1408, 1965.

[99] JJ Rasmussen and K Rypdal. Blow-up in nonlinear Schrödinger equations I: a general review. *Physica Scripta*, 33:481, 1989.

[100] D Redfern. *The Maple Handbook: Maple V release 3*. Springer-Verlag, New York, 1994.

[101] D Redfern and C Campbell. *The MATLAB 5 Handbook*. Springer, New York, 1997.

[102] M Remoissenet. Low-amplitude breather and envelope solitons in quasi-one-dimensional physical models. *Phys. Rev. B*, 33:2386, 1985.

[103] M Remoissenet. *Waves Called Solitons. Concepts and Experiments, third edition*. Springer-Verlag, Berlin, 1999.

[104] P Rosenau. Dynamics of nonlinear mass-spring chains near the continuum limit. *Phys. Lett. A*, 118:222, 1986.

[105] P Rosenau. Dynamics of dense lattices. *Phys. Rev. B*, 36:5868, 1987.

[106] FM Russell. Identification and selection criteria for charged lepton tracks in mica. *Nucl. Tracks Radiat. Meas.*, 15:41, 1988.

[107] FM Russell and DR Collins. Lattice-solitons in radiation damage. *Nucl. Inst. Meth. Phys. Res. B*, 105:30, 1995.

[108] B Sánchez-Rey, G James, J Cuevas, and JFR Archilla. Bright and dark breathers in Fermi-Pasta-Ulam lattices. *Phys. Rev. B*, 70:014301, 2004.

[109] KW Sandusky and JB Page. Interrelation between the stability of extended normal modes and the existence of intrinsic localized modes in nonlinear lattices with realistic potentials. *Phys. Rev. B*, 50:2866, 1994.

[110] KW Sandusky, JB Page, and KE Schmidt. Stability and motion of intrinsic localized modes in nonlinear periodic lattices. *Phys. Rev. B*, 46:6161, 1992.

[111] M Sato and AJ Sievers. Direct observation of the discrete character of intrinsic localized modes in an antiferromagnet. *Nature*, 432:486, November 2004.

[112] J Schjødt-Eriksen, YB Gaididei, and PL Christiansen. Collapse arresting in an inhomogeneous two-dimensional nonlinear Schrödinger model. *Phys. Rev. E*, 64:066614, 2001.

[113] UT Schwarz, LQ English, and AJ Sievers. Experimental generation and observation of intrinsic localized spin wave modes in an antiferromagnet. *Phys. Rev. Lett.*, 83:223, 1999.

[114] AC Scott. *Nonlinear Science, second edition*. Oxford University Press, Oxford, 1999.

[115] H Segur and MD Kruskal. Nonexistence of small amplitude breather solutions in ϕ^4 theory. *Phys. Rev. Lett.*, 58:747, 1987.

[116] DS Sholl and BI Henry. Perturbative calculation of superperiod recurrence times in nonlinear chains. *Phys. Lett. A*, 159:21, 1991.

[117] A Sievers and S Takeno. Intrinsic localized modes in anharmonic crystals. *Phys. Rev. Lett.*, 61:970, 1988.

[118] AJM Spencer, DF Parker, DS Berry, AH England, TR Faulkner, WA Green, JT Holden, D Middleton, and TG Rogers. *Engineering Mathematics: Volume 2*. Van Nostrand Reinhold, New York, 1977.

[119] WA Strauss. *Nonlinear Wave Equations*. American Mathematical Society, Providence, R. I., 1989.

[120] C Sulem and P-L Sulem. *The Nonlinear Schrödinger Equation*. Springer, New York, 1999.

[121] B Swanson, J Brozik, S Love, G Strouse, A Shreve, A Bishop, W Wang, and M Salkola. Observation of intrinsically localised modes in a discrete low-dimensional material. *Phys. Rev. Lett.*, 82:3288, 1999.

[122] S Takeno. Theory of stationary anharmonic localized modes in solids. *J. Phys. Soc. Japan*, 61:2821, 1992.

[123] S Takeno. P-like stationary self-localized modes in pure one-dimensional lattice with quartic lattice anharmonicity. *J. Phys. Soc. Japan*, 59:3861, 1990.

[124] S Takeno. Localized modes in the long-time behavior of anharmonic lattice. *J. Phys. Soc. Japan*, 59:1571, 1990.

[125] S Takeno and K Hori. A propagating self-localized mode in a one-dimensional lattice with quartic anharmonicity. *J. Phys. Soc. Japan*, 59:3037, 1990.

[126] S Takeno and K Hori. Self-localized modes in a pure one-dimensional lattice with cubic and quartic lattice anharmonicity. *J. Phys. Soc. Japan*, 60: 947, 1991.

[127] S Takeno, K Kisoda, and AJ Sievers. Intrinsic localized vibrational modes in anharmonic crystals. *Prog. Theor. Phys. Suppl.*, 94:242, 1988.

[128] JM Tamga, M Remoissenet, and J J Pouget. Breathing solitary waves in a sine-Gordon two-dimensional lattice. *Phys. Rev. Lett.*, 75:357, 1995.

[129] M Toda. *Theory of Nonlinear Lattices*. Springer, Berlin, 1978.

[130] GP Tsironis. If "discrete breathers" is the answer, what is the question? *Chaos*, 13:657, 2003.

[131] JL Tuck and MT Menzel. The superperiod of the nonlinear weighted string (FPU) problem. *Adv. Math.*, 9:399, 1972.

[132] S Wang. Localized vibrational modes in an anharmonic chain. *Phys. Lett. A*, 182:105, 1993.

[133] S Wang. Influence of cubic anharmonicity on high frequency modes. *Phys. Lett. A*, 200:103, 1995.

[134] JAD Wattis. Approximations to solitary waves on lattices. II. quasi-continuum methods for fast and slow waves. *J. Phys. A: Math. Gen.*, 26: 1193, 1993.

[135] JAD Wattis. Solitary waves on a two-dimensional lattice. *Physica Scripta*, 50:238, 1994.

[136] JAD Wattis. Stationary breather modes of generalized nonlinear Klein-Gordon lattices. *J. Phys. A: Math. Gen.*, 31:3301, 1998.

[137] MI Weinstein. Excitation thresholds for nonlinear localized modes on lattices. *Nonlinearity*, 12:673, 1999.

[138] HC Yuen and BM Lake. Nonlinear deep-water waves: theory and experiment. *Phys. Fluids*, 18:956, 1975.

[139] NJ Zabusky and MD Kruskal. Interaction of "solitons" in a collisionless plasma and the recurrence of initial states. *Phys. Rev. Lett.*, 15:240, 1965.

[140] VE Zakharov. Collapse of Langmuir waves. *Zh. Éksp. Teor. Fiz.*, 62:1745, 1972. Also published in Sov. Phys. JETP 35:908, 1972.

[141] VE Zakharov and EA Kuznetsov. Optical solitons and quasisolitons. *Journal of Experimental and Theoretical Physics*, 86:1035, 1998. Also published in Zh. Éksp. Teor. Fiz. 113:1892, 1998.

[142] GZ Zhou and CT Zhang. A short review on the nonlinear motion in DNA. *Physica Scripta*, 453:347, 1991.